Universidade de Aveiro Departamento de Engenharia Civil
2013

Vitor Emanuel Marta da Silva

DESENVOLVIMENTO DE MODELOS E FERRAMENTAS PARA A AVALIAÇÃO DO RISCO SÍSMICO: APLICAÇÃO A PORTUGAL

DEVELOPMENT OF OPEN MODELS AND TOOLS FOR SEISMIC RISK ASSESSMENT: APPLICATION TO PORTUGAL

Universidade de Aveiro Departamento de Engenharia Civil
2013

Vitor Emanuel Marta da Silva

DESENVOLVIMENTO DE MODELOS E FERRAMENTAS PARA A AVALIAÇÃO DO RISCO SÍSMICO: APLICAÇÃO A PORTUGAL

DEVELOPMENT OF OPEN MODELS AND TOOLS FOR SEISMIC RISK ASSESSMENT: APPLICATION TO PORTUGAL

Tese apresentada à Universidade de Aveiro para cumprimento dos requisitos necessários à obtenção do grau de Doutor em Engenharia Civil, realizada sob a orientação científica do Prof. Doutor Humberto Salazar Amorim Varum, Professor Associado com Agregação do Departamento de Engenharia Civil da Universidade de Aveiro, e coorientação do Prof. Doutor Rui Jorge Silva Moura Pinho, Professor Associado do Departamento de Mecânica Estrutural da Universidade de Pavia.

Apoio financeiro da FCT através da bolsa com referência SFRH/BD/60967/2009.

Júri

presidente

Prof. Doutor Fernando Manuel dos Santos Ramos
professor catedrático da Universidade de Aveiro, Portugal

Prof. Doutora Emily So
professora associada da Universidade de Cambridge, Reino Unido

Doutora Helen Marie Crowley
investigadora sénior do EUCENTRE, Itália

Doutor Alfredo Campos Costa
investigador principal do Laboratório Nacional de Engenharia Civil, Portugal

Prof. Doutor Aníbal Guimarães da Costa
professor catedrático da Universidade de Aveiro, Portugal

Prof. Doutor Humberto Salazar Amorim Varum
professor associado com agregação da Universidade de Aveiro, Portugal

Prof. Doutor Rui Jorge Silva Moura Pinho
professor auxiliar da Universidade de Pavia, Itália

agradecimentos

acknowledgements

I would like to start by expressing my gratitude to Professor Humberto Varum, who has been the coordinator of my academic and professional career since I started this journey. His role has been crucial in my life, not only academically, with his vast experience and knowledge, but personally as well, with his permanent motivation and constantly challenging me to accomplish more.

To Dr. Rui Pinho, my co-advisor, I would like to express my infinite appreciation for his restless and relentless encouragement, which allowed me to achieve what I thought unachievable. His unending energy and leadership skills were a truly inspiration throughout these years.

To Dr. Helen Crowley, I would like to express my admiration and gratitude for stimulating me and for giving me the opportunity to take part in many other activities. To her, I owe a fair amount of my scientific knowledge and interest in structural and seismic risk analysis. Most important, I am thankful for her friendship and faith in my work.

My sincere gratitude goes also to everyone at the Global Earthquake Model Foundation, in particular to Graeme Weatherill, Christopher Burton, Damiano Monelli and Marco Pagani, with whom I had the pleasure to work with. Without their numerous explanations about the various challenging topics, my work would have not been possible.

To my Pavia companions, namely Luis Sousa, Cecilia Nievas and Romain Sousa, I would like to express my gratitude for the late nights full of complex hypothesis and impossible theories. Thank you for helping me dealing with my homesickness, and making me feel at home in a foreign country.

To all of my dear friends, I am thankful for their patience and affection, for providing me with numerous wonderful moments and endless support in the worst ones, specially Daniel, Alexandra, Rui, Eurico, Samuel, Hugo, Rossana, Maria João and Filipa.

To my beautiful fiancée Daniela, whose love and support have been my guiding light in these last years, I would like to say a very special thank you. My academic and professional achievements would have been meaningless without the chance of sharing the happy moments with my love.

Finally, I would like to dedicate my work to my family, in particular to my parents and sister, whose support throughout these years has been unconditional and without which the distance would have been unbearable.

palavras-chave

Perigosidade sísmica, risco sísmico, cálculo de perdas, exposição, vulnerabilidade estrutural, modelação numérica, edifícios de betão armado.

resumo

O contínuo crescimento da população mundial tem levado a uma massificação dos centros urbanos, frequentemente localizados em áreas propensas a desastres naturais, de entre os quais os sismos. Consequentemente, e apesar dos avanços do conhecimento no domínio da modelação de catástrofes naturais e das ações de mitigação do risco, o número de fatalidades continua a aumentar e, recentemente, perdas económicas sem precedentes têm vindo a ser registadas. No presente trabalho, são investigados vários aspetos da engenharia sísmica e sismologia, e é desenvolvido como caso de estudo Portugal continental.

A avaliação rigorosa do risco sísmico é um instrumento fundamental para a redução do número de vítimas e de danos como consequência dos eventos sísmicos. Este reconhecimento despoletou o desenvolvimento de ferramentas numéricas e de *software* para o cálculo do risco. No presente trabalho, uma plataforma *open-source* para o cálculo de perigosidade e risco sísmico foi desenvolvida, que permite calcular a distribuição das perdas e danos para um cenário específico da ação sísmica (evento determinístico), ou das perdas acumuladas devidas a todos os eventos sísmicos que podem ocorrer numa determinada região e num dado período de tempo. Como resultado deste trabalho foi desenvolvido um *software*, que é disponibilizado a qualquer indivíduo ou instituição.

A determinação do risco sísmico depende principalmente de três componentes: perigosidade sísmica, exposição e vulnerabilidade. A última componente assume particular importância, na medida em que uma eventual intervenção ao nível do reforço estrutural pode ter influência direta na redução do risco sísmico associado. O recurso a metodologias analíticas é fundamental para a avaliação da vulnerabilidade estrutural, particularmente em regiões onde a informação sobre danos em edifícios após sismos é escassa ou inexistente. Neste trabalho foram analisadas várias metodologias conhecidas, discutindo-se a eficiência e rigor dos vários métodos, nomeadamente no respeitante à relação entre precisão e esforço computacional exigido. Complementarmente é proposta uma abordagem simplificada que permite o cálculo expedito de curvas de fragilidade.

É ainda proposto um modelo de vulnerabilidade para edifícios de betão armado em Portugal, utilizando dados recolhidos na análise de centenas de projetos de edifícios existentes. Foi adotada uma abordagem analítica, baseada em análises não-lineares dinâmicas, que permitiu avaliar a influência de vários parâmetros, nomeadamente a influência dos critérios na definição do dano ou o tipo de medida de intensidade usada na representação da ação sísmica.

É apresentada uma revisão abrangente dos estudos e contributos anteriores de outros autores que contribuíram para a compreensão da perigosidade e risco sísmico em Portugal. Neste estudo, para o cálculo da perigosidade sísmica em Portugal continental foi usado um modelo disponível de zonas sismogénicas, e modelos de atenuação recentemente propostos. Estes resultados foram combinados com dados provenientes do recente Recenseamento Geral, de 2011, e com o modelo de vulnerabilidade desenvolvido neste trabalho, obtendo-se mapas de perdas económicas para um período de retorno da ação de 475 anos. A desagregação para as diferentes tipologias construtivas estudadas permitiu aferir quais os tipos de construção poderão ter maior impacto nas perdas económicas totais num eventual evento sísmico.

keywords seismic hazard, seismic risk, loss estimation, exposure, structural vulnerability, numerical modelling, reinforced concrete buildings

abstract

The exponential growth of the world population has led to an increase of settlements often located in areas prone to natural disasters, including earthquakes. Consequently, despite the important advances in the field of natural catastrophes modelling and risk mitigation actions, the overall human losses have continued to increase and unprecedented economic losses have been registered. In the research work presented herein, various areas of earthquake engineering and seismology are thoroughly investigated, and a case study application for mainland Portugal is performed.

Seismic risk assessment is a critical link in the reduction of casualties and damages due to earthquakes. Recognition of this relation has led to a rapid rise in demand for accurate, reliable and flexible numerical tools and software. In the present work, an open-source platform for seismic hazard and risk assessment is developed. This software is capable of computing the distribution of losses or damage for an earthquake scenario (deterministic event-based) or earthquake losses due to all the possible seismic events that might occur within a region for a given interval of time (probabilistic event-based). This effort has been developed following an open and transparent philosophy and therefore, it is available to any individual or institution.

The estimation of the seismic risk depends mainly on three components: seismic hazard, exposure and vulnerability. The latter component assumes special importance, as by intervening with appropriate retrofitting solutions, it may be possible to decrease directly the seismic risk. The employment of analytical methodologies is fundamental in the assessment of structural vulnerability, particularly in regions where post-earthquake building damage might not be available. Several common methodologies are investigated, and conclusions are yielded regarding the method that can provide an optimal balance between accuracy and computational effort. In addition, a simplified approach based on the displacement-based earthquake loss assessment (DBELA) is proposed, which allows for the rapid estimation of fragility curves, considering a wide spectrum of uncertainties.

A novel vulnerability model for the reinforced concrete building stock in Portugal is proposed in this work, using statistical information collected from hundreds of real buildings. An analytical approach based on nonlinear time history analysis is adopted and the impact of a set of key parameters investigated, including the damage state criteria and the chosen intensity measure type.

A comprehensive review of previous studies that contributed to the understanding of the seismic hazard and risk for Portugal is presented. An existing seismic source model was employed with recently proposed attenuation models to calculate probabilistic seismic hazard throughout the territory. The latter results are combined with information from the 2011 Building Census and the aforementioned vulnerability model to estimate economic loss maps for a return period of 475 years. These losses are disaggregated across the different building typologies and conclusions are yielded regarding the type of construction more vulnerable to seismic activity.

parole chiave

pericolosità sismica, rischio sismico, valutazione delle perdite, esposizione, vulnerabilità delle strutture, modellazione numerica, edifici in cemento armato

sommario

La crescita esponenziale della popolazione mondiale ha portato a un aumento di insediamenti spesso localizzati in aree propense a disastri naturali, tra cui terremoti. Di conseguenza, nonostante gli importanti avanzamenti nel campo della modellazione delle catastrofi naturali e nelle azioni di mitigazione del rischio, le perdite umane complessive sono continuate a crescere e sono state registrate perdite economiche senza precedenti. Nel lavoro di ricerca presentato di seguito, varie aree dell'ingegneria sismica e della sismologia sono investigate a fondo e applicate come caso studio al Portogallo continentale.

La definizione del rischio sismico è un punto critico nella riduzione di vittime e danni dovuti a eventi sismici. Il riconoscimento di tale importanza ha portato a una rapida crescita della richiesta di strumenti e software accurati, affidabili e flessibili. Nel presente lavoro è stata sviluppata una piattaforma open-source per la definizione della pericolosità e del rischio sismico. Questo software è capace di calcolare la distribuzione di perdite o danni per un determinato scenario sismico (evento deterministico) o le perdite dovute a tutti i possibili eventi sismici che potrebbero accadere in una regione in un dato intervallo di tempo. Questo risultato è stato perseguito seguendo una filosofia aperta e trasparente e quindi è disponibile a qualsiasi individuo o istituzione.

La stima del rischio sismico dipende soprattutto da tre componenti: la pericolosità sismica, la esposizione e la vulnerabilità. L'ultima componente assume speciale importanza, poiché intervenendo con soluzioni appropriate di adeguamento, è possibile far diminuire direttamente il rischio sismico. L'utilizzo di metodologie analitiche nella definizione della vulnerabilità delle strutture è fondamentale particolarmente in regioni dove potrebbero non essere disponibili informazioni sul danno a edifici conseguente un terremoto. Numerose metodologie tra le più comuni sono state analizzate, e si è concluso su quale metodo può offrire un equilibrio ottimale tra accuratezza dei risultati e impegno computazionale. Inoltre si propone un approccio semplificato a partire dalla metodologia di determinazione delle perdite sismiche basata sugli spostamenti (DBELA), che permette di derivare velocemente curve di fragilità, considerando un ampio spettro di incertezze.

Si propone un nuovo modello di vulnerabilità per edifici in cemento armato in Portogallo, usando informazioni statistiche raccolte da centinaia di edifici reali. Si è utilizzato un approccio analitico basato su analisi dinamiche non lineari e si è investigato sull'impatto di un gruppo di parametri chiave, tra cui i criteri di definizione dello stato di danno e il tipo di misura di intensità scelta.

É presentata un'ampia revisione di studi precedenti che hanno contribuito alla comprensione della pericolosità sismica e del rischio per il Portogallo. Per calcolare la pericolosità sismica probabilistica sull'intero territorio si è fatto uso di un modello esistente di fonti sismiche con modelli di attenuazione proposti recentemente. Questi ultimi risultati sono stati combinati con informazioni dal Censimento degli Edifici del 2011 e il suddetto modello di vulnerabilità per stimare mappe di perdite economiche per un periodo di ritorno di 475 anni. Le perdite sono state disaggregate per le diverse tipologie di edifici e sono state riportate conclusioni sul tipo di costruzione più vulnerabile all'attività sismica.

“Remember that all models are wrong;
the practical question is how wrong
do they have to be to not be useful.”
George E. Box

Table of Contents

Chapter 1 - Introduction **1**
1.1. The Need for Earthquake Loss Modelling **1**
1.2. The importance of physical vulnerability **4**
1.3. Seismic risk in Portugal **6**
1.4. Organization of the thesis **8**

Chapter 2 - Development of OpenQuake, an Open-source Software for Seismic Risk Assessment **11**
2.1. Summary **11**
2.2. Introduction **12**
2.3. OpenQuake: Seismic hazard and risk software **14**
2.3.1. Development of OpenQuake 14
2.3.2. OpenQuake Data Model and the Natural hazards Risk Markup Language (NRML) 14
2.3.3. Seismic Source model 15
2.3.4. Logic Tree model 16
2.3.5. Rupture model 16
2.3.6. Vulnerability model 17
2.3.7. Fragility model 17
2.3.8. Exposure model 18
2.3.9. Hazard Curves, Hazard Maps, and Ground Motion Fields 18
2.3.10. Loss Curves and Loss Maps 19
2.3.11. Damage distribution and collapse maps 19
2.4. OpenQuake Risk Calculation Workflows **20**
2.4.1. Scenario Risk Calculation Workflow 20
2.4.2. Scenario Damage Calculator Workflow 21
2.4.3. Probabilistic Event-Based Risk Calculation Workflow 22
2.4.4. Classical PSHA-Based Risk Calculation Workflow 24
2.4.5. Benefit-Cost Ratio Calculator Workflow 26
2.5. Case study applications **27**
2.5.1. Introduction 27
2.5.2. PSHA model 28
2.5.3. Deterministic rupture model 30
2.5.4. Building Exposure Model 30
2.5.5. Fragility and Vulnerability Model 31
2.6. Output **33**
2.6.1. Ground motion fields for Istanbul 33
2.6.2. Seismic Hazard Map for Turkey 34

2.6.3. Scenario Risk for Istanbul 35
2.6.4. Comparison with other studies 37
2.6.5. Scenario Damage for Istanbul 37
2.6.6. Probabilistic risk assessment for Istanbul 39
2.6.7. Probabilistic event-based approach 39
2.6.8. Using the classical PSHA-based approach 40
2.6.9. Retrofitting Benefit-Cost Analysis 42
2.7. Final Remarks 43

Chapter 3 - Evaluation of Analytical Methodologies used to Derive Vulnerability Functions 45
3.1. Summary 45
3.2. Introduction 46
3.3. Description of the Framework 48
3.3.1. Generation of Synthetic RC frames 50
3.3.2. Numerical Modelling of the RC Frames 52
3.3.3. Ground Motion Input 52
3.4. Pushover curves 54
3.4.1. Conventional Pushover 54
3.4.2. Adaptive Pushover 56
3.4.3. Convergence in the statistics 57
3.5. Nonlinear static procedures 58
3.5.1. Capacity Spectrum Method 59
3.5.2. Displacement Coefficient Method 62
3.5.3. N2 Method 63
3.5.4. Adaptive Capacity Spectrum Method 64
3.6. Nonlinear dynamic analysis 65
3.7. Discussion of results 66
3.7.1. Variability in the Capacity Curves 66
3.7.2. Variability in the Fragility Functions 68
3.7.3. Variability in the Vulnerability Functions 69
3.7.4. Variability in Seismic Risk Assessment 72
3.7.5. Computational performance 75
3.8. Final remarks 76

Chapter 4 - Extending the Displacement-Based Earthquake Loss Assessment (DBELA) for the Computation of Fragility Curves 79
4.1. Summary 79
4.2. Introduction 80
4.3. DBELA Fragility Function Calculator 81
4.3.1. Summary of DBELA 81
4.3.1.1. Displacement capacity 82
4.3.1.2. Displacement demand 86
4.3.2. Proposed Fragility Functions Methodology 88
4.3.3. Vulnerability Functions Calculation 92
4.4. Case study application 95

4.4.1. Characterization of the RC Building Portfolio 95
4.4.2. Ground Motion Input 97
4.4.3. Results 98
4.5. Comparison with Other fragility models 101
4.5.1. Using Nonlinear Dynamic Analysis 102
4.5.2. From previous studies 106
4.6. Final remarks 109

Chapter 5 - Investigation of the Characteristics of the Portuguese RC Building Stock and Development of a Vulnerability Model 111
5.1. Summary 111
5.2. Introduction 112
5.2.1. Portuguese RC building stock 114
5.2.2. Geometric properties of Portuguese RC building stock 115
5.2.2.1. Inter-story height 116
5.2.2.2. Column properties 117
5.2.2.3. Beam properties 119
5.2.2.5. Slab thickness 121
5.2.3. Material properties of Portuguese RC building stock 122
5.2.3.1. Concrete properties 122
5.2.3.2. Steel properties 123
5.3. Development of the vulnerability model 125
5.3.1. Structural Modelling of the RC frames 125
5.3.2. Damage state definition criteria 129
5.3.2.1. Maximum global drift 129
5.3.2.2. Maximum inter-story drift 130
5.3.2.3. Residual inter-story drift 131
5.3.3. Selection of ground motion records 132
5.3.4. Evaluation of consequence models 133
5.3.5. Fragility methodology 135
5.4. Results 136
5.4.1. Evaluation of the RC frames 136
5.4.1.1. Elastic period of vibration 136
5.4.2. Capacity curves 138
5.4.3. Fragility functions 139
5.4.4. Vulnerability functions 142
5.5. Final remarks 145

Chapter 6 - Seismic Risk Assessment for mainland Portugal 147
6.1. Summary 147
6.2. Introduction 148
6.3. Review of existing studies 149
6.4. Description of the input models 152
6.4.1. Probabilistic seismic hazard model 152
6.4.2. Selection of ground motion prediction equations 153
6.4.3. Consideration of site effects 156
6.4.3.1. V_{s30} mapping for Portugal 157

6.4.4. Exposure model 161
6.4.4.1. Portuguese building stock 161
6.4.4.2. Development of the exposure model 163
6.4.5. Vulnerability model 166
6.5. Results 169
6.5.1. Seismic hazard 169
6.5.2. Seismic risk 171
6.6. Final remarks 175
Chapter 7 - Conclusions and future developments 177
7.1. Conclusions 177
7.2. Future developments 179

List of Figures

Figure 1.1. Overall losses and insured losses from 1980 until 2011 (MunichRe, 2012). 2
Figure 1.2. Absolute population and GDP exposed to natural disasters (adapted from UNISDR, 2009). 2
Figure 1.3. Distribution of average annual cost of natural disaster in low-, middle- and high-income countries (adapted from Cummins and Mahul, 2009). 4
Figure 1.4. Cumulative distribution of buildings in Portugal according to the period of construction, at the time of the 2011 Building Census. The dashed vertical lines mark the introduction of a design code. 7
Figure 2.1 - Illustration of a discrete vulnerability function. 17
Figure 2.2 – Continuous (left) and discrete (right) fragility models. 18
Figure 2.3 - Workflow of the Scenario Risk calculator. 21
Figure 2.4 – Workflow of the Scenario Damage Distribution. 22
Figure 2.5 - Workflow of the Probabilistic Event-Based Risk calculator. 24
Figure 2.6 - Workflow of the Classical PSHA-Based Risk calculator. 26
Figure 2.7 - Workflow of the Benefit/Cost Ratio Calculator. 27
Figure 2.8 - Fault source model for Turkey. Faults are assumed to be vertical, so only fault traces are shown. Colours represent maximum magnitude (M_w) 29
Figure 2.9 - Area source model for Turkey. Large-scale rectangular background sources cover the entire country, whilst most of the small-scale area sources follow fault source geometries. 29
Figure 2.10 – Representation of rupture trace (in red). 30
Figure 2.11 - Distribution of building economic value in the Metropolitan Area of Istanbul. 31
Figure 2.12 - Fragility (left) and vulnerability (right) functions for low-rise RC frames built after the 1979 design code. 33
Figure 2.13 - Median ground motion field in terms of peak ground acceleration (g). 34
Figure 2.14 - Mean hazard map for a probability of exceedance of 10% in 50 years in Turkey. 35
Figure 2.15 - Aggregated loss statistics for the four types of calculation. 36
Figure 2.16 - Loss map with the distribution of mean economic losses for the Metropolitan Area of Istanbul. 36
Figure 2.17 – Mean damage distribution for RC building with irregular masonry infill walls. 38
Figure 2.18 - Collapse map for the Metropolitan Area of Istanbul. 38
Figure 2.19 - Aggregated loss curves for the three types of calculations. 40
Figure 2.20 - Loss map with a probability of exceedance of 10% in 50 years. 41
Figure 2.21 - Loss map with a probability of exceedance of 1% in 50 years. 41
Figure 2.22 - Vulnerability function for the original and retrofitted design of low-rise RC buildings. 42

Figure 2.23 - Benefit-cost ratio map for mid-rise RC buildings built before the 1979 design code. 43
Figure 3.1. Scheme of the developed framework. 48
Figure 3.2. Schematic view of the RC frame model: front (left), side (centre) and isometric view (right). 50
Figure 3.3 - Distribution of the PGA (g), PGV (m/s) and Arias Intensity (m/s) for the set of ground motion records. 54
Figure 3.4 – Acceleration spectra (g) versus period of vibration (sec) for the set of ground motion records. 54
Figure 3.5. Capacity curves using a uniform (left), triangular (centre) and multi-modal (right) loading pattern. 56
Figure 3.6. Capacity curves using DAP. 57
Figure 3.7 – Mean relative error as a function of the size of the sample, for 5 repetitions 58
Figure 3.8 - Bilinear curves according to ATC-40 (left) and FEMA-273 (right) for a "weak" response spectrum. 61
Figure 3.9 - Bilinear curves according to ATC-40 (left) and FEMA-273 (right) for a "strong" response spectrum. 61
Figure 3.10. Fragility functions using ACSM 65
Figure 3.11. Fragility functions using dynamic analysis. 66
Figure 3.12 – Mean (a) and median (b) capacity curves and capacity curves generated using the mean characteristics of the RC frames (c). 67
Figure 3.13 – Fragility curves for the first (a), second (b) and third (c) limit states, according to the different methodologies. 68
Figure 3.14 – Consequence model for buildings in California (HAZUS) (FEMA-443, 2003) and Turkey (Bal *et al*., 2008b). 70
Figure 3.15 – Vulnerability functions per NSP using the HAZUS consequence model. 70
Figure 3.16 – Vulnerability functions per NSP using the Turkish consequence model 71
Figure 3.17 – Mean vulnerability function for each NSP according to the HAZUS (FEMA-443, 2003) (left) and Turkish (Bal *et al*., 2008b) (right) consequence models. 72
Figure 3.18 – Economic value (EUR) for mid-rise RC pre-code buildings in the MAI. 73
Figure 3.19 – Hazard map for 10% probability of exceedance in 50 years for the Marmara Region 74
Figure 3.20 - Relative variation in the AAL (top), level of losses for frequent events (centre) and level of losses for rare events (bottom). 75
Figure 3.21 – Relative required computational time for each vulnerability methodology. 76
Figure 4.1 - Comparison between limit state capacity and the associated demand (adapted from Bal *et al*., 2010) 82
Figure 4.2 – Definition of effective height coefficient (Glaister and Pinho, 2003) 83
Figure 4.3 – Deformed profiles for beam-sway (left) and column-sway (right) mechanisms (adapted from Paulay and Priestley, 1992). 83
Figure 4.4 - Workflow of the DBELA fragility functions calculator. 89
Figure 4.5 - Derivation of fragility curves based on building damage distribution. 90
Figure 4.6 - Statistical treatment of the parameters defining the curve. 92
Figure 4.7 - Correlation between a) logarithmic means of limit state 1 and 2; b) logarithmic mean of limit state 1 and logarithmic standard deviation of limit state 3; c) logarithmic mean and standard deviation of limit state 1. 94
Figure 4.8 - Set of vulnerability functions and uncertainty per intensity measure level. 95
Figure 4.9 – Histogram of the PGA (left) and PGV (centre) in the selected ground motion records. 98

Figure 4.10 - Correlation between the results and the set of intensity measure levels for low rise, non-compliant reinforced concrete frames within infill panels. 100
Figure 4.11 - Scatter of the results for RCW-LC-MR for the first, second and third limit state. 100
Figure 4.12 - Comparison between mean capacity curves and respective limit states, estimated using the strain levels (DBELA) and top displacement (DAP) criteria..... 103
Figure 4.13 - Fragility models derived through dynamic analyses (left) and applying the proposed DBELA methodology (right). 104
Figure 4.14 – Comparison between fragility models derived using dynamic analyses and the proposed DBELA methodology. 104
Figure 4.15 - Vulnerability curve using dynamic analyses (left), the proposed DBELA methodology (centre) and comparison between both (right)..... 106
Figure 4.16 - Vulnerability curve using dynamic analyses (left), the proposed DBELA methodology (centre) and comparison between both (right)..... 106
Figure 4.17 - Comparisons between fragility functions produced using the DBELA methodology and from other studies for RC buildings: high code and low-rise (a), low code and low-rise (b), low code and mid-rise (c)..... 109
Figure 5.1 - Percentage of RC buildings according to year of construction and number of floors (left), and spatial distribution throughout Portugal at the parish level (right), according to the 2011 Census Survey..... 115
Figure 5.2 - Number of buildings analysed per number of storeys and date of construction (left) and the distribution per district in Portugal (right). 116
Figure 5.3 - Distribution of ground story (left) and regular story (right) heights for all RC buildings. 117
Figure 5.4 - Distribution of beam length (left) and width (right) for all RC buildings..... 119
Figure 5.5 - Distribution of beam depth for pre-code (left) and post-code (right) RC buildings. 120
Figure 5.6 – Correlation between beam length and depth for pre-code (left) and post-code (right) RC buildings. 121
Figure 5.7 – Distribution of slab thickness for pre-code (left) and post-code (right) RC buildings. 121
Figure 5.8 - Concrete compressive strength distribution. 123
Figure 5.9 – Idealized force-displacement relationship for each infill strut (adapted from Sattar and Liel, 2010). 127
Figure 5.10 – Probability of demolition as a function of the inter-story residual drift. 131
Figure 5.11 - Distribution of the PGA (left), PGV (centre) and Arias Intensity (right) in the selected records. 133
Figure 5.12 - Consequence models for a) Italy (Di Pasquale and Goretti, 2001); b) Greece (Kappos *et al*. 2006); c) Turkey (Bal *et al*., 2008b) and d) California (FEMA-443, 2003). 134
Figure 5.13 - Analytical fragility methodology workflow. 136
Figure 5.14 – Comparison between the elastic periods for the bare frames computed herein and FEMA and NIBS (1999) (left) and between the elastic period for infilled frames computed herein and various authors (right). 137
Figure 5.15 – Capacity curves for the building typologies built before (left) and after (right) the 1983 design code. 138
Figure 5.16 – Mean capacity curve for a sample of a hundred of pre-code frames with 4 storeys (left) and top displacement time history of a single frame of the same building typology (right). 139

Figure 5.17 - Variation of the coefficient of correlation between the intensity measure levels and the cumulative percentage of frames in each damage state for pre-code low-rise (left) and post-code high-rise (right) RC structures, as a function of the period. 140
Figure 5.18 - Fragility model for pre-code low-rise RC buildings, considering the global drift (left) and inter-story drift (right) damage criteria. 141
Figure 5.19 - Percentage of nonlinear dynamic analysis (per damage state and in total), in which collapse occurred due to excessive residual inter-story drift. 143
Figure 5.20 - Fragility model for pre-code high-rise RC frames with (WR) and without (NR) considering collapse due to excessive residual inter-story drift. 143
Figure 5.21 - Vulnerability model for RC building in Portugal assuming a global drift (black) and an inter-storey drift (grey) damage criteria. 144
Figure 6.1 – Economic loss map for a return period of 475 (left) and 975 (right) years, (adapted from Sousa, 2006). 151
Figure 6.2 – Source zonation and earthquake catalogue (adapted from Vilanova and Fonseca, 2007). 152
Figure 6.3 – Logic tree used for the hazard calculations defining the epistemic uncertainties in the seismic source model (adapted from Vilanova and Fonseca, 2007). 153
Figure 6.4 - V_{s30} map based on the methodology proposed by Wills and Clahan (2006) (left) and Wald and Allen (2009) (right). 160
Figure 6.5 – Distribution of population per each soil type category for Portugal mainland. 160
Figure 6.6 - Distribution of buildings according to type of construction, year of construction and number of storeys. 162
Figure 6.7 - Exposure model for Portugal following a parish-based (left) and 30 arc sec grid (right) resolutions. 164
Figure 6.8 – Average number of dwelling in function of the number of floors for each CCRD region. 165
Figure 6.9 - Performance points for each limit state and associated acceleration spectrum (left), and resulting fragility model for a masonry building with 3 storeys (right). 168
Figure 6.10 - Vulnerability functions for M2 low-rise (a), mid-rise (b) and M3 low-rise (c) typologies. 169
Figure 6.11- Mean seismic hazard map and 16th and 86th percentile maps in peak ground acceleration (g) for rock, for a probability of exceedance of 10% in 50 years (return period of 475 years). 170
Figure 6.12 – Economic loss map for a probability of excedance of 10% in 50 years (475 years return period), considering the parish-based exposure model. 171
Figure 6.13 - Economic loss map for a probability of excedance of 10% in 50 years (475 years return period), considering the grid-based exposure model. 172
Figure 6.14 - Economic loss per building typology, for a probability of exceedance of 10% in 50 years (return period of 475 years). The error bars indicate the 16th and the 84th percentiles. 173
Figure 6.15 – Percentage of economic loss per building typology, for a probability of exceedance of 10% in 50 years (return period of 475 years). The error bars indicate the 16th and the 84th percentiles. 174

List of Tables

Table 2.1 - Summary of the seismic risk software evaluated. 12
Table 2.2 - Correspondence between damage states and damage ratio. 32
Table 2.3 – Description of the four calculation configurations for the scenario risk assessment. 35
Table 3.1. Probabilistic distributions of the material and geometric properties. 51
Table 3.2. Mean spectral displacement and acceleration for each limit state, per loading pattern. 56
Table 3.3. Mean spectral displacement and acceleration for each limit state. 57
Table 3.4. Lognormal parameters of the fragility functions produced using the CSM. 62
Table 3.5. Lognormal parameters of the fragility functions produced using the DCM. 62
Table 3.6. Lognormal parameters of the fragility curves produced using the N2 Method. 64
Table 3.7. Lognormal parameters of the fragility functions using ACSM 65
Table 3.8. Lognormal parameters of the fragility functions using nonlinear dynamic analysis. 66
Table 4.1 - Limits for the deformation-based sway index. 86
Table 4.2 - Classification of the building typologies used in this study. 96
Table 4.3 - Limit state definition according to Crowley *et al.* (2004) and Turkish Design Code (2007). 99
Table 4.4 Logarithmic mean and logarithmic standard deviation of each fragility curve in terms of spectral acceleration for the elastic period. 101
Table 4.5 - Probabilistic distribution of the statistics of the limit state fragility curves. 105
Table 4.6 - Summary of proposed fragility models from the past 10 years. 107
Table 5.1 - Probabilistic distribution of column depth for each RC building typology. 118
Table 5.2 - Probabilistic distribution of column width for each RC building typology. 118
Table 5.3 - Probabilistic distribution of steel yielding strength (produced in Portugal) proposed by Pipa (1995). 124
Table 5.4 – Limit state inter-story drifts for infilled MRF proposed by Rossetto and Elnashai (2003). 130
Table 5.5 – Consequence model used in the development of the vulnerability model for the Portuguese RC building stock. 134
Table 5.6 – Logarithmic mean (λ), logarithmic standard deviation (ζ) and coefficient of correlation (R^2) for each limit state fragility function, according to the adopted damage criterion. 142

Table 6.1 - Ground motion prediction scheme for SCR and ASCR proposed by Delavaud *et al.* (2012)..... 154
Table 6.2 - Correspondence between the geological units in Portugal and the equivalent categories in Wills and Clahan (2006) and Stewart *et al*. (2008). 158
Table 6.3 - Relation between V_{s30} values and topographic slope (Allen and Wald, 2009)..... 159
Table 6.4 - Vulnerability classes for Portuguese building stock. 163
Table 6.5 – Construction costs for each zone according to Directive nº 291 (2011). 165
Table 6.6 - Area per dwelling for each CCRD region. 166
Table 6.7 - Logarithmic mean (λ) and logarithmic standard deviation (ζ) for each limit state fragility function. 169

Chapter 1

Introduction

1.1. The Need for Earthquake Loss Modelling

In 2011 the world celebrated the birth of the 7 billionth citizen. It has been estimated that in 10 years the world population will reach 8.1 billions, and 9.4 billions in the year of 2050 (PRB, 2010). This uncontrolled growth of the population has led to an increase of megacities (with a population greater than 2 million), often located in areas prone to natural disasters, such as earthquakes (Crowley *et al.*, 2006). This peril has been responsible for a death toll of over 60 thousand people per year in the last decades and economic losses that can reach a great fraction of a country's welfare. In the last 50 years in Central America, the earthquakes of Guatemala (1976), Nicaragua (1972), and El Salvador (1986) caused economic losses of approximately 98%, 82% and 40% of the nominal gross domestic product (GDP) of each country, respectively (Daniell *et al.*, 2010). In the Haiti earthquake of 2010, the economic losses were above the nominal GDP (120%) and more than 300 thousand people are believed to have perished. In addition to these direct consequences in the vicinity of the seismic event, business disruption of multi-national enterprises can induce a negative impact at a global scale. After the Great East Japan earthquake in 2011, the industry of electronics suffered systematic delays in the supply of numerous components produced by some of the affected factories, which led to a worldwide rise of the prices due to the reduction in the stocks.

The global economic losses and insured losses due to great natural disasters from 1980 to 2011 are illustrated in Figure 1.1.

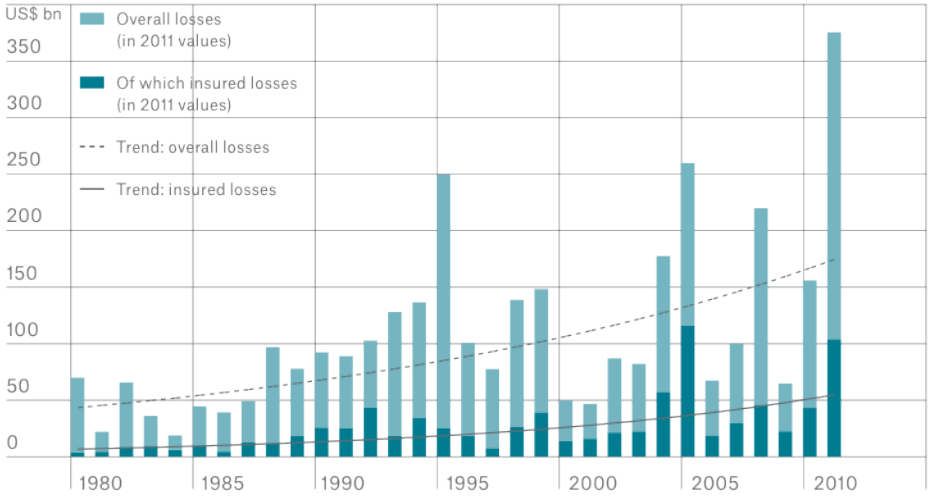

Figure 1.1. Overall losses and insured losses from 1980 until 2011 (MunichRe, 2012).

Earthquakes constitute on average 20% of the overall losses, but in some years, this portion can be as high as 60% (e.g. 2010, 2011). Despite the great advances that have been made in the last decades in the areas of probabilistic seismic hazard assessment (e.g. Abrahamson, 2006; Bommer and Abrahamson, 2006), evaluation of building seismic vulnerability (e.g. Calvi *et al*, 2006) and collection of information regarding the elements exposed to the hazards (e.g. Gamba *et al*., 2012), an increase in the trend of earthquake losses is still observed. The Global Assessment Report (UNISDR, 2009) points out two probable causes for this tendency. Firstly, the significant increase of population and capital stock in hazard prone areas that have a direct impact in the associated catastrophe risk. Figure 1.2 illustrates the amount of population and GDP exposed to hazard in the 20 countries with the highest values.

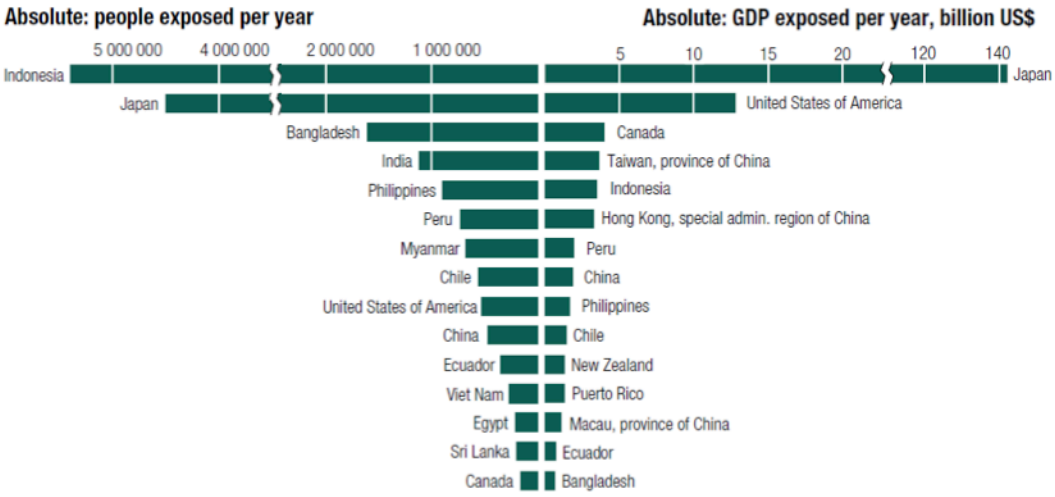

Figure 1.2. Absolute population and GDP exposed to natural disasters (adapted from UNISDR, 2009).

Secondly, besides this growth in the property and property value, modern societies strongly rely on inter-related systems (building stock, power, finance, transport), which in case of a natural catastrophe might initiate a cascade effect, where a disaster triggers another disaster. Modelling this system of systems might be very challenging due to the required understanding of each component, and lack of numerical tools to carry out such calculations.

The Great East Japan earthquake (2011) and tsunami sent a clear message that both developed and developing countries are exposed to high risks. The year of 2011 was the most expensive year ever registered, far exceeding the 2005 economic losses (hurricane Katrina), which yield the previous record. From the overall cost of 380 billion US$, the earthquake disasters in Japan and New Zeeland alone accounted for absolute losses of 228 billion US$. Such losses can have a crippling effect in the economy of countries whose governments have the legal liability to cover the full costs of rebuilding. In the Kocaeli and Düzce earthquakes of 1999 (with a combined fraction of GDP loss of approximately 8%), the Turkish government was faced with an enormous financial burden due to its statuary obligation in covering the costs of reconstruction. This situation propelled the creation of the Turkish Catastrophe Insurance Pool (TCIP), which allowed transferring large parts of the financial burden due to seismic losses to the world's reinsurance market (Bommer *et al*. 2002). In this project, the creation of an earthquake loss model was fundamental to the development of the economic model used to evaluate the impact of catastrophe risk in the Turkish economy. Furthermore, earthquake loss modelling also serves as the foundation to many other seismic risk mitigation actions. These may include prioritization of zones within a country where the structural seismic vulnerability of the building stock should be improved, planning of post-disaster emergency response or definition of regulations to impose seismic-proof construction practices. However, in less developed countries, the required resources, datasets and tools might not exist in order to perform a comprehensive assessment of the seismic risk. In fact, the evaluation of the annual costs of natural disasters from the last decades between low/middle-income countries and high-income countries shows considerably lower costs in the latter category, where catastrophe models are more frequently available. This trend can be seen in Figure 1.3.

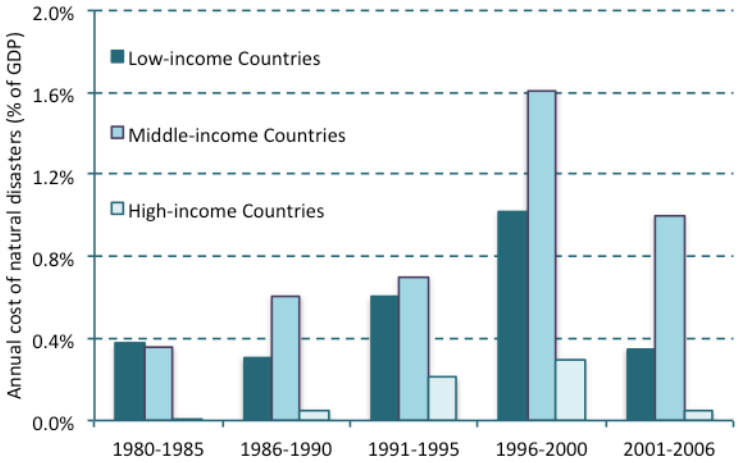

Figure 1.3. Distribution of average annual cost of natural disaster in low-, middle- and high-income countries (adapted from Cummins and Mahul, 2009).

With the purpose of facilitating earthquake loss modelling to any individual or institution, within this thesis, an open-source platform (OpenQuake-engine) capable of calculating seismic hazard and risk at any scale was developed. The activities developed in this thesis were focused in the development, testing and scientific verification of a set of seismic risk calculators capable of estimating earthquake losses due to a single earthquake (scenario event-based), or due to all the possible seismic events that might occur in a region within a certain time span (probabilistic event-based). OpenQuake-engine has been developed following an open-source philosophy and its methodologies, algorithms and assumptions have been documented and made available through a public repository [1]. This endeavour was carried out as part of the Global Earthquake Model [2] (Pinho, 2012), an initiative that aims to calculate and communicate seismic hazard and risk worldwide.

Despite the fact that these risk calculators were developed with the objective of estimating earthquake losses, its main algorithms can also be employed in the estimation of losses due to other perils, such as hurricanes or floods.

1.2. The importance of physical vulnerability

Structural vulnerability can be defined as the likelihood of a certain element to suffer loss due to the effects of an earthquake. The influence of the vulnerability of the exposed elements to seismic events is fundamental in the magnitude of losses. A simple comparison between earthquakes that occurred in developing regions and

developed countries reveals the critical importance of vulnerability. For example, the Spitak (Armenia) earthquake of December 1988 had a magnitude of M_s 6.7 and left a death toll of about 25000 casualties. Less than a year after, an earthquake with a greater magnitude (M_s 7.0) occurred in Loma Prieta (California, USA) causing a number of human losses smaller than 70 (Bommer, 2002), this way, the structural vulnerability assumes special importance in the estimation of seismic risk, not only for reflecting directly the damage susceptibility of a structure, but also because by intervening with appropriate strengthening solutions, it may be possible to significantly reduce the vulnerability, and consequently the seismic risk (Vicente, 2008).

The recognition of the importance in understanding the vulnerability of the exposed elements led to a rapid rise in demand for accurate and flexible methodologies for its evaluation (Calvi *et al*, 2006). These may include empirical methods that take advantage of post-earthquake damage data to derive fragility functions (e.g. Colombi *et al*., 2008, Rota *et al*., 2008); simplified approaches where a set of structural parameters are employed to derive a vulnerability index, which is then used to calculate a curve relating levels of damage with a set of intensity measure levels (e.g. GNDT, 1994; Lagomarsino and Giovinazzi, 2006); or analytical methodologies that rely on numerical models to simulate the seismic performance of structures against increasing levels of ground motion (e.g. Vamvatsikos and Cornell, 2002; Freeman, 2004; Rossetto and Elnashai, 2005). The latter category of methods has the advantage of not depending on the availability of post-earthquake damage data, and depending on the level of complexity of the numerical models, these approaches can still incorporate fundamental structural characteristics in the analysis such as vertical or plan irregularities or influence of higher modes of vibration (Chopra and Goel, 2002; Casarotti and Pinho, 2007). Each analytical method considers different simplifications, assumptions and algorithms, mainly in the way the structural nonlinearity is handled. Consequently, the structural response will be dependent on the chosen methodology, and discrepancies in the order of 2 can be observed (Chopra and Goel, 2000; Lin *et al*, 2004). The investigation of this epistemic uncertainty and its impact in the resulting seismic risk was a research question addressed in this thesis.

Despite the recognition that current analytical methodologies can provide satisfactory results in terms of accuracy, the computational effort and calculating time required to derive reliable sets of vulnerability functions are still a strong

short-coming. With the intention of overcoming this drawback, a simplified methodology capable of providing sets of vulnerability curves considering a large spectrum of uncertainties (such as the material and geometric aleatory uncertainty or the record-to-record variability) and with reduced calculating time was developed within this thesis. The proposed method uses Monte Carlo simulations to generate thousands of structures compliant with the characteristics of real buildings of a given region, which are then tested against hundreds of ground motion records using the Displacement-Based Earthquake Loss Assessment (DBELA) (Crowley *et al*, 2004; Bal *et al*., 2010). This process results in a probabilistic distribution of loss ratio for a set of intensity measure levels, which can then be used for earthquake loss estimation. The various modules employed by this methodology have been developed following the same open-source philosophy of OpenQuake-engine, and can be found in a public repository [3].

1.3. Seismic risk in Portugal

Portugal has its past marked by the occurrence of very destructive earthquakes. In the well-known 1755 Lisbon earthquake, despite the various estimates proposed by the scientific community (França, 1988; Oliveira, 1988, Farinha, 1997), it is fair to assume that in Lisbon, more than 50% of the buildings were heavily damaged or collapsed and approximately 10% of the population perished. In the beginning of the last century, a moderate event of magnitude 6.6 Mw struck the village of Benavente, causing 46 casualties and damaging more than 3000 dwellings (Choffat, 1912). A scenario loss assessment performed by Sousa (2006) indicated that if such historical were to occur again, large economic and human losses would still be observed.

Notwithstanding the important studies that have been developed in the last decades in the seismic hazard and risk field for Portugal (Carvalho *et al.,* 2002; Sousa, 2006; Vilanova and Fonseca, 2007; Carvalho, 2008; Vicente, 2008; Campos-Costa *et al*., 2009; Azevedo *et al.*, 2009, Sousa *et al*., 2010), efforts towards the reduction of the seismic risk, raise of risk awareness throughout the society or creation of regulations promoting the improvement of the seismic performance of existing buildings does not seem to have been extensively explored. Furthermore, recent studies in probabilistic seismic hazard analysis allied with the existence of buildings that have not been designed according to the most rigorous design codes, indicate that a great portion of the population might be at risk. The distribution of

existing buildings in Portugal according to their construction period at the time of the 2011 Building Census is depicted in Figure 1.4. The vertical dashed lines highlight the periods of time in which a design code was released.

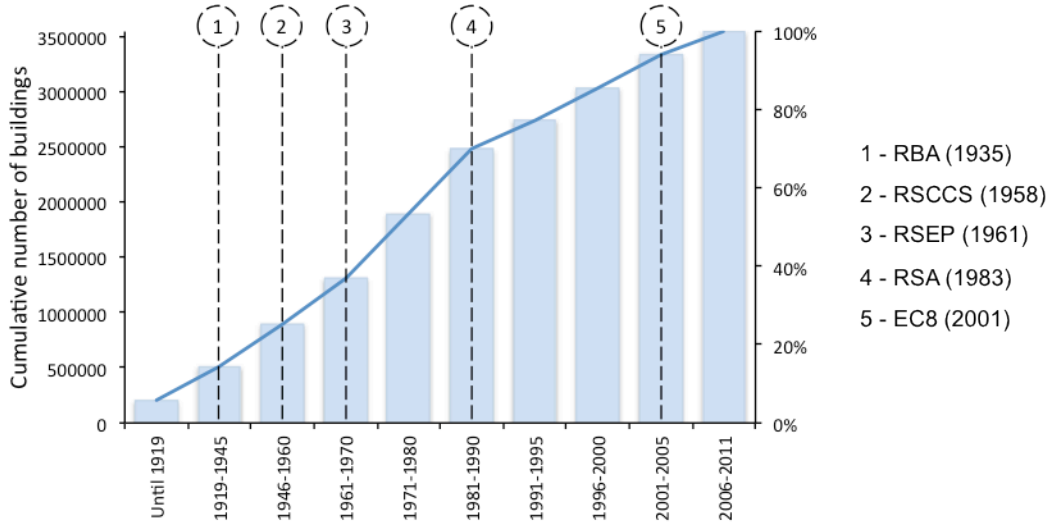

Figure 1.4. Cumulative distribution of buildings in Portugal according to the period of construction, at the time of the 2011 Building Census. The dashed vertical lines mark the introduction of a design code.

Portugal was one of the first countries to endorse a design code (RSCCS, RSEP) with provisions regarding the consideration of a possible seismic event. These recommendations included a simplified method to estimate some horizontal loads according to three geographic zones with different levels of seismicity. However, due to the simplicity of the method and inadequate hazard zonation, these regulations are recognized as insufficient (Sousa, 2006). Later in 1983, a more demanding design code (RSA) was introduced, which is still in force nowadays. The comparison between the design code evolution and rate of construction in Portugal indicates that at the time of the Building Census Survey of 2011, 25% of the buildings were designed with no explicit seismic provisions, 37% while a design code (RSCCS, RSEP) that might not be capable of providing an adequate seismic performance was in use, and 38% were designed according to the current regulations (RSA, EC8).

The seismic vulnerability of each existing building typology in Portugal, for the aforementioned construction periods is discussed in Carvalho *et al.* (2002). In the latter study, a simplified approach proposed by FEMA and NIBS (1999) is employed to derive sets of fragility functions. These results were used in the work of Sousa (2006), along with other macroseismic methodologies, to estimate probabilistic

seismic risk for mainland Portugal and losses for three past earthquakes. Notwithstanding the importance and pioneering character of these studies, new advances in the creation of probabilistic seismic hazard models, development of ground motion prediction equations, evaluation of structural vulnerability and evolution in the building stock call for a revision of the modelling seismic risk in Portugal. In the present work, the material and geometric properties of the reinforced concrete building stock were investigated, through the analysis of hundreds of drawings and design specifications of real buildings located in different regions of the country. The statistics from this study were used to derive vulnerability functions for a set of reinforced concrete building typologies, using hundreds of nonlinear time history analysis. This vulnerability model was employed in the probabilistic assessment of the seismic risk for mainland Portugal, which allowed the calculation of loss maps (for a return period of 475 years) and economic loss disaggregation according to the different building typologies.

1.4. Organization of the thesis

The present thesis has been divided into seven chapters, which can be grouped into four sections. The first chapter provides a general introduction to the various subjects addressed in this thesis. Chapter two deals with the development of OpenQuake-engine, the open-source software for seismic hazard and risk assessment. Chapter three and four are concerned with the evaluation of several analytical approaches to derive vulnerability functions and derivation of the DBELA-based methodology for the computation of fragility functions. The following two chapters present the development of a vulnerability model for the Portuguese building stock and seismic hazard and risk assessment for mainland Portugal, and the last chapter discusses the main conclusions and present possible future developments. The contents of each chapter are described in further detail in the next.

The second chapter presents a brief review of some of existing seismic risk software, which served the purposes of defining a list of scientific requirements for OpenQuake-engine. The various risk calculators are described, highlighting the necessary input models, calculation workflows and main outputs. A test case application using the Metropolitan Area of Istanbul was carried out to demonstrate

the capabilities of each calculator. For a single event, economic losses and damage distribution are demonstrated, and considering all the possible seismic events within the region of interest, a seismic hazard and risk map are shown.

In the third chapter, several analytical static and dynamic methodologies used to derive vulnerability functions are investigated. A brief introduction to each technique is presented and comparisons are made regarding the variability in the resulting capacity curves, fragility functions, vulnerability functions and ultimately, in the seismic risk parameters. Some conclusions are yield regarding the methodology that provides the optimal balance between computational efficiency and accuracy.

The fourth chapter presents the latest developments in the displacement-based earthquake loss assessment and describes the proposed methodology to derive fragility functions. A probabilistic procedure to convert the resulting fragility functions into vulnerability functions, capable of propagating the various uncertainties, is presented. This methodology is tested against existing fragility functions, as well as results obtained through nonlinear time history analysis. In addition, a set of fragility functions for typical Turkish reinforced concrete buildings is provided.

The fifth chapter of this thesis deals with the development of a novel vulnerability model for the reinforced concrete building stock in Portugal. Probabilistic distributions are derived to model a set of geometric and material parameters, based on information collected from hundreds of drawings and design specifications of real buildings. A set of fundamental aspects in the development of vulnerability functions is discussed, such as the limit state criteria, the selection of the ground motion records, the consideration of a consequence model or the intensity measure type used to derive each function. Two vulnerability models are proposed based on two damage criteria: global drift and inter-storey drift.

In the sixth chapter a review of the most relevant studies that contributed to the understanding of the seismic hazard and risk in Portugal is presented. Various components that influence greatly the level of hazard are investigated, such as the source model, ground motion prediction equations or local soil conditions. A risk

map is calculated using an existing probabilistic hazard model; an exposure model is derived based in the 2011 Building Census survey; the vulnerability model calculated in the previous chapter for reinforced concrete buildings and a set of vulnerability functions derived using a simplified methodology for the masonry building typologies. Moreover, conclusions are yield regarding the building typologies that may contribute the most to the overall economic loss.

Finally, chapter seven summarizes the main conclusions of the present work and presents a description of the future developments envisaged to improve each of the subjects addressed herein.

Chapter 2

Development of OpenQuake, an open-source software for seismic risk assessment

Silva, V., Crowley, H., Pagani, M., Modelli, D., Pinho, R. (2013) "Development of the OpenQuake engine, the Global Earthquake Model's open-source software for seismic risk assessment". *Natural Hazards*, DOI 10.1007/s11069-013-0618-x.

2.1. Summary

The Global Earthquake Model (GEM) aims to combine the main features of state-of-the-art science, global collaboration and buy-in, transparency and openness in an initiative to calculate and communicate earthquake risk worldwide. One of the first steps towards this objective has been the open source development of a software for seismic hazard and risk assessment called OpenQuake-engine. This software comprises a set of calculators capable of computing human or economical losses for a collection of assets, caused by a deterministic seismic event, or due to all the possible events that might happen within a region for a certain time span. This chapter provides an insight of the current status of the development of this tool and presents a comprehensive description of each calculator. With the purpose of demonstrating the functionalities of the OpenQuake-engine, an exemplificative test case application was carried out using the Metropolitan Area of Istanbul as the region of interest.

2.2. Introduction

The recognition of seismic hazard and risk analysis as a critical link in the reduction of casualties and damages due to earthquakes, led to a rapid rise in demand for accurate, reliable and flexible risk assessment tools and software. The OpenQuake[4] project was initiated as part of the Global Earthquake Model (Pinho, 2012), a global collaborative effort that brings together state-of-the-art science and national/regional/international organizations and individuals with the aim of establishing uniform and open standards for calculating and communicating earthquake risk worldwide. In January 2009, GEM launched a pilot project named GEM1, which had the objective of developing the initial IT infrastructure of GEM. As part of this effort, a number of existing hazard and risk software applications were reviewed (Danciu *et al*. 2010; Crowley *et al*. 2010). The purpose of this study was not to validate or test the accuracy of any of the applications, but rather to understand their capabilities and limitations, thus allowing the specification of the first scientific requirements of OpenQuake. The selection of the seismic risk software to be evaluated was done based on the level of public availability, reliability and openness, thus leaving the commercial software out of this list. Table 2.1 describes some of the features of the seismic risk software evaluated in this first phase.

Table 2.1 - Summary of the seismic risk software evaluated.

Software	Institution	Programming language	Applicability	Availability	Graphical user interface	Type of calculations
Selena[5]	NORSAR	Matlab/C	User-defined	OS	Yes	D/P
EQRM[6]	GA	Python	User-defined	OS	No	D/P
ELER[7]	KOERI	Matlab	User-defined	SA	Yes	D
QLARM[8]	WAPMEER	Java	World	SC	Yes	D
CEDIM[9]	CEDIM	Visual Basic	User-defined	SC	Yes	D
CAPRA[10]	World Bank	Visual Basic	Central America	SC	Yes	D/P
RiskScape[11]	GNS	Java	New Zeeland	SA	Yes	D
LNECLOSS[12]	LNEC	Fortran	Portugal	SC	No	D/P
MAEVIZ[13]	MAE Center	Java	User-defined	OS	Yes	D
OPENRISK[14]	SPA Risk	Java	USA	SA	Yes	P

OS – Open-source (code can be acquired freely)
SA – Standard application (available under request)
SC – Source code only (available under request)
D – Deterministic seismic risk (one event).
P – Probabilistic seismic risk (many events).

The well-known HAZUS software (FEMA-443, 2003) is also recognized herein as a very useful tool, as it was a pioneering application in seismic risk assessment. However, its high demanding hardware requirements, lack of transparency and inability to be applied in other regions besides California, made it a less appealing software to be evaluated. Nevertheless, it is evident that the methodologies behind this software have been the basis for many of the codes tested herein and it is thus implicitly part of the evaluation. These reviews are documented in Crowley *et al*. (2010), and were fundamental in order to understand the current state of the practice in seismic hazard and risk software, as well as to identify the standard functionalities that OpenQuake should feature and the gaps that it needed to fill. Currently, OpenQuake differs from some of the aforementioned software in the following aspects:

- free, publically available and open-source;
- has technical support and documentation;
- allows users to upload their own hazard, vulnerability and exposure models (and thus not tied to any specific region in the world);
- combines hazard and risk calculations within a single software, but also allows users to run hazard-only calculations;
- considers site effects through the usage of Vs30 values (velocity of seismic shear waves in the upper 30 meters layer);
- estimates both deterministic and probabilistic seismic hazard and risk;
- makes use of logic trees to consider the epistemic uncertainty;
- allows many different types of assets to be modelled (e.g. buildings, population);
- incorporates the modelling of spatial correlation of ground motion residuals;
- allows the consideration of correlation of the uncertainty in the vulnerability;
- is scalable and hence, can be used on a single processor laptop as well as on a cloud of computers;
- produces a full spectrum of products such as stochastic event sets, ground motion fields, uniform hazard spectra, hazard curves and maps, disaggregation plots, loss curves and maps and damage maps.

Despite this list of achievements, other important features were also identified during the review of the various software, such as the incorporation of a user-friendly and intuitive user interface or the capability of running the calculations in any platform, which are part of the development road map. The current status of OpenQuake and supported calculators are described in this chapter, giving more emphasis to the seismic risk component. Then, its functionalities are demonstrated through a series of test case applications for the Metropolitan Area of Istanbul (MAI).

2.3. OpenQuake: Seismic hazard and risk software

2.3.1. Development of OpenQuake

OpenQuake is an open-source software written in Python for calculating seismic hazard and risk at any scale. It makes use of a number of other, independent, open-source projects such as Celery [15] and RabbitMQ [16]. The current version of OpenQuake (v0.9) is a 'developer' release to be executed through a command line interface, though a graphics user interface is currently being developed. OpenQuake is licensed with an Affero General Public License (AGPL), and therefore it is Free Open Source Software (FOSS). Currently it is hosted on GitHub [1], a web-based hosting service for software development projects. An important characteristic of OpenQuake is the strong emphasis on testing, which ensures that the same results are obtained following any changes or additions. A number of verification tests are being implemented such as the PEER tests that have been set up by Thomas *et al*. (2010) to test hazard calculations. All such testing ensures that the code is fully checked for correctness, completeness and quality. For what concerns "validation" (i.e. checking that the results match reality), such tests are not part of OpenQuake development and will instead be carried out as part of a wider GEM effort through the Testing and Evaluation Facility, as validation relates more to the testing of models rather than software.

2.3.2. OpenQuake Data Model and the Natural hazards Risk Markup Language (NRML)

OpenQuake relies on a data model to represent the objects used in hazard and risk calculations, that is being developed in parallel with a transparent and standard

markup language utilized to transfer different types of information within and out of the software. This language – called the Natural hazards Risk Markup Language (NRML) - is XML-based and it leverages from the previous GEM1 experience (Pagani *et al*., 2010a) and existing standards, such as the Geography Markup Language (GML) and QuakeML [17], a markup language for seismic catalogues.

NRML is being hosted in the OpenQuake repository at GitHub [18] and information regarding how to create and edit these files can be found at the OpenQuake User Manual (GEM, 2012a). Although the present scope of NRML is seismic risk, it is planned to extend this markup language to cover other natural hazards such as hurricanes, floods or tsunamis. Currently, NRML is being used to represent input data such as hazard source zone models, logic trees, finite ruptures, vulnerability models, exposure models, and output data including hazard curves, hazard maps, loss curves and loss maps, damage distribution, which are described in the following sections.

2.3.3. Seismic Source model

A seismic source model provides information about location, geometry, and activity of seismic sources. A seismic source model is defined as a sequence of seismic sources, and in NRML each seismic source can be one of four possible typologies:

- Area: Polygonal region describing area of uniform seismicity.
- Point: Single location describing a point of concentrated seismicity.
- Simple Fault: 3D surface describing seismicity on a simple (i.e. regular) fault plane.
- Complex Fault: 3D surface allowing description of seismicity occurring on a complex fault plane.

These four categories have been derived after an extensive evaluation of seismic hazard models that was carried out during the GEM1 project (Pagani *et al*., 2010b). For instance, area sources have been widely used during the GSHAP project (Giardini, 1999), whilst point, simple fault and complex fault sources are often utilized in the USGS models, such as in the calculation of the latest hazard maps for United States (Petersen *et al*., 2008). Collections of point sources can be used to represent gridded seismicity models, whilst simple fault source are employed to

describe active shallow crust sources, and complex faults are usually adopted for modelling subduction interface seismicity.

2.3.4. Logic Tree model

Logic Trees are widely used in modern PSHA (e.g. Bommer and Scherbaum, 2008). The goal of a logic tree is to systematically describe epistemic uncertainties (uncertainties arising from a lack of knowledge or data) to be considered in a seismic hazard/risk analysis. In the current schema, a logic tree is structured as a sequence of branch sets, each branch set being a collection of logic tree branches. The schema implicitly assumes that a branch set defines a branching level in the logic tree, thus currently allowing only the definition of symmetric logic trees. An uncertainty model (e.g. fault dip equal to 40°) and an uncertainty weight define a logic tree branch. The uncertainty model specifies a particular realization of epistemic uncertainty, and the uncertainty weight specifies the degree of belief or probability associated to that particular realization.

2.3.5. Rupture model

The NRML schema allows the definition of a rupture model, which is a key input for scenario risk analysis. Together with an ID, name and description, a rupture is specified by a magnitude and a tectonic region definition. The geometry associated with a rupture can be described using one out of four available options:

- Point rupture (described by a focal mechanism and hypocentre location);
- Simple fault rupture (described by a rake angle and by the same geometrical attributes of a simple fault source);
- Complex fault rupture (described by a rake angle and by the same geometrical attributes of a complex fault source);
- Arbitrarily complex rupture (described by a rake angle and a rupture surface defined as a sequence of arbitrarily shaped polygons);

The above options offer a wide range of possibilities for rupture modelling. For instance, a point rupture can be used if the ground motion modelling is performed by means of a ground-motion prediction equation (GMPE) that adopts hypocentral distance as the distance metric. The three extended rupture options can be used

depending on the level of knowledge of the fault surface geometry, ranging from basic to very detailed.

2.3.6. Vulnerability model

Physical or structural, vulnerability is defined as the probability distribution of loss ratio, given an intensity measure level. In the current version of OpenQuake, discrete vulnerability functions are used to directly losses which might, for example, be fatalities or repair costs, where the loss ratio for the former would be the ratio of fatalities to exposed population, and for the latter the ratio would be that of cost of repair to cost of replacement for a given building typology. Discrete vulnerability functions are described by a list of intensity measure levels and corresponding mean loss ratio, associated coefficient of variation and probability distribution. The uncertainty in the loss ratio can currently be assumed as following a lognormal or beta distribution. Figure 2.1 presents an example of a discrete vulnerability function, compatible for use with OpenQuake.

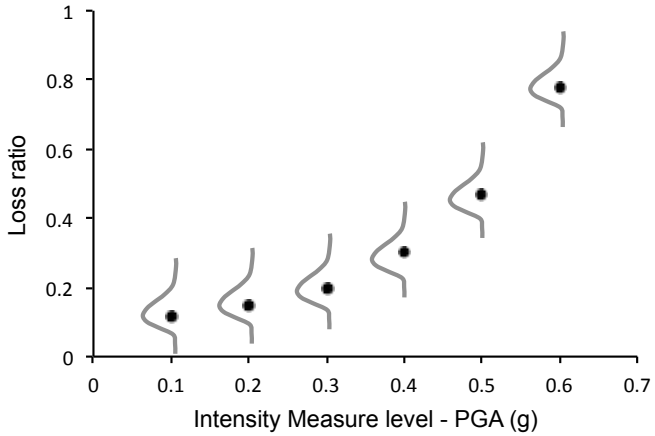

Figure 2.1 - Illustration of a discrete vulnerability function.

2.3.7. Fragility model

Fragility is defined as the probability of exceeding a list of limit states, given a range of intensity measure levels. Currently, a fragility model can be defined in two manners: following a discrete approach, in which a list of probabilities of exceedance per limit state are provided for a set of intensity measure levels or in alternative, by means of modelling each limit state curve as a cumulative lognormal function, represented by a mean and standard deviation (see Figure 2.2).

OpenQuake deals with any fragility models regardless the number or nomenclature of the list of limit states.

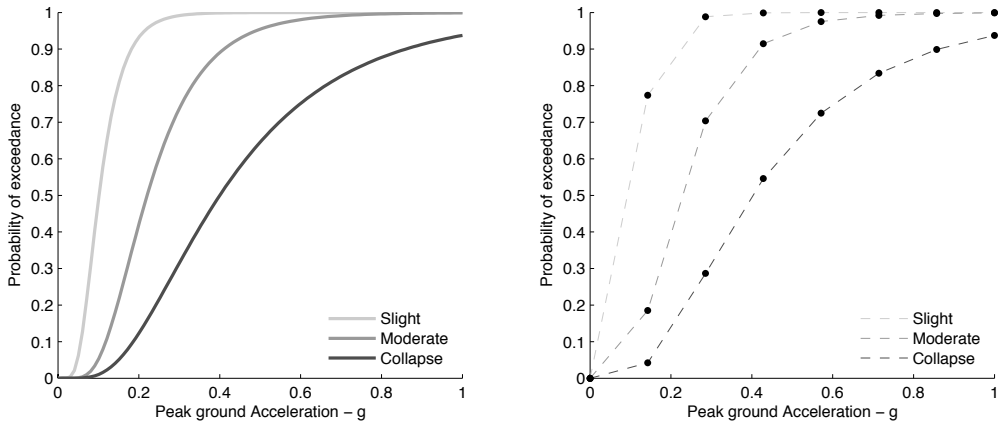

Figure 2.2 – Continuous (left) and discrete (right) fragility models.

2.3.8. Exposure model

The exposure model contains the information regarding the assets within the region of interest, where the term asset is used to define something of value. A number of parameters are required to define the characteristics of each asset, such as the taxonomy that allows OpenQuake to relate the asset with the appropriate vulnerability function, the value of the asset, and the geographic coordinates that will allow the calculators to relate the asset with the respective seismic hazard. The taxonomy is a classification scheme and is of particular use for buildings, which can have very different attributes (such as material, height, age) that need to be documented. The user can apply any taxonomy, which might be the recently proposed GEM Building Taxonomy V2.0 [19] or the HAZUS taxonomy (FEMA-443, 2003), as long as the same taxonomy is used for the exposure and the vulnerability models. Uncertainty in the exposure model is not currently incorporated, but will be considered in future development; furthermore the extension of the hazard logic tree to consider different exposure and vulnerability models will be undertaken.

2.3.9. Hazard Curves, Hazard Maps, and Ground Motion Fields

The typical outputs of a probabilistic seismic hazard analysis are hazard curves and hazard maps. Scenario hazard analysis produces sets of ground motion fields, which can then be used for risk calculations. If the PSHA input model contains a logic tree structure for both seismic sources and GMPEs, OpenQuake generates several

results each one corresponding to a specific realization of the logic tree structure (i.e. a seismic source model and a set of GMPEs). The NRML schema allows the representation of results referring to a single realization (i.e. a hazard map computed with a given seismic source model and set of GMPEs) as well as of results summarizing the entire set produced, i.e. results giving a description of the variability due to epistemic uncertainty.

2.3.10. Loss Curves and Loss Maps

Each loss exceedance curve produced in OpenQuake is represented by a list of losses and respective probabilities of exceedance. Furthermore, each curve is associated with an end branch label (that allows the curve to be connected to the set of specifications used in the calculations) and an asset ID (that permits tracking of the asset that each loss curve was computed for). With regards to the second output, loss maps are comprised by a set of "loss nodes", which are associated with a pair of coordinates. For each node, one or more loss values might exist, due to the fact that several different assets can be located at the same location. A probability of exceedance and time span are also attributes of loss maps, if they are supporting results from a probabilistic risk assessment and not from a deterministic scenario.

2.3.11. Damage distribution and collapse maps

OpenQuake is capable of estimating the distribution of buildings in each damage state (according to a fragility model), due to the occurrence of a single seismic event. The damage distribution output is comprised by a set of "damage nodes" (defined by a pair of coordinates) for which the amount of buildings in each damage state is described. Currently, OpenQuake can also provide a damage distribution per building typology (amount of buildings in each damage state within the same building taxonomy) or the total damage distribution (sum of all the buildings in each damage state). Using the distribution of buildings in the last damage state (usually defined as collapse or total destruction), collapse maps can be extracted. In this output, the spatial distribution of the percentage of collapsed buildings is provided.

Despite the fact that GEM is working closely with many regions in the world to develop seismic hazard models, to collect information about the local building typologies and proposing guidelines to estimate vulnerability and fragility models, it

is emphasized here that no data is incorporated in OpenQuake, and each user is free of using its own models.

2.4. OpenQuake Risk Calculation Workflows

OpenQuake currently comprises five risk calculation workflows: two computing losses and damage distribution due to a single event, other two computing seismic risk due to most or all of the possible events that might occur in a given region within a certain time span, and a last one that uses probabilistic losses to assess whether retrofitting measures would be economically viable or not. A comprehensive description of the methodologies included in OpenQuake can be found in the OpenQuake Book (GEM, 2012b). In the following sections, a description of the properties characterizing each risk calculation methodology is provided.

2.4.1. Scenario Risk Calculation Workflow

This calculation sequence is capable of computing losses and loss statistics due to a single, deterministic earthquake, for a collection of assets. Such analyses are of importance, for example, for emergency management planning and for raising societal awareness of risk.

The hazard input consists of a finite rupture and a single GMPE. By repeating the same rupture, and sampling the inter- and intra-variability from the GMPE each time, many ground motion fields can be computed to account for the aleatory variability in the ground motion. During the generation of each ground motion field, the spatial correlation of the intra-event variability can be considered, so that assets located close to each other are likely to have similar ground motion levels (see e.g. Crowley *et al*., 2008 for a summary of ground motion variability treatment in loss models). The set of ground motion fields is then provided to the Scenario Risk calculator, together with the vulnerability and exposure models, to compute the losses for each asset in the exposure model, per ground motion field. The correlation in the uncertainty in the vulnerability functions is incorporated such that when sampling the uncertainty in the vulnerability of two assets with the same taxonomy, the residuals can be perfectly correlated, uncorrelated or modelled with a specific correlation coefficient. The mean or median value of losses across all ground motions fields can be found for a given asset, and the spatial variation of this value

for a given asset typology can be plotted in a loss map. The losses to all assets across the region of interest can also be aggregated per ground motion field, to obtain a list of aggregated losses, which can then be used to compute the mean and standard deviation of the aggregated losses. This calculation type was found in many of the codes reviewed in GEM1, but the robust modelling of uncertainty and its correlation (in the ground motion residuals and the vulnerability uncertainty) was not found to be present in the reviewed software. In Figure 2, the procedure of this workflow is illustrated.

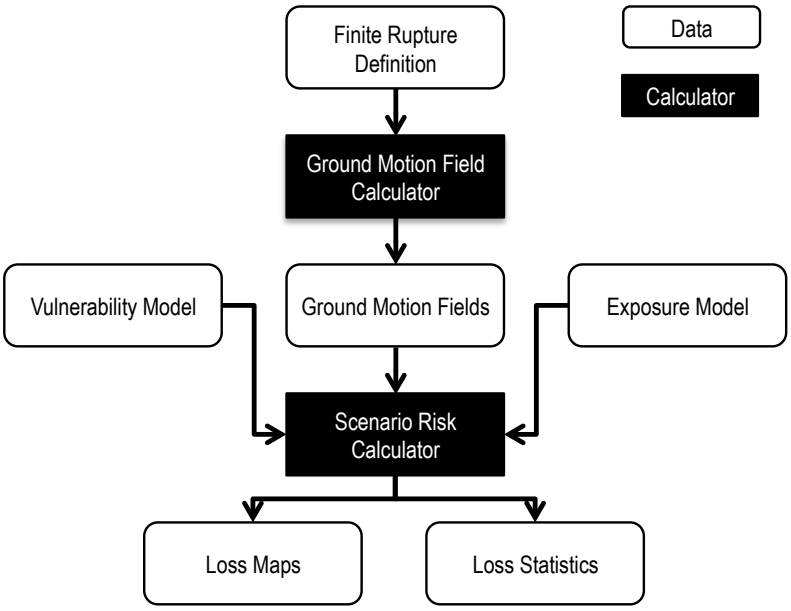

Figure 2.3 - Workflow of the Scenario Risk calculator.

2.4.2. Scenario Damage Calculator Workflow

This calculation workflow serves the purposes of estimating the distribution of damage due to a single deterministic earthquake, for a spatially distributed building portfolio. Similarly to the previous calculator workflow, this tool is fundamental for the same risk mitigation activities. Again, a finite rupture definition needs to be provided, along with the GMPE intended to be used. A set of ground motion fields is computed, with the possibility of considering the spatial correlation of the ground motion residuals. Then, the Scenario Damage Distribution Calculator computes for each asset, the fraction of buildings in each damage state. This percentage of buildings in each damage state is calculated based on the vertical distance between consecutive limit state curves. By repeating this process for each ground motion field, a list of fractions (one per damage state) for each asset is obtained. The

damage distribution output is comprised by the mean and standard deviation of this list of fractions for each asset. By multiplying the number or area of buildings by the respective fractions, the absolute buildings damage distribution is attained. Finally, The Scenario Damage Distribution Calculator also uses the amount of buildings in the last damage state (commonly defined as collapse) to output collapse maps (i.e.: spatial distribution of number or area of collapsed buildings).

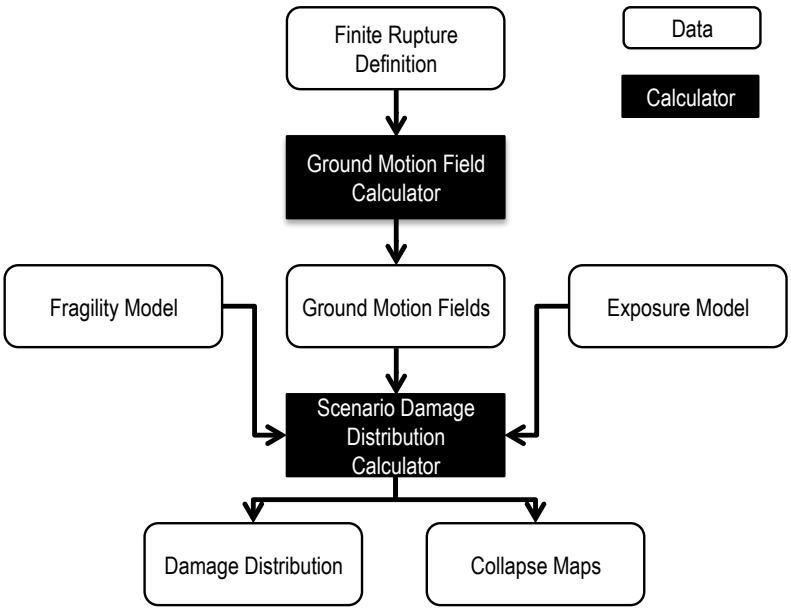

Figure 2.4 – Workflow of the Scenario Damage Distribution.

2.4.3. Probabilistic Event-Based Risk Calculation Workflow

This calculation workflow computes the probability of losses and loss statistics for a collection of assets, based on the probabilistic hazard. The losses are calculated with an event-based approach, such that the simultaneous losses to a set (or portfolio) of assets can be calculated.

This workflow requires a number of calculators in order to calculate ground motion fields. Firstly, a Logic Tree Processor calculator uses information contained within the seismic source system together with a Monte Carlo approach to sample the logic tree structure and produce a seismic source model (SSM). Each seismic source model computed is used by the Earthquake Rupture Forecast (ERF) calculator to produce a list of all the possible ruptures occurring on all the sources in the SSM; each rupture is associated with a probability of occurrence in the time span specified by the user in the configuration file. Then, the Stochastic Event Set calculator uses the ERF to create one or several groups of ruptures. Each group

represents a possible realization of the seismicity generated in the specified time span by the entire set of seismic sources included in the seismic source model. Afterwards, the Logic Tree Processor is again used to process the GMPEs system and provide the ground motion relationship that shall be used by the Ground Motion Field calculator, together with each earthquake rupture, to compute the ground motion values at a set of sites. The spatial correlation of the intra-event residuals of the ground motion model can also be considered. As mentioned previously, in that case, sites that are closer are more likely to have similar levels of ground motion. This set of ground motion fields is combined with the exposure and vulnerability model (again with correlation of the uncertainty in the vulnerability) in the Probabilistic Event-Based Risk calculator, to compute the losses for each asset per ground motion field. The list of losses per asset can be used to build a cumulative histogram which gives the number of losses in selected bins of loss over the time span, from which the loss exceedance curve is computed (loss versus probability of exceedance in a given time span). This approach can be used to compute a loss curve for each asset within the exposure model, or by summing all the losses throughout the region per ground motion field, a total loss curve representative of the whole set of assets within the exposure file is obtained. The workflow in Figure 3 describes this procedure.

This calculation type was found to be in only a few of the codes reviewed in GEM1, and those where it was present did not include a robust modelling of uncertainly and its correlation (in the ground motion residuals and the vulnerability uncertainty).

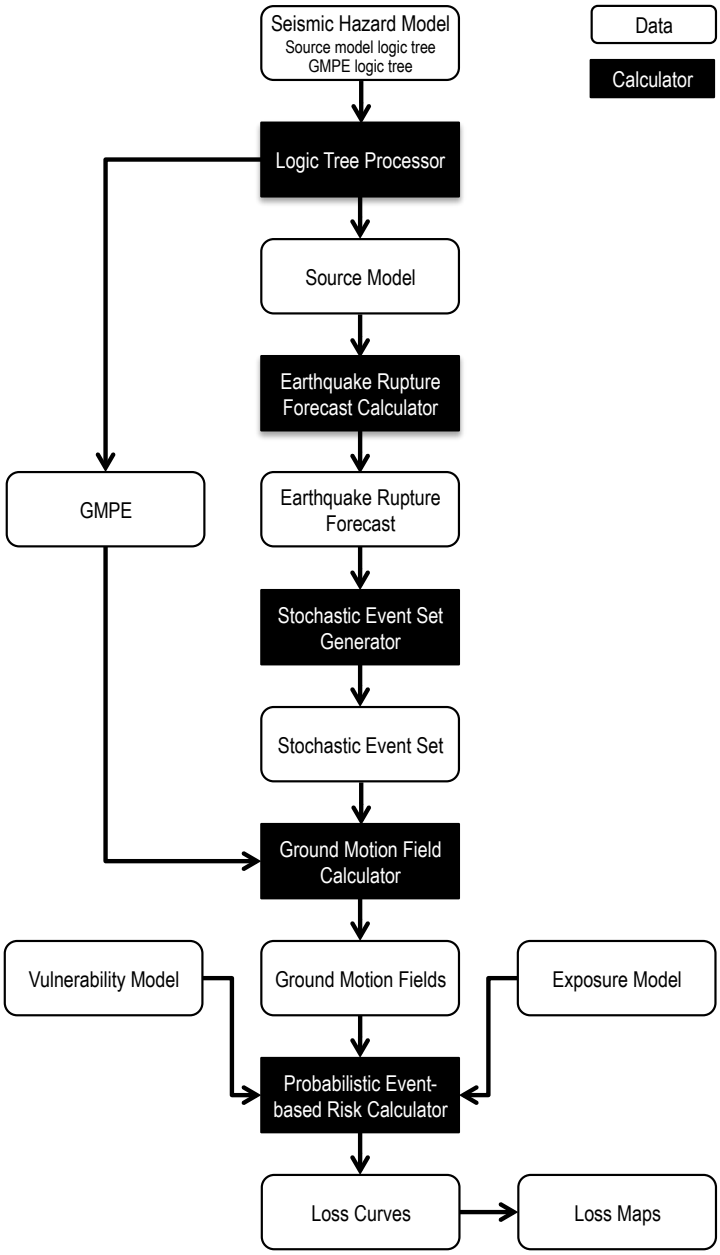

Figure 2.5 - Workflow of the Probabilistic Event-Based Risk calculator.

2.4.4. Classical PSHA-Based Risk Calculation Workflow

This calculation workflow leads to the computation of the probability of losses and loss statistics for single assets, based on the probabilistic hazard. The output of this calculator is useful for comparative risk assessment between assets at different locations.

This workflow has an initial architecture similar to the previous one, in which a Logic Tree Processor uses the structure defined in the Seismic Source System to provide the required parameters to the Earthquake Rupture Forecast (ERF)

calculator, which produces a list of all the possible ruptures occurring on all the sources included in the seismic hazard model. Then, using the GMPEs system, the Logic Tree processor states which GMPEs the Classical Hazard Curves calculator will use. This calculator uses the classical PSHA approach (Cornell, 1968, McGuire, 2004) following the methodology presented by Field *et al*. (2003) to compute a hazard curve at each site. This set of hazard curves is then provided, together with the vulnerability and exposure model to the Classical PSHA-based Risk calculator. Here, the first step is to convert each discrete vulnerability function into a loss ratio exceedance matrix (e.g. a matrix which describe the probability of exceedance of each loss ratio for a discrete set of intensity measure levels). Once these matrices are built, the values of each column are multiplied by the probability of occurrence of the associated intensity measure level. This probability is extracted from the previously computed hazard curves. Finally, the list of probabilities of exceedance of the loss ratio curve is obtained by summing all the values per loss ratio. This loss ratio curve is then converted into a loss curve by multiplying each loss ratio by the associated asset value. The workflow in Figure 3b describes the architecture of this calculator.

Some of software reviewed in GEM1 feature risk calculations based on hazard maps (for a single return period), but only one other software explicitly used hazard curves.

The loss exceedance curves produced using the Probabilistic Event-Based and the Classical PSHA-Based calculators, can also be used to create loss maps representing the distribution of the expected loss per location for a certain probability of exceedance within a given time span. Furthermore, mean losses within the given time span (e.g. average annual loss) can also be extracted by integrating the loss exceedance curves.

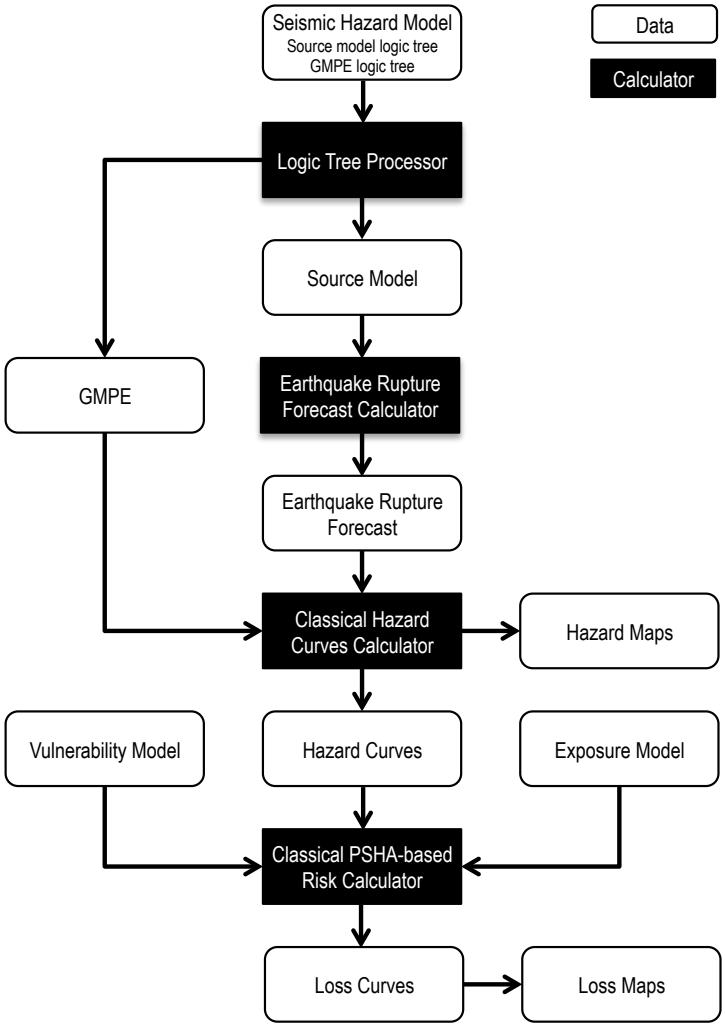

Figure 2.6 - Workflow of the Classical PSHA-Based Risk calculator.

2.4.5. Benefit-Cost Ratio Calculator Workflow

This calculation sequence supports users in deciding whether employing retrofitting/strengthening measures to a collection of existing buildings is advantageous from an economical point of view. This functionality uses probabilistic seismic risk (loss curves) that can be computed using either the Probabilistic Event-based Risk calculator or the Classical PSHA-based Risk calculator. Two sets of loss curves need to be calculated: one considering the original asset vulnerability, and a second one using the retrofitted vulnerability configuration. Then, the Annual Average Loss (AAL) is estimated for each configuration, by summing the product of each loss with the corresponding probability of occurrence, extracted from the loss curves. The associated economical benefit is computed using the AAL for both configurations, according to the following formula:

$$Benefit = \frac{\left(AAL_{retrofitted} - AAL_{original}\right)}{r} \times (1 - e^{rt}) \quad (2.1)$$

where t stands for the life expectancy of the building stock and r represents the discount interest rate. The later parameter serves the purpose of taking into account the variation of building value throughout time. Thus, a rate close to zero signifies that no changes in the building stock value are expected, whilst a positive discount rate indicates that each year the economic value is reduced according to the associated rate. The final ratio is computed by dividing the aforementioned benefit, by the cost of retrofitting. The output of this calculator is a benefit/cost ratio spatial distribution, which if higher than 1, indicates that employing retrofitting measures is economically viable.

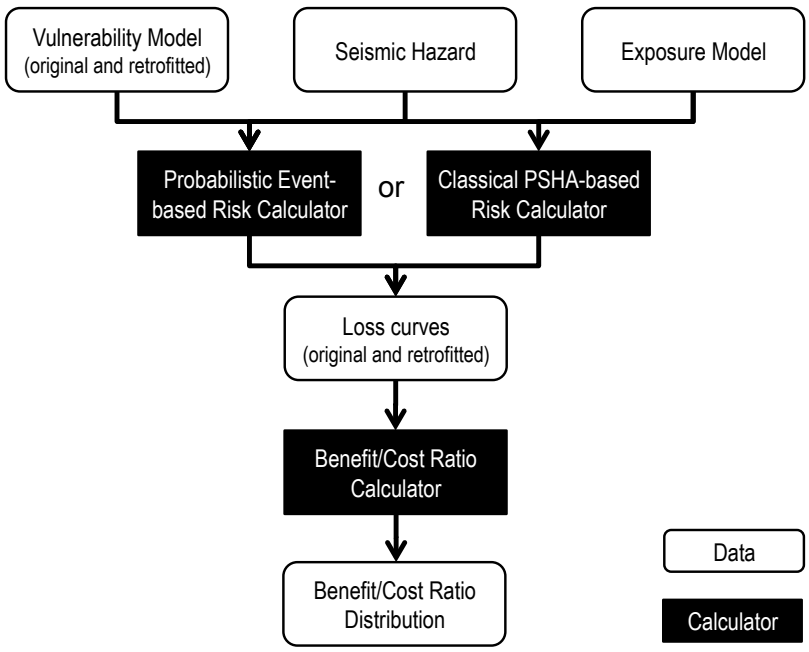

Figure 2.7 - Workflow of the Benefit/Cost Ratio Calculator.

2.5. Case study applications

2.5.1. Introduction

Turkey as been the subject of various studies in the past (e.g. Erdik *et al.,* 2003; Kalkan *et al*., 2008, Bal *et al*., 2008a) hence, there is a wide variety of seismic hazard, exposure and vulnerability/fragility models available, being this the main reason for choosing the Metropolitan Area of Istanbul as the region of interest for this case

study application. This region is located in one of the most seismically active region in the world with a large amount of population exposed to a significant risk of major earthquakes (Bommer *et al.*, 2002). Proof of this is given by the numbers from the last two catastrophic earthquakes that occurred in the region: Kocaeli (August, 1999) and Duzce (November, 1999), in which over 18 thousand people lost their life and more than 50 thousand were injured. Furthermore, it is believed that a similar earthquake will hit the southern region of Istanbul with a probability of 62% in the next 30 years (Bakıra and Boduroglu, 2002). Within this section, the OpenQuake capabilities are demonstrated, focusing mainly on the risk component. The input data is described and some exemplificative hazard and risk results are presented. It is highlighted herein that it is not the objective to validate any of the input models, but simply to show the OpenQuake-engine functionalities.

2.5.2. PSHA model

The seismic hazard input data utilized to exercise the OpenQuake calculators comes from a preliminary seismic hazard model developed for Turkey (Demicioglu *et al.*, 2008). The PSHA model consists of a seismic source model based on two source typologies: area and faults. Faults are utilized to model large magnitude events (i.e. with moment magnitude $M_w \geq 6.7$), while area sources describe distributed seismicity for Mw ≥ 5.0. Area sources are employed for two different purposes: to model large-scale background seismicity ($5.0 \leq M_w \leq 6.5$), as well as seismicity around faults (that is, events not occurring on the fault plane but within its neighbourhood). Earthquake ruptures inside area sources are modelled as points, while on fault sources ruptures are modelled as rectangles, whose dimension (length and width) are derived from the Wells and Coppersmith (1994) magnitude-area scaling relationship. Figure 2.8 and Figure 2.9 depict the fault and area-based source models in terms of maximum moment magnitude, respectively.

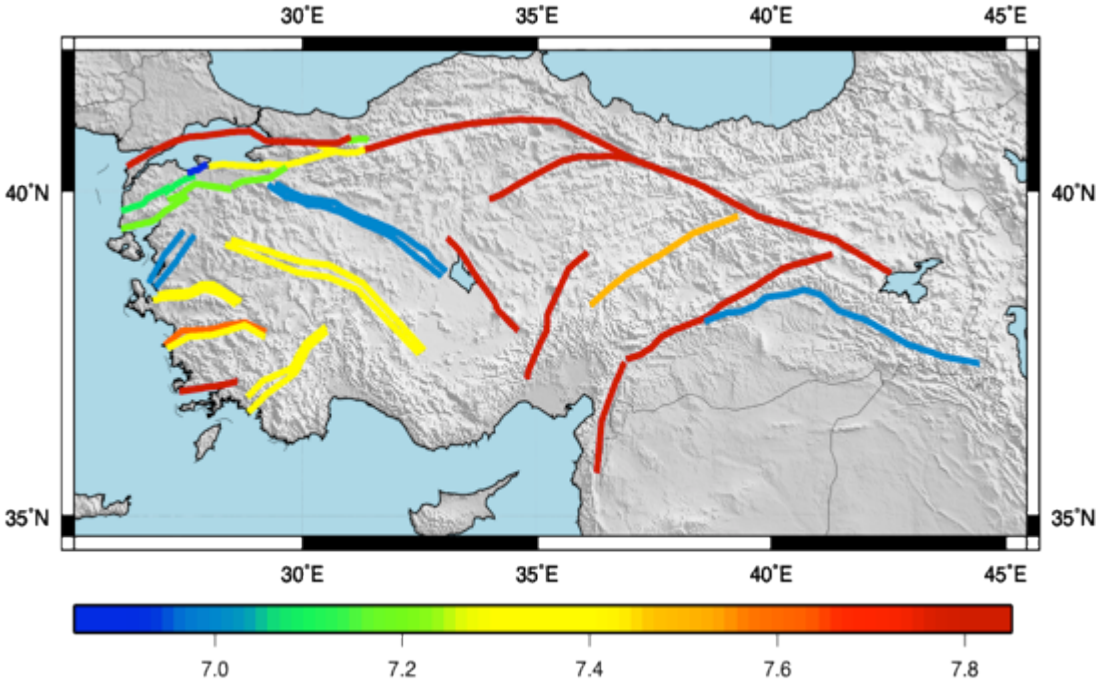

Figure 2.8 - Fault source model for Turkey. Faults are assumed to be vertical, so only fault traces are shown. Colours represent maximum magnitude (M_w).

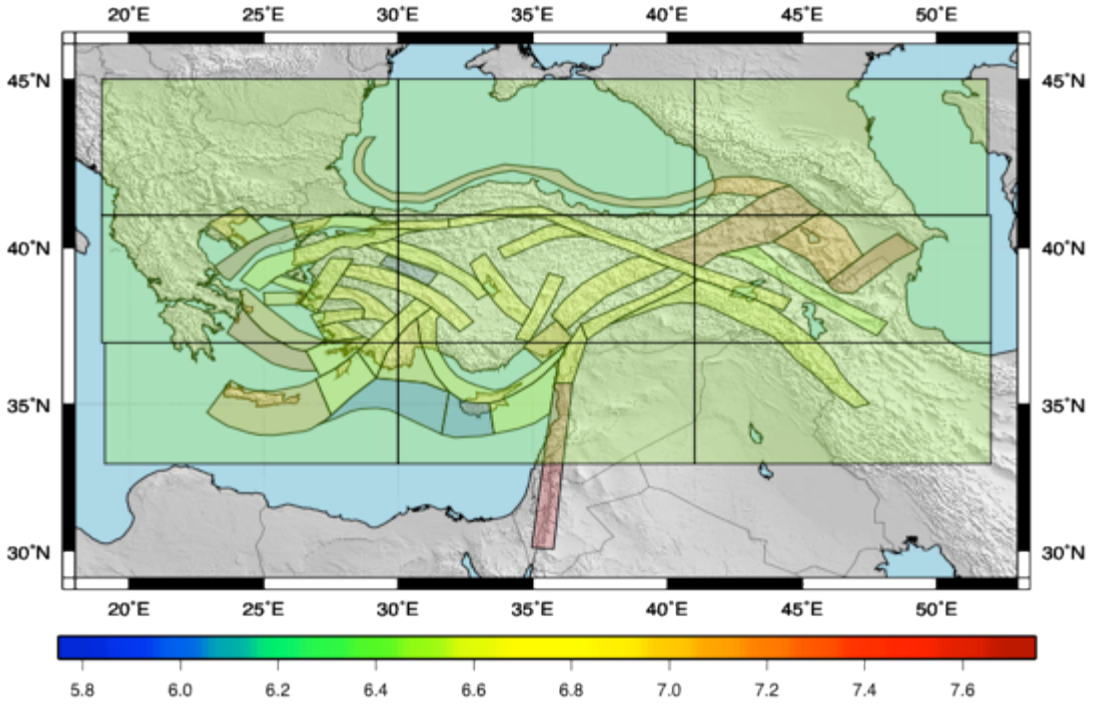

Figure 2.9 - Area source model for Turkey. Large-scale rectangular background sources cover the entire country, whilst most of the small-scale area sources follow fault source geometries.

Faults are assumed to be vertical (dip angle equal to 90 degrees) with a strike-slip mechanism (rake angle equal to 0 degrees according to the Aki and Richards convention). Fault surfaces extend from 0 to 15 km depth. Area sources are

associated to an average hypocentral depth of 3 km. Both faults and area sources occurrence rates follow a truncated Gutenberg-Richter magnitude frequency distribution.

The ground motion model contains a logic tree consisting of three GMPEs: Boore and Atkinson (2008), Campbell and Bozorgnia (2008), and Chiou and Youngs (2008). All three GMPEs received an equal weight.

2.5.3. Deterministic rupture model

The deterministic scenario model for the city of Istanbul considers a single rupture equivalent to a magnitude of 7.5. A rake of 0° and a dip of 90 ° were assumed, characterizing the rupture as a pure strike-slip mechanism. The rupture extends for 120 km along the North Anatolian fault, on a section close to the Bosphorus strait, as shown in Figure 2.10.

Figure 2.10 – Representation of rupture trace (in red).

2.5.4. Building Exposure Model

The building inventory for the metropolitan area of Istanbul was created based on a combination of data from aerial photos taken in 1995 and 1998 and census data from 2000 conducted by the Turkish State Statistics Institute. In this dataset, buildings are organized according to construction type (RC frames, RC shear walls, Masonry and Pre-cast buildings), height (low-, mid- and high-rise) and code level (pre-1979 or post-1980) (BU-ARC, 2002). The dataset uses an evenly spaced grid

with a 0.005×0.005 decimal degree spatial resolution and for each grid cell, the number of buildings for each typology is provided. This exposure model has been used in several past studies such as the NERIES project (Strasser *et al.*, 2008), in which 5 different earthquake loss estimation methodologies were used to compute the distribution of building damage for the same earthquake rupture. For the purposes of this case study, this exposure model has also been extended to provide the economic value (replacement cost) for each building typology per grid cell. This conversion was carried out by multiplying each building count, by the associated replacement cost. The total economic value of the estimated building portfolio has been estimated in 66.1 billion EUR. In order to understand the distribution of building count and economic cost throughout the metropolitan area of Istanbul, the values per grid cell were aggregated and the results are illustrated in Figure 2.11.

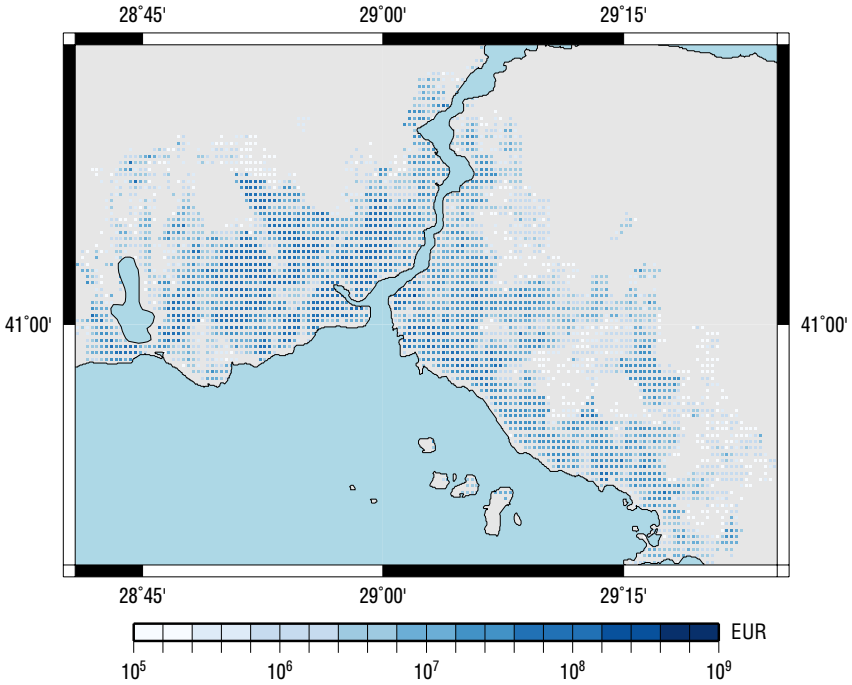

Figure 2.11 - Distribution of building economic value in the Metropolitan Area of Istanbul.

2.5.5. Fragility and Vulnerability Model

Several studies have been carried out in the past to calculate fragility functions of typical Turkish buildings (e.g. Akkar *et al.*, 2005, Kirçil and Polat, 2006, Erberik, 2008, Ozmen *et al.*, 2010). However, such endeavours often focus only in a few types of structures, turning the task of collecting fragility functions that follow the same damage state definition and intensity measure types for every building typology very challenging. In the present work, the vulnerability indexes estimated for the

same building typologies considered herein, were extracted from the software ELER [7]. Then, using the procedure proposed by Lagomarsino and Giovinazzi (2006), a set of fragility functions were derived for each building typology. This approach uses EMS as the intensity measure type and considers six damage states (D0, D1, D2, D3, D4 and D5), as defined in Grunthal (1998). These fragility functions were combined with a consequence model (i.e.: ratio between the repair cost and replacement cost for each damage state, also known as damage ratio) to derive a vulnerability model. In this process, a set of loss ratios (*LR*) are computed for a range of intensity measure levels (*IML*), by summing the product of the percentage of buildings in each damage state with the respective damage ratio (DR), as described in the following expression:

$$LR|IML_i = \sum_{j=1}^{n} \%_j|IML_i \times DR_j \tag{2.2}$$

where n stands for the number of damage states considered in the fragility model and $\%_j$ represents the fractions of buildings in damage state j, for a given IML_i. This fraction for each damage state is equal to the vertical distance between the bounding limit state curves, at the IML_i. In this study, the consequence model developed for Typical Turkish buildings by Bal *et al*. (2008b) was employed. The relation between each damage state defined within the fragility model and the corresponding damage ratio is described in Table 2.2.

Table 2.2 - Correspondence between damage states and damage ratio.

Damage definition by Grunthal (1998)			Consequence model by Bal *et al*. (2008b)	
Damage state	Non-structural damage	Structural damage	Damage state	Damage ratio
D1	Slight	None	None	0.00
D2	Moderate	Slight	Slight	0.16
D3	Heavy	Moderate	Moderate	0.33
D4	Very heavy	Heavy	Extensive	1.05
D5	Destruction		Collapse	1.04

It is noted that this consequence model proposes a damage ratio of 1.05 for extensive damage, because Turkish law endorses a total replacement of a building when it experiences very heavy damage, which implies additional costs due to its demolition and removal of debris. The extra cost of removing the debris is also considered in the collapse damage ratio (1.04). The resulting fragility and vulnerability functions for the most common building typology in Istanbul (low-rise

RC frames with unreinforced masonry infill walls built after the 1979 design code) are depicted in Figure 2.12.

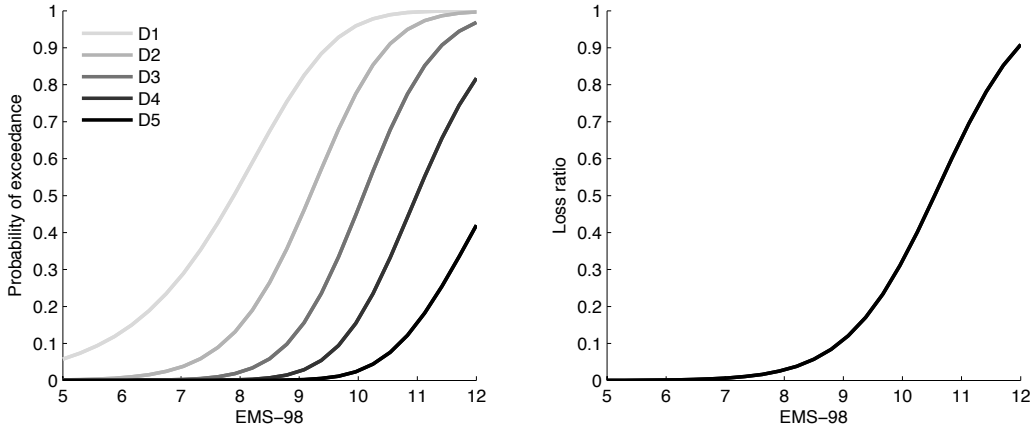

Figure 2.12 - Fragility (left) and vulnerability (right) functions for low-rise RC frames built after the 1979 design code.

All of the fragility functions were truncated for a minimum intensity of V, as it is assumed that no damage is observed for such low values. The intensity measure levels from the fragility and vulnerability model were converted from macroseismic intensity (EMS-98) to peak ground acceleration (PGA), in order to allow the employment of spatially correlated ground motion fields using the model proposed by Jayaram and Baker (2009). At the time of writing, no models were available in the peer review literature capable of correlating the intra-event variability of macroseismic intensity, that could be implemented in OpenQuake. The conversion equation developed for the Marmara Region by Sorensen *et al.* (2008) was employed for this purpose.

2.6. Output

2.6.1. Ground motion fields for Istanbul

Using a single GMPE (Boore and Atkinson, 2008), a set of ground motion fields was generated, sampling the inter- and intra-event variability at each time. OpenQuake allows the consideration of the spatial correlation of the intra-variability. Figure 2.16 presents the median ground motion field in terms of peak ground acceleration, for a region around the fault rupture, following a spatial resolution of 0.05x0.05 decimal degrees (800 locations).

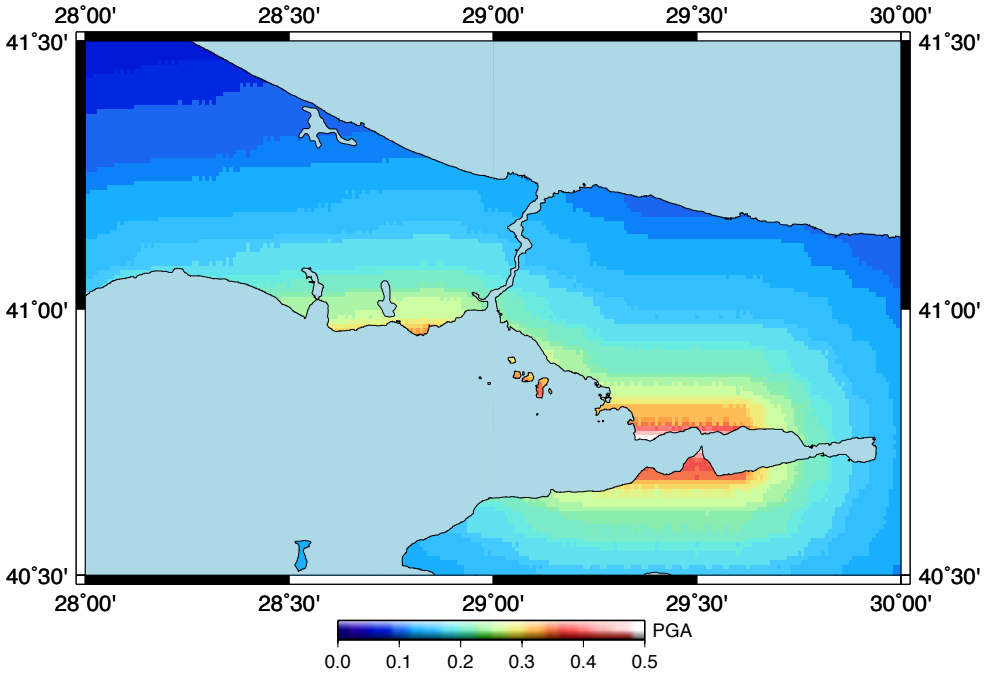

Figure 2.13 - Median ground motion field in terms of peak ground acceleration (g).

2.6.2. Seismic Hazard Map for Turkey

By using the Classical PSHA-Based Risk Calculator, OpenQuake is able to produce hazard curves, from which a hazard map (corresponding to a certain probability of exceedance in a given time span) can be derived. Hazard curves for all the three GMPEs defined in the ground motion model logic tree (see section 2.5.2) were computed, and a mean hazard map was obtained (as shown in Figure 2.14). Hazard curves have been computed from 35.0 to 43.0 degree north, and from 25.0 to 47.0 degree east, every 0.05 degrees. A total of 71001 hazard curves have been derived for each GMPE. As can be seen, the hazard is mostly driven by fault sources, especially the North Anatolian fault, with levels of PGA of about 1.3g along the fault trace. Area sources surrounding fault sources also play an important role. Their effect it to widen the region of significant hazard around fault sources. Large-scale background area sources produce instead a rather stable value of PGA of about 0.2g in all locations that are far from small-scale area sources or fault sources.

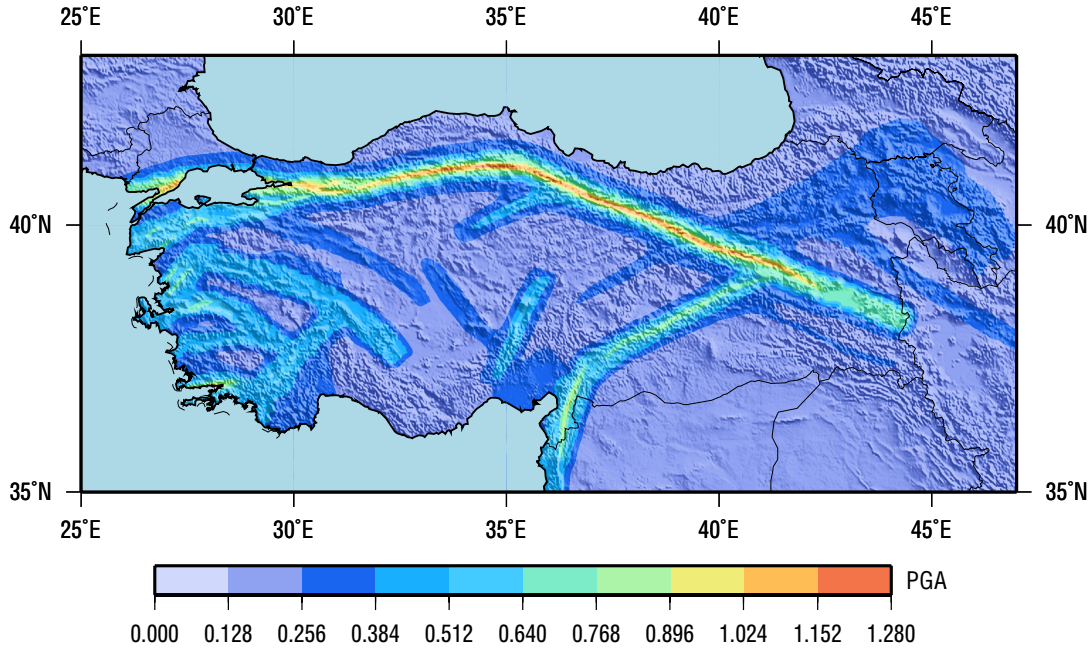

Figure 2.14 - Mean hazard map for a probability of exceedance of 10% in 50 years in Turkey.

2.6.3. Scenario Risk for Istanbul

Using the previously described input data, losses for a deterministic scenario in the metropolitan area of Istanbul were computed using the Scenario Risk Calculator. In this process, about 1000 ground motion fields were produced for the same rupture. In order to test the influence of how the ground motion and vulnerability variabilities are modelled, four different configurations were considered, as described in Table 2.3.

Table 2.3 – Description of the four calculation configurations for the scenario risk assessment.

Type	Ground motion uncertainty	Vulnerability uncertainty
A	No sampling (only the median GMF was used)	No sampling (only mean loss ratio was used)
B	Sampling 1000 GMFs without spatial correlation	Sampling the loss ratio without vulnerability correlation
C	Sampling 1000 GMFs with spatial correlation	Sampling the loss ratio without vulnerability correlation
D	Sampling 1000 GMFs with spatial correlation	Sampling the loss ratio with vulnerability correlation (perfectly correlated)

For each of the aforementioned configurations, the aggregated mean loss and associated standard deviation were computed. The results are depicted in Figure 2.15.

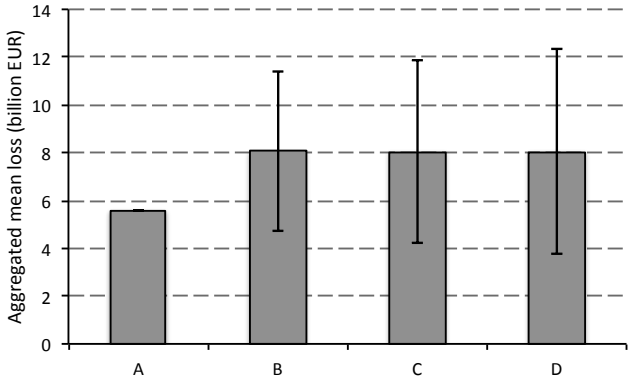

Figure 2.15 - Aggregated loss statistics for the four types of calculation.

As can be inferred from Figure 2.15, not considering the uncertainty in the ground motion (Type A) considerably underestimates the resulting losses. Regarding the other calculation configurations (B, C and D), no significant changes in the aggregated mean loss were observed, but an increase in the standard deviation of 15% from type B to C and of 29% from type B to D were obtained. These variations in the results demonstrate that the way the variability in the ground motion and vulnerability is handled can relevantly affect the aggregated distribution of losses. Figure 2.16 presents a loss map with the distribution of mean economic losses (across all ground motion fields), using the type D configuration. When many building typologies existed simultaneously in a given grid cell, the loss values were aggregated.

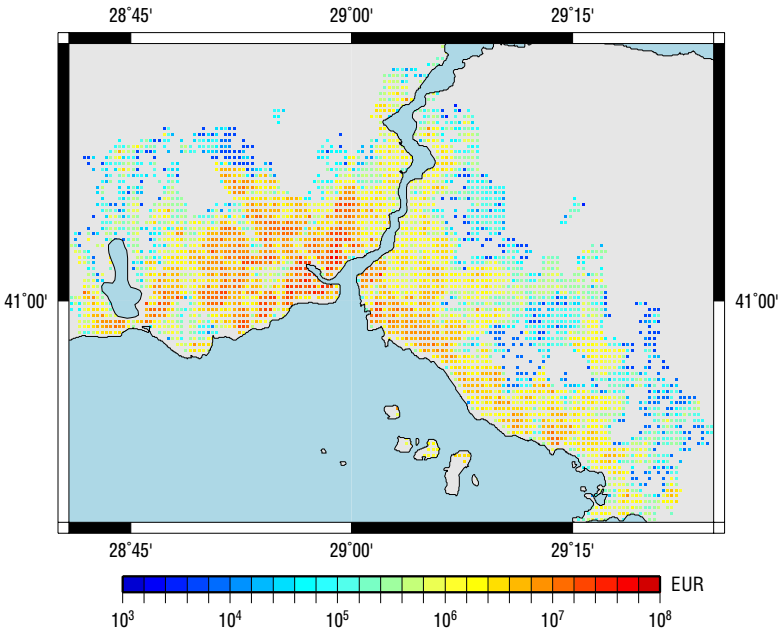

Figure 2.16 - Loss map with the distribution of mean economic losses for the Metropolitan Area of Istanbul.

2.6.4. Comparison with other studies

It is recognized that comparing the computed results with real post-event data is fundamental for the testing of earthquake loss models. Despite the fact that Istanbul has been the target of many studies in the past, no data currently exists that could allow an intensive validation of the results (i.e. testing that the modelled results reflect reality). However, a sanity test can be carried out, by comparing the results presented herein with the ones from previews studies. Such an exercise needs to be performed carefully and taking into account the different assumptions from each study. For example, the size of the region, the magnitude of the rupture, or the consideration of site affects are aspects that are often not common to all of the studies developed for this region. Sozen (2006) has suggested that an event similar to the 7.5 magnitude scenario considered herein would cause the collapse of 10% of the building stock, leading to a loss of about 6.6 billion EUR. Griffiths *et al*. (2007) propose a much drastic estimate of collapses at least 40%, representing an economic loss of approximately 26.4 billion EUR. The aforementioned study was discussed by Erdik (2007), who claimed that such a scenario would actually lead to losses 2.5 times smaller (10.5 billion EUR). Bal *et al*. (2008a) performed a loss assessment using the same exposure model and rupture magnitude considered in the study presented in this chapter, and estimated that about 17.6% of the buildings would collapse or be damaged beyond repair (i.e. be extensively damaged), 27.5% would suffer moderate damage and 54.9% would experience none to slight damage. This damage distribution would lead to an economic loss of 19.7 billion EUR. Although these comparisons have only a qualitative character due to the inherent differences in the studies, it is fair to conclude that the scenario presented herein (8.1 billion EUR with a standard deviation of 3.4 billion EUR) falls within the expected range.

2.6.5. Scenario Damage for Istanbul

The damage distribution for the same deterministic seismic event was estimated using the fragility model described in 2.5.5. Again, several spatially correlated ground motion fields were generated and for each location, the amount of buildings in each damage state was calculated. OpenQuake can also aggregate these results according to the building typologies (defined by the taxonomy attribute in the exposure model) or across the whole building portfolio, thus providing the total building damage distribution. The mean relative damage distribution for low- (LR),

mid- (MR) and high-rise (HR) reinforced concrete buildings built before (PC) and after (C) the implementation of the 1979 design code is illustrated in Figure 2.17.

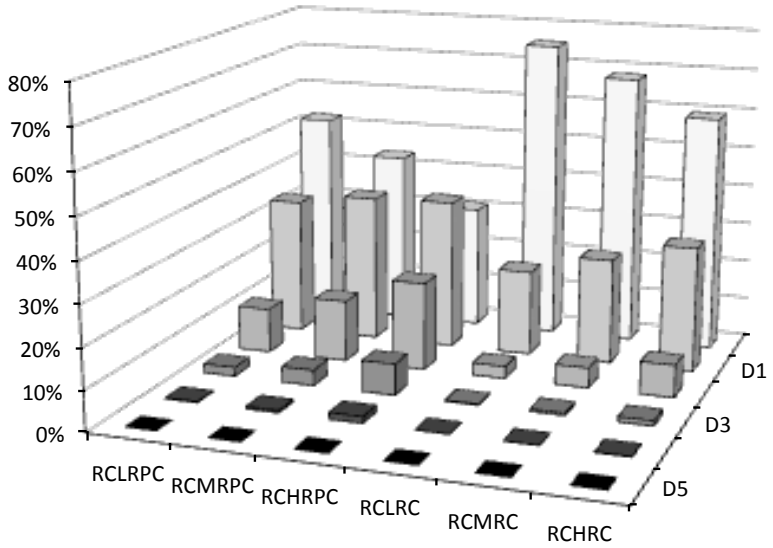

Figure 2.17 – Mean damage distribution for RC building with irregular masonry infill walls.

Using this calculator, it is also possible to extract maps presenting the spatial distribution of collapse in the region of interest. Figure 2.18 presents this type of output for the scenario considered herein. For locations where more than one asset exists, the number of collapses has been aggregated.

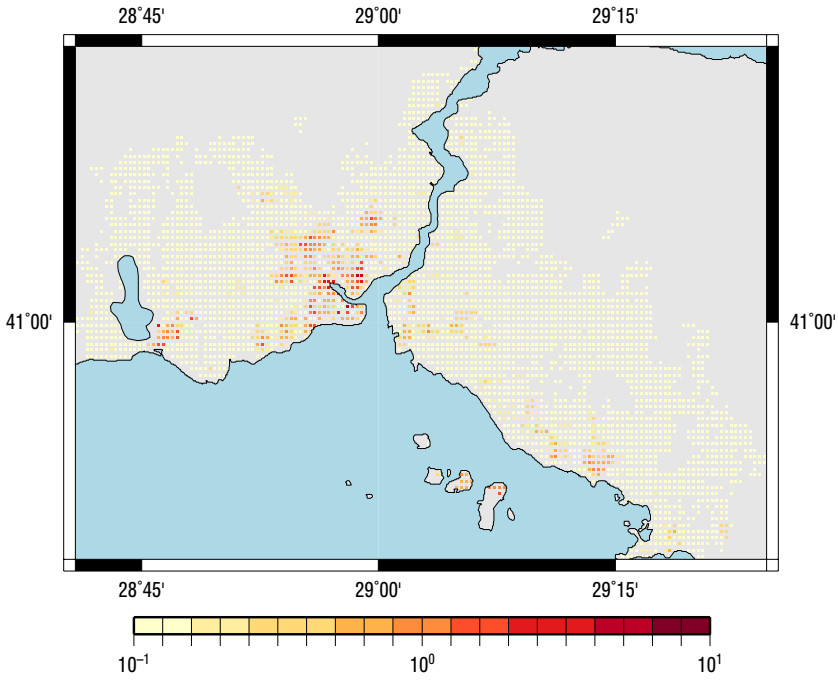

Figure 2.18 - Collapse map for the Metropolitan Area of Istanbul.

2.6.6. Probabilistic risk assessment for Istanbul

Currently in OpenQuake, probabilistic seismic risk can be computed following two approaches: a probabilistic event-based or a classical PSHA-based. The former approach has the advantage of considering the intra-event variability of the ground motion, allowing a more realistic aggregation of the losses per event, and consequently, the computation of aggregated loss curves. However, in order to have stability in the results, it may be necessary to generate thousands of ground motion fields, making this calculation workflow very computationally expensive. This issue will be solved in OpenQuake, through the employment of efficient sampling algorithms (e.g. Jayaram and Baker, 2010), which preferentially generate the ruptures that actually produce significant ground motion in the region. In the other hand, if there is no need of aggregating the losses or in the case the assets are too distant for spatial correlation be irrelevant, the second approach can be followed. In this case, hazard curves for each location are used to derive seismic risk. The first approach is used herein to produce aggregated loss exceedance curves representative of the whole building stock, and the second workflow is utilized to estimate loss maps for different probabilities of exceedance in 50 years.

2.6.7. Probabilistic event-based approach

About two hundred realizations of the seismicity, with a 50 years time span in each case, were used for this probabilistic risk assessment, leading to more than 10,000 ground motion fields. Although area and background sources are also presented in the PSHA model section, only fault sources were considered in this demonstration in order to reduce the computation time for these illustrative results. Furthermore, as mentioned previously, the hazard is mostly driven by the fault sources. Again, the ground motion and vulnerability variability were modelled following different configurations. In this case, the calculation configuration of type B, C and D were considered, as described in Table 2.3. The three aggregated loss exceedance curves computed using this calculator workflow are presented in Figure 2.19.

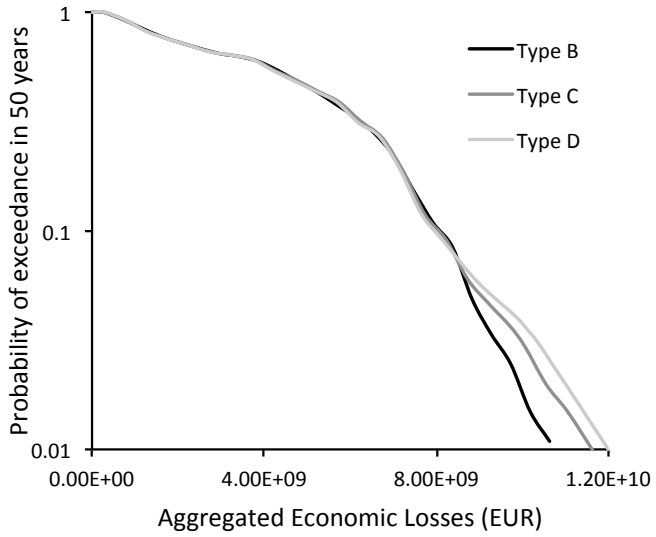

Figure 2.19 - Aggregated loss curves for the three types of calculations.

Once again, the consideration of different approaches to model the variability in the ground motion and vulnerability proved to lead to distinct results. In this case, it can be concluded that ignoring the spatial correlation in the ground motion or the correlation in the vulnerability in the assets of the same building typology (type B curve) underestimates the aggregated losses. This aspect is more evident for low probabilities of exceedance (usually corresponding to large rare events). As an example, for a probability of exceedance of 2% in 50 years (equivalent to a return period of 2450 years), considering the type C configuration led to an increase in the expected aggregated loss of 7%, while for the type D configuration, an increase of 12% was observed.

2.6.8. Using the classical PSHA-based approach

Using the Classical PSHA-Based Risk Calculator, approximately 4,000 hazard curves were computed for each GMPE, as defined in the ground motion model logic tree in section 2.5.2. Then, the mean hazard curve at each location was used to compute the distribution of losses for each asset, totalling 43.194 loss exceedance curves. Currently, OpenQuake is not capable of computing losses for each branch of the logic tree within this approach, but only to use the mean hazard results. However, such capability (extending the logic tree to the risk calculations) is in the future developments plan. Linear interpolation was applied in each loss curve to

calculate the expected economic loss for probabilities of exceedance of 10% and 1% in 50 years. The resulting loss maps are illustrated in Figure 2.20 and Figure 2.21.

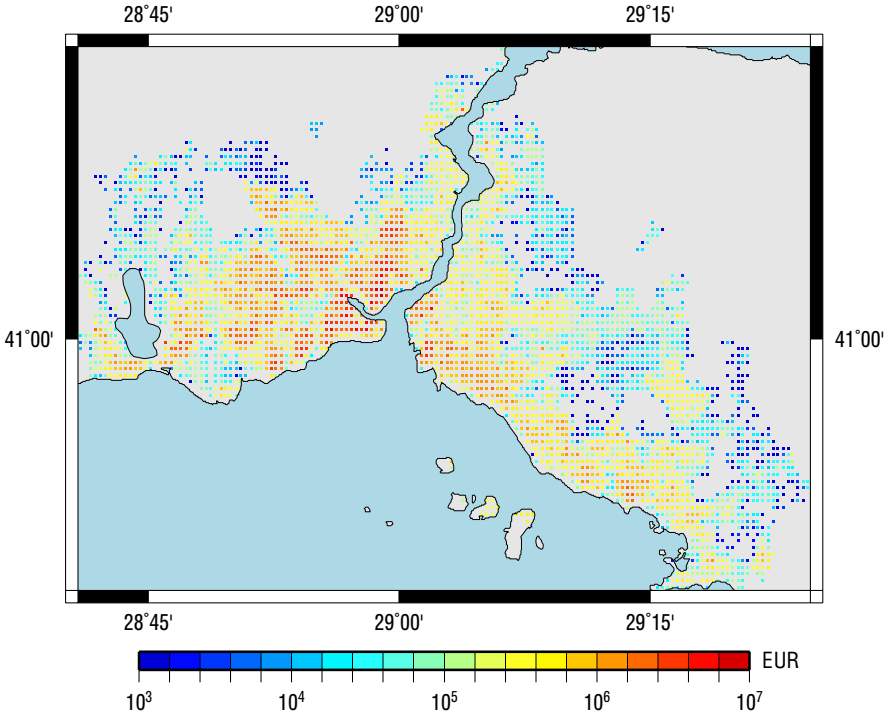

Figure 2.20 - Loss map with a probability of exceedance of 10% in 50 years.

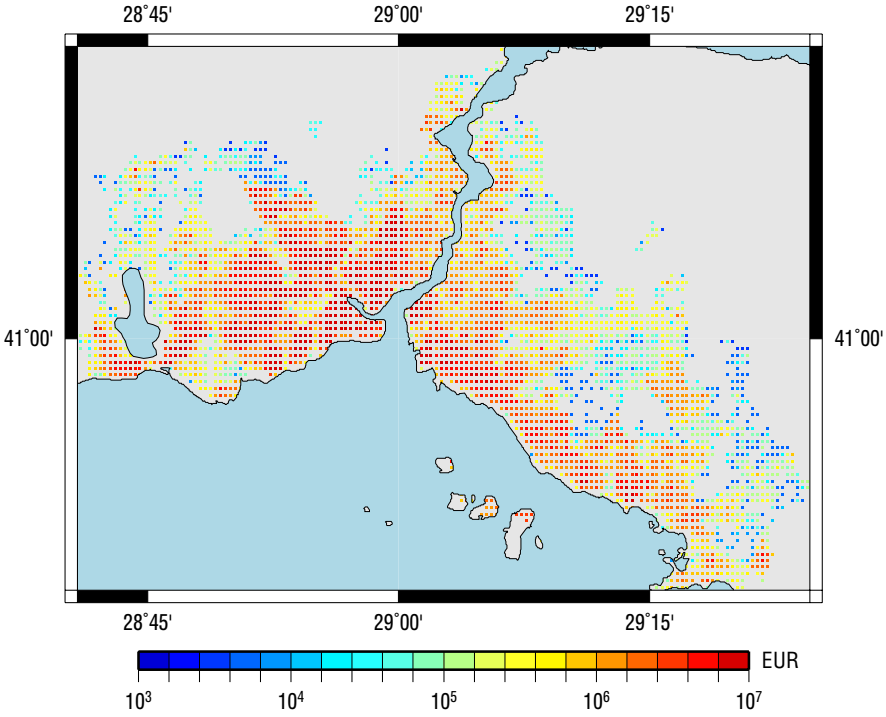

Figure 2.21 - Loss map with a probability of exceedance of 1% in 50 years.

2.6.9. Retrofitting Benefit-Cost Analysis

For the purpose of assessing whether a certain building typology would benefit from an economically point of view by being seismic retrofitted, the distribution of low-rise RC buildings built before the implementation of the 1979 design code was used. This structure type represents the most common building typology designed with inadequate seismic standards in the region. As described in section 2.4.5, in order to carry out this assessment, it is necessary to provide a vulnerability function representing the distribution of loss for the retrofitted design of this building typology. In this exercise, it was assumed that after the employment of a retrofitted intervention, the considered building typology would possess a seismic vulnerability equivalent to a low-rise RC building built after the implementation of the 1979 design code. These two vulnerability functions are represented in Figure 2.22.

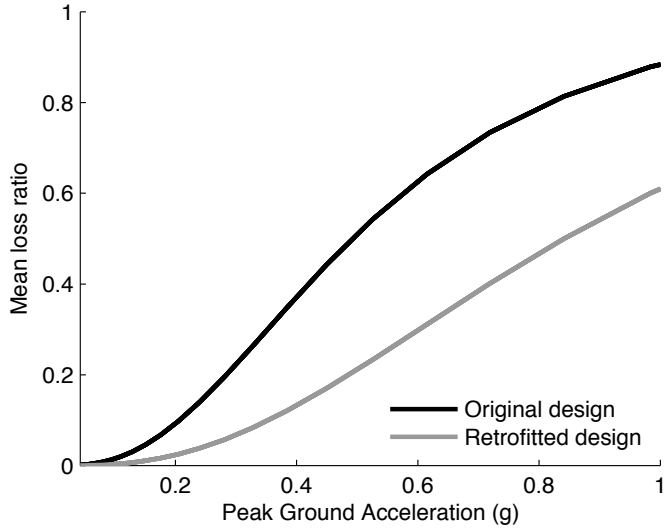

Figure 2.22 - Vulnerability function for the original and retrofitted design of low-rise RC buildings.

The Classical PSHA-based Risk calculator was used to compute a loss curve for each asset, with the original and the retrofitted configuration. Then, the Average Annual Loss for both designs was estimated and using equation (2.1), the benefit-cost ratio was estimated for each asset, as presented in Figure 2.23. It was assumed an interest rate of 2% and a 50 years life expectancy for all the assets.

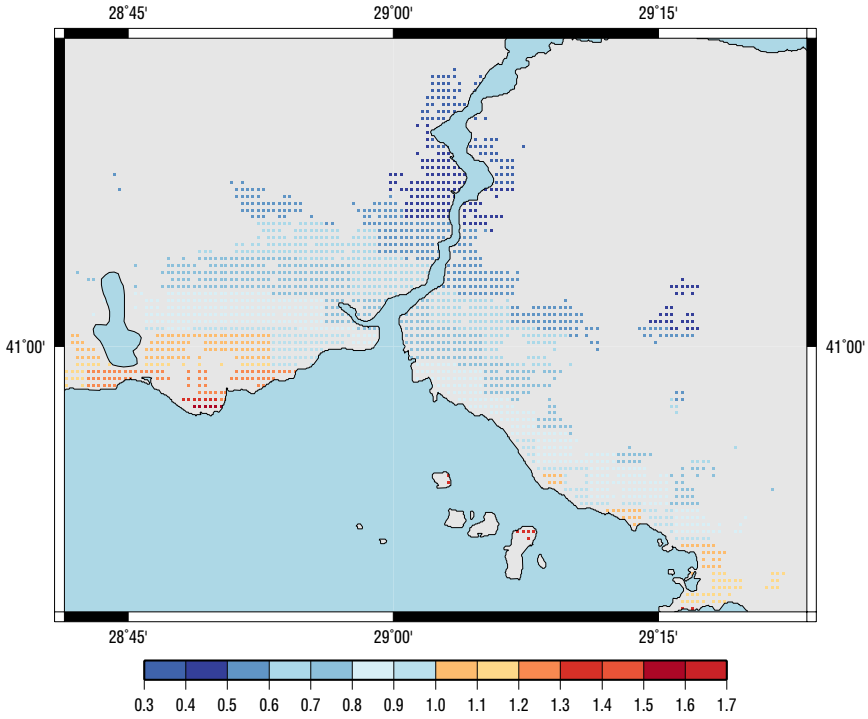

Figure 2.23 - Benefit-cost ratio map for mid-rise RC buildings built before the 1979 design code.

The benefit-cost ratio map revealed a region close to the location of the fault sources, where subjecting the existing buildings to a seismic retrofitting intervention would be economically advantageous, as the savings due to having a more adequate seismic design would overcome the cost of retrofitting.

2.7. Final Remarks

An open-source software capable of computing seismic hazard and risk was presented, with focus given to the risk component. Currently, OpenQuake is comprised by five main calculation workflows. Two capable of computing loss and damage distribution due to single events, two with the purpose of estimating probabilistic seismic risk considering all possible events within a region for a given time span, and a last one that uses loss exceedance curves to carry out retrofitting benefit-cost analysis. Notwithstanding the usefulness of such features, it is recognized that other functionalities still need to be explored, such as the application of analytical methodologies for the loss estimation or the consideration of networks.

Due to its transparent, modular and test-driven development philosophy, OpenQuake aims to be a community effort in which anyone can contribute with their

own methods and formulae. This differs from traditional practice, where a closed "enterprise" development tends to be followed, even if the source code is eventually openly released.

Chapter 3

Evaluation of Analytical Methodologies used to Derive Vulnerability Functions

Silva, V., Crowley, H., Pinho, R., Varum, H. and Sousa, R. (2013) "Evaluation of analytical methodologies to derive vulnerability functions". *Earthquake Engineering and Structural Dynamics*, in review.

3.1. Summary

The recognition of fragility and vulnerability functions as a fundamental tool in seismic risk assessment has led to the development of more and more complex and elaborate procedures for their computation. Although these functions have been traditionally produced using observed damage and loss data, more recent studies propose the employment of analytical methodologies as a way to overcome the frequent lack of post-earthquake data. The variation of the structural modelling approach on the estimation of building capacity has been the target of many studies in the past; however, its influence on the resulting vulnerability model for classes of buildings, the impact in loss estimations or propagation of the uncertainty to the seismic risk calculations has so far been the object of limited scrutiny. In this chapter, an extensive study of static and dynamic procedures for estimating the nonlinear response of buildings has been carried out in order to evaluate the impact of the chosen methodology on the resulting capacity, fragility, vulnerability and risk outputs. Moreover, the computational effort and numerical stability provided by

each approach has been evaluated and conclusions drawn regarding the optimal balance between accuracy and complexity.

3.2. Introduction

Fragility functions, a fundamental component in the process of assessing seismic risk, can be defined as the probability of exceeding a set of limit states given a certain level of ground motion. Building damage data from past earthquakes can be used to derive these types of functions (e.g. Sabetta *et al*., 1998; Rossetto and Elnashai, 2003; Rota *et al.,* 2008). However, empirical methodologies can have some disadvantages such as the subjectivity in allocating each building to a damage state, or the lack of accuracy in the determination of the ground motion affecting the region. Furthermore, there are only a few dozen places in the world where post-earthquake damage data has been collected from a number of buildings large enough to permit the development of reliable vulnerability functions (i.e. loss ratios, such as the ratio of cost of repair to cost of replacement, for a set of intensity measure levels). To overcome these limitations, analytical methodologies can be employed in either a single structure that is believed to be representative of a class of buildings, or a set of randomly generated buildings, modelled using structural analysis techniques, and subjected to specific lateral loading patterns or accelerograms (e.g. Singhal and Kiremidjian, 1997; Dumova-Jovanoska, 2004; Akkar *et al*., 2005; Erberik, 2008).

As discussed by Rosetto and Elnashai (2005), there is no unique methodology for the development of fragility functions and therefore, the resulting curves will be conditional on the assumptions and techniques followed within the selected methodology. These discrepancies due to the different approaches will consequently introduce differences in the risk assessments, even when considering the exact same region, seismicity and types of structures (Strasser *et al.,* 2008). Despite the existence of various studies that have evaluated the differences in the seismic response of buildings provided by alternative methodologies (e.g. Chopra and Goel, 2000; Dolsek and Fajfar, 2005; Casarotti *et al.*, 2009), the impact of this epistemic uncertainty in the computation of fragility functions and estimation of seismic risk has been the subject of reduced investigation.

The various analytical methodologies for structural assessment can be categorized in two main groups: nonlinear dynamic analysis and nonlinear static analysis, each one having its own strengths and shortcomings. The main advantage in employing nonlinear dynamic analysis is certainly the fact that the actual dynamic phenomenon is reproduced by applying an acceleration time history at the base of the structure, leading in theory to more accurate results. However, the intrinsic modelling complexity (e.g. hysteric response models, equivalent viscous damping) combined with the heavy computational effort, is often impractical, thus favouring the employment of simpler methods, comprising nonlinear static analysis (Antoniou and Pinho, 2004a). In this second approach, pushover curves are computed and used to estimate the maximum displacement response experienced by the structure for a given ground motion record. The main drawback of this simplified methodology lies with the assumption that the structural response obtained from horizontal static loading is representative of the one attained in the dynamic analysis.

In this study, several analytical methodologies are used to derive fragility functions for the same structural typology. A number of static approaches are investigated herein based on conventional and adaptive pushover analyses together with nonlinear static procedures (e.g. Capacity Spectrum Method (ATC-40, 1996), Displacement Coefficient Method (FEMA-440, 2005), N2 Method (Fajfar, 1999)), using hundreds of ground motion records, to derive fragility functions for different levels of ground motion (intensity measure levels). Then, dynamic analysis is used as the baseline method in this sensitivity study, to yield conclusions regarding the relative accuracy of each method. Each set of fragility functions is transformed into vulnerability functions (i.e. probability of loss for a given level of ground motion) by calculating the mean damage ratio (i.e. ratio of cost of repair to cost of replacement) for a number of intensity measure levels. In all methods, hundreds of 2D reinforced concrete bare frames have been simulated using a Monte Carlo approach based on the variability in the material and geometric properties of real buildings. In this study, advantage was taken of the availability of detailed characteristics of reinforced concrete buildings in Turkey assembled by Bal *et al.* (2008b).

3.3. Description of the Framework

For the purposes of this study, a comprehensive probabilistic framework was developed and its architecture is schematically represented in Figure 3.1.

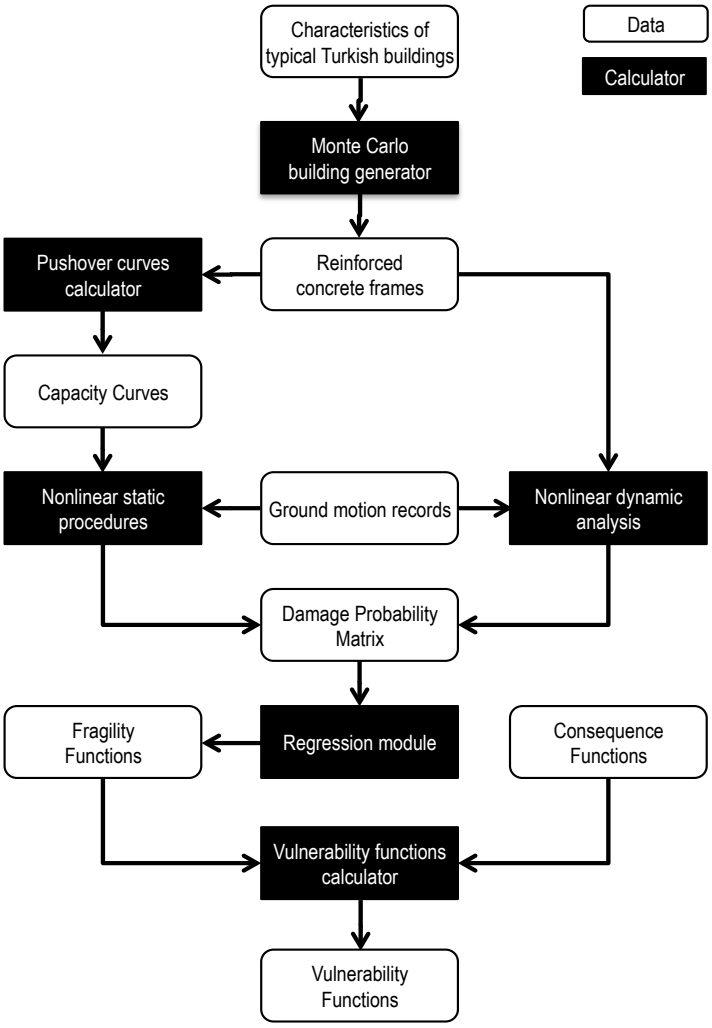

Figure 3.1. Scheme of the developed framework.

Within this framework, regardless of the chosen analytical methodology, the process of computing fragility curves always starts with the generation of a population of 2D Reinforced concrete frames through Monte Carlo simulation. Then, the sample of synthetic frames is subjected to a set of ground motion records through the use of either static or dynamic analysis. In the static analysis, a pushover curve is generated for each frame and transformed into the capacity curve of the equivalent SDOF system. Then, for each capacity curve, the nonlinear target displacement for a set of ground motion records is estimated, using a Nonlinear Static Procedure (NSP). The target displacement for each ground motion record is

employed to allocate each frame in a damage state, according to limit state criteria. In the dynamic analysis each frame is assigned a global damage state based on the maximum top displacement registered during the nonlinear time history analysis, which is again compared with the limit state displacements. Thus, for each record, the number of frames in each damage state will be obtained. This distribution of buildings in each damage state can be organized in a damage probability matrix, with a number of columns equal to the number of ground motion records and a number of rows equal to the number of damage states. Regression analysis (mean least squares method) can then be applied to this data to fit a lognormal curve for each limit state (leading to a fragility curve). All the fragility functions were derived using spectral acceleration for the fundamental period, $Sa(T_{el})$, which is an intensity measure type capable of providing a good correlation to building damage (Shome *et al.*, 1998; Bommer *et al.*, 2002). Each set of fragility functions has been combined with a consequence model (relating physical damage to percentage of loss) to produce a vulnerability model.

Regarding the damage criterion adopted in the present study, as discussed in Akkar *et al.* (2005), there are several options regarding criteria to allocate buildings to a damage state. These may include the maximum roof displacement, inter-storey drift ratio, steel or concrete strain level, maximum base shear, etc. Each option will naturally lead to different damage distributions, and consequently, different fragility functions. The influence of these criteria has been discussed in previous studies (Priestley, 1998) and will not be further investigated in this work. In this study, the maximum top displacement has been used to identify the threshold between each damage state, as described below:

- Limit state 1: top displacement when 75% of the maximum base shear capacity is achieved;
- Limit state 2: top displacement when the maximum base shear capacity is achieved;
- Limit state 3: top displacement when the base shear capacity decreases 20%.

Until limit state 1 the structure can be assumed to have none to slight damage; between limit state 1 and 2 the structure is presumed to have moderate damage; extensive damage occurs between limit state 2 up to 3; and collapse is achieved when limit state 3 is exceeded. It is recognized that the maximum top displacement

is a very simplified criterion to allocate buildings to a damage state, and that the findings from this study should be tested against results using other limit state criteria. The influence of this aspect in the development of fragility/vulnerability functions is the subject of another on-going investigation.

3.3.1. Generation of Synthetic RC frames

In all methods applied herein, hundreds of 2D reinforced concrete bare frames have been simulated using a Monte Carlo approach based on the variability in the material and geometric properties of real typical Turkish buildings gathered by Bal *et al.* (2008b). In the latter work, hundreds of drawings from buildings located in the Marmara region were used to measure several geometrical properties. Then, for each property, the statistical parameters from the probabilistic distribution that provided the best fit were calculated. With regards to the steel and concrete material properties, Bal *et al.* (2008b) took advantage of some existing studies from Akyuz and Uyan (1992) and Bal and Yildiz (2005).

In order to maintain the computational effort at a reasonable level, a single type of frame was considered, with 4 storeys and 3 bays, as demonstrated in Figure 3.2.

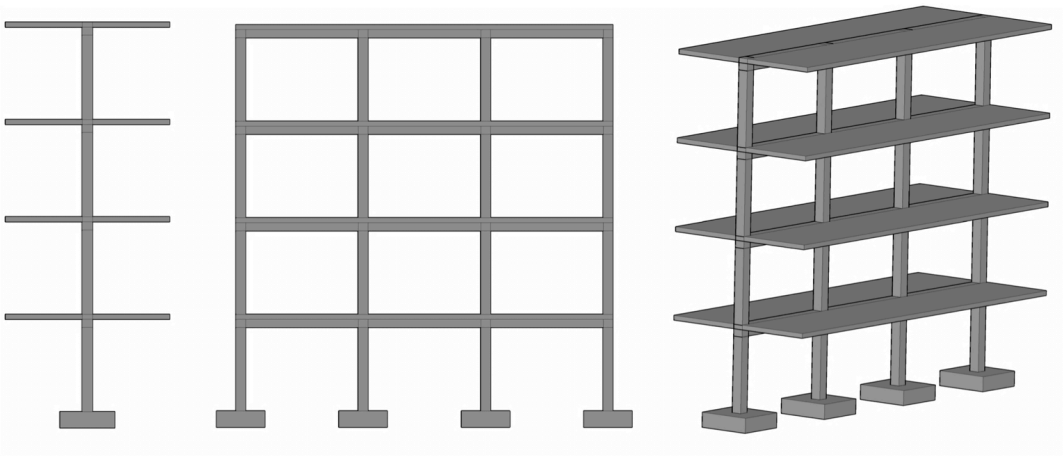

Figure 3.2. Schematic view of the RC frame model: front (left), side (centre) and isometric view (right).

A Matlab[20] script was developed to individually produce and design each frame. In a first phase, controlled Monte Carlo simulation is used to randomly sample several parameters based on the probabilistic distributions proposed by Bal *et al*. (2008b). These parameters and the associated statistical model are described in Table 3.1.

Table 3.1. Probabilistic distributions of the material and geometric properties.

Parameter	Mean	COV	A*	B*	Type of distribution
Steel modulus (GPa)	210	5%	-	-	Normal
Steel yield strength (MPa)	371.1	24%	-	-	Normal
Concrete strength (MPa)	16.7	50%	2	40	Gamma
Regular height (m)	2.84	8%	-	-	Lognormal
Ground/regular height ratio	1.13	14%	1	1.4	Exponential
Beam length (m)	3.37	38%	-	-	Gamma
Column depth (m)	0.49	30%	0.4	1	Lognormal

*A and B indicate the lower and the upper bounds respectively of the truncated distribution.

Each parameter was sampled independently (without correlation), though for the bay lengths within a given frame, a correlation factor of 0.7 was used, to avoid the generation of highly irregular structures. Bal *et al*. (2008b) also suggested probabilistic distributions for the beam depth, but no information has been provided with regards to the correlation between the depth and length of the beams. Thus, independently sampling these two parameters could lead to unrealistic situations (e.g. very long beams with a small depth).

Once the set of parameters for a given frame was sampled, an automatic process was triggered to calculate beam depth and area of steel of each structural element, for gravity loads only, as was the common practice for many existing buildings (prior to the implementation of the 1998 Turkish seismic design code). The maximum bending moment (M_{max}) was computed for each beam based on the appropriate dead and live loads and the following formula was employed for the beam depth calculation:

$$D_{beam} = \sqrt{\frac{M_{max}}{0.15 \times W_{beam} \times f_c}} \tag{3.1}$$

where W_{beam} stands for the beam width and f_c represents the concrete compressive strength.

The maximum negative and positive bending moment were used respectively to estimate the top and bottom reinforcement steel area (A_s) of the beam section using the following classic formulae:

$$M_{red} = \frac{M_{max}}{W_{beam} \times D_{beam}^2 \times f_c} \qquad w = 0.973\left(1 - \sqrt{1 - 2.056 \times M_{red}}\right) \tag{3.2, 3.3}$$

$$A_s = \frac{w \times D_{beam} \times W_{beam} \times f_c}{f_y} \tag{3.4}$$

where f_y represents the steel yield strength. For what concerns the reinforcement steel in the columns, the following formula was used:

$$A_s = \frac{N - 0.85 A_c \times f_c}{f_y} \tag{3.5}$$

where N and Ac stand for the axial load and area of concrete in the column section respectively. A minimum criterion for the area of steel of at least 1% of the concrete sectional area was established. Once the areas of steel of the beams and columns were computed, a number of reinforcement bars capable of providing the previously estimated amount of steel were attributed to each element, completing the design of the frames.

3.3.2. Numerical Modelling of the RC Frames

In order to use the randomly generated RC frames in the various analyses, the developed framework was connected to OpenSEES [21], a platform for structural modelling and assessment. Each frame was modelled using a 2D environment, thus considering only 3 degrees of freedom per node (2 translational and 1 rotational) and all the columns and beams were modelled as force-based elements, using fibre sections in order to capture the nonlinear behaviour of the materials, with a mesh of 5x40 fibres. The unconfined and confined concrete constitutive relationships were assumed to follow the Kent-Park model modified by Scott *et al*. (1982) with a confinement coefficient equal to 1.15, whereas the behaviour of the steel was represented by the model suggested by Giuffrè and Pinto (1970). The gravity loads were applied in the structure in the form of uniformly distributed loads on the beams, and P-delta effects were considered.

3.3.3. Ground Motion Input

The selection of the set of accelerograms used for this study was undertaken based on local seismic hazard properties such as range of magnitude and peak ground acceleration, most common fault failure mechanism, frequency content, duration and epicentral distance. This use of suites of accelerograms allows the consideration of the influence of the record-to-record variability of the seismic input on the structural response. Currently there appear to be no formal guidelines for the selection of ground motion records to use in fragility curves generation. Many

authors choose to gather sets of natural or synthetic records that are subsequently scaled to cover the range of ground motion levels that might occur in the region of interest (e.g. Singhal and Kiremidjian, 1997; Dumova-Jovanoska, 2004; Watson-Lamprey and Abrahamson, 2006; Katsanos *et al*., 2010). However, often the scaling process selected does not introduce changes in other properties of the records such as the frequency content or event duration, which are inherent to the magnitude of the event.

There have been a number of recent advances in the selection of ground motion records to ensure compatibility with the seismic characteristics of the region, whilst also maintaining the variability (Jayaram *et al*., 2011). It is intended to investigate the influence of using such selection methods on the development of vulnerability functions, but for the purposes of the current research, a decision was taken to employ natural ground motion records due to the wide availability of strong motion databases (e.g. ITACA [22] (Italy), K-Net/NIED [23] (Japan), ISMN [24] (Iran), GeoNet [25] (New Zealand), Daphne [26] (Turkey), ESD [27] (Europe), PEER [28] (global), COSMOS [29] (global)) with records that can be applicable to the region from where the characteristics of the RC buildings were compiled. For the selection of the accelerograms, the work of Kalkan *et al*. (2008), in which a probabilistic seismic hazard analysis for the Marmara region was performed, was used to identify the following characteristics of the seismic events:

- Range of magnitude: 6.0 to 7.4 Mw;
- Range of distance: 15 to 150 km;
- Rupture mechanism: strike-slip.

A decision was also made not to include records that were at a distance lower than 15 km, with the purpose of avoiding accelerograms with near field effects, where it has been observed that the inelastic spectral displacements can be much larger, and with higher variability than the respective elastic response (Baez and Miranda, 2000). Another factor that was taken into account was the frequency range featured by each accelerogram. Records that did not cover the full frequency range within this study (i.e. spectral ordinates between 0.05 and 5 seconds) were also excluded. About 100 ground motion records were finally extracted from the ESD [27] and PEER [28] databases. Histograms illustrating the variation of PGA, PGV and Arias Intensity of the selected records are presented in Figure 3.3.

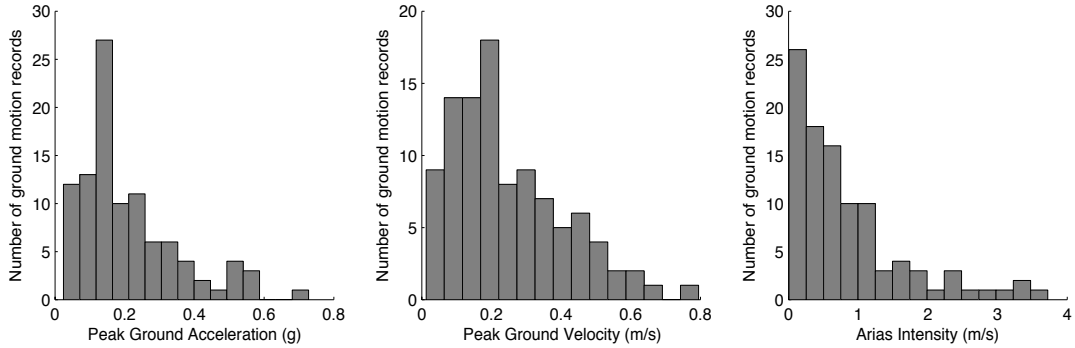

Figure 3.3 - Distribution of the PGA (g), PGV (m/s) and Arias Intensity (m/s) for the set of ground motion records.

In order to understand the variability in the spectral shape and frequency content, the elastic acceleration spectra for 5% viscous damping were evaluated, as depicted in Figure 4.

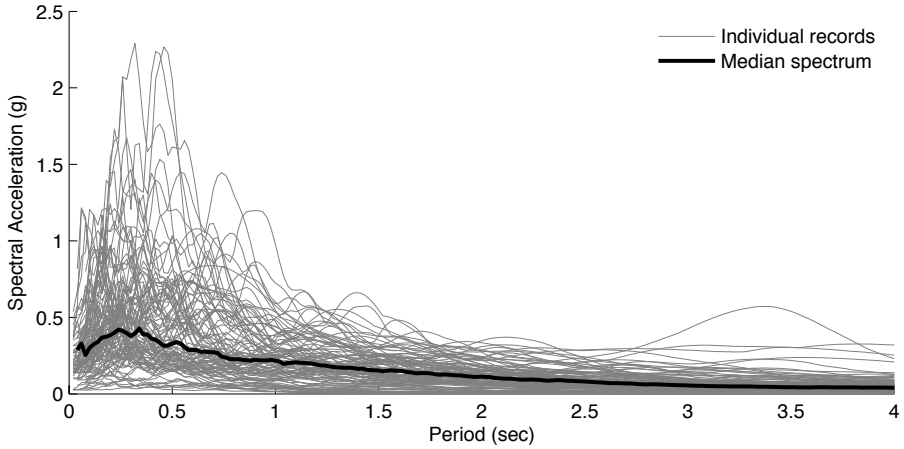

Figure 3.4 – Acceleration spectra (g) versus period of vibration (sec) for the set of ground motion records.

3.4. Pushover curves

This Section presents the derivation of pushover and capacity curves (in terms of spectral acceleration and spectral displacement) for one hundred randomly generated frames using a number of different methodologies and assumptions. Further discussion of the variability in the capacity curves from the different procedures is presented in Section 6.1.

3.4.1. Conventional Pushover

A conventional pushover curve describes the relation between base shear and top displacement of a multi-degree of freedom (MDOF) structure when an

increasing lateral force is applied. The use of pushover curves in earthquake engineering somewhat originates from the pioneering work or Gulkan and Sozen (1974), in which simplified SDOF models were created to represent MDOF structures and used in nonlinear static analysis. This methodology has many advantages and disadvantages that have been the focus of several studies for the past years, in particular that by Krawinkler and Seneviratna (1998). The latter stated that such approach is a valuable tool in vulnerability assessment due to its simplicity, ease of use and reduced running time, despite its inability to reproduce certain phenomena such as viscous damping, strength deterioration or pinching effect. These authors also highlighted the constant loading pattern as one of the weakest points of this method, as it ignores some deformation modes that are propelled by dynamic response and inelastic response characteristics. This invariant loading pattern usually adopts a uniform, triangular or a first deformation mode shape. In this study, the first two patterns were considered but not the latter since the regularity of the RC frames led to a first deformation mode approximately of a triangular shape, thus leading to the same structural behaviour. Instead, a decision was taken to apply a modal loading pattern with the resulting shape from the contribution of the first 3 modes of vibration.

The transformation of the pushover curve from the MDOF system to a capacity curve in terms of spectral acceleration (Sa) versus spectral displacement (Sd) for an equivalent SDOF structure can be carried out in various ways, under the condition that the deformed shape of the structure is not significantly altered during the dynamic loading. The top displacement has been converted to Sd herein based on the participation factor of the first mode of vibration, while the base shear has been reduced to Sa using the same factor and the first modal mass. One hundred capacity curves were derived for the randomly generated RC frames and the results are presented in Figure 3.5, along with the mean and median capacity curves. A single RC frame was also modelled using the mean material and geometric properties (see Table 3.1), and the resulting capacity curve is also presented in the same figure.

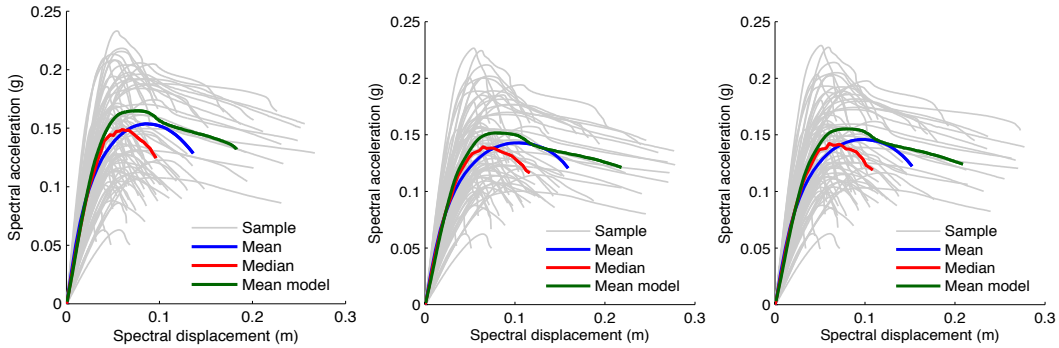

Figure 3.5. Capacity curves using a uniform (left), triangular (centre) and multi-modal (right) loading pattern.

These results show a very large dispersion in the capacity of the RC frames, strengthening the idea that using a single or few structures to represent a building typology might be insufficient to properly capture their characteristics. The mean limit state spectral displacements and accelerations in the capacity curves (i.e. the spectral ordinates at which each limit state is reached) considering all of the RC frames, are presented in Table 3.2 for the purpose of comparing the different load profiles that have been applied.

Table 3.2. Mean spectral displacement and acceleration for each limit state, per loading pattern.

	Uniform		Triangular		Multi-modal	
	Sd (m)	Sa (g)	Sd (m)	Sa (g)	Sd (m)	Sa (g)
Limit state 1	0.030	0.119	0.035	0.112	0.033	0.114
Limit state 2	0.064	0.158	0.080	0.149	0.072	0.151
Limit state 3	0.136	0.126	0.218	0.119	0.152	0.120

3.4.2. Adaptive Pushover

As an attempt to overcome some of the previously mentioned shortcomings of conventional pushover, several authors (Bracci et al., 1997; Elnashai, 2001; Antoniou and Pinho, 2004b) have developed adaptive or fully adaptive pushover procedures. These innovative techniques have the advantage of better accounting for stiffness degradation, influence of higher mode effects and spectral amplifications due to ground motion frequency content. In this method, instead of applying an invariant load vector, the structural properties of the model are evaluated at each step of the analysis, and the loading pattern is updated accordingly. In this way, the variation in the structural stiffness at different deformation levels, and consequently the system degradation and period elongation can be accounted for. The only apparent drawback of this methodology can be the

additional computation time required to assess the structural characteristics at every step.

In this study, a displacement based adaptive pushover (DAP - Antoniou and Pinho, 2004b) technique was used, in which a SRSS approach was employed in the modal combination to update the lateral load profile. It was decided that considering other modal combinations techniques such as CQC or ABSolute would not bring any benefit to this study since the RC frames are highly regular with periods of vibration for each mode that are sufficiently distinct from each other. One hundred capacity curves were derived for the randomly generated RC frames, as well as for the frame model with the mean characteristics. Figure 3.6 and Table 3.3 present these results considering the complete sample of RC frames.

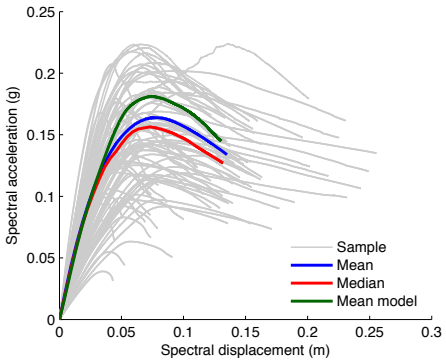

Figure 3.6. Capacity curves using DAP.

Table 3.3. Mean spectral displacement and acceleration for each limit state.

	Adaptive capacity curve	
	Sd (m)	Sa (g)
Limit state 1	0.038	0.133
Limit state 2	0.074	0.178
Limit state 3	0.131	0.142

A large scatter in the capacity of the RC frames is still observed but in this case the capacity curve obtained using the model with the mean characteristics is much closer to the mean of the capacity curves. In the work of Akkar *et al*. (2005), JICA (2002) and Bogaziçi (2002) the lateral capacity of common building typologies in Turkey (comparable to the one that is being considered herein) was evaluated and similar capacity curves were observed.

3.4.3. Convergence in the statistics

When using a Monte Carlo approach to randomly generate portfolios of buildings, it is important to ensure that convergence in the results is achieved. In the study presented herein it was necessary to understand how many RC frames would have to be generated, to ensure that additional specimens would not alter the statistics of the sample, within a certain tolerance. The level of variability in the capacity of the

randomly generated RC frames is obviously connected to the variability of the material and geometric properties used in the sampling process. Bal *et al*. (2008b) estimated that a minimum of 35 buildings would be required in order to have stability in the mean geometric properties. In the present study, 10.000 RC frames were used to estimate the mean capacity curve and due to the very large size of the sample, these statistics were assumed to provide the exact solution. Subsequently, a number of samples with increasing sizes (from 5 to 500) were produced and their mean capacity curves were compared with the results generated using the 10.000 RC frames. This process was repeated several times and, as shown in Figure 3.7, the variation of the mean error (i.e. the relative difference between the mean curve of each sample and the exact solution) for the uniform-based pushover curves is shown for 5 repetitions.

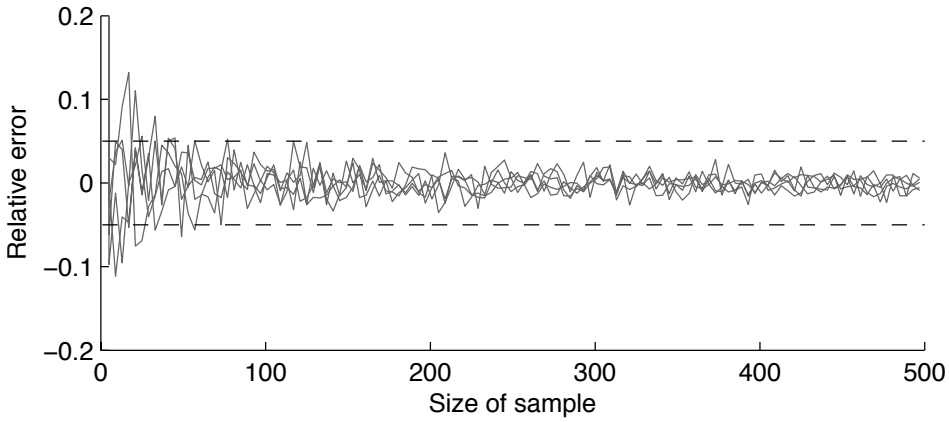

Figure 3.7 – Mean relative error as a function of the size of the sample, for 5 repetitions

As can be seen from Figure 3.7, every time that a sample of 100 RC frames is reached, no significant changes were observed in the mean results within a 5% tolerance. The same procedure was also repeated for the other types of pushover curves and an identical number of RC frames required to achieve convergence was obtained. Thus, throughout this study, a sample of 100 RC frames was always used to test each methodology.

3.5. Nonlinear static procedures

The so-called Nonlinear Static Procedures (NSP) represent a simplified approach for the assessment of the seismic behaviour of structures, included in guidelines such as the ATC-40 (1996) and FEMA-440 (2005) in the United States or the

Eurocode 8 (CEN, 2005) in Europe. In this study, four distinct methodologies were employed: the Capacity Spectrum Method (CSM) (ATC-40, 1996), the Coefficient Displacement Method (CDM) (FEMA-440, 2005), the N2 Method (Fajfar, 1999) and the Adaptive Capacity Spectrum Method (ACSM) (Casarotti and Pinho, 2007), which are further described in the following sections. These methodologies make use of capacity curves in terms of Sa versus Sd (i.e. the capacity of the equivalent SDOF). Each Nonlinear Static Procedure is employed to estimate the target displacement obtained for each ground motion record, and this level of displacement is used to allocate the building in a damage state (according to the limit state criteria define in section 2). This target displacement can be equated to the maximum top displacement that would be experienced by the equivalent SDOF structure in a nonlinear dynamic analysis. For each of the 100 randomly generated frames, this displacement is compared with the limit state displacements to identify the damage state of each frame. The distribution of buildings in each global damage state per ground motion record can then be used to derive a fragility function for each limit state by estimating the cumulative percentage of buildings exceeding each limit state and relating this to an intensity measure of the ground motion record. In this study the selected intensity measure type is spectral acceleration (in g) at the yield period of vibration. A lognormal distribution is then fit to the data using least squares regression leading to a logarithmic mean (λ) and a logarithmic standard deviation (ζ) for each fragility function.

Other NSPs such as the Modal Pushover Analysis (MPA) (Chopra and Goel, 2002) or the Adaptive Modal Combination Procedure (AMCP) (Kalkan and Kunnath, 2006) have not yet been considered. The main reason for this is that one of the main strengths of such methodologies is the consideration of the influence of higher modes of vibration, which is not relevant in this study, given the high level of regularity and number of storeys of the considered building typology.

3.5.1. Capacity Spectrum Method

The capacity spectrum method (CSM) was initially proposed by Freeman *et al*. (1975), and it represents a simplified methodology for many purposes such as the evaluation of a large inventory of buildings, assessment of new or existing structures or to identify the correlation between damage states and level of ground motion Freeman (2004). ATC-40 (1996) proposes three different procedures (A, B and C)

for the application of the Capacity Spectrum Method. However, procedure B adopts some simplifications that might not always be valid and procedure C has a very strong graphical component, making it difficult to program (Monteiro, 2011). Hence, procedure A, which is characterized by its intuitiveness and simplicity, was employed herein. This procedure iteratively compares the capacity and the demands of a structure, using a capacity curve (for the simplified SDOF) and a damped response spectrum, respectively. The ground motion spectrum is computed for a level of equivalent viscous damping that is estimated as a function of the displacement at which the response spectrum crosses the capacity curve, in order to take into account the inelastic behaviour of the structure. Iterations are needed until there is a match between the equivalent viscous damping of the structure and the damping applied to the spectrum. The final intersection of these two curves approximates the displacement response of the structure.

The initial proposal of this method was criticized by Fajfar (1999) and Chopra and Goel (2000), due to its tendency to underestimate the deformation of the structures. Thus, in FEMA-440 (2005), some modifications were proposed mainly regarding the calculation of the equivalent viscous damping, which were followed in this study. Another aspect worth further investigation in this method is how well the bilinear curves represent the yielding point for different response spectra, as this value is crucial for the calculation of the equivalent viscous damping.

ATC-40 (1996) defines the slope of the first segment of the bilinear curve based on the initial stiffness, which in order to respect the equal energy dissipated rule (i.e. the area under the capacity curve needs to be equal to the area under the bilinear curve), a yielding point located in the elastic portion of the capacity curve might be obtained. This misrepresentation of the yielding occurs mostly when combining this method with response spectra with low levels of ground motion. An alternative for this procedure has been proposed in FEMA-273 (1997), in which the slope of the first segment of the bilinear is computed based on the effective stiffness, allowing a more realistic shape of the bilinear curves. This aspect is shown in Figure 3.8 and Figure 3.9, where the same capacity curve was used against a weak (PGA=0.74 m/s^2) and a strong (PGA=1.42 m/s^2) accelerogram for each procedure.

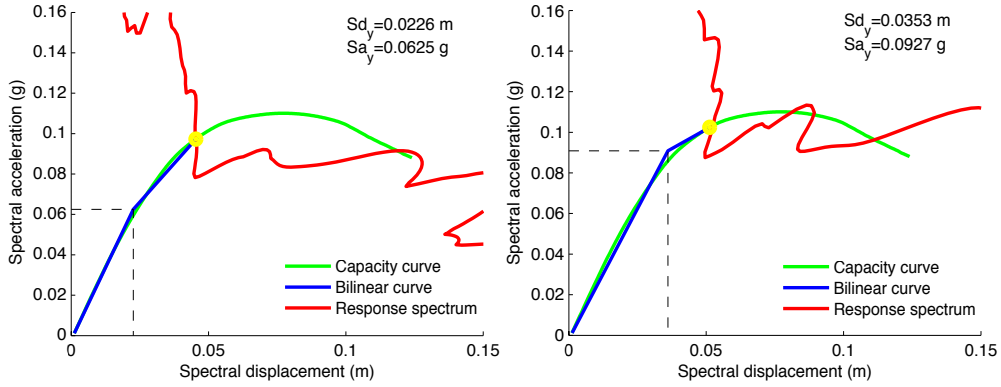

Figure 3.8 - Bilinear curves according to ATC-40 (left) and FEMA-273 (right) for a "weak" response spectrum.

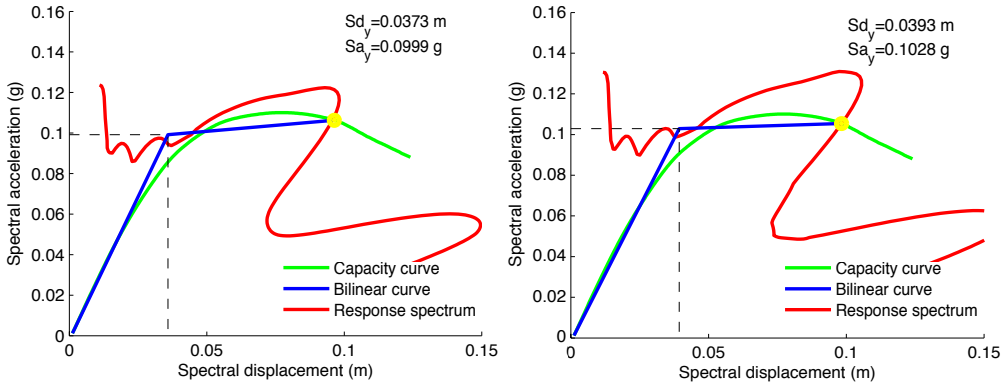

Figure 3.9 - Bilinear curves according to ATC-40 (left) and FEMA-273 (right) for a "strong" response spectrum.

A significant discrepancy is observed in the bilinear curves for the "weaker" response spectrum. In fact, in the case where the ATC-40 guidelines were followed, an equivalent viscous damping equal to 8.94% was obtained, whilst in the second case where the FEMA-273 was used, a lower equivalent damping of 5.91% was attained. This poor performance of the ATC-40 procedure for response spectra with low ground motion was also observed in the work of Lin *et al.* (2004). With regards to the second situation in which a stronger spectrum is employed, both methods seem to provide reasonable results (equivalent damping of 13.21% and 12.30% for ATC-40 and FEMA-273, respectively). Despite the fact that FEMA-273 recommendations seem to lead consistently to more reasonable results, it was decided to follow the ATC-40 procedure regarding the bilinearisation, in order to evaluate the practices that currently seem more common in use.

The capacity curves computed for all the RC frames, using the different pushover methods presented in the previous section, were used with this NSP to derive

fragility functions for each limit state, the lognormal parameters of which are presented in Table 3.4.

Table 3.4. Lognormal parameters of the fragility functions produced using the CSM.

	Uniform		Triangular		Modal		DAP	
	λ (g)	ζ (g)	λ (g)	ζ (g)	λ (g)	ζ (g)	λ (g)	ζ (g)
Limit state 1	-2.071	0.225	-2.121	0.261	-2.169	0.259	-2.070	0.317
Limit state 2	-1.439	0.323	-1.364	0.254	-1.438	0.285	-1.327	0.291
Limit state 3	-1.084	0.575	-1.043	0.508	-1.043	0.552	-0.975	0.408

3.5.2. Displacement Coefficient Method

The Displacement Coefficient Method (DCM) represents a methodology for the assessment of the seismic response of a building, proposed initially in ATC-40 (1996) and further developed in FEMA-440 (2005). This method consists of modifying the elastic spectral displacement for the effective fundamental period (extracted from the capacity curve), according to four coefficients. These four parameters have the purpose of introducing the effect of the difference in the response of the SDOF and the MDOF systems (C_0), the variation between elastic and inelastic response (C_1), possible degradation of stiffness and energy dissipation (C_2) and the influence of P-delta effects (C_3). The resulting maximum displacement can be determined through the following formula:

$$\delta_t = C_0 C_1 C_2 C_3 Sa \frac{T_e^2}{4\pi^2} \tag{3.6}$$

where Sa stands for the spectral acceleration response for the elastic period (T_e). These coefficients are tabled in FEMA-440 and have been derived based on statistics from dynamic analysis of SDOF models with various characteristics. It can be applied to new or existing buildings, that are regular and do not have adverse torsional or multimode effects. The capacity curves computed for all the RC frames, using the different pushover methods presented in the previous section, were used with this NSP to derive fragility functions for each limit state, the lognormal parameters of which are presented in Table 3.5.

Table 3.5. Lognormal parameters of the fragility functions produced using the DCM.

	Uniform		Triangular		Modal		DAP	
	λ (g)	ζ (g)	λ (g)	ζ (g)	λ (g)	ζ (g)	λ (g)	ζ (g)
Limit state 1	-2.133	0.269	-2.055	0.194	-2.126	0.296	-2.080	0.292
Limit state 2	-1.424	0.376	-1.384	0.383	-1.394	0.376	-1.471	0.362
Limit state 3	-0.932	0.607	-0.856	0.673	-0.882	0.660	-0.823	0.526

3.5.3. N2 Method

Fajfar (1999) firstly proposed this simplified nonlinear procedure for the estimation of the seismic response of structures. It is somehow similar to the Capacity Spectrum Method as it also uses capacity curves and response spectra, but it differs in the fact that it uses inelastic spectra rather than elastic overdamped spectra for an equivalent viscous damping and period. Moreover, it also has the distinct aspect of assuming an elasto-perfectly plastic force-displacement relationship in the construction of the bilinear curve.

To estimate the target displacement within this methodology, it is necessary to assess whether the SDOF structure is in the short-period or medium/long-period ranges. If the structure is in the latter category, it is assumed that the target displacement is equal to the elastic spectral displacement for the fundamental period of the idealized SDOF. If on the other hand it is located in the short-period range, a procedure is carried out to check if the capacity of the SDOF at the yielding point (taken from the bilinear curve) is lower than the spectral acceleration response for the same period. If this is verified, then the structure is assumed to have an elastic response and once again, the target displacement will be equal to the elastic spectral displacement for the fundamental period. In case the capacity is higher than the response for the yielding point, the structure is assumed to have an inelastic response and the following formula is employed to determine the target displacement:

$$\delta_t = \frac{Sd(T_{el})}{q_u}\left(1 + (q_u - 1)\frac{T_C}{T_{el}}\right) \geq Sd(T_{el}) \tag{3.7}$$

where $Sd(T_{el})$ stands for the spectral displacement for the fundamental period of the idealized SDOF (T_{el}), T_C stands for the corner period and q_u represents the ratio between the spectral acceleration for T_{el} and the acceleration at the yielding point. Considering the capacity curves computed for all the RC frames for the different pushover methods presented in the previous section, this NSP was used to derive fragility functions for each limit state, the lognormal parameters of which are presented in Table 3.6.

Table 3.6. Lognormal parameters of the fragility curves produced using the N2 Method.

	Uniform		Triangular		Modal		DAP	
	λ (g)	ζ (g)	λ (g)	ζ (g)	λ (g)	ζ (g)	λ (g)	ζ (g)
Limit state 1	-2.133	0.313	-2.047	0.193	-2.061	0.235	-2.112	0.292
Limit state 2	-1.477	0.359	-1.432	0.354	-1.414	0.353	-1.440	0.346
Limit state 3	-0.941	0.627	-0.864	0.676	-0.878	0.661	-0.813	0.536

3.5.4. Adaptive Capacity Spectrum Method

This NSP proposed by Casarotti and Pinho (2007) allows the estimation of the seismic response of structures using a fully adaptive perspective. Pushover curves are generated following a displacement-based adaptive procedure (as described in section 3.2), but instead of using any elastic or inelastic mode of vibration to convert the MDOF pushover curve to the equivalent SDOF system, the deformed shape at every step is used, leading to a more realistic equivalent capacity curve. Then, an iterative process identical to that described for the Capacity Spectrum Method has been employed to estimate the target displacement. This method also uses equivalent viscous damping to take into account the nonlinear behaviour of the structure, however, unlike CSM, no specific damping model has been suggested. From the many existing damping models, it was decided to apply the one by Priestley *et al*. (2007), as it seemed to provide more accurate results in a parametric study carried out by Casarotti *et al*. (2009). The lognormal parameters of the fragility functions computed combining this method with the previously presented capacity curves for the adaptive pushover method are presented in Table 3.7. In Figure 3.10, the scatter used to derive each fragility function is displayed along with the associated curve. Each point represents the cumulative percentage of buildings in a given damage state, for a certain ground motion record. For example, a given record ($Sa_{el} = 0.14g$) led to 88% of the frames that exceeded the first limit state, 30% that exceeded the second limit state and 4% that collapsed (exceeded limit state 3).

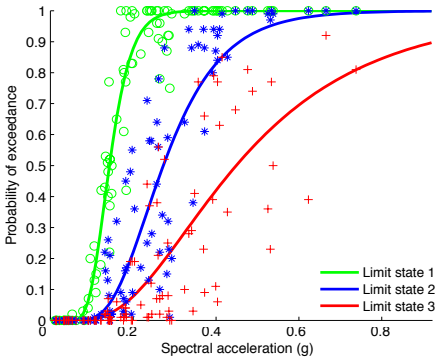

Figure 3.10. Fragility functions using ACSM.

Table 3.7. Lognormal parameters of the fragility functions using ACSM.

	λ (g)	ζ (g)
Limit state 1	-2.065	0.289
Limit state 2	-1.419	0.422
Limit state 3	-0.882	0.566

3.6. Nonlinear dynamic analysis

Nonlinear dynamic analysis, when adequately used, tends to be considered as the most accurate and reliable methodology to estimate the seismic response of structures. The requirements around this approach in comparison to the previously presented NSPs are considerably more demanding, mainly on the level of detail of the model, the necessity to represent the masses in the structure, the need to model the equivalent viscous damping, the definition of time integration algorithms and the treatment of the ground motion input. This higher level of complexity comes also with a significant increase in the computation time, and frequent difficulties with convergence in the analyses.

In this study, nonlinear time history analyses were performed for the one hundred randomly generated frames, using the set of ground motion records presented in Section 2.3. As mentioned previously, the maximum roof displacement for each record was compared with the limit state displacements to identify the damage state of the structure. In order to substantially reduce the computation time of each analysis, these accelerograms were filtered and trimmed based on the 5% maximum PGA threshold, as discussed by Bommer and Pereira (1999). The resulting fragility functions are presented in Figure 3.11, and their lognormal parameters are given in Table 3.8.

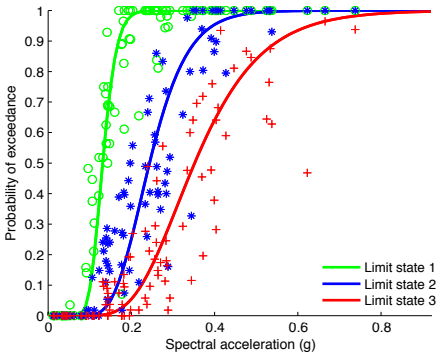

Figure 3.11. Fragility functions using dynamic analysis.

Table 3.8. Lognormal parameters of the fragility functions using nonlinear dynamic analysis.

	λ (g)	ζ (g)
Limit state 1	-2.098	0.298
Limit state 2	-1.452	0.354
Limit state 3	-0.833	0.514

3.7. Discussion of results

3.7.1. Variability in the Capacity Curves

With regards to the variation of the capacity curves based on their method of calculation, an underestimation of the capacity in most of the randomly generated RC frames was consistently observed when employing conventional pushover procedures, in comparison with the adaptive pushover technique. This behaviour is probably due to the fact that in the former approach, the structures may be forced to deform in an "unnatural" manner. It was also noticed that the capacity curve generated using the RC frame following the mean geometric and material properties was significantly different from the mean of the capacity curves from the randomly generated frames. In fact, this capacity curve presented a considerably higher displacement capacity, which suggests that if such output would be used in seismic risk assessment, the losses could be underestimated. This observation is conditional on the probabilistic distribution of the geometric and material properties proposed by Bal *et al.* (2008b) and therefore, it should not be generalized to other building typologies.

Regarding the differences due to the application of the different loading patterns, it was observed that a uniform load led to higher values of base shear capacity, whilst greater displacement capacity was attained when employing a triangular load. Such results are in agreement with other studies (Antoniou and Pinho, 2004a; Papanikolau and Elnashai, 2005). Applying a loading pattern based on the contribution of the first three modes of vibration generated intermediate results, as

expected. With regards to the variations between conventional and adaptive techniques, it is possible to conclude that the latter approach led to slightly superior base shear capacity and significantly higher top displacements in more cases. These differences in the statistics will naturally have a direct impact on the associated fragility functions, as explained in the following section. In Figure 3.12, the mean and median capacity curves are presented, as well as the capacity curve generated using the mean characteristics of the RC frames.

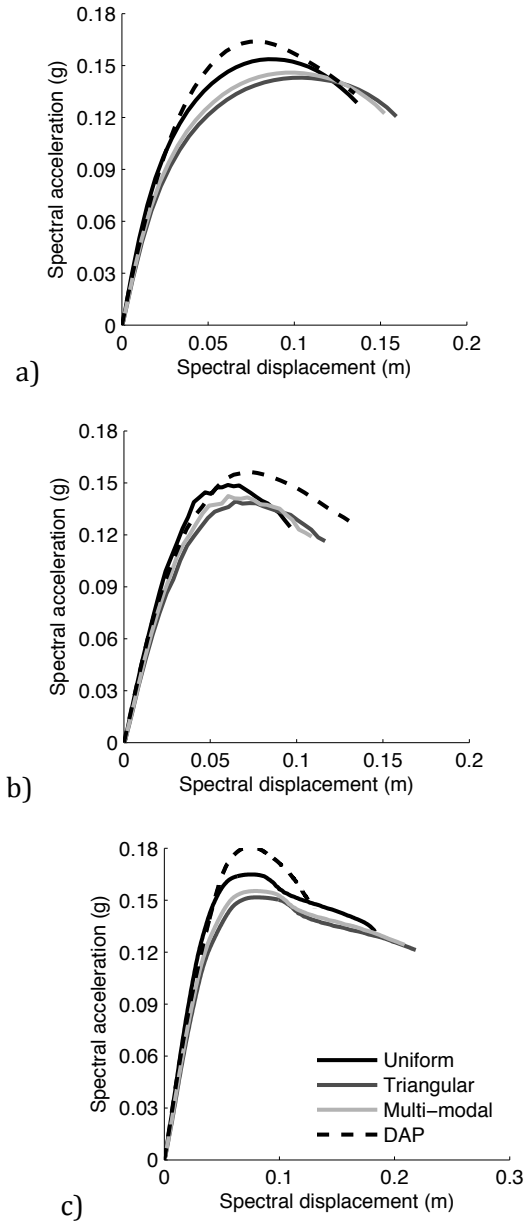

Figure 3.12 – Mean (a) and median (b) capacity curves and capacity curves generated using the mean characteristics of the RC frames (c).

3.7.2. Variability in the Fragility Functions

In order to investigate the impact of the various pushover methods and NSPs on the fragility, all of the computed functions were plotted together, as illustrated in Figure 3.13. For the sake of clarity, these curves were separated according to the limit states.

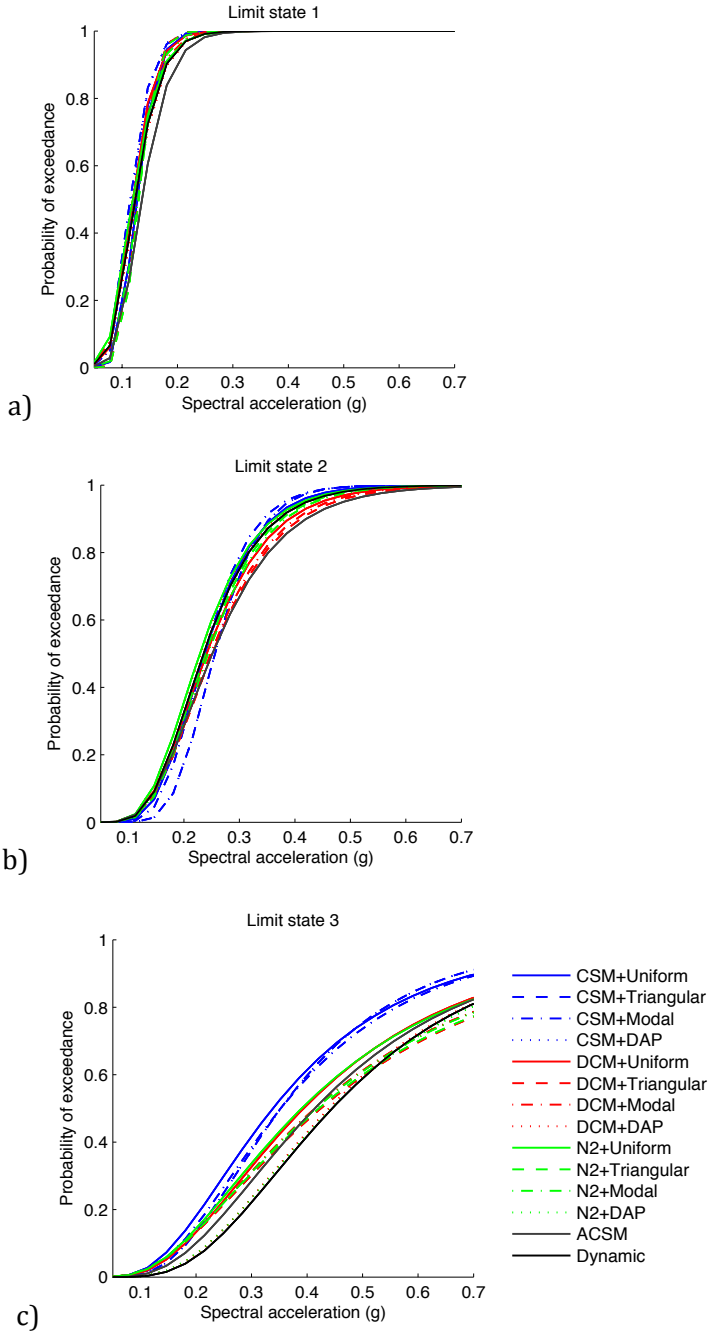

Figure 3.13 – Fragility curves for the first (a), second (b) and third (c) limit states, according to the different methodologies.

The evaluation of the curves between different limit states shows higher variations for the third limit state, and a lower sensitivity regarding the chosen methodology for the first limit state. This aspect is probably due to the fact that for low levels of ground motion (when only limit state 1 is reached), the response of the RC frames is mainly elastic. Therefore, each methodology provides similar results. For stronger levels of ground motion, damage begins to occur (reaching limit state 2 and 3) and the RC frames starts to deform nonlinearly. The manner in which each combination of methodology estimates the nonlinear response is different, and consequently so will be the associated results.

Regarding the differences in the fragility curves between the various combinations of methodologies, it is fair to state that the Capacity Spectrum Method systematically overestimated the collapse (limit state 3) fragility, whilst the Displacement Coefficient Method + DAP and N2 + DAP provided results identical to those obtained using the nonlinear dynamic analysis.

3.7.3. Variability in the Vulnerability Functions

Each set of fragility functions was transformed into a vulnerability function (i.e. a probabilistic distribution of loss ratio given an intensity measure level). To do so, for a set of intensity measure levels, each fragility model was used to compute the percentage of buildings in each damage state and these results were multiplied by the associated damage ratios, according to a consequence model. These consequence models establish the relation between physical damage and the ratio between cost of repair and cost of replacement (herein called damage ratio), and can differ significantly based on the region, building typology and definition of damage states (e.g. Greece - Kappos *et al*., 2006; Italy - Di Pasquale and Goretti, 2001; Turkey - Bal *et al*., 2008b; California (HAZUS) - FEMA-443, 2003). The consequence model will naturally have a direct impact on the shape of the vulnerability function, as it defines the contribution of each damage state to the resulting loss ratio per intensity measure level. In Figure 3.14, the consequence models employed in this study are represented.

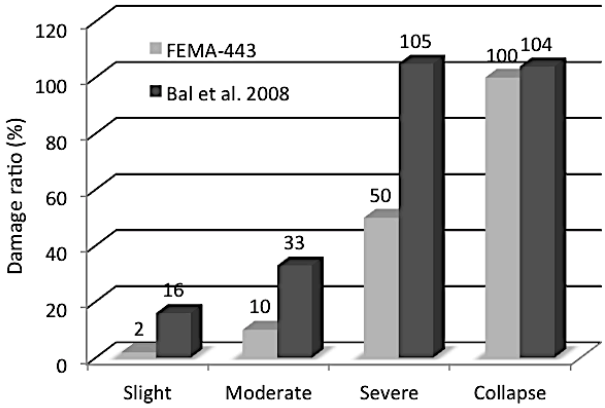

Figure 3.14 – Consequence model for buildings in California (HAZUS) (FEMA-443, 2003) and Turkey (Bal *et al*., 2008b).

The resulting vulnerability functions from the combination of the different pushover techniques with the various NSPs are presented in Figure 3.15 (with the HAZUS consequence model) and in Figure 3.16 (with the Turkish consequence model). The vulnerability curve resulting from the nonlinear dynamic analysis has also been included for comparison purposes. For the sake of clarity, the vulnerability functions have been organized according to the nonlinear static procedure.

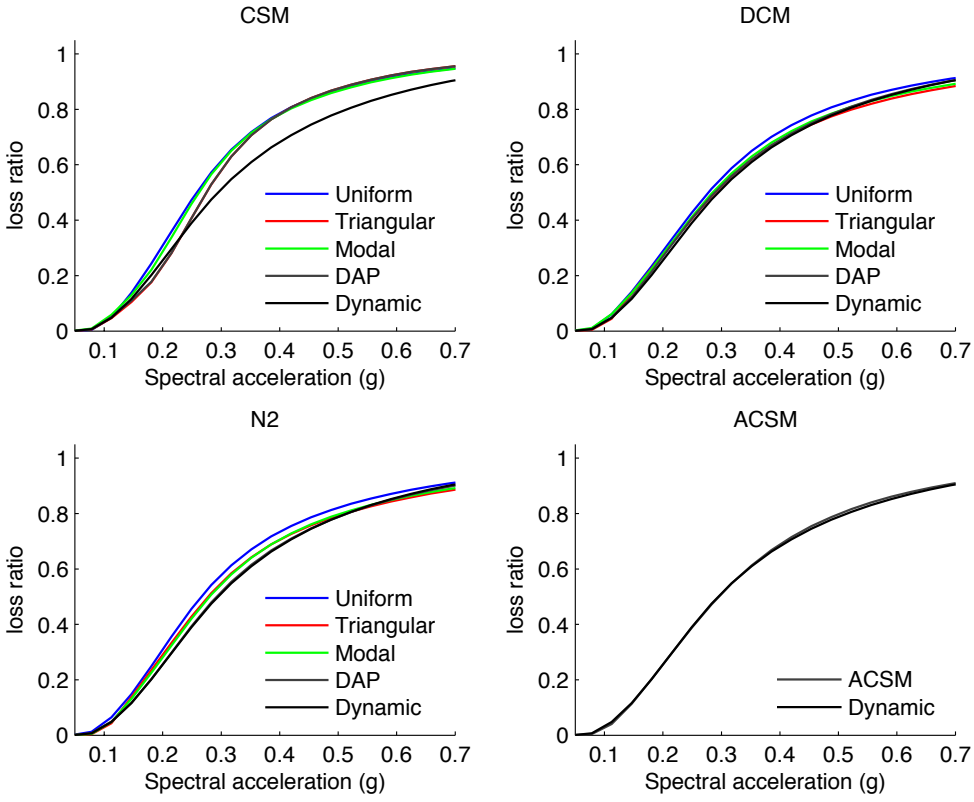

Figure 3.15 – Vulnerability functions per NSP using the HAZUS consequence model.

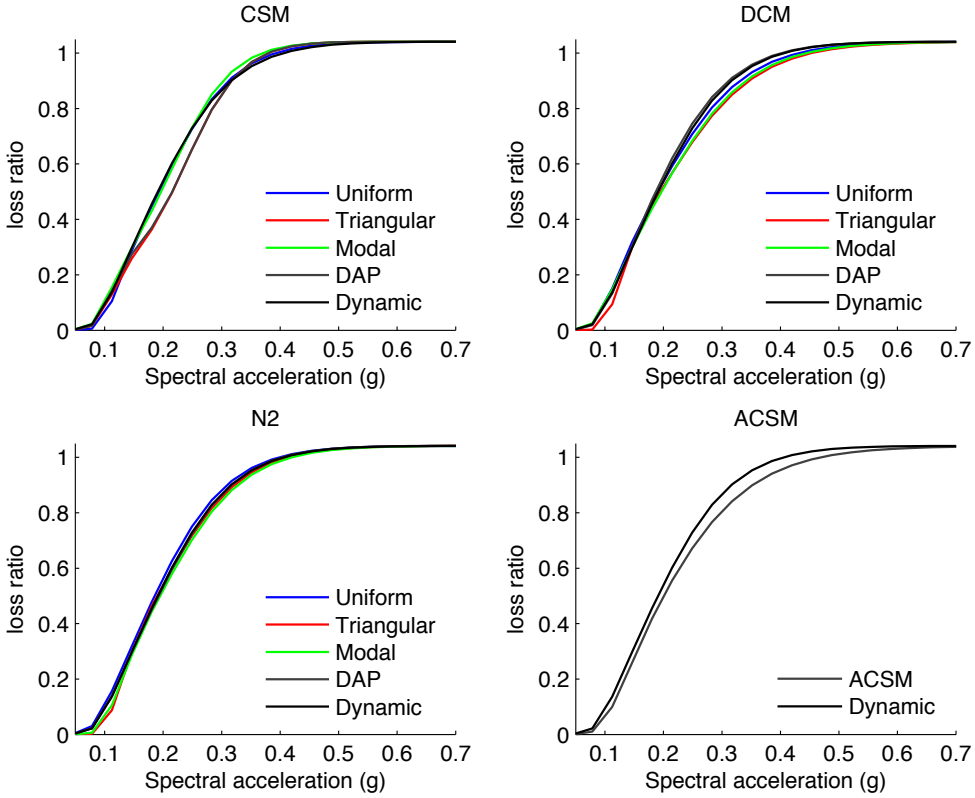

Figure 3.16 – Vulnerability functions per NSP using the Turkish consequence model.

Through the observation of the results, it is fair to state that despite the differences in the applied analysis, no major discrepancies were obtained in the vulnerability functions across the pushover methods within each NSP. For what concerns the influence of the consequence model, a higher discrepancy was observed between the vulnerability functions using the HAZUS model. This aspect is connected to the differences in the limit state curves, and the weight of each damage state in the resulting loss ratio. In general, the fragility curves for the first two limit states are very similar regardless of the methodology employed to produce them, but for the last limit state the differences are more pronounced (as shown previously in Figure 3.13). Hence, a consequence model like the Turkish one that attributes high damage ratios not just for the last damage state (collapse), but also for the second (moderate) and third (severe), will produce vulnerability functions whose loss ratios is not just influenced by the last damage state. On the other hand, the HAZUS consequence model has a distribution of damage ratios that defines the last damage state (which varies more significantly amongst the different methodologies), as the one that influences the most the resulting loss ratio, leading to higher variations in the vulnerability functions. In order to yield conclusions

regarding the differences obtained when using different NSPs, the mean vulnerability function for each NSP was derived, as presented in Figure 3.17.

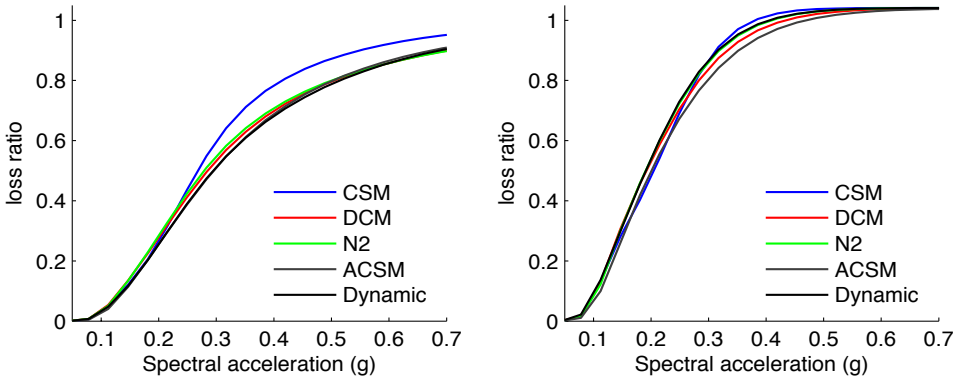

Figure 3.17 – Mean vulnerability function for each NSP according to the HAZUS (FEMA-443, 2003) (left) and Turkish (Bal *et al*., 2008b) (right) consequence models.

The functions for which the Capacity Spectrum Method was employed presented consistently higher loss ratios, whilst those using the N2 and Displacement Coefficient Method were very similar and presented slightly lower loss ratios with respect to the dynamic analyses. Considering all of the results, the vulnerability function with the lowest loss ratios is obtained when employing the Adaptive Capacity Spectrum Method, whilst the highest loss ratios are produced when using the Capacity Spectrum Method combined with uniform-based pushover curves. In fact, a mean and maximum average difference amongst vulnerability functions of 12% and 18%, respectively, are observed. This underestimation in the capacity of the structures when employing the Capacity Spectrum Method was also verified in an experimental exercise performed by Lin *et al.* (2004), in which the estimated seismic response was 20% lower than experimental observations. With regards to the differences between the results obtained using the aforementioned combinations and those attained with the nonlinear dynamic analysis, it was observed that the N2 method associated with the adaptive capacity curves led to almost identical results.

3.7.4. Variability in Seismic Risk Assessment

As previously presented, different methodologies to analyse the nonlinear response of structures lead to slightly different vulnerability functions. The influence of these discrepancies in seismic risk assessment was also evaluated within this study. A decision was taken to not just consider only one or a few

scenarios (single seismic events), but rather to carry out a probabilistic seismic risk assessment, in which all the possible ruptures for the region of interest are covered; relying only in a set of scenarios could easily lead to ambiguous conclusions, as depending on the magnitude of the events, only certain portions of the vulnerability functions would have been used in the calculations.

The reinforced concrete building portfolio of the Metropolitan Area of Istanbul (MAI) was used for the seismic risk assessment. The exposure model is a combination of data from aerial photos taken in 1995 and 1998 and census data from 2000 conducted by the Turkish State Statistics Institute (BU-ARC, 2002) and it follows a 0.005x0.005 decimal degrees grid. Each grid cell contains the economic value of a set of building typologies, and for this study only the mid-rise RC buildings built before the implementation of the 1998 Turkish design code were considered, as they represent the building class considered herein. With regards to the hazard model, the work of Demircioglu *et al.* (2007) was used, in which a distribution of area and fault sources were compiled for the whole Turkish territory. The combination of a spatially distributed exposure model with a comprehensive seismic hazard model allowed the consideration of a large spectrum of ground motions and, consequently, a full coverage of the vulnerability functions. Figure 3.18 and Figure 3.19 present the spatial distribution of building economic value (in EUR) and the hazard map with a 10% probability of exceedance in 50 years in the Marmara Region, respectively.

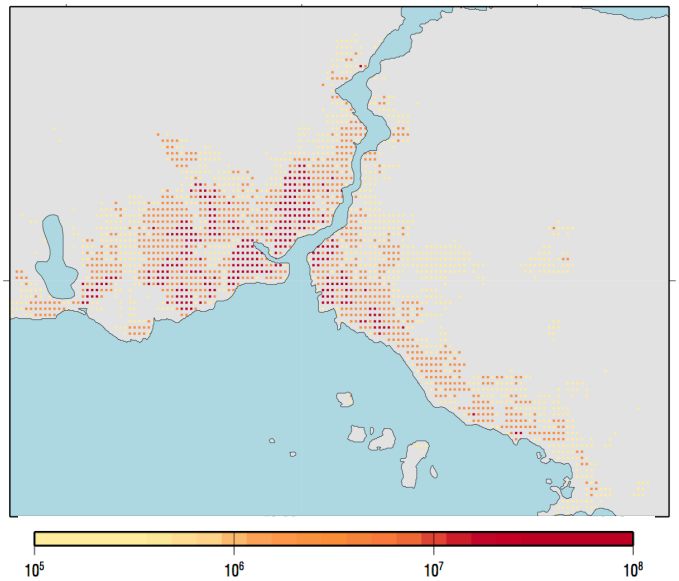

Figure 3.18 – Economic value (EUR) for mid-rise RC pre-code buildings in the MAI.

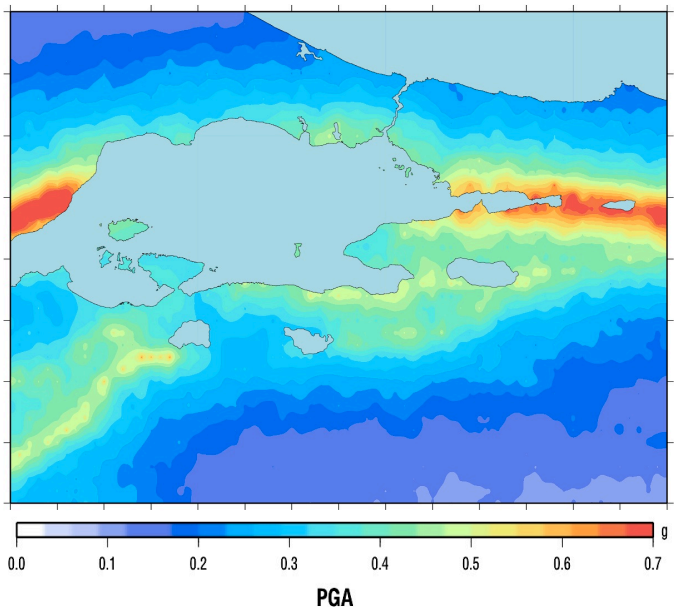

Figure 3.19 – Hazard map for 10% probability of exceedance in 50 years for the Marmara Region.

The exposure model, seismic hazard model and the set of vulnerability functions (generated using the Turkish consequence model) were introduced in the open source software OpenQuake (Chapter 2) and total loss exceedance curves (representing the aggregate losses of the whole building portfolio) were computed, using each vulnerability function. Then, using these curves, the average annual loss (AAL) and the losses for probabilities of exceedance of 1% and 10% in 50 years were extracted. The results using the vulnerability function derived through nonlinear dynamic analysis were used as the baseline solution to compute the relative variation of each methodology, as presented in Figure 3.20.

The comparison of the seismic risk results revealed slight differences amongst the different vulnerability methodologies. With regards to the differences between the nonlinear static procedures, a lower variation was observed when employing the N2 Method, closely followed by the Displacement Coefficient Method. Furthermore, within these two procedures, an improvement in the results was found when adaptive-based pushover curves (DAP) were utilized. The Adaptive Capacity Spectrum Method also revealed satisfactory results, with an average variation of 4%.

Regarding the differences between the three seismic risk parameters, the results for the average annual losses showed a slightly higher sensitivity for some of the methods. This risk parameter is highly influenced by the losses due to frequent

events, which generally have lower levels of ground motion. Therefore, in the methods that led to vulnerability functions with significantly different loss ratio values in the low spectral acceleration region than those derived using dynamic analysis, a higher relative variation was obtained.

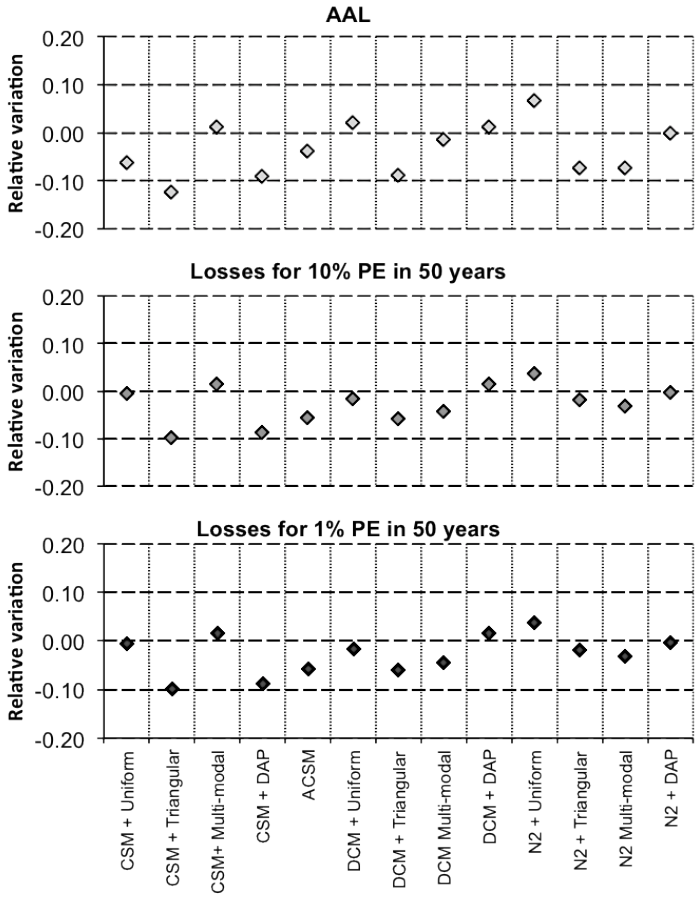

Figure 3.20 - Relative variation in the AAL (top), level of losses for frequent events (centre) and level of losses for rare events (bottom).

3.7.5. Computational performance

In order to yield conclusions regarding the balance between reliability and computational efficiency, the required time to complete each vulnerability methodology was registered (from the generation of the one hundred random RC frames until the estimation of the vulnerability functions). The performance provided by each methodology has been normalized with regards to the most computationally efficient one, as presented in Figure 3.21.

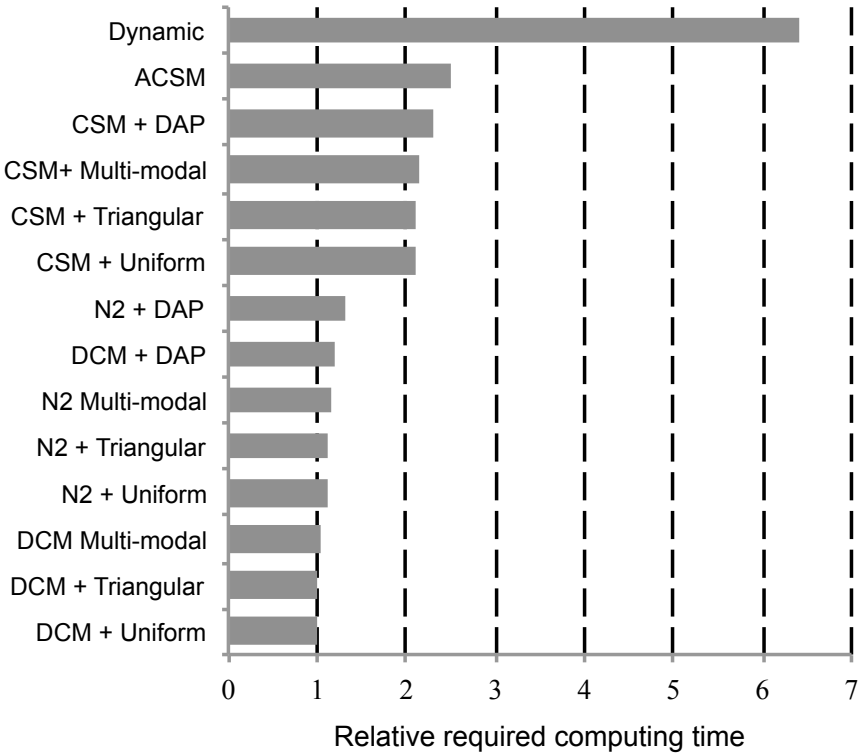

Figure 3.21 – Relative required computational time for each vulnerability methodology.

In general, the DCM and N2 represent the most efficient methodologies, falling in the same performance category regardless of the type of pushover curve. The methodologies that rely on the capacity spectrum approach to estimate the seismic response (CSM and ACSM) are more time demanding, due to the necessary iterative process that often requires several trials for convergence to be achieved. Moreover, carrying out these methodologies in an automatic manner can be very challenging if real accelerograms are employed, mainly due to the fact that the corresponding response spectra can intersect the capacity curve in many points. Finally, the nonlinear dynamic analysis proved to be the most time consuming, as expected. This last methodology also has the drawback of often presenting convergence problems, thus requiring constant monitoring throughout the analysis.

3.8. Final remarks

In this study, 13 sets of fragility functions were produced based on many different combinations of pushover curves and nonlinear static procedures, as well as a set of fragility functions using nonlinear dynamic analysis, totalling more than 140.000 simulations. It is important to establish that any conclusions yielded herein are conditional on the building typology, methodologies and assumptions followed

that were followed, and extrapolation to other cases calls for due care. Extending this study to cover 3D structures and to consider more accurate damage state criteria (such as inter-storey drift or chord rotations) is the subject of future studies.

Despite the discrepancies in the estimated seismic response of structures when employing different methodologies, as already shown by many authors (Chopra and Goel, 2000, Lin *et al*., 2004, Casarotti *et al*., 2009), it has been concluded in this study that those notable differences are not necessarily propagated into the resulting fragility/vulnerability functions. This decrease in the discrepancies between different methodologies is due to the fact that the focus is not on the member level performance (in terms of bending moments or shear forces) of an individual structure, but rather on the global damage state of the building, which is correlated with the maximum roof displacement. Thus, instead of obtaining differences that can reach magnitudes of 50% (Chopra and Goel, 2000), the maximum variation in the results did not exceed 18% in the vulnerability functions and 14% in the seismic risk parameters.

Considering the results from nonlinear dynamic analysis as the baseline method, it can be stated that the application of the DCM or the N2 method gave more accurate results than those provided by the CSM. However, as discussed in Section 4.1, improvements to the ATC-40 CSM in the bilinearisation process have been proposed, but have not been adopted herein (as it was felt that the more common practices should be investigated). It is expected that more accurate results would be attained with the consideration of these improvements. Although very different from a practical point of view, the DCM and the N2 method both use inelastic spectra to estimate the target displacement, which is probably one of the causes of the similarity in the results. Furthermore, the employment of N2 combined with adaptive pushover curves provided results within 2% of those attained with the nonlinear dynamic analysis, which shows that a simplified methodology with a much lower computational effort can still provide reliable and accurate results. Regarding the ACSM, which differs from the CSM + DAP configuration in the process to build the bilinear curve, in the damping model and in the way the equivalent SDOF capacity curve is calculated, also satisfactory results were obtained.

It can be concluded from the results presented herein that the best balance between accuracy and efficiency is obtained for the N2 + DAP configuration,

providing similar vulnerability functions to those obtained with nonlinear dynamic analysis, but at a rate that is almost seven times faster.

Chapter 4

Extending Displacement-Based Earthquake Loss Assessment (DBELA) for the Computation of Fragility Curves

Silva, V., Crowley, H., Pinho, R., Varum, H. (2013) "Extending Displacement-Based Earthquake Loss Assessment (DBELA) for the Computation of Fragility Curves". *Engineering Structures*, in review.

4.1. Summary

This Chapter presents a new procedure to derive fragility functions for populations of buildings that relies on the displacement-based earthquake loss assessment (DBELA) methodology. The recent developments in this methodology are also presented herein, such as the development of new formulae for the calculation of the yield period or the consideration of infilled frame structures. In the fragility method proposed herein, thousands of synthetic buildings have been produced considering probabilistic distributions describing the variability in their geometrical and material properties. Then, their nonlinear capacity has been estimated using the DBELA method and their performance against a large set of ground motion records has been calculated. Global limit states are used to estimate the distribution of buildings in each damage state for different levels of ground motion, and a regression algorithm is applied to derive fragility functions for each limit state. The proposed methodology is demonstrated for the case of ductile and

non-ductile Turkish reinforced concrete buildings with and without masonry infill walls, and compared with results obtained using nonlinear dynamic procedures and with the results from previous studies.

4.2. Introduction

Fragility functions representing the probability of exceeding a set of damage states conditional on a level of ground motion are a fundamental component to describe the physical vulnerability of a population of buildings. The increase in the demand for reliable and more accurate loss estimations has triggered the development of fragility functions based on analytical/mechanical approaches which tend to provide a better representation of the structural behaviour of the building typologies. As discussed by Rossetto and Elnashai (2005), there is no unique methodology for the development of fragility functions and therefore, each approach will have its limitations and advantages. Several methodologies (Singhal and Kiremidjian, 1996; Dumova-Jovanoska, 2000; Akkar *et al.*, 2005; Erberik, 2008; amongst others) have been proposed with different levels of simplification and efficiency in the past years. However, it is well established that one of the main drawbacks of any analytical methodology is the required computational and modelling effort. For this reason, a simplified methodology is proposed in this study.

The so-called DBELA methodology (e.g. Crowley *et al*., 2004; Bal *et al*., 2010) is employed to estimate the nonlinear capacity of thousands of reinforced concrete (RC) frames randomly generated and the associated demand from a large set of ground motion records. The fact that several synthetic buildings and ground motion records are used in the calculations allows the consideration of the material and geometrical uncertainties, as well as (to some extent) the record-to-record variability. These calculations are performed within a probabilistic framework and therefore, the parameters that define the fragility functions (i.e. logarithmic mean and logarithmic standard deviation) are also described by a probabilistic distribution, which permits the propagation of the uncertainty in the vulnerability to the risk analysis. This procedure proved to provide a good balance between computational efficiency and reliability, allowing a quick and simple assessment of the physical vulnerability of many different building typologies (e.g. reinforced concrete frames or shear walls, masonry buildings with concrete or timber slabs).

This methodology is applied herein to estimate the statistics of fragility functions for real Turkish reinforced concrete frames with and without masonry infills walls. Then, these results are compared with previous studies, as well as with results obtained using complex nonlinear dynamic analysis, showing that despite the simplicity of the proposed methodology, satisfactory results are still attained.

4.3. DBELA Fragility Function Calculator

Since the initial publications of the DBELA methodology (Glaister and Pinho, 2003; Crowley *et al*, 2004), several improvements have been suggested, such as the development of new period/height relationships or the consideration of other building typologies. The new developments that concern the assessment of reinforced concrete frames have been compiled and are described in this section. Then, the proposed methodology to derive fragility functions is comprehensively explained. A procedure to use these results in the calculation of vulnerability functions (i.e. the probability distribution of loss for a set of intensity measure levels) that propagates the uncertainties from the fragility functions and consequence functions (which relate damage to loss) is also presented. These efforts have been developed within an open-source and transparent philosophy and therefore, all of these calculators can be found in a public code repository at GitHub [3].

4.3.1. Summary of DBELA

The DBELA methodology is a simplified nonlinear static analysis method for the seismic risk assessment of buildings. The method builds upon the urban assessment methodology proposed by Calvi (1999), in which the principles of structural mechanics and seismic response of buildings were used to estimate the seismic vulnerability of classes of buildings. In this method, the displacement capacity and demand for a number of limit states needs to be calculated. Each limit state marks the threshold between the levels of damage that a building might withstand, usually described by a reduction in strength or by exceedance of certain displacement/drift levels. Once these parameters are obtained, the displacement capacity of the first limit state is compared with the respective demand. If the demand exceeds the capacity, the next limit states need to be checked successively, until the demand no longer exceeds the capacity and the building damage state can be defined. If the

demand also exceeds the capacity of the last limit state, the building is assumed to have collapsed. This procedure is schematically depicted in Figure 4.1, in which the capacities for three limit states are represented by Δ_i and the associated demand by Sd_i.

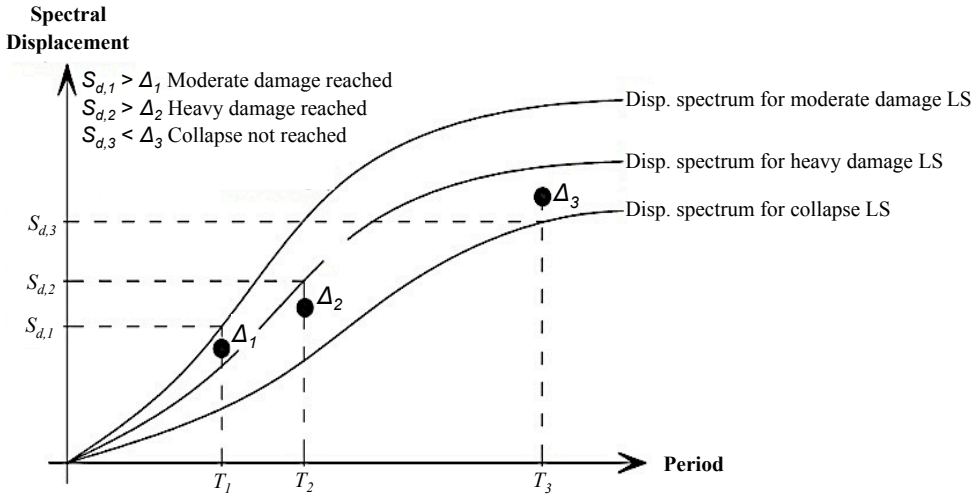

Figure 4.1 - Comparison between limit state capacity and the associated demand (adapted from Bal *et al.*, 2010).

In this example, the demand exceeds the capacity in the first and second limit state but not in the third limit state, thus allocating the building to the third damage state.

4.3.1.1. Displacement capacity

As explained above, the demand in this methodology is represented by a displacement spectrum which can be described as the expected displacement induced by an earthquake on a single-degree-of-freedom (SDOF) oscillator of given period and damping. Therefore, the displacement capacity equations that are derived must describe the capacity of a SDOF substitute/equivalent structure and hence must give the displacement capacity at a given limit state (which could be structural or non-structural) at the centre of seismic force of the original structure.

When considering structural limit states, the displacement at the height of the centre of seismic force of the original structure (H_{CSF}) can be estimated by multiplying the base rotation by the height of the equivalent SDOF structure (H_{SDOF}), which is obtained by multiplying the total height of the actual structure (H_T) by an effective height ratio (ef_h) (see Figure 4.2).

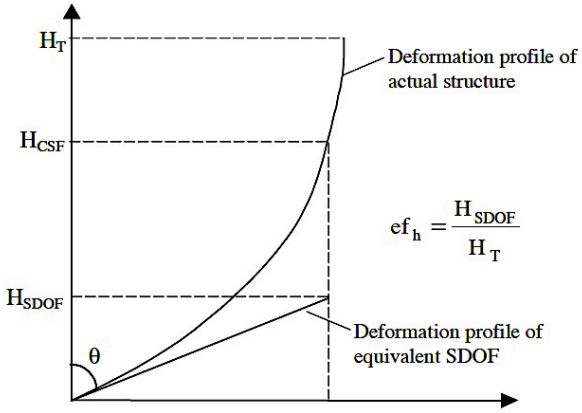

Figure 4.2 – Definition of effective height coefficient (Glaister and Pinho, 2003).

Pinho *et al.* (2002) and Glaister and Pinho (2003) proposed formulae for estimating the effective height coefficient for different response mechanisms. For what concerns the beam sway mechanism (or distributed plasticity mechanism, as shown in Figure 4.3), a ratio of 0.64 is proposed for structures with 4 or less storeys, and 0.44 for structures with 20 or more storeys. For any structures that might fall within these limits, linear interpolation should be employed. With regards to the column-sway mechanism (or concentrated plasticity mechanism, as shown in Figure 4.3), the deformed shapes vary from a linear profile (pre-yield) to a non-linear profile (post-yield). As described in Glaister and Pinho (2003), a coefficient of 0.67 is assumed for the pre-yield response and the following simplified formula can be applied post-yield (to attempt to account for the ductility dependence of the effective height post-yield coefficient):

$$ef_h = 0.67 - 0.17 \cdot \frac{\varepsilon_{s(LS_i)} - \varepsilon_y}{\varepsilon_{s(LS_i)}} \tag{4.1}$$

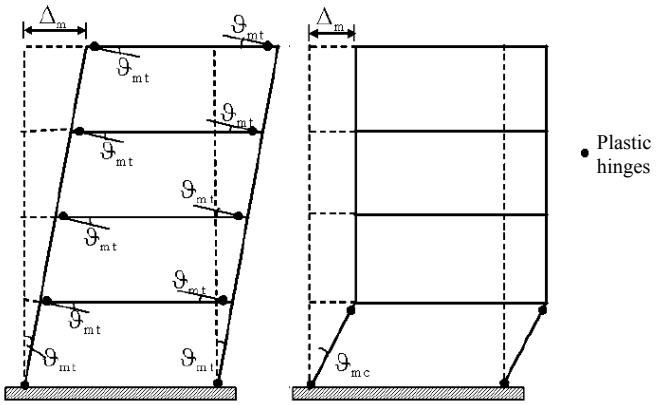

Figure 4.3 – Deformed profiles for beam-sway (left) and column-sway (right) mechanisms (adapted from Paulay and Priestley, 1992).

The displacement capacity at different limit states (either at yield (Δ_y) or post-yield (Δ_{LSi})) for bare frame structures can be computed using simplified formulae, which are distinct if the structure is expected to exhibit a beam- or column-sway failure mechanism. The formulation of these equations is not described in detail here and interested readers are referred to Crowley *et al.* (2004) for more details.

For a beam-sway mechanism:

$$\Delta_y = 0.5 \cdot ef_h \cdot H_T \cdot \varepsilon_y \cdot \frac{l_b}{h_b} \tag{4.2}$$

$$\Delta_{LS_i} = \Delta_y + 0.5 \cdot ef_h \cdot H_T \cdot \left(\varepsilon_{c(LS_i)} + \varepsilon_{s(LS_i)} - 1.7 \cdot \varepsilon_y\right) \tag{4.3}$$

For a column-sway mechanism:

$$\Delta_y = 0.43 \cdot ef_h \cdot H_T \cdot \varepsilon_y \cdot \frac{h_s}{h_c} \tag{4.4}$$

$$\Delta_{LS_i} = \Delta_y + 0.5 \cdot ef_h \cdot h_s \cdot \left(\varepsilon_{c(LS_i)} + \varepsilon_{s(LS_i)} - 2.14 \cdot \varepsilon_y\right) \tag{4.5}$$

where the different symbols stand for:

- ef_h is the effective height ratio;
- H_T is the total height;
- l_b is the beam length;
- h_b is the beam depth;
- h_s is the average of the inter-storey height;
- h_c is the column depth;
- ε_y is the yield strain of the reinforcement steel;
- $\varepsilon_{c(Lsi)}$ and $\varepsilon_{s(LS1)}$ are the strain levels for sectional limits states for concrete and steel respectively;

The aforementioned parameters h_b, l_b, h_c and l_c should be representative of the geometric characteristics of a given structure, and not specific to a given story. Each of these geometric parameters can be modelled as random variables, with respective mean, standard deviation and probability distribution (e.g. Bal *et al.*, 2008b). The concrete and steel strains (ε_y, $\varepsilon_{c(Lsi)}$, $\varepsilon_{s(Lsi)}$) used to compute the displacement capacities for each limit state can also be defined in a probabilistic manner and the material strains are sampled from a probabilistic distribution that needs to be defined for each strain, at each limit state. The consideration of the uncertainty in the limit states thresholds is in agreement with existing guidelines

(FEMA-445, 2006) and studies (Cornell *et al*., 2002; Crowley *et al*., 2004; Erberik, 2008). The limit states that can be reached for a given level of damage depend on the level of confinement; it is thus important to distinguish between structures that have an adequate level of confinement and will respond in a *ductile* manner to seismic actions, and those where the level of confinement is inadequate and will thus have a *non-ductile* response.

In the work of Bal *et al.* (2010), the formulae to calculate the displacement capacity have been adapted to take into consideration the influence of infill walls; in this type of structure, an increase in strength and slight decrease in displacement capacity is observed, in comparison to bare frame structures. This decrease in the displacement capacity has been introduced through the employment of reduction parameters β_1 *and* β_2 in the previously presented equations (4.2)-(4.5), leading to the following formulae:

For a beam-sway mechanism:

$$\Delta_{LS_i}= \left[0.5 \cdot ef_h \cdot H_T \cdot \varepsilon_y \cdot \frac{l_b}{h_b}\right] \cdot \beta_1 + 0.5 \cdot ef_h \cdot H_T \cdot \left(\varepsilon_{c(LS_i)} + \varepsilon_{s(LS_i)} - 1.7 \cdot \varepsilon_y\right) \cdot \beta_2 \qquad (4.6)$$

For a column-sway mechanism:

$$\Delta_{LS_i}= \left[0.43 \cdot ef_h \cdot H_T \cdot \varepsilon_y \cdot \frac{h_s}{h_c}\right] \cdot \beta_1 + 0.5 \cdot ef_h \cdot h_s \cdot \left(\varepsilon_{c(LS_i)} + \varepsilon_{s(LS_i)} - 2.14 \cdot \varepsilon_y\right) \cdot \beta_2 \qquad (4.7)$$

The β_1 parameter serves the purpose of reducing the yield displacement capacity, whilst the β_2 parameter adjusts the post-yield displacement capacity. In order to estimate these parameters, Bal *et al.* (2010) carried out several nonlinear analyses in a set of structures with infills and another set without infill walls, and the mean ratio between the top displacements of the two sets was estimated for each limit state. A mean value of 0.52 was obtained for β_1, while for β_2, a mean value of 0.46 and 0.28 was attained for limit state 2 and limit state 3, respectively.

In order to identify which displacement capacity equation should be applied to a given structure, the expected sway mechanism needs to be estimated. Indices to estimate whether plastic hinges will form in the beams or columns have been proposed in the past as part of capacity design (e.g. Paulay and Priestley, 1992). These indices consider the relative yield strength of the beams and the columns at

the joints of a given floor to allow the designer to ensure there is enough overstrength in the columns, which should yield after the beams. However, in order to estimate whether a given frame will respond with a beam- or a column-sway mechanism, the properties of the storey, rather than the floor, are of more importance. Furthermore, it is well known that frames with flexible columns are more likely to exhibit a soft storey mechanism. Hence, an alternative, deformation-based index has been proposed by Abo El Ezz (2008) which reflects the relation between the stiffness of the beams and columns. This index can be computed using the following formula:

$$R = \frac{h_b/l_b}{h_c/l_c} \tag{4.8}$$

where l_c stands for the column length. Abo El Ezz (2008) proposed some limits for this index applicable to bare and fully infilled frame structures, as described in Table 4.1.

Table 4.1 - Limits for the deformation-based sway index.

Building typology	Failure mechanism	
	Beam sway	Column Sway
Bare frames	R ≤ 1.5	R > 1.5
Fully infilled frames	R ≤ 1.0	R > 1.0

4.3.1.2. Displacement demand

The displacement demand is initially represented by the 5% damped spectra. The displacement is computed for the period at each limit state and modified by a correction factor (η), representative of the equivalent viscous damping and limit state ductility. In EC8 (CEN, 2004), the following equation is proposed for the calculation of the correction factor:

$$\eta = \sqrt{\frac{10}{5 + \xi_{eq}}} \tag{4.9}$$

where ξ_{eq} stands for the equivalent viscous damping, which can be estimated using the formula proposed by Priestley *et al*. (2007) for RC structures with a non negative post-yield ratio:

$$\xi_{eq} = 0.05 + 0.565\left(\frac{\mu_{LS_i+1}}{\mu_{LS_i}\pi}\right) \quad (4.10)$$

where μ_{LSi} stands for the ductility at the considered limit state (assumed as the ratio between Δ_{LSi} and Δ_y). More accurate approaches have recently been proposed to estimate the correction factors (η), considering additional parameters, such as the magnitude or source-to-site distance (Rezaeian *et al*., 2012). The integration of such methods in the calculation of the displacement demand is in the future development plans of the proposed methodology.

It is important to emphasize that this approach to estimate the displacement demand is simplified, and might underestimate the record-to-record variability as only the spectral properties of the records are considered. For example, if a set of accelerograms whose spectra has been matched to a certain target spectrum are employed within this methodology, the same response spectra would always be obtained, thus leading to zero record-to-record variability, even though the same response would not be obtained from nonlinear dynamic analysis. This limitation could thus be overcome through the calculation of the response spectrum using nonlinear time history analysis of the single degree of freedom oscillators. However, such approach would compromise one of the advantages of the current methodology, which is the computational speed. One way to improve the estimation of the record-to-record variability in the proposed approach would be to consider the uncertainties in Equations (4.9) and (4.10); however, these are not generally reported and thus this solution has not yet been implemented.

With regards to the calculation of the yield period (T_y in seconds) for bare frame structures, Crowley and Pinho (2004) and Crowley *et al*. (2008) proposed a relationship between the period and the total height of $0.10H_T$ and $0.07H_T$ for structures without and with lateral load design, respectively. For infilled frames, a relation equal to $0.06H_T$ has been recommended by Crowley and Pinho (2006) for structures without lateral load design. Considering that lateral load designed bare frames have a period that is 70% of those without lateral load, until further analyses are undertaken, it is assumed herein that the same relationship holds for infilled frames, and a formula of $0.042H_T$ can be used for infilled structures designed for lateral loads.

The elongated period of vibration for any of the limit states (T_{LSi}) can be computed using the following formula:

$$T_{LS_i} = T_y \sqrt{\frac{\mu_{LS_i}}{1 + \alpha \cdot \mu_{LS_i} - \alpha}} \tag{4.11}$$

where α stands for the post-yield stiffness ratio. In cases where this ratio can be assumed as zero, the relation between T_{LSi} and T_y will depend purely on the limit state ductility as follows:

$$T_{LS_i} = T_y \sqrt{\mu_{LS_i}} \tag{4.12}$$

This procedure has been employed within a probabilistic framework in the work of Crowley *et al*. (2004) and extended to other building typologies such as dual structures (combination of frames and shear walls) and masonry (with concrete or timber slabs) by Bal *et al*. (2010).

4.3.2. Proposed Fragility Functions Methodology

The employment of analytical methods to create fragility functions has been widely used, mainly through the employment of capacity spectrum (Freeman, 2004) methodologies or nonlinear dynamic analysis (e.g. Vacareanu *et al*, 2004, Akkar *et al*., 2005, Rossetto and Elnashai, 2005, Erberik, 2008, amongst others). The methodology that is being proposed herein differs from some of the already proposed methods because: i) it does not require nonlinear modelling of structures; ii) it does not require nonlinear static or dynamic analysis; iii) it allows the consideration of the dispersion in the geometric and material properties, the variability in the damage state thresholds, and (partially) the record-to-record variability; iv) the method to calculate the nonlinear response of the buildings is simplified, avoiding the common convergence problems often experienced when using the capacity spectrum method with real accelerograms (e.g. Chopra and Goel, 2000). For these reasons, this methodology proved to be considerably less time demanding in comparison to other fragility methodologies.

The proposed simplified methodology to derive fragility functions using the DBELA methodology is summarized in Figure 4.4.

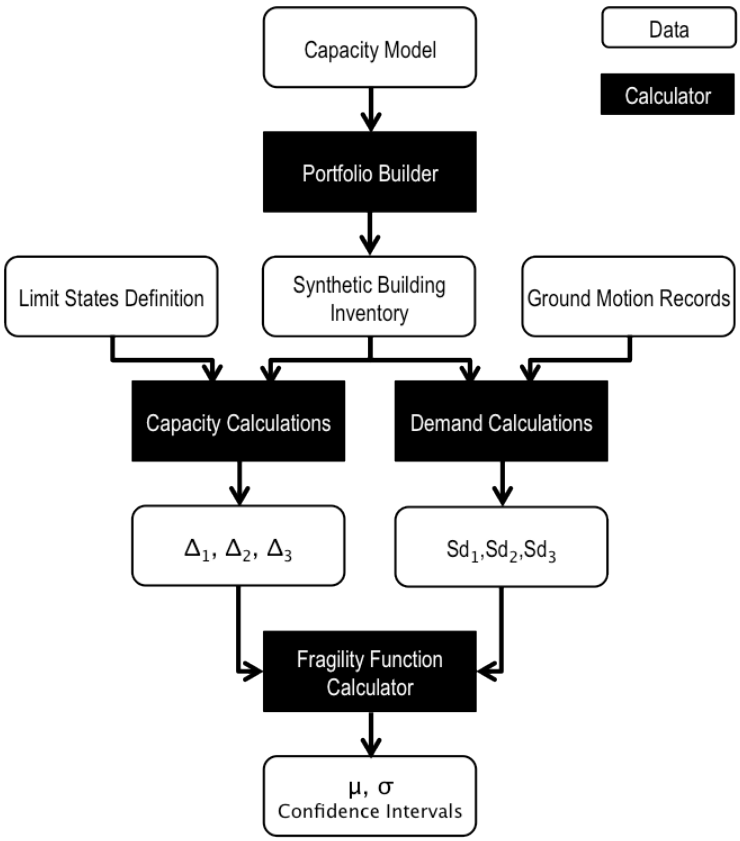

Figure 4.4 - Workflow of the DBELA fragility functions calculator.

In this methodology, a randomly generated population of buildings is produced, according to the probabilistic distribution of a set of material and geometrical properties. These distributions are defined based on information gathered from real Turkish buildings, as described in Bal *et al*. (2008b).

The set of synthetic buildings is then passed to two distinct modules. The first one computes the displacement capacity Δ_i based on the material and geometrical properties of the building typology, with the equations described in section 2.1.1. The second module calculates the displacement demand Sd_i for each limit state period using over-damped spectra at a level of equivalent viscous damping, representative of the combined elastic damping and hysteretic energy absorbed during the inelastic response, from a set of accelerograms. In order to compute the displacement spectrum from each ground motion record, a module that uses a Newmark integration process (Newmark, 1959) was developed. However, if a user wishes to avoid this additional computational effort, the displacement spectra can also be provided directly as an input to the calculator. The displacement demand for

each limit state is then computed by modifying the elastic displacement spectrum by a correction factor η_i, representative of the equivalent viscous damping and limit state ductility.

The selection of the set of accelerograms is a key parameter in this methodology and it should comprise a large variety of records, respecting the local seismicity characteristics, as also explained in Section 3.3.3. Employing suites of accelerograms partially allows the consideration of the effect of the record-to-record variability of the seismic input, though as mentioned previously, this might be underestimated.

Once the capacity and demand displacements for the whole group of synthetic buildings are computed, a module is called to compare both sets of displacements, and allocate each building in a certain damage state. Thus, for each ground motion record, percentages of buildings in each damage state can be obtained and fragility curves can be extrapolated. In Figure 4.5, the building damage distributions for 4 records with different levels of spectral acceleration at the fundamental period are presented. Each generated building will have unique geometrical characteristics, as well as a distinct natural period of vibration. Thus, in order to plot the cumulative percentage of buildings in each damage state against the associated spectral acceleration for a single period of vibration, the mean period was calculated for the population of random buildings.

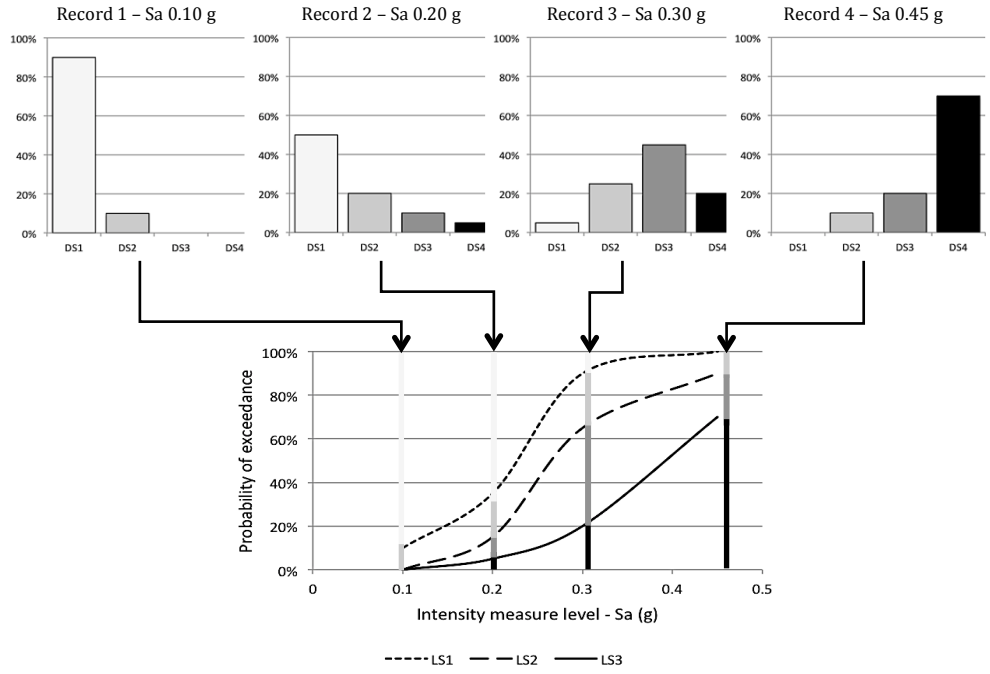

Figure 4.5 - Derivation of fragility curves based on building damage distribution.

Each ground motion record needs to be represented by an intensity measure level. Within this methodology, it is possible to choose any intensity measure type to represent the record, as long as the necessary information is available. Macroseismic intensities such as MMI or EMS could be a natural choice since there is a direct relationship with the levels of damage in different building typologies. However, keeping track of the intensity at the location where the record was captured is not common and furthermore, macroseismic intensity does not take into account the influence of the frequency content on the structural response. Peak ground motion also shares this last shortcoming and even more importantly, it does not have a clear correlation with damage. The influence of the frequency content on the ground motion can be considered by choosing spectral acceleration or displacement to represent each record (Bommer *et al.*, 2002). Other factors might play an important role in choosing the appropriate intensity measure type such as the availability of accurate GMPE or the possibility of taking advantage of existing seismic hazard data such as USGS ShakeMaps (Allen *et al*., 2008).

The fitting of a curve to the list of cumulative percentages versus intensity measure levels is done using the mean least squares method and assuming a lognormal distribution. As shown in the European SYNER-G project, where hundreds of fragility curves from the past 30 years were collected (SYNER-G, 2011), this type of distribution is very common to model fragility curves. However, other distributions such as exponential or normal have been used in past vulnerability studies (e.g. Lang, 2002; Rossetto and Elnashai, 2003) and for this reason, the definition of the probabilistic distribution has not been hard coded, and can easily be modified to other models. The logarithmic mean, λ, and logarithmic standard deviation, ζ, that are estimated for each curve will naturally have some uncertainty, due to the scatter of the results. Hence, a sampling method was implemented to properly evaluate the uncertainty on the statistics. This method consists in a continuous bootstrap sampling with replacement from the original dataset (Wasserman, 2004). Figure 4.6 shows an example of the estimated limit state exceedance probability from 250 records. A number of synthetic datasets are randomly extracted from these results, each with 250 data points; it is clear that in many of these datasets some of the data points will be repeated. For each synthetic dataset that is generated, the associated logarithmic mean and logarithmic standard deviation are estimated. This process is repeated N times, generating N different

pairs of logarithmic mean and logarithmic standard deviation, whose distribution can be assumed as normal (Bradley, 2010). From these distributions, confidence intervals for different levels of confidence can be extracted. In Figure 4.6 a curve was fitted to a dataset of 250 points and the sampling method was used to derive the distributions of the associated logarithmic mean and logarithmic standard deviation. A number of synthetic datasets equal to 100 proved to be sufficient to achieve a satisfactory convergence on the first and second moments of the distribution.

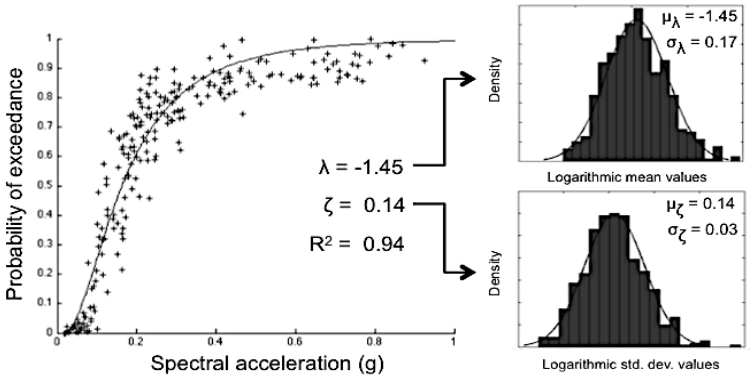

Figure 4.6 - Statistical treatment of the parameters defining the curve.

4.3.3. Vulnerability Functions Calculation

Fragility functions are commonly converted into vulnerability functions, which can then be used in loss assessment. Thus, this framework was also extended to the derivation of these curves, through the employment of a consequence model. For each intensity measure level, a loss ratio is computed, by multiplying the percentage of buildings in each damage state by the associated damage ratio (ratio of repair cost to cost of replacement). The damage ratio per damage state varies significantly according to the building typology. The damage ratio per damage state varies significantly according to the building typology and for the purposes of this study, the consequence model for typical Turkish buildings proposed by Bal *et al*., 2008b (see Figure 3.14) was employed.

The previously described methodology to derive vulnerability functions must be applied not only to the mean values of the parameters of each fragility curve, but rather to a set of randomly generated pairs of parameters (logarithmic mean and logarithmic standard deviation per fragility curve), allowing the propagation of this uncertainty to the vulnerability curves. This sampling process needs to be done taking into account the possible correlation between each parameter of the fragility

curves. For example, if the correlation coefficient between two parameters is close to 1, then during the sampling process if one of them is sampled to be above the mean, it is likely that the second one will also be sampled with a positive residual. On the other hand, if the pair of parameters has a coefficient of correlation close to 0, then the sampling process is done independently and the manner in which one parameter is sampled does not affect the other one. As previously described, in the bootstrap methodology a set of logarithmic means and a set of logarithmic standard deviations are obtained for each limit state (of which there are 3), making a total of six sets of parameters. The correlation coefficients are then computed by analysing the variation of each set of parameters with respect to the others. An example is presented below to better explain this relation.

A set of fragility curves was computed for low-rise Turkish buildings and the bootstrap methodology was used to estimate the probabilistic distribution of the statistics of the three curves. In this process, 100 synthetic datasets were generated (as previously described) for the first limit state and the associated data points for the second and third limit states were selected. For each dataset, for each limit state, the logarithmic mean (λ) and logarithmic standard deviation (ζ) for each curve were computed. Then, the parameters associated to each dataset were plotted against each other; three of these plots with the respective correlation coefficient are presented in Figure 4.7.

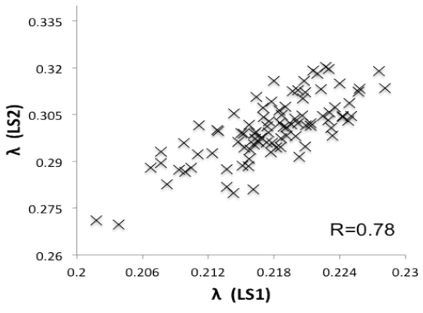

a)

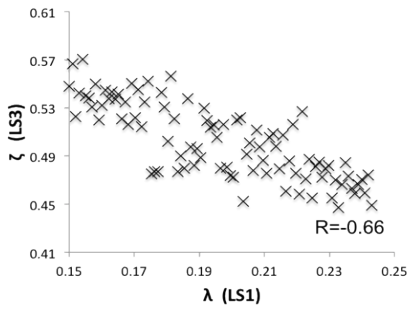

b)

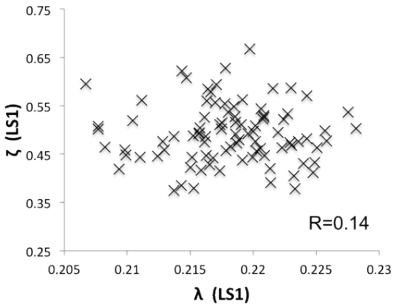

c)

Figure 4.7 - Correlation between a) logarithmic means of limit state 1 and 2; b) logarithmic mean of limit state 1 and logarithmic standard deviation of limit state 3; c) logarithmic mean and standard deviation of limit state 1.

The correlation between the parameters can be inferred by analysing the shape of the scatter. In the first combination, there is a thin dispersion of the data with a positive slope, which means that the values vary relatively linearly and proportionally. In other words, during the bootstrap method every time that a synthetic dataset led to a low mean for the first limit state, it also tended to produce a low mean for the second limit state, and vice-versa. In the second combination there is also a clear correlation between the two parameters but in this case it is negative, which means that the values tend to vary somewhat linearly but inversely. In the last combination, the scatter of the data is characterized by a wide dispersal and therefore, the correlation is not significant.

Different approaches can be followed to randomly sample correlated normal distributions (e.g. Martinez and Martinez, 2002). In this work, a multivariate normal with Cholesky factorization of the covariance matrix approach is followed. This procedure can be described by the following expression:

$$X = ZR + \mu^T \tag{4.13}$$

where X represents the resulting n× d matrix with the randomly sampled parameters, Z represents a n× d matrix of standard normal random variable, R is a d× d upper triangular matrix obtained by applying a Cholesky factorization to the covariance matrix, μ^T stands for a n×d matrix containing the mean of each distribution, n is equal to the number of required samples and d is equal to the number of normal distributions. In this case, d is equal to 6 (a logarithmic mean and a logarithmic standard deviation for each of the three limit state curves) and n should not be lower than 50.

Using the statistics from the previous example and the mean values of the damage ratios proposed by Bal *et al*. (2008b), a set of 100 vulnerability curves was calculated. Then, for each intensity measure level, the distribution of the loss ratios was evaluated and a lognormal curve was fit to the data. In Figure 4.8 these results are presented, along with a histogram of the loss ratios and associated lognormal curve for a given spectral acceleration.

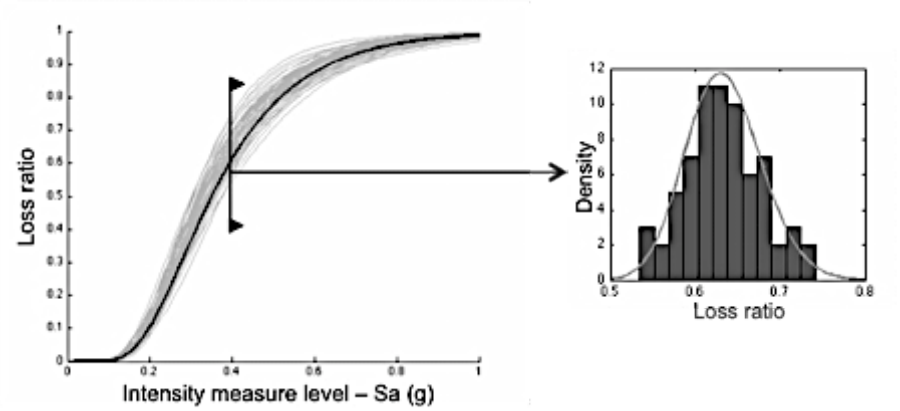

Figure 4.8 - Set of vulnerability functions and uncertainty per intensity measure level.

During this process, it is also possible to include the uncertainty from the consequence function, by sampling a set of damage ratios each time a vulnerability curve is computed. In the case of the last example, a set of damage ratios would be sampled 100 times. In order to do so, it is necessary to have the damage ratio for each damage state modelled according to a probabilistic distribution, with the associated statistics.

4.4. Case study application

4.4.1. Characterization of the RC Building Portfolio

A detailed description of the material and geometric properties of typical reinforced concrete buildings situated in the Marmara region can be found in Bal *et al*. (2008b). In the latter study, hundreds of buildings were used to derive the probabilistic distribution of a list of parameters such as the number of storeys, ground floor and regular height, dimensions of the structural elements, concrete and steel strength, amongst others. To prove that the statistics for each parameter are representative of the population, Bal *et al*. (2008b) carried out an exercise in which the number of buildings considered to derive each statistic was continuously

reduced, and the respective results were compared with the ones based on the complete sample. It was concluded that even considering a reduced number of buildings, the results were still similar (within a 5% tolerance).

The buildings that were "legal" and designed according to the 1998 Turkish Earthquake Code (herein termed as "compliant") were treated separately from the ones that were illegal or built before the implementation of the aforementioned design code (herein termed as "non-compliant"), allowing the correct estimation of some parameters that are greatly influenced by the code level (e.g. steel and concrete resistance, beam and column width). This classification of the buildings according to the design code was also followed by Bal *et al.* (2008b). With regards to the building height, it was necessary to aggregate the buildings into three categories: low-rise (1-3 storeys), mid-rise (4-7 storeys) and high-rise (8-9 storeys). Buildings above 9 storeys (tall buildings) are not considered herein, as it is recognized that the simplified methodology could lead to unreliable results. In Table 4.2, the organization of the building typologies is presented for reinforced concrete frames with and without masonry infill walls, along with the attributed code and percentage of each building height within each typology.

Table 4.2 - Classification of the building typologies used in this study.

Structure type	Code level	Height	Code	# of storeys	Percentage
RC frames without masonry infills	Low code (non-ductile)	Low-rise	RCB-LC-LR	1	82
				2	9
				3	9
		Mid-Rise	RCB-LC-MR	4	10
				5	40
				6	31
				7	19
		High rise	RCB-LC-HR	8	47
				9	53
	High code (ductile)	Low-rise	RCB-HC-LR	1	11
				2	22
				3	67
		Mid-rise	RCB-HC-MR	4	49
				5	32
				6	17
				7	2
		High-rise	RCB-HC-HR	8	50
				9	50
RC frames with masonry infills	Low code (non-ductile)	Low-rise	RCW-LC-LR	1	17
				2	40

			3	43
	Mid-Rise	RCW-LC-MR	4	33
			5	34
			6	22
			7	7
	High rise	RCW-LC-HR	8	50
			9	50
High code (ductile)	Low-rise	RCW-HC-LR	1	11
			2	22
			3	67
	Mid-rise	RCW-HC-MR	4	49
			5	32
			6	17
			7	2
	High-rise	RCW-HC-HR	8	50
			9	50

The presented percentages in Table 3 were derived based on Turkish Census Data from 2000, and used for the Monte Carlo sampling process to ensure that the distribution of building height for each typology was in fair agreement with what exists in reality.

4.4.2. Ground Motion Input

The process for the selection of the ground motion records employed herein was similar to what has been described in Section 3.3.3. Thus, the work of Kalkan *et al*. (2008) was used in order to understand the selection criteria for the set of ground motion records.

Since the methodology proposed herein is considerably less computational demanding in comparison to the methods considered in Chapter 3, a decision was made to use a larger number of accelerograms. About 250 ground motion records were extracted from the PEER database [28]; the histograms of PGA and PGV are presented in Figure 4.9 and the spectral acceleration versus period of vibration for the whole sample of records is depicted in Figure 3.4.

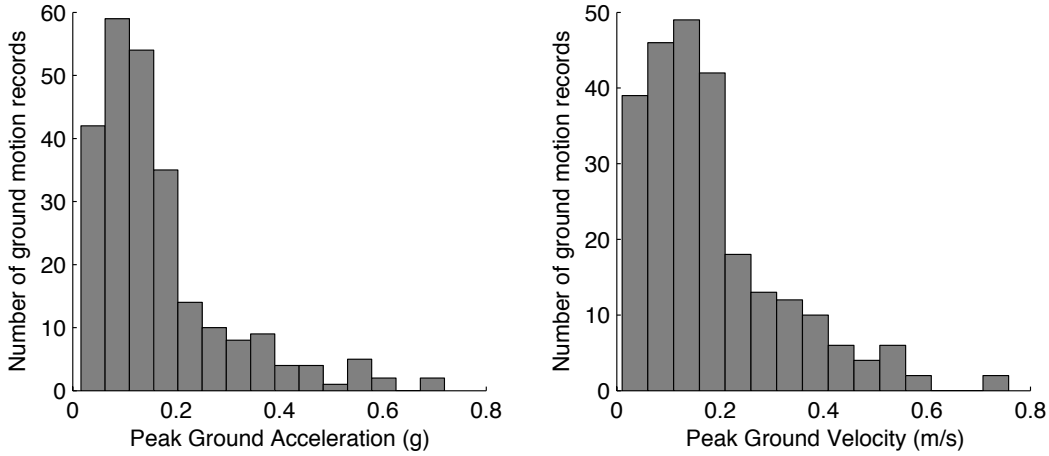

Figure 4.9 – Histogram of the PGA (left) and PGV (centre) in the selected ground motion records.

4.4.3. Results

Considering the previously defined building typologies, twelve sets of fragility functions were derived, each set comprised of three limit state curves, establishing the limits between four damage states (none to slight, moderate, extensive and complete). These damage states are defined according to certain steel and concrete strain levels, as described in section 4.3.1. These strain levels are defined herein in a probabilistic manner, as discussed by Crowley *et al*. (2004). For the building typologies designed before the implementation of the 1998 Turkish Design Code (termed as "non-compliant" and assumed to have inadequately confined members) the mean of the range of strain levels suggested by Crowley *et al*. (2004) was considered, whilst for the remaining building typologies designed after the implementation of the aforementioned code (termed as "compliant" and assumed to have adequately confined members), the values proposed by the most recent Turkish Earthquake Code (2007) were used for the mean strain levels, as presented in Table 4.3. The steel yielding strain was assumed to follow a normal distribution with a coefficient of variation of 10% (as recommended by Mirza and MacGregor, (1979) and JCSS, (2001)), whilst the concrete and steel strains for the second and third limit states were modelled as lognormal distributions with a coefficient of variation of 50% (as observed by Kappos *et al*., 1999 and discussed in Crowley *et al*., 2004).

Table 4.3 - Limit state definition according to Crowley *et al.* (2004) and Turkish Design Code (2007).

Limit state	Description	Mean		Coefficient of variation		Distribution
		Non-compliant	Compliant	Non-compliant	Compliant	
First	Threshold between none to slight and moderate damage states. Limit state is defined by the steel yielding strain: $\varepsilon_{sy} = {F_y}/{E}$ (E = Young Modulus)	ε_{sy} = 0.0018	ε_{sy} = 0.0023	24%	15%	Normal
Second	Threshold between moderate and extensive damage states. Limit state is defined by the steel and concrete strains: Inadequately confined members: ε_c=0.004 - 0.005, ε_s=0.010 - 0.015. Adequately confined members: ε_c=0.0035, ε_s=0.040	ε_c = 0.0045; ε_s = 0.0125	ε_c = 0.0035; ε_s = 0.040	50%		Lognormal
Third	Threshold between extensive and complete damage states. Limit state is defined by the steel and concrete strains: Inadequately confined members: ε_c=0.005 - 0.010, ε_s=0.015 - 0.030. Adequately confined members: ε_c=0.004, ε_s=0.060	ε_c = 0.0045; ε_s =0.015	ε_c = 0.004; ε_s = 0.060	50%		Lognormal

Although it is widely recognized that spectral ordinates provide a better correlation with damage than peak ground motion (e.g. Shome *et al.*, 1998), an exercise was briefly carried out to observe how such correlation varies using the methodology proposed herein. Thus, the correlation between the results and four different intensity measure types was evaluated for each building typology. For low rise, non-compliant RC frames with infill panels, peak ground acceleration, peak ground velocity and spectral acceleration for the periods at each limit state. The average coefficient of correlation and standard deviation across all of the building typologies, for each limit state, is presented in Figure 4.10.

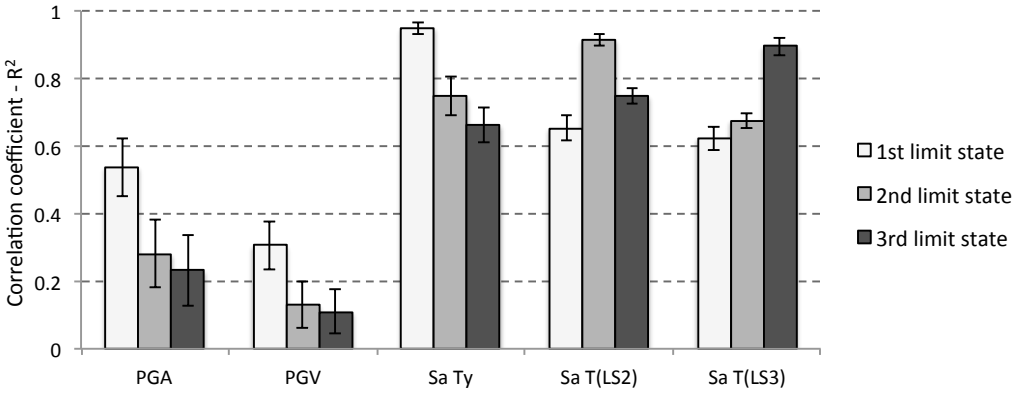

Figure 4.10 - Correlation between the results and the set of intensity measure levels for low rise, non-compliant reinforced concrete frames within infill panels.

As expected, there is clearly a stronger correlation between probability of exceedance of each limit state and spectral ordinates than with peak ground motion. Regarding the consideration of different periods of vibration, each limit state period provided a better correlation for the associated limit state. For the purposes of this study, a decision was made to use the spectral acceleration at the yielding period (*Ty*), as it is a measurement that provided a reasonable correlation across the three limit states, and uses a period that can be easily computed using the formulae presented in section 4.3.1.2. For this intensity measure type, a reduction in the correlation in the second and third limit state was consistently observed. This decrease is characterized by a larger dispersion of the results, as illustrated in Figure 4.11.

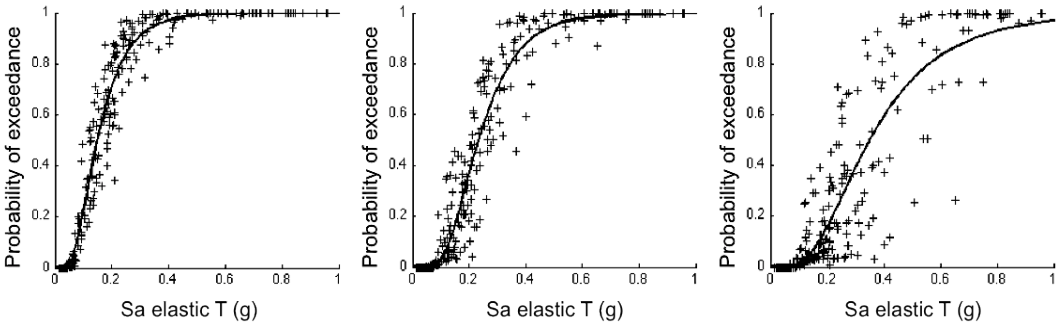

Figure 4.11 - Scatter of the results for RCW-LC-MR for the first, second and third limit state.

It is recognized that other ground motion parameters or combinations between different intensity measures types could decrease the dispersion in the data (Vamvatsikos and Cornell, 2005). However, for the sake of simplicity, only the

aforementioned intensity measurements have been investigated in the present study.

The logarithmic mean (λ), logarithmic standard (ζ) deviation and coefficient of correlation (R^2) per limit state for each building typology in terms of spectral acceleration at the yielding period (Ty) are presented in Table 4.4.

Table 4.4 Logarithmic mean and logarithmic standard deviation of each fragility curve in terms of spectral acceleration for the elastic period.

Building typology	T (sec)	LS1			LS2			LS3		
		λ (g)	ζ (g)	R^2	λ (g)	ζ (g)	R^2	λ (g)	ζ (g)	R^2
RCB-LC-LR	0.39	-1.036	0.541	0.966	-0.394	0.549	0.900	-0.071	0.628	0.798
RCB-LC-MR	1.61	-2.587	0.454	0.977	-1.612	0.485	0.879	-1.116	0.697	0.732
RCB-LC-HR	2.42	-3.067	0.381	0.987	-2.024	0.512	0.836	-1.354	0.841	0.629
RCB-HC-LR	0.72	-1.185	0.464	0.969	0.107	0.764	0.718	1.264	1.208	0.452
RCB-HC-MR	1.34	-1.901	0.296	0.973	-0.456	0.669	0.674	0.195	0.773	0.484
RCB-HC-HR	2.42	-2.570	0.277	0.991	-0.605	1.037	0.432	0.442	1.277	0.277
RCW-LC-LR	0.40	-1.265	0.525	0.964	-0.656	0.544	0.894	-0.564	0.551	0.878
RCW-LC-MR	0.88	-2.205	0.382	0.979	-1.365	0.548	0.882	-1.227	0.543	0.869
RCW-LC-HR	1.46	-2.735	0.330	0.993	-1.871	0.449	0.866	-1.721	0.503	0.839
RCW-HC-LR	0.35	-0.418	0.465	0.949	0.630	0.764	0.646	0.698	0.774	0.633
RCW-HC-MR	0.64	-1.096	0.341	0.972	0.000	0.522	0.707	0.052	0.533	0.693
RCW-HC-HR	1.16	-1.773	0.252	0.990	-0.531	0.616	0.711	-0.437	0.642	0.685

4.5. Comparison with Other fragility models

In In order to verify the proposed methodology, a study was carried out to compare the results obtained with this method, against the ones achieved using: 1) nonlinear dynamic analysis and 2) from previous studies. The first exercise had the advantage of using exactly the same probabilistic distributions of the material and geometric properties, damage state definition and intensity measure type. Thus, differences in the results should be mainly due to the different nonlinear response approaches and not due to the fact that distinct building classes or damage scales are being considered. For the second comparison, fragility models developed for RC building for Turkey in the past years were gathered, and for a selected number of these studies, the proposed methodology was employed to derive fragility models for those building classes.

4.5.1. Using Nonlinear Dynamic Analysis

In the work of Silva *et al*. (2012a), one hundred RC 2D frames were modelled using the software OpenSEES [21] and several nonlinear dynamic analyses were performed in order to derive fragility functions. A reinforced concrete four storey building typology without infill panels designed before the implementation of the 1998 Turkish Design Code was considered, whose material and geometric characteristics follow the distributions proposed by Bal *et al.* (2008b). The non-linearity of the materials was modelled using fibre elements and the top displacement was used to define the limit states. This global parameter was chosen to establish each limit state, because the focus of this study is to derive fragility functions for building typologies and therefore, more detailed criteria based on member deformation, local strains or hinge mechanisms usually adopted for the evaluation of individual structures would not be appropriate (Akkar *et al.,* 2005; Erberik, 2008).

In order to estimate the top displacement for each limit state, a displacement-based adaptive pushover curve (Antoniou and Pinho, 2004) was computed for each generated 2D frame, and the three limit state displacements were defined according to the following criteria:

- Limit state 1: top displacement when 75% of the maximum base shear capacity is achieved;
- Limit state 2: top displacement when the maximum base shear capacity is achieved;
- Limit state 3: top displacement when the base shear capacity decreases 20%.

The mean pushover curve (base shear versus top displacement) across all the generated 2D frames was calculated and transformed into a capacity curve (spectral acceleration versus spectral displacement) as depicted in Figure 4.12, along with the associated limit states. The equivalent mean capacity curve generated using the strain levels employed in the DBELA approach is also presented. For this latter curve, the spectral displacements for each limit state were computed according to the formulae presented in section 4.3.1.1, and the respective spectral accelerations were derived through the following expression:

$$Sa_{LS_i} = \frac{4\pi^2 Sd_{LS_i}}{T_{LS_i}^2} \tag{4.14}$$

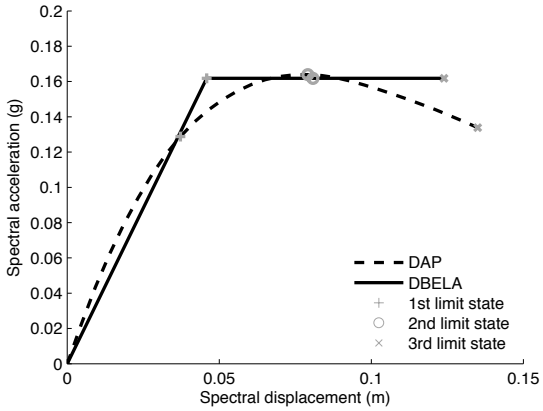

Figure 4.12 - Comparison between mean capacity curves and respective limit states, estimated using the strain levels (DBELA) and top displacement (DAP) criteria.

From Figure 4.12 it is possible to observe a bias in the spectral displacements between the different methodologies. Such discrepancies are expected, as the damage state criteria between the two methods are very distinct (maximum top displacement in the nonlinear dynamic analysis and strain levels in the concrete and steel in the DBELA method). The impact of these differences in the fragility and vulnerability functions is discussed later.

After the computation of the pushover curve, one hundred ground motion records were randomly extracted from the ground motion input described in section 4.4.2, and used to perform nonlinear dynamic analyses for each frame. This reduction in the number of accelerograms used for this comparison exercise served the purpose of keeping the computation time to a reasonable level. The maximum top displacement observed during the dynamic analyses of each analysis was compared to the three limit state displacements in order to allocate each frame in a damage state.

Using the same building typology and ground motion input, two sets of fragility functions were derived, one following the simplified methodology proposed herein and another one using the nonlinear dynamic analyses. In Figure 4.14, the resulting limit state curves are shown, along with the associated data points used to derive them.

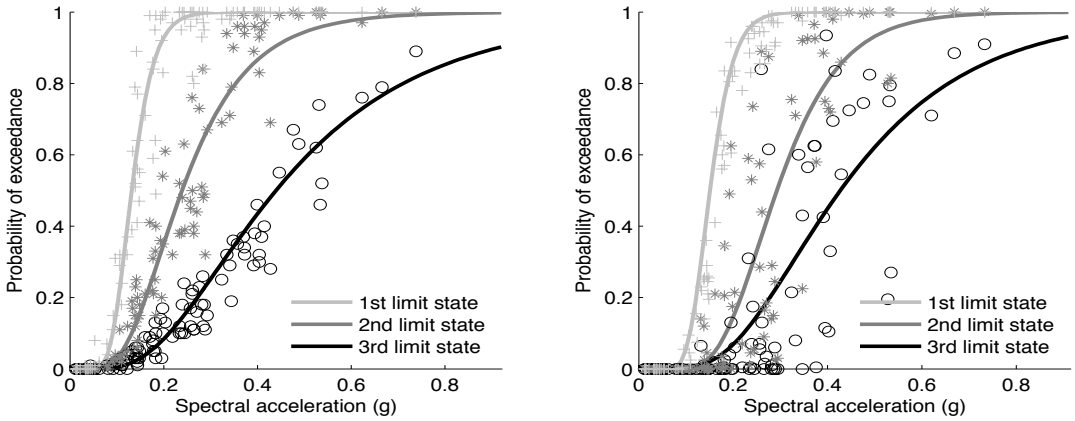

Figure 4.13 - Fragility models derived through dynamic analyses (left) and applying the proposed DBELA methodology (right).

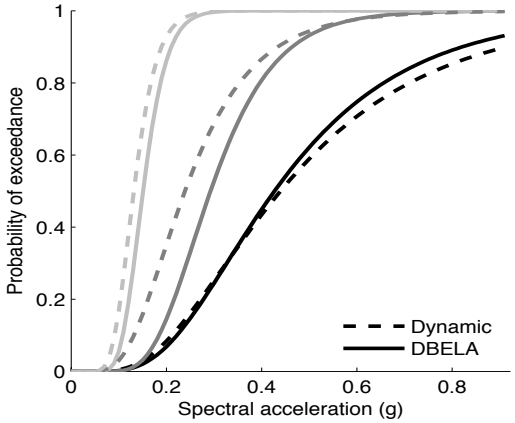

Figure 4.14 – Comparison between fragility models derived using dynamic analyses and the proposed DBELA methodology.

With the exception of the fragility curves for the second limit state in which a maximum absolute difference of about 0.19 in the probability of exceedance was observed, it is fair to state that a satisfactory matching of the results was obtained. Considering the whole set of limit state curves, an average absolute discrepancy of 0.09 was obtained.

As mentioned in the description of the spectral ordinates for the different limit states, there is a discrepancy mostly in the first and third limit states between these two methodologies. In the nonlinear dynamic analysis the first limit state is achieved for a smaller spectral displacement and the DBELA methodology seem to have a lower displacement capacity. This trend is also observed in the resulting fragility functions, in which the fragility curve for the first limit state using dynamic analysis shows a smaller mean spectral displacement. Likewise, a lower mean spectral

displacement is also observed in the third limit state curve when employing the proposed DBELA methodology. These statistics are described in Table 4.5.

Through the observation of the distribution of the data points from each approach, it is possible to notice that a larger dispersion is obtained with the DBELA approach, mainly for the third limit state. This scatter implies that the uncertainty in the statistics (mean and standard deviation) used to define each limit state curve will be greater in the results from the DBELA procedure. These uncertainties were quantified with the bootstrap methodology previously mentioned. In Table 4.5, the mean and coefficient of variation of each parameter is presented, as well as the respective probability density function.

Table 4.5 - Probabilistic distribution of the statistics of the limit state fragility curves.

Limit state	Approach	Logarithmic mean			Logarithmic standard deviation		
		Mean	COV	PDF*	Mean	COV	PDF*
First	Dynamic	-2.036	0.02	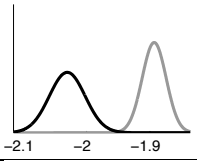	0.329	0.12	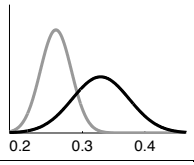
	DBELA	-1.892	0.01		0.258	0.09	
Second	Dynamic	-1.431	0.02	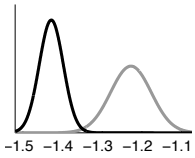	0.400	0.07	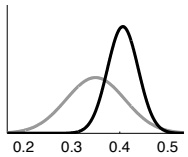
	DBELA	-1.233	0.04		0.359	0.18	
Third	Dynamic	-0.803	0.05	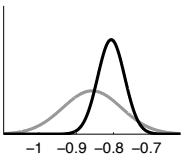	0.531	0.09	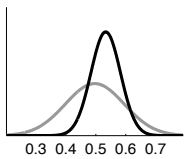
	DBELA	-0.861	0.10		0.512	0.23	

* Probability density function for the parameters obtained in the dynamic (black) and DBELA (grey) methodologies.

As mentioned already, the mean and standard deviation for each limit state curve obtained using the methodology proposed herein have a greater associated uncertainty, with the exception of the first limit state curve where both approaches showed variability of the same order. Moreover, the standard deviation of the lognormal distribution using the DBELA methodology is systematically lower, in comparison with the standard deviation when employing the nonlinear dynamic analysis. This behaviour might be due to the underestimation of the record-to-record variability, as mentioned in section 4.3.1.2.

These statistics were used to sample one hundred sets of fragility functions, which were then combined with the consequence model proposed by Bal *et al*. (2008b) (see Figure 3.14), to derive vulnerability functions. Then, at each intensity measure level the distribution of loss ratio was evaluated and the mean, 10% and 90% percentile were estimated, as illustrated in Figure 4.15 and Figure 4.16.

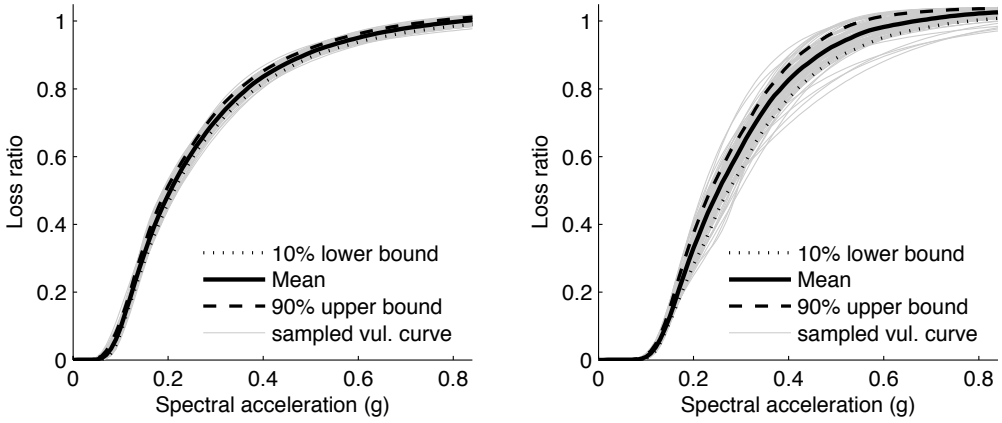

Figure 4.15 - Vulnerability curve using dynamic analyses (left), the proposed DBELA methodology (centre) and comparison between both (right).

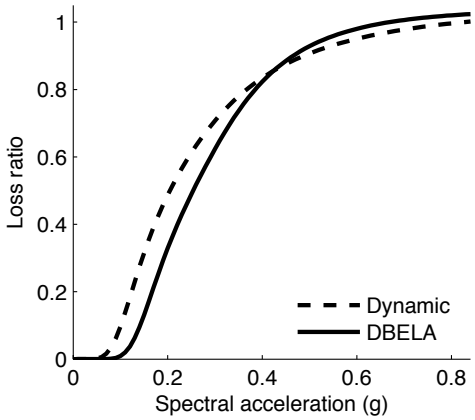

Figure 4.16 - Vulnerability curve using dynamic analyses (left), the proposed DBELA methodology (centre) and comparison between both (right).

Again, despite the satisfactory correspondence between the two approaches, it is relevant to note the larger variability in the loss ratio at each intensity measure level when employing the simplified methodology proposed herein.

4.5.2. From previous studies

In the past years, the vulnerability of the Turkish building stock has been the subject of many studies, mainly for what concerns RC buildings designed before the

implementation of the 1998 design code (the most recent and rigorous regulation). In Table 4.6 some of the characteristics of these studies are summarised.

Table 4.6 - Summary of proposed fragility models from the past 10 years.

Author	Building typologies	Applicability	Intensity Measure type	Damage Scale	Methodology
Erdik *et al.* (2003)	Low-, mid- and high-rise RC frame buildings built before and after 1980.	Turkey	MSK-81 Sd (T_{el})*	Slight; moderate; extensive; complete.	Empirical; Simplified analytical method.
LESSLOSS (2005)	Low-, mid- and high-rise RC frame buildings before and after 1980.	Istanbul	MSK-81 Sd (T_{LS})**	Slight; moderate; extensive; complete.	Empirical; Simplified analytical method.
Akkar *et al*. (2005)	Low- (4 and 5 storeys) mid-rise (RC buildings mainly from the 1970's.	Turkey	PGV	Light; moderate; severe.	2D Nonlinear dynamic analysis using equivalent SDOF.
Kirçil and Polat (2006)	Mid-rise (3, 5, and 7 storeys) RC frame buildings built according to the 1975 design code.	Turkey	PGA Sa (T_{el})* Sd (T_{el})*	Yielding; collapse.	3D Nonlinear dynamic analysis using MDOF.
Hancilar *et al*. (2006)	Mid-rise RC frame with RC shear walls (schools).	Istanbul	PGA Sd (T_y)***	Slight; moderate; extensive; complete.	3D Nonlinear dynamic analysis using MDOF.
Erberik (2008)	Low- (3 storeys) and mid-rise (4, 5 and 6 storeys) RC frame buildings with and without infills.	Turkey	PGV	Serviceability; damage control; collapse prevention.	2D Nonlinear dynamic analysis using equivalent SDOF.
Ahmad *et al.* (2010)	Low- (2 storeys), mid- (5 storeys) and high-rise (8 storeys) RC frame ductile and nonductile buildings.	Italy, Greece and Turkey	PGA Sd (T_{LS})**	Slight; moderate; extensive; complete.	DBELA-based analytical method.
Ozmen *et al*. (2010)	Low- and mid-rise RC frame buildings built according to the 1975 design code.	Turkey	PGA	Immediate occupancy; life safety; collapse prevention.	2D Nonlinear dynamic analysis using equivalent SDOF.

* Spectral ordinate for the elastic period.
** Spectral ordinate for the inelastic period.
*** Spectral ordinate for the yielding period.

The variability in aspects such as building typologies covered or the damage states that were considered in each study, renders the comparison process of the results using the proposed methodology with those obtained from previous authors very difficult, and for some of the cases, even impossible. For instance, some of the fragility models developed within the LESSLOSS (2005) European project or by Erdik *et al*. (2003) and Ahmad *et al*. (2010) used macroseismic intensity (MSK-81) or spectral displacement for the inelastic period ($Sd(T_{LS})$), which are intensity

measure types not currently supported by the proposed methodology. The damage scale (number and definition of each limit state) also varies significantly from author to author, representing the main obstacle to the direct comparison of fragility curves; as can be seen from Table 4.6, the number of limit states varies from only 2 up to 4. Furthermore, even when the same number of limit states is employed, different criteria for the definition of these limits are frequently assumed; as an example, the fragility models in LESSLOSS (2005), Hancilar *et al*. (2006) and Ahmad *et al*. (2010) all use the same damage scale (slight, moderate, extensive and complete) but in the first study, roof top displacement is used to estimate the damage state of each building, whilst in the second, inter-storey drift was preferred and in the last work, steel and concrete strain levels were utilized. Despite these differences in the damage scale, there are two thresholds that are roughly assumed across the majority of the studies: yielding and collapse. The first limit state is commonly established as the boundary between slight and moderate damage, while the second usually refers to the last limit state curve of the fragility model. Thus, it was decided to carry out these comparisons considering only these two limits, as comparing intermediate limit states would not be reliable. The fragility models selected for this exercise were chosen so that different intensity measure types and building typologies would be considered. Then, the proposed methodology was employed to derive sets of fragility curves for the building typologies that were considered in each study. The results for three cases are illustrated in Figure 4.17.

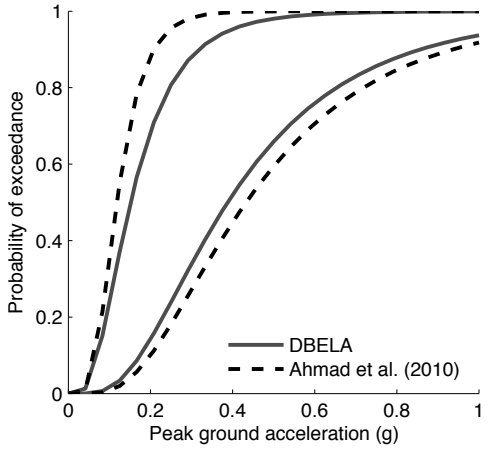

a)

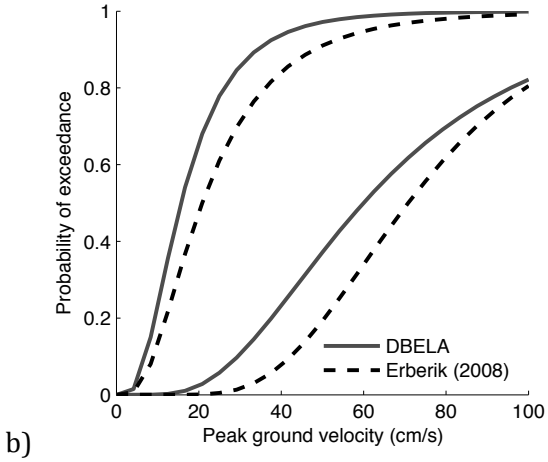

b)

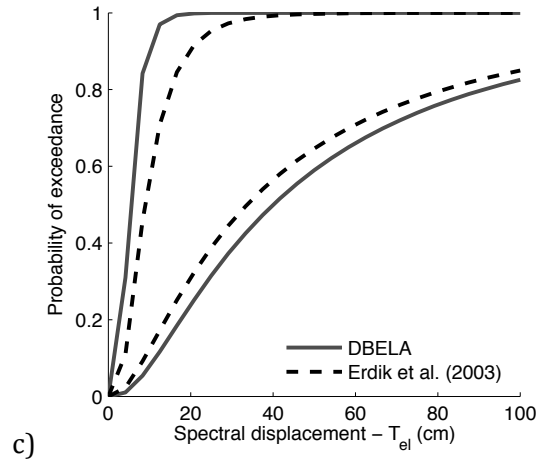

c)

Figure 4.17 - Comparisons between fragility functions produced using the DBELA methodology and from other studies for RC buildings: high code and low-rise (a), low code and low-rise (b), low code and mid-rise (c).

Notwithstanding the differences in the methodologies and assumptions in each case, the procedure proposed herein managed to provide a reasonable approximation of the fragility curves, mainly for the collapse limit state, which usually has a higher importance in loss assessment.

4.6. Final remarks

In this Chapter, a simplified methodology for the derivation of fragility and vulnerability functions based on the DBELA approach was presented. The procedure relies on a probabilistic framework, which allows the consideration of the material, geometric and limit state uncertainties of the considered building typology, as well as, to some extend, the variability in the ground motion records.

A set of fragility functions has been derived for twelve distinct RC building typologies, organized based on the time of construction, number of storeys and presence of masonry infill panels. Since the building characteristics employed herein were developed based on real information from buildings located in Istanbul, the application of these fragility functions in loss assessment in other regions calls for due care.

This procedure provided a good balance between computational efficiency and reliability, allowing a quick but still accurate assessment of the physical vulnerability. The proposed procedure does not require the employment of any finite element analysis, which reduces its computing time by a order of 100, in comparison to the approaches in which nonlinear dynamic analysis are utilised.

The reliability of this method has been thoroughly investigated by comparing its results with those obtained using nonlinear dynamic analysis, as well as with fragility functions developed in previous studies by other research groups. Despite the good correlation between the results using this methodology and those employing nonlinear dynamic analyses, it is important to acknowledge the increase in the uncertainty in the resulting fragility and vulnerability functions. Furthermore, the simplified methodology adopted herein only partially considers the record-to-record variability, due to the employment of a deterministic procedure to estimate the nonlinear damped response. The improvement of the estimation of the nonlinear structural response is part of the future development plan. This includes the possible employment of nonlinear time history analysis in single degree of freedom oscillators or the employment of magnitude- and distance-dependent methods to reduce the elastic spectrum to its inelastic counterpart (Rezaeian *et al*., 2012).

The fragility and vulnerability models produced with this tool can be directly used in the open source software described on Chapter 2 (OpenQuake-engine), for seismic risk assessment and loss estimation.

Chapter 5

Investigation of the characteristics of the Portuguese RC Building Stock and Development of a Vulnerability Model

Silva, V., Crowley, H., Pinho, R., Varum, H. (2013) "Investigation of the characteristics of the Portuguese RC building stock and development of a vulnerability model". *Bulletin of Earthquake Engineering*, in review.

5.1. Summary

A vulnerability model capable of providing the probabilistic distribution of loss ratio for a set of intensity measure levels is a fundamental tool to perform earthquake loss estimation and seismic risk assessment. The aim of the study presented herein is to develop a set of vulnerability functions for six reinforced concrete building typologies, categorized based on the date of construction (which has a direct relation with the design code level) and number of storeys (height of the building). An analytical methodology was adopted, in which thousands of nonlinear dynamic analyses were performed on 2D moment resisting frames with masonry infills, using one hundred ground motion records as much as possible compatible with the Portuguese tectonic environment. The generation of the structural models was carried out using the probabilistic distribution of a set of geometric and material properties, compiled based on information gathered from a large sample of drawings and technical specifications of typical Portuguese reinforced concrete buildings, located in various regions in the country. Various key aspects in the

development of the vulnerability model are investigated herein, such as the selection of the ground motion records, the modelling of the infilled frames, the definition of the damage criterion and the evaluation of dynamic (i.e. period of vibration) and structural (i.e. displacement and base shear capacity) parameters of the frames. A statistical bootstrap method is employed to analyse the variability of the loss ratio at each intensity measure level, allowing the estimation of the mean, as well as 10% and 90% percentile vulnerability curves.

5.2. Introduction

Earthquake loss estimation can play a fundamental role in the sustainable development of a given region, providing local governments and other decision makers with valuable information necessary to the creation of risk mitigation actions. These may include post-disaster emergency planning, building retrofitting campaigns, creation of insurance pools, strategic urban planning, amongst other measures. An important component for this purpose is a vulnerability model that allows the estimation of losses from structural/non-structural damage due to earthquakes, as a function of a set of ground motion parameters.

The structural vulnerability of the Portuguese building stock has been the target of only limited investigation in recent years. However, in the European project LESSLOSS (2004-2007) (Calvi and Pinho, 2004), in which the metropolitan area of Lisbon was used as test case (Spence, 2007), various fragility functions were developed by Carvalho *et al.* (2002) for a set of building typologies. These curves were computed using the simplified methodology from HAZUS (FEMA, 1999) that relies on a capacity curve that is constructed from a group of parameters (related to the design of the structure), which is then used to extract a set of spectral displacements (one per limit state) according to pre-defined global drift thresholds. Each spectral displacement is used as the median of a cumulative lognormal distribution, with a given pre-established logarithmic standard deviation, to represent the respective limit state fragility function. For each building typology, a number of curves describing the probability of exceeding a set of damage states was computed, using damped spectral displacement at the inelastic period to represent the various levels of ground motion. Such output can be used together with capacity spectrum-based methodologies (e.g. N2 – Fajfar, 1999; Capacity Spectrum Method –

Freeman, 2004) to assess the distribution of buildings throughout a set of damage states, which can then be converted into an economic loss.

Notwithstanding the importance and contribution of the above fragility model, which has already been employed in a seismic risk assessment in Portugal (Campos-Costa *et al.*, 2009), there are a number of reasons that may justify the development of a novel fragility model for Portugal: i) the use of spectral ordinates for the inelastic period (thus a specific period for each level of ground motion) complicates the seismic risk assessment, as it does not allow the direct use of commonly available ground motion prediction equations (GMPE) to compute the ground motion at the location of the assets; ii) the design parameters used in the construction of the capacity curve (strength coefficient, over-strength factor, elastic period and ductility factor) have been specifically calibrated for structures typically found in the United States; iii) the shape of the simplified capacity curve fails to account for the decrease in the base shear capacity due to P-delta effects; and, iv) in the case of reinforced concrete building typologies, the influence of eventual masonry infill panels has been neglected.

Despite the availability of other fragility models developed for generic European buildings (Mouroux and Brun, 2006), or for other countries whose building stock could have some similarities to the Portuguese one (e.g. Spain - Vargas *et al*. (2010), Italy - Borzi *et al*. (2008), Greece - Kappos *et al*. (2006)), the characteristics in the structural capacity and response might not be realistically representative of Portuguese buildings, and consequently they could affect the reliability of the resulting earthquake loss estimation.

This Chapter hence focuses on the structural vulnerability of reinforced concrete buildings in Portugal, which represent about 50% of the total building stock in the country, according to the 2011 Census Survey [30]. Due to the lack of data regarding post-earthquake damage for this type of buildings in Portugal, an analytical methodology has been adopted herein. Thus, hundreds of models of moment resisting frames were produced to represent the RC building stock in Portugal, and subjected to one hundred ground motion records, using nonlinear dynamic analyses. In order to generate frames capable of reproducing the structural characteristics of the RC building stock in Portugal, 400 drawings were collected in many parts of the country, from public institutions, design offices and private practitioners, and subsequently analysed with the purpose of estimating the probabilistic distribution

of a set of geometric parameters. Each generated frame was subjected to a nonlinear dynamic analysis per ground motion record, and two different criteria were employed to allocate each frame into a damage state. Six building typologies were considered herein, based on the data of construction (or seismic design philosophy and practice) and number of storeys (or height of the structure), leading to six fragility models in terms of spectral acceleration for the inelastic period. These results were combined with a consequence model (fraction of loss for each damage state), to produce a vulnerability model (set of loss ratios for a set of intensity measure levels), which can be used directly for economic loss estimation. The results from this study were applied in a probabilistic seismic risk assessment for mainland Portugal, as described in the following Chapter.

5.2.1. Portuguese RC building stock

Reinforced concrete construction accounts for approximately 50% of the Portuguese building stock and hosts 60% of the national population, since on average it contains more dwellings than the other building typologies. Within this building class, at the time of the 2011 Census Survey, 49% of the buildings had not been designed according to the most recent seismic code (RSA, 1983), which represents approximately 3.1 million habitants living in structures that might not be capable of withstanding the effects on an eventual earthquake. Thus, the year of construction plays an important role in classifying the building portfolio according to the seismic design level.

In Portugal, the first design codes that contained provisions regarding the consideration of seismic action date from 1958 (RSCCS) and 1961 (RSEP). In 1967, a regulation was introduced for reinforced concrete structures (REBA). However, such recommendations were overly simplified and did not impose adequate seismic performance requirements. Later, in 1983, a new and more demanding design code (RSA) was introduced, which is still in use nowadays, along with Eurocode 2 (CEN, 2004). Thus, buildings constructed before 1983 are categorized herein as pre-code (PC), whilst the ones built after are termed post-code (C).

Regarding the number of floors, three categories are considered herein: up to three storeys as low-rise (LR), between four and six storeys as mid-rise (MR) and seven or more storeys as high-rise (HR). A summary of the RC building stock

following the aforementioned parameters and their spatial distribution throughout mainland Portugal are illustrated in Figure 5.1.

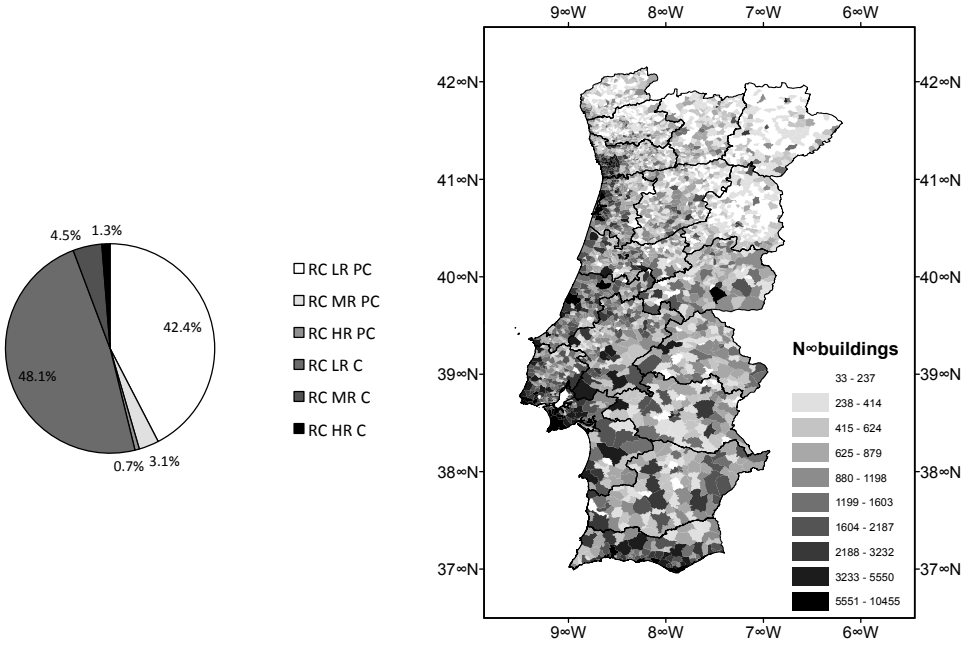

Figure 5.1 - Percentage of RC buildings according to year of construction and number of floors (left), and spatial distribution throughout Portugal at the parish level (right), according to the 2011 Census Survey.

5.2.2. Geometric properties of Portuguese RC building stock

In this study, the material and geometric properties of the RC buildings with a moment-resisting frame as the structural system were thoroughly analysed. In order to do so, 400 drawings and design specifications from real buildings were gathered throughout the country, in cooperation with private practitioners, design offices and public institutions. The collection of blueprints from many parts of the country and from different entities was done with the purpose of capturing the variability in the structural design and construction practices endorsed in the different regions. Nevertheless, the set of blueprints that were considered were conditioned to the availability and willingness of the various private and public institutions to cooperate in this study. From the 400 drawings, only 50% were used to estimate the statistics of each geometric parameter, as the remaining blueprints were from structures mainly composed by masonry or shear walls, vertically or horizontally very irregular or were related to industrial, public infrastructures or purely commercial buildings. The number of drawings analysed per building typology and its distribution per district in Portugal is presented in Figure 5.2.

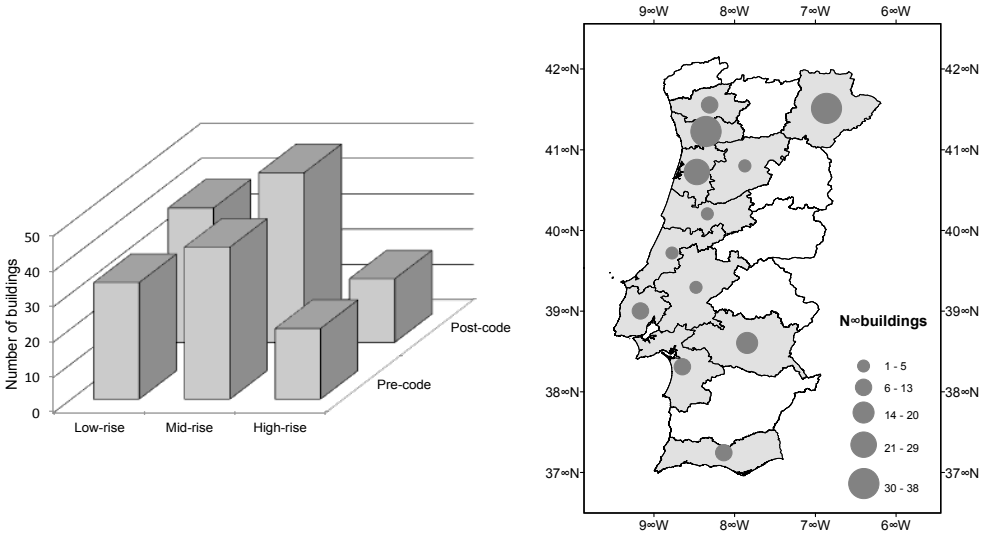

Figure 5.2 - Number of buildings analysed per number of storeys and date of construction (left) and the distribution per district in Portugal (right).

For each building drawing, the main frames in the structure that would resist lateral loads were chosen in order to measure the following set of geometric parameters: ground story and upper storeys heights, column widths and depths, beam lengths, widths and depths, and slab thicknesses. Then, the data for the various parameters was disaggregated according to the six building typologies, in order to assess if some geometric properties were directly related to the date of construction and/or number of storeys and hence they should be considered separately from the data of the other typologies.

To model each geometric property, several probabilistic distributions (normal, lognormal, exponential, gamma, beta and weibull) were considered, and their statistical parameters derived using the maximum likelihood approach. Then, each distribution was evaluated in terms of the best-fit (i.e. the size of the residual between the reference and the modelled data) and goodness-of-fit (i.e. the capability of providing a satisfactory fit given a certain level of significance). For the latter, the Chi-square test was used for levels of 1%, 5% and 10% significance. A similar study was carried out by Bal *et al*. (2008b) for the Turkish building stock and was used to guide the work undertaken and presented herein.

5.2.2.1. Inter-story height

RC buildings in Portugal frequently present differences in height between the ground story and the remaining upper floors (herein termed as the regular story

height), usually due to the need to have wider spaces at the ground floor for commercial purposes or garages. The Portuguese legislation (RGEU, 2007) has established since 1951 that a minimum clear height between the floor and the ceiling of 2.7 meters should be present in dwellings, and a minimum clear height of 3.0 meters is required in public areas, commercial spaces and offices. No significant differences were observed in the statistics when disaggregating the data according to date of construction or number of storeys and therefore, all of the data was considered together in order to estimate these distributions. The ground story height was found to follow a lognormal distribution with a mean height of 3.21 meters and a coefficient of variation of 13%, whilst the regular story height was modelled with a normal distribution with a mean value of 2.88 meters and a coefficient of variation of 7%. Both distributions proved to pass the Chi-square test with a significance level of 1%. In Figure 5.3, the histograms and associated probabilistic distributions of these parameters are illustrated.

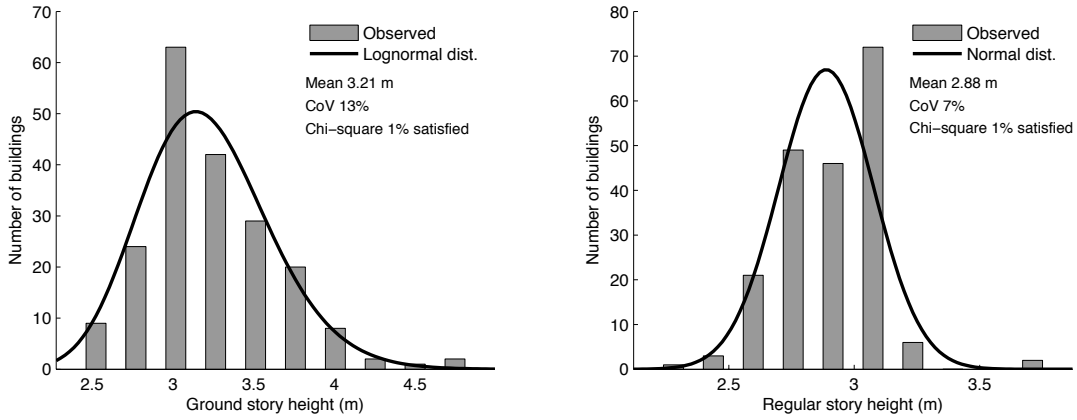

Figure 5.3 - Distribution of ground story (left) and regular story (right) heights for all RC buildings.

The correlation between these two heights was estimated as 0.24, which can be considered insignificant. Thus, if the aforementioned statistics are used to generate synthetic frames, these two parameters can be sampled independently.

5.2.2.2. Column properties

For what concerns the column depth, the disaggregation of the data revealed a strong influence, as expected, in the number of storeys and time of construction. The dependence with the building height is certainly due to the higher axial loads in taller buildings, which consequently leads to columns with larger sections. Regarding the time of construction, the increase in the column depth and width is

probably due to the implementation of the seismic code of 1983, imposing higher bending moments in the design process, thus leading to longer sections, as was also verified in the depth of the beams. The statistics for the column depth are summarized in Table 5.1.

Table 5.1 - Probabilistic distribution of column depth for each RC building typology.

Building typology		Number of buildings	Probabilistic distribution	Mean (m)	Coefficient of variation	A[a] (m)	B[a] (m)	Chi-square test
Pre-code	Low-rise	33	Lognormal	0.28	15%	0.20	0.44	NS[b]
	Mid-rise	43	Normal	0.36	23%	0.24	0.55	10%
	High-rise	20	Lognormal	0.57	40%	0.28	1.00	10%
Post-code	Low-rise	38	Normal	0.38	20%	0.26	0.60	10%
	Mid-rise	48	Lognormal	0.43	20%	0.28	0.70	5%
	High-rise	18	Lognormal	0.51	36%	0.30	0.95	10%

[a] A and B represent the minimum and maximum values of the observed data respectively.

[b] NS signifies that the Chi-square test could not be satisfied for any of the established significance levels.

With regards to the column width, a slightly different behaviour was observed. For the pre-code buildings, no relevant discrepancies were verified in the column width between buildings with a distinct number of stories. In fact, during the process of evaluating the drawings, it was noticed that the majority of the columns from the pre-code buildings were only designed to withstand the bending moment in a single direction. Therefore, the column width was frequently established a priori within a range between 0.20 and 0.30 meters, as it was assumed that these elements would not have to resist any significant bending moment in this direction. Concerning the column width for the post-code buildings, the implementation of the 1983 seismic code, the introduction of automatic tools and the three-dimensional design of the structures propelled the consideration of larger bending moments in the two directions, leading to columns with increasing sections (not just a greater depth but also width as discussed before) with the number of storeys. The results for this parameter are described in Table 5.2.

Table 5.2 - Probabilistic distribution of column width for each RC building typology.

Building typology		Number of buildings	Probabilistic distribution	Mean (m)	Coefficient of variation	A[a] (m)	B[a] (m)	Chi-square test
Pre-code		96	Lognormal	0.27	16%	0.20	0.53	NS[b]
Post-code	Low-rise	38	Normal	0.25	11%	0.20	0.30	1%
	Mid-rise	48	Normal	0.27	13%	0.20	0.37	1%
	High-rise	18	Lognormal	0.31	23%	0.21	0.53	NS[b]

[a] A and B represent the minimum and maximum values of the observed data respectively.

[b] NS signifies that the chi-square test could not be satisfied for any of the established significance levels.

5.2.2.3. Beam properties

As previously mentioned, for each drawing only the frames that provided the main lateral load resistance to the building were considered. This approach allowed the elements that were built mainly for aesthetics or to support secondary elements (e.g. balconies) to be neglected. The investigation of the beam properties covered the beam length, width and depth.

Regarding the first two parameters, no significant differences in the statistics were observed when disaggregating the data based on the date of construction or number of storeys, probably due to the fact that the beam length is more influenced by architectural requirements and the beam width is related with the thickness of the walls and depth of the beams, rather than code guidelines or the height of the building. Beam length was found to have a mean of 4.37 meters with a coefficient of variation of 11%, while for the beam width a mean of 0.27 meters with a coefficient of variation of 16% was calculated. Both geometric parameters were modelled using a lognormal distribution, but the former satisfied the Chi-square test for a significance level of 5% whilst the latter did not satisfy this test for any of the established significance levels. The results for these parameters are presented in Figure 5.4.

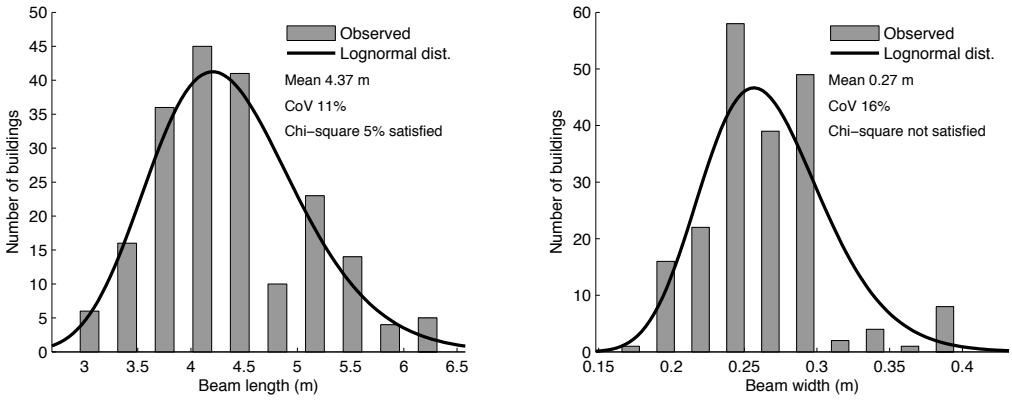

Figure 5.4 - Distribution of beam length (left) and width (right) for all RC buildings.

For the beam depth, a relevant discrepancy was observed in the statistics between the buildings constructed before and after the implementation of the design code of 1983. Thus, the data has been separated and the beam depth for the pre-code was assumed to follow a normal distribution with a mean of 0.44 meters and associated coefficient of variation of 22%, whilst for the post-code buildings a lognormal distribution was used with a mean of 0.50 meters and coefficient of

variation of 18%. For the pre-code beam depth, it was possible to satisfy the Chi-square test for a significance level of 1%, though for the post-code beam depth, in which despite the low residual between the observed data and the probabilistic model, none of the significance levels were respected. Figure 5.5 presents the results for this geometric parameter.

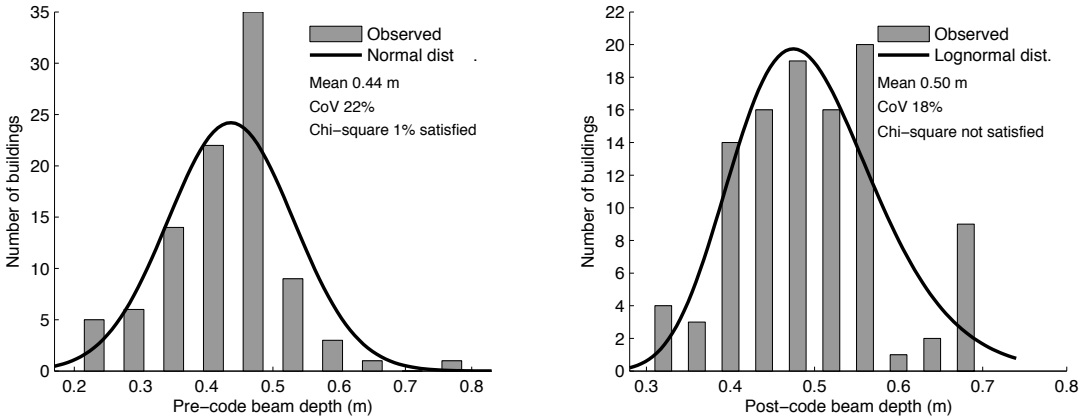

Figure 5.5 - Distribution of beam depth for pre-code (left) and post-code (right) RC buildings.

A clear increase in the beam depth can be seen between the pre- and post-code buildings, probably due to the fact that the adequate consideration of the lateral loads due to the seismic action led to higher bending moments in the beams, and consequently a greater depth to withstand such demands.

Moreover, the correlation between the beam geometric parameters has been investigated, as the calculation of beam depth should be directly related to the beam length. For the pre-code buildings, a correlation of 0.53 was estimated while for the post-code buildings, a larger correlation of 0.76 was observed. This increase in the correlation for the post-code buildings might be due to the introduction of automatic tools in the design of the buildings, leading to section dimensions uniquely calculated for each structural element. In fact, during the process of evaluating the drawings and design specifications, it was observed that buildings with similar dimensions but with distinct construction times had a striking difference in the variability of the structural elements dimensions. Buildings built more recently were frequently designed with tens of different beam sections whilst for the pre-code buildings, only a few sections were designed and applied repeatedly in beams often with different lengths. The employment of the correlation factor during the generation of synthetic RC building frames using a Monte Carlo sampling approach is fundamental to ensure that unrealistic structural elements are not created (e.g.

long beams with very small section depth). The scatter between the beam depths and the respective beam lengths are depicted in Figure 5.6.

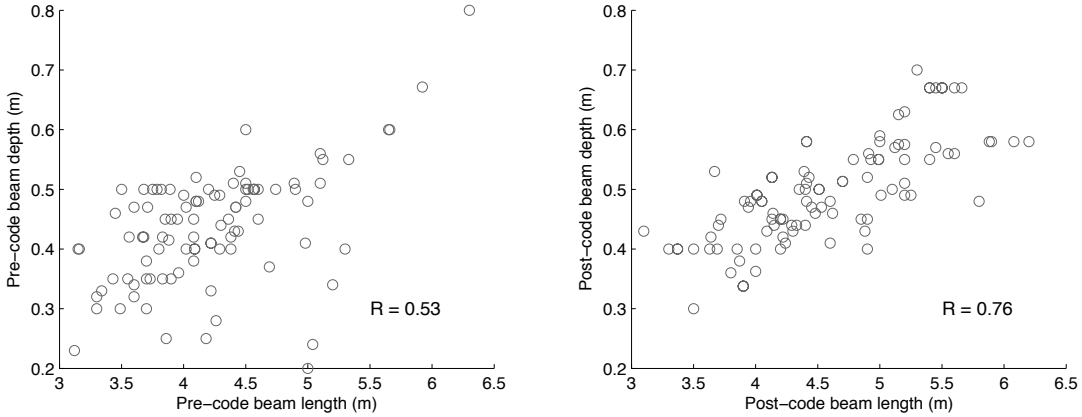

Figure 5.6 – Correlation between beam length and depth for pre-code (left) and post-code (right) RC buildings.

5.2.2.4. Slab thickness

The floors of the common RC buildings in Portugal are mostly composed of pre-cast pre-stressed RC beams with clay hollow blocks and a cast-in-place concrete topping layer. It is also possible to find purely cast-in-place reinforced concrete slabs, mainly in floors with long spans or more recently, in flat slab buildings only consisting of columns and slabs, without the use of beams. The thickness of the slabs was also investigated, as it is an important parameter to be considered in the estimation of the gravity loads. Again, the data was disaggregated based on the date of construction (pre- and post-code), and the respective results are illustrated in Figure 5.7.

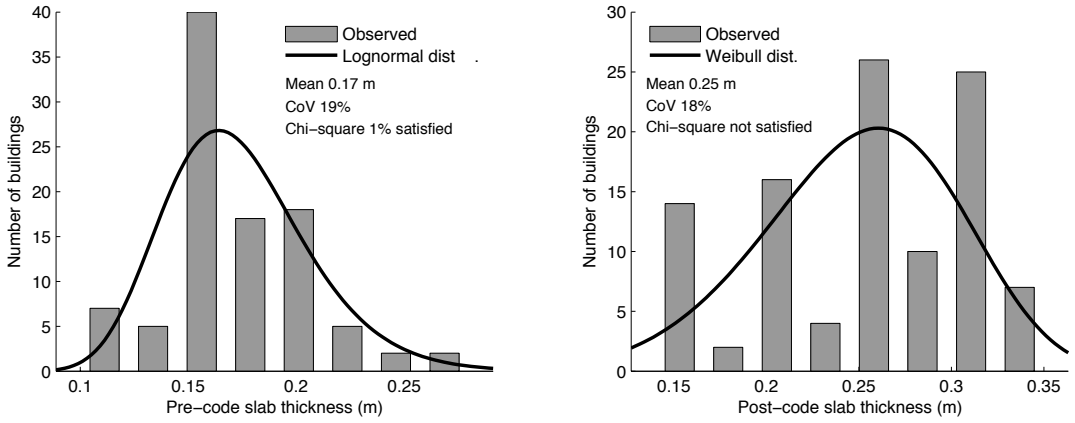

Figure 5.7 – Distribution of slab thickness for pre-code (left) and post-code (right) RC buildings.

5.2.3. Material properties of Portuguese RC building stock

An attempt has also been made herein to investigate the probabilistic distribution of the concrete and steel mechanical properties of Portuguese buildings. In order to estimate such statistics, ideally a large number of random buildings should be selected, and field tests should be carried out to calculate properties such as the concrete compressive strength and steel rebar yielding and ultimate strength. Since such endeavor would require a great amount of human and economic resources, for the concrete compressive strength, it was decided to take advantage of the availability of data from measurements on buildings that were subjected to structural retrofitting/rehabilitation or demolition, provided by public and private institutions that carried out those tests on the concrete. The measurements were mostly done through destructive approaches, in which a concrete drilling core was extracted from a column or beam, and compressed until rupture in the laboratory. For the steel properties, the results from previous studies have been investigated and employed.

5.2.3.1. Concrete properties

Regarding the code specifications for concrete properties, the first regulation that imposed minimum requirements for the compressive strength dates from 1918 (120 kg/cm^2 or ≈12 MPa), which was later replaced by another regulation in 1935 (RBA) (180 kg/cm^2 or ≈18 MPa). These thresholds were established for the mean concrete compressive strength (f_{cm}), which had the disadvantage of allowing the possibility of using concrete with considerably lower resistance. Hence, in 1967 the regulation was changed (REBA) enforcing the use of the characteristic compressive strength (f_{ck}), a minimum resistance value that features a 95% probability of being exceeded. This regulation also introduced the concept of classes of concrete resistance, each one with a characteristic compressive strength, varying from approximately 18 to 40 MPa. Finally, in the 1983 regulation (RSA), and in the more recently proposed Eurocode 2 (CEN, 2004), the concrete classes were adjusted to the international units (MPa) and extended to a compressive strength of 55 MPa.

To derive the concrete compressive strength statistics, the experimental results from core drilling tests in 76 buildings located mainly in the centre and north of Portugal were employed. Unfortunately, it was not possible to disaggregate this data

based on the date of construction or resistance class, since privacy restrictions prevented access to such complementary information. A gamma distribution seemed to provide the best fit with a mean value of 23.8 MPa and a coefficient of variation of 49% (leading to a characteristic compressive strength of 8 MPa), as depicted in Figure 5.8.

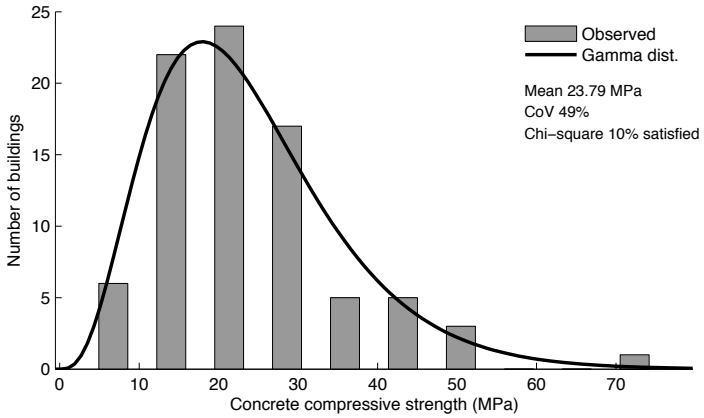

Figure 5.8 - Concrete compressive strength distribution.

The scatter of the results is characterized by a large coefficient of variation, probably due to the fact that the samples were taken from buildings constructed in different time periods, meaning that the structures were designed considering different resistance classes and different design codes. In fact, Almunia (1993) suggested a significantly lower coefficient of variation (between 6% and 11%) for the variability of the concrete compressive strength within the same resistance class. Nevertheless, in the work of Bal *et al.* (2008b), in which a similar process was employed to estimate the probabilistic distribution of this parameter, a similar coefficient of variation was obtained (51%).

5.2.3.2. Steel properties

The development of the code specifications regarding the steel properties followed an evolution similar to that described previously for the concrete. The first regulations date from 1918 and 1935, and required an ultimate tensile strength greater than 3800 kg/m^2 (≈387 MPa) and 3700 kg/m^2 (≈377 MPa) for reinforced plain steel bars, respectively. By the end of the 1940's, high resistance steel was introduced in Portugal and in order to fully explore this higher level of resistance, the interaction between concrete and steel was enhanced by the application of ribs on the bars, which are now mandatory by the design codes (Pipa, 1995). In the 1967

code (REBA), steel resistance classes (A24, A40, A50) were adopted, each class defined by a characteristic yielding tensile strength (f_{yk}). Later in the 1983 regulation (RSA) and in the Eurocode 2 (CEN, 2004), these classes were modified to A230/A400/A500 and S400/S500/S600, respectively.

In Portugal, the majority of the buildings have been designed using steel ribbed bars with a nominal strength of 400 and 500 MPa, and a smaller fraction with plain bars with a lower resistance, mainly in reinforced concrete buildings constructed until the 1970's. In the work of Pipa (1995), several material parameters (yielding and ultimate strength and strain) of A400 and A500 steel classes were analysed using experimental results from a sample with about 700 specimens, coming from many European producers (e.g. Italy, Portugal, Spain, United Kingdom). Each parameter was assumed to follow a normal distribution and a mean and standard deviation was computed for the complete sample. More specifically for the steel yielding strength, its probabilistic distribution was estimated considering only the steel bars produced in Portugal. The latter statistics are presented in Table 5.3, and will be used in the development of the vulnerability model for the reinforced concrete building stock in Portugal.

Table 5.3 - Probabilistic distribution of steel yielding strength (produced in Portugal) proposed by Pipa (1995).

Steel class	Size of sample	Mean yielding strength (f_{ym}) - (MPa)	Standard deviation of yielding strength (σ_y) – (MPa)	Coefficient of variation (%)
A400	84	495	22	4.4
A500	51	589	30	5.1

The variability in the steel material properties is usually fairly constrained, due to the industrialized process used in its production that can be well controlled. Its effective yielding strength is considerably higher than the nominal strength, probably due to the safety factors considered in its production process. In the work of Fernandes *et al*. (2011), Rodrigues *et al*. (2012), Lopes (2012) and Melo *et al*. (2012), the yielding strength of a smaller sample of steel bars was estimated, and results within the range proposed by Pipa (1995) were obtained.

From the evaluation of the technical specifications from the sample of RC buildings constructed after the 1983 regulation, both steel classes seemed to be used with the same frequency. Hence, both types of steel were used with equal weight in the development of the vulnerability model herein. For buildings prior to

this code, the employment of steel of class A230 (or A24) was also found. A comprehensive statistical study regarding the material properties of this class of steel for Portugal does not seem to exist. For this reason, the mean yielding strength of 344.3 MPa for European and Mediterranean buildings proposed in Carvalho and Coelho (2001) was adopted. Regarding the uncertainty in the yielding strength, it was assumed that the production process of that era was less controlled, allowing a higher variability of this property. Thus, a coefficient of variation of 20% was adopted, as this leads to a characteristic yielding strength (5% fractile) equal to the nominal strength of the steel class – 230 MPa. The values of these statistics are in agreement with the findings of Akyuz *et al.* (1999), in which more than 200 steel samples (S220 class) in Turkey were evaluated, leading to a mean yielding strength of 371 MPa, with a coefficient of variation of 24%. For the development of the vulnerability functions for buildings constructed prior to the 1983 regulation, a steel of class A400 was used with a relative weight of 0.5 and steel of classes A500 and A230 were used with equal weights of 0.25 each.

5.3. Development of the vulnerability model

In this Section, an analytical methodology that uses nonlinear dynamic analysis to calculate a fragility model (i.e. a collection of curves describing the probability of exceeding a number of limit states for a set of intensity measure levels) is described. Then, these results are converted into a vulnerability model (i.e. mean loss ratio and associated coefficient of variation for a set of intensity measure levels) through the employment of a consequence model (i.e. the ratio between repair cost and replacement cost for each damage state). When applying such approach to derive a set of vulnerability functions, there are four main aspects that strongly affect the results: i) the structural modelling of the building typologies; ii) the damage state criteria; iii) the selection of the ground motion records; and iv) the consequence model employed to convert fragility curves into vulnerability curves. The various assumptions and main results from each of the aforementioned components are further discussed in what follows.

5.3.1. Structural Modelling of the RC frames

The geometric and material probabilistic distributions presented in the previous Section have been used to randomly generate one hundred assets for each building

typology. Then, the percentage of flexural reinforcement in each structural element is estimated taking into account the code level of the building typology within which the building falls: i) pre-code (before the 1983 code) - designed only for gravity loads; ii) post-code (after the 1983 code) - designed for gravity and lateral loads, which were calculated based on the uniform hazard spectra for both types of seismicity (short distance with moderate magnitude and far distance with large magnitude) in very hard soils (Vs30 > 360 m/s), which are the most common soil type in Portugal, as will be .

To keep the computational effort at a reasonable level, each asset is represented by a 2D frame with 3 bays. This approach has the advantage of allowing the consideration of the uncertainties in the capacity, rather than using a single structure believed to be representative of a given building typology. Each frame was modelled using a 2D structural analysis environment, thus considering only 3 degrees of freedom per node (2 translations and 1 rotation) and all the columns and beams were modelled as force-based fibre elements with five integration points. The cross-sections were discretized in fibres in order to capture the nonlinear behaviour of the materials, with a mesh of 5x50 fibres. The unconfined and confined concrete constitutive relationships were assumed to follow the Kent-Park model modified by Scott *et al*. (1982) with a confinement coefficient equal to 1.15, whereas the behaviour of the steel was represented by the model suggested by Giuffrè and Pinto (1970). The gravity loads were applied in the structure as distributed uniform loads on the beams, and P-delta effects were considered.

The infill panels were modelled with two diagonal compression struts, which is a common approach adopted in some guidelines (FEMA273, 1997; NZSEE, 2006). Such model has the disadvantage of neglecting the interaction between the two diagonal elements (Rodrigues *et al.*, 2010) or the local shear forces introduced by the panel near the column ends (Smyrou *et al*., 2006). However, given the large sample of assets and the wide spectrum of variables considered in this study, it was concluded that these improvements in the model were not worth the significant increase in the complexity of the analyses. The force-displacement model used to represent the strut's nonlinear response is depicted in Figure 5.9.

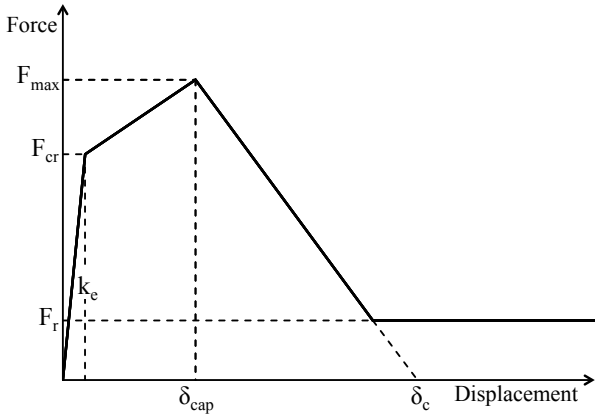

Figure 5.9 – Idealized force-displacement relationship for each infill strut (adapted from Sattar and Liel, 2010).

Several other relationships for the force-displacement model can be found in the literature (e.g. FEMA273, 1997; Hashemi and Mosalan, 2007; Dolsek and Fajfar, 2008; Rodrigues *et al.*, 2010). Nevertheless, the majority of the models are comprised by an initial branch with a linear behaviour, followed by a reduction in stiffness due to the formation of cracks in the infill panel, a short plateau due to the low ductility characteristic of masonry walls, and ending with an abrupt loss in strength capacity due to shear or crushing failure. Some models also consider some residual strength, such as the one adopted herein.

The equivalent strut width (w_{inf}) was computed considering the proposal from Stafford-Smith and Carter (1969), which uses the following formula:

$$w_{inf} = 0.58\left(\frac{L_{inf}}{h_{inf}}\right)^{-0.445}(\lambda_i h_{col})^{0.335} r_{inf}\left(\frac{L_{inf}}{h_{inf}}\right)^{0.064} \tag{5.1}$$

where h_{col} stands for the column height and L_{inf}, h_{inf} and r_{inf} represent the length, height and diagonal length of the infill, respectively. The λ_i stands for a non-dimensional parameter expressing the relative stiffness of the frame to the infill and can be calculated through the following formula:

$$\lambda_i h_{col} = \left(\frac{E_{inf} t_{inf} sin(2\theta)}{4 E_f I_{col} h_{inf}}\right)^{0.25} \tag{5.2}$$

where E_{inf} and t_{inf} represent the elasticity modulus and the thickness of the infill panel, respectively; E_f stands for the elasticity modulus of the frame; θ is the angle

between the diagonal of the infill and the horizontal; and I_{col} refers to the moment of inertia of the columns.

The initial stiffness (k_e) was computed as suggested by Sattar and Liel (2010) with the formula:

$$k_e = 2\left(\frac{E_{inf} w_{inf} t_{inf}}{r_{inf}}\right)\cos(2\theta)^2 \tag{5.3}$$

The formula proposed by Dolsek and Fajfar (2008) was used to compute the maximum force (F_{max}), the cracking force of the infill (F_{cr}) was assumed as 55% of the latter, the deformation at maximum force (δ_{cap}) was assumed as 0.10% (for panels with openings) or 0.20% (for panels without openings) and the deformation at zero wall strength (δ_c) was established as 5 times the latter deformation (Dolsek and Fajfar, 2008; Sattar and Liel, 2010; Uva *et al*., 2012). The strength and the initial stiffness in panels with openings were reduced by a factor λ_0, according to the work of Dawe and Seah (1988):

$$\lambda_0 = 1 - \frac{1.5 L_{op}}{L_{inf}} \tag{5.4}$$

where L_{op} represents the horizontal length of the opening. The consideration of openings in the infill panels allows a more realistic modelling of the frame, rather than considering it bare or fully infilled. In this study, in order to keep a fair balance between the different types of panels, it was decided to consider one bay as fully infilled, one bay with large openings (i.e. doors) and another bay with small openings (i.e. windows). Their position was randomly allocated within the floor. Regarding the ground floor, some frames were modelled with no infill panels at this level, in order to take into account the portion of buildings with open-space configurations for commercial purposes. The ratio of frames with and without infill walls at the ground story was derived based on information from the Building Census survey of 2011, where about 10% of the buildings were categorized as partially residential/commercial buildings, and thus no infill walls were considered at the ground story.

5.3.2. Damage state definition criteria

The possible options for the limit state criterion can vary significantly and a recognized common approach regarding which criteria should be employed for the development of fragility functions does not seem to exist. As discussed by Akkar *et al.* (2005) and Erberik (2008), the employment of a local criterion (e.g. member deformation, hinge mechanisms or concrete/steel strains) to define the limit states when generating fragility curves for population of buildings may not be appropriate. Hence, a global parameter such maximum global drift (e.g. Akkar *et al.,* 2005) or maximum inter-story drift (e.g. Hancilar *et al*., 2006; Rossetto and Elnashai, 2005) was preferred in this study. Both of these approaches have been independently considered herein.

5.3.2.1. Maximum global drift

For the estimation of the global drift limits, a displacement-based adaptive pushover curve (Antoniou and Pinho, 2004) was derived for each frame without the masonry infills (bare frame), and four limit state global drifts were extracted based on the following criteria:

- Slight damage: global drift when 50% of the maximum base shear capacity is achieved;
- Moderate damage: global drift when 75% of the maximum base shear capacity is achieved;
- Extensive damage: global drift when the maximum base shear capacity is achieved;
- Collapse: global drift when the base shear capacity decreases by 20% or 75% of the ultimate global drift taken from the pushover curve, whichever is achieved first.

Similar thresholds for the global drift limits have been used by various authors (e.g. Erberik, 2007; Papailia, 2011). The consideration of the infill panels in the numerical models causes a significant decrease in the displacement capacity. In order to take into account this aspect, the reduction parameters proposed by Bal *et al.* (2010) for each limit state were employed. The latter study suggests a factor of 0.52 for the displacement until the yielding point (moderate damage), a factor of 0.40 for the displacement between the yielding point and the third limit state

(extensive damage) and a factor of 0.28 for the displacement between the same point and the fourth limit state (collapse).

5.3.2.2. Maximum inter-story drift

For the estimation of the inter-story drift limits, Kirçil and Polat (2006) demonstrated a procedure to estimate the inter-story drift for yielding and collapse limit states by employing Incremental Dynamic Analysis (IDA - Vamvatsikos and Cornell, 2002) in single structures. However, applying such approach would soon become impractical due to the large sample of structures considered herein. As an alternative, instead of computing these values for each structure, a fixed set of inter-story drifts (one per limit state) proposed by Rossetto and Elnashai (2003) were applied to the complete sample. In the latter study, the authors evaluated the progression of the global damage with increasing inter-story drift in 25 dynamic tests for RC moment resisting frames (MRF) and the maximum inter-story drift was estimated for six limit states, as described in Table 5.4.

Table 5.4 – Limit state inter-story drifts for infilled MRF proposed by Rossetto and Elnashai (2003).

Damage State	Inter-story drift (%)
Slight	0.05
Light	0.08
Moderate	0.30
Extensive	1.15
Partial collapse	2.80
Collapse	> 4.40

In order to adapt this damage scale (six levels), to the one previously adopted for the global drift parameter (four levels), the light and slight damage states were merged as one (since both are related only to non-structural damage) with an inter-story drift threshold of 0.05%. Partial collapse and collapse were equally merged, becoming a single damage state with an inter-story drift limit of 2.8%.

Clearly, both global parameters have strengths and limitations. Inter-story drift tends to provide a better correlation with damage, but it is not easily assessed for each structure and thus often a fixed set of limit state values are used, regardless of the structural properties. On the other hand, the global drift for each limit state can be derived taking into account the structural characteristics of each frame at a low

computational effort. However, in frames where a soft-story failure mechanism might develop or in vertically irregular structures in which the maximum lateral displacement might occur at intermediate floors, this global parameter could fail to establish the level of damage. For these reasons and to comprehend how the damage state criteria might affect the resulting limit state curves, fragility models were developed using each global parameter criterion.

5.3.2.3. Residual inter-story drift

Residual inter-story drifts were also evaluated, as buildings with permanent large displacements are often likely to be demolished. The probability of demolition is related with the level of residual drift sustained by the building after the earthquake. Ramirez and Miranda (2012) suggest that the probability of demolition should follow a cumulative lognormal distribution with a median of 0.15% and a logarithmic standard deviation of 0.3%. With such a distribution, a building with a residual inter-story drift of 1% would lead to a probability of demolition of 10%, whilst a building with a residual drift of 3% would be almost certainly demolished (99%). This process is clarified in Figure 5.10.

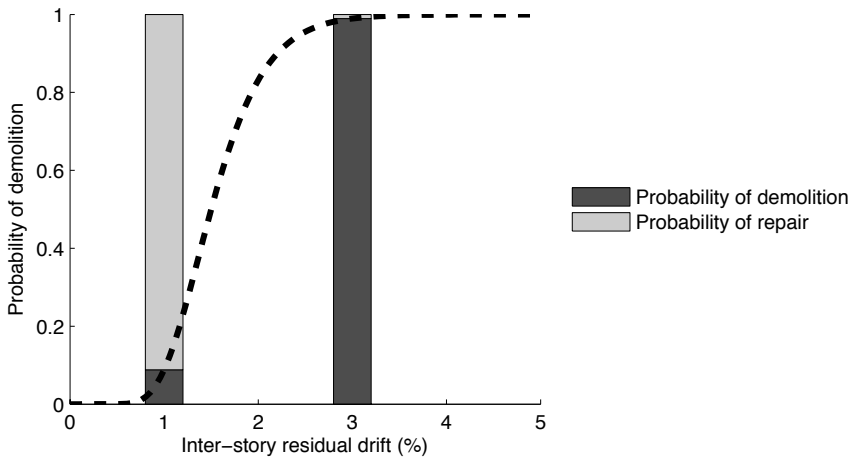

Figure 5.10 – Probability of demolition as a function of the inter-story residual drift.

Hence, a building sustaining moderate or extensive damage might actually represent a greater loss, due to the necessity of its full replacement. This aspect might not be relevant in the development of a fragility model, whose main purpose is to simply provide the distribution of buildings in a number of damage states for a set of intensity measure levels, but it is certainly fundamental in the development of a vulnerability model, which should be capable of providing percentages of

economic loss for various levels of seismic intensity. For this reason, in the calculation of the vulnerability functions, a second fragility model was developed in which after each nonlinear dynamic analysis, if the RC frame presented considerable residual inter-story drifts, the probabilistic distribution proposed by Ramirez and Miranda (2012) was used to assess whether the frame should be placed in the collapse damage state, or remain in the one indicated by the global damage criteria.

5.3.3. Selection of ground motion records

For what concerns the selection of a set of ground motion records to carry out the nonlinear dynamic analyses, Portugal represents a challenging case as only three seismic events with significant ground motion were ever recorded. For this reason, records from other regions in the world with similar geological and tectonic characteristics (e.g. Spain, France, Switzerland, Northwest Africa, Central and Eastern North America) were gathered. For further information regarding the Portuguese tectonic environment, readers are referred to Vilanova and Fonseca (2007) and Sousa and Campos-Costa (2009).

In order to understand what are the earthquake magnitude and distance intervals that contribute the most to the hazard in Portugal, the hazard disaggregation carried out by Montilla *et al*. (2002) and Sousa and Campos-Costa (2009) was used. Despite the different conclusions between these studies, it is fair to state that significant ground motion in Portugal is mainly produced by shallow earthquakes with low to moderate magnitude (4.5 – 6.5 Mw) at short distances (10 - 80 km) generated in stable continental regions (SCR) and deep earthquakes with moderate to large magnitudes (6.5 – 8.0 Mw) at long distances (100 – 200 km) generated in active shallow crustal regions (ASCR). These combinations of magnitude/distances were respected in the selection of the accelerograms to ensure a sample of records compatible with the seismicity in Portugal. One hundred ground motion records were extracted from the PEER [28], ESD [27], RAP [31] and SED [32] databases, and the variation of PGA, PGV and Arias Intensity of these records is presented in Figure 4.9.

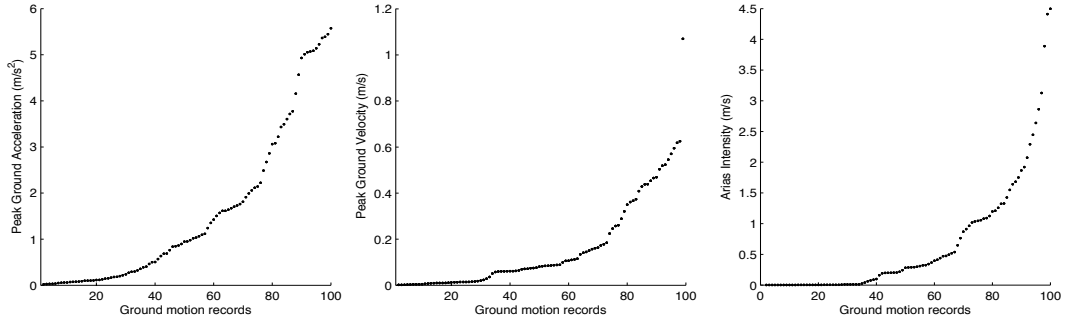

Figure 5.11 - Distribution of the PGA (left), PGV (centre) and Arias Intensity (right) in the selected records.

5.3.4. Evaluation of consequence models

Consequence models can be used to convert a set of fragility functions (probability of exceeding a set of limit states versus a set of intensity measure levels) into a vulnerability function (mean loss ratio and corresponding coefficient of variation versus a set of intensity measure levels). A model describing the distribution of cost ratio (also known as damage ratio, providing the ratio of cost of repair to cost of replacement) for a set of damage states does not seem to currently exist for Portugal. Such models are commonly derived based on information regarding the repair costs claimed by householders after the occurrence of an earthquake, which hampers the development of consequence models for countries such as Portugal, where earthquakes are not frequent. For this reason, consequence models developed for other regions (Italy, Greece, Turkey and California) were considered (see Figure 5.12).

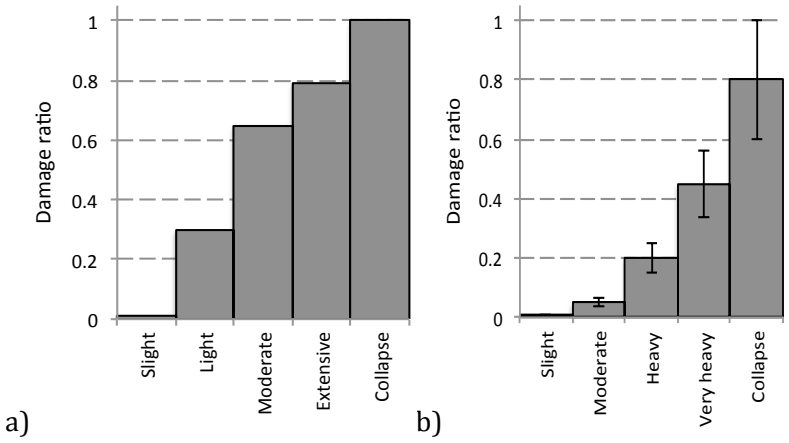

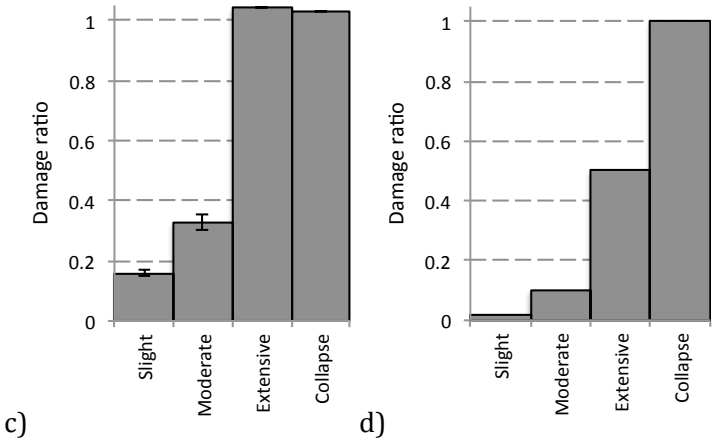

Figure 5.12 - Consequence models for a) Italy (Di Pasquale and Goretti, 2001); b) Greece (Kappos *et al*. 2006); c) Turkey (Bal *et al*., 2008b) and d) California (FEMA-443, 2003).

These models can present different damage scales and each damage ratio might be influenced not just by the level of damage in the structure, but also by the local policy. For example, Turkish law states that a building sustaining extensive damage should not be repaired, and must be demolished instead. The aforementioned four models were used to estimate a consequence model to be used in the development of the vulnerability functions for the Portuguese RC building stock. To do so, an average between the cost ratios of the damage states equivalent to the ones considered herein was estimated. The damage ratio for extensive damage in the Turkish model was neglected, as the criteria behind this value is not valid for Portugal. The resulting distribution of damage ratio used in the present study is described in Table 5.5.

Table 5.5 – Consequence model used in the development of the vulnerability model for the Portuguese RC building stock.

Damage state	Damage ratio
Slight	0.10
Moderate	0.30
Extensive	0.60
Collapse	1.00

It is worth mentioning that such damage ratios can be described not only by a deterministic value, but instead by a probabilistic distribution (e.g. consequence model for Greece illustrated in Figure 5.12), allowing the propagation of this uncertainty into the vulnerability functions. However, in the present work, due to lack of information regarding these variability for some of the consequence models, a decision was made to consider a fixed damage ratio for each damage state.

5.3.5. Fragility methodology

For the purposes of deriving a set of fragility functions for each RC building typology, a framework was developed in Matlab [20] to handle the various inputs/outputs, to generate the RC frames and to perform the final statistical regressions. This framework was connected to OpenSEES [21], an open source software for structural analysis, to derive the pushover curves and to carry out the nonlinear dynamic analysis. The overall process can be summarized in the following steps:

1. Random generation of a population of RC frames through Monte Carlo simulation, considering the material and geometric variability, code level and distribution of buildings regarding the number of storeys within each building typology;
2. Computation of a displacement-based adaptive pushover curve for each frame, with the purpose of estimating a set of limit state global drifts;
3. Perform nonlinear dynamic analyses for each RC frame using a large selection of ground motion records, with the purpose of extracting the maximum global and inter-story drifts;
4. Allocate each RC frame into a damage state based on the global (step 2) or inter-story drift criteria and verify if collapse was achieved due to excessive residual inter-story drift;
5. Calculate the cumulative percentage of buildings for each limit state versus the representative intensity measure of the each accelerogram (e.g. $Sa(T_{el})$, PGA);
6. Carry out regression analysis to calculate the parameters (mean and standard deviation) of the fragility functions (assumed to follow a lognormal distribution).

This process is schematically illustrated in Figure 5.13.

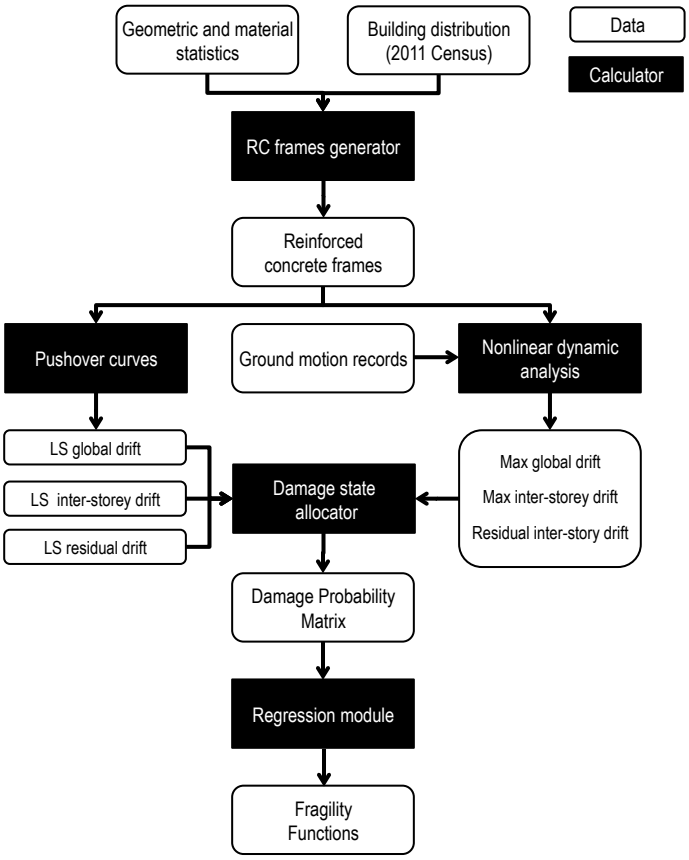

Figure 5.13 - Analytical fragility methodology workflow.

5.4. Results

5.4.1. Evaluation of the RC frames

5.4.1.1. Elastic period of vibration

When employing an analytical methodology to derive a vulnerability model, in which Monte Carlo sampling is used to create a synthetic collections of assets, it is important to verify whether the structures that are being generated are reasonable and in agreement with the real characteristics of the building stock. To carry out this verification, various structural and dynamic parameters were estimated, and compared with results from previous studies and experimental campaigns. The first verification was done in terms of the elastic period (first mode) of the frames with and without the infill panels. For the former comparison, the elastic periods calculated by Carvalho *et al.* (2002) according to the FEMA (1999) methodology for Portuguese building typologies were used. For the latter, a set of empirical formulae providing the elastic period as a function of the number of floors was employed.

These equations were derived based on field measurements of the period of vibration of tens of real RC buildings with infill walls in Barcelona, Spain (Espinoza, 1999); Caracas, Venezuela (Enomoto *et al.*, 1999); Granada, Spain (Kobayashi *et al.*, 1996) and Lisbon, Portugal (Navarro and Oliveira, 2004). One hundred frames were randomly generated for each number of storeys, and the mean period and respective probability density function are presented in Figure 5.14, along with the results from the aforementioned studies.

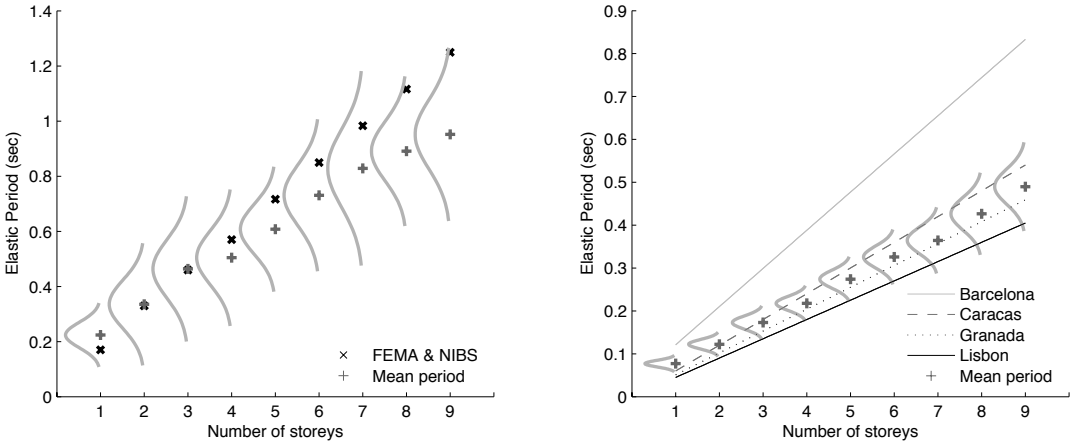

Figure 5.14 – Comparison between the elastic periods for the bare frames computed herein and FEMA and NIBS (1999) (left) and between the elastic period for infilled frames computed herein and various authors (right).

For what concerns the period of vibration of the bare frames, a fairly good agreement is observed in the frames with four or less storeys, followed by an increase in the discrepancies, in which the periods estimated herein are lower than the ones calculated with the FEMA methodology. These variations are mainly due to the fact that in the latter approach, a fixed inter-story height of 3.3 meters was assumed, as opposed to the lower height with a mean of 2.89 meters and 7% coefficient of variation considered herein. Moreover, as indicated by Oliveira and Navarro (2010), the FEMA methodology has been developed for buildings in the United States, whose geometric characteristics tend to impart a more flexible behaviour, and consequently, a longer period. Regarding the evaluation of the periods of the infilled frames, a reasonable matching was observed for all the empirical relationships, with the exception of Barcelona whose results were considerably higher. The longer periods calculated herein in comparison with the estimation for Lisbon might be due to the non-consideration of the additional stiffness provided by structural elements such as stair cases, elevator shafts or

eventual shear walls. Other empirical relationships for the period of vibration of buildings in other cities (e.g. Almeria, Spain; Grenoble, France; Potenza, Italy) were also evaluated. Their results, however, are between the ranges presented for Lisbon and Caracas, and so were omitted from Figure 5.14 for the sake of visual clarity.

5.4.2. Capacity curves

The global displacement and base shear capacities for each building typology were analysed. Thus, for each typology, a set of bare frames was randomly generated and used to derive several displacement-based adaptive pushover curves. Then, each pushover curve (top displacement versus base shear for the multi degree-of-freedom system) was transformed into a capacity curve (spectral displacement versus spectral acceleration for the equivalent single degree-of-freedom system), using the deformed shape of the frame at each step, as proposed by Casarotti and Pinho (2007). The mean capacity curve for each building typology is depicted in Figure 5.15.

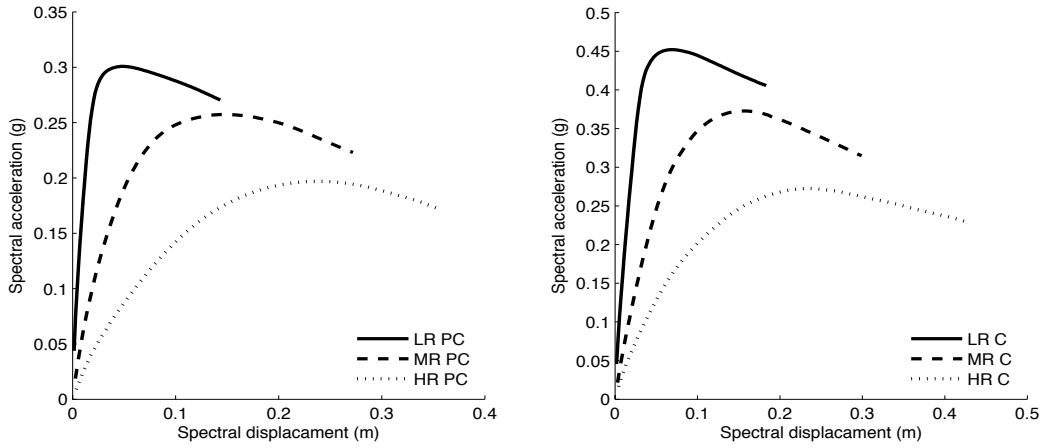

Figure 5.15 – Capacity curves for the building typologies built before (left) and after (right) the 1983 design code.

The results in terms of spectral acceleration are in agreement with the values estimated by Carvalho *et al.* (2002) and slightly lower regarding the spectral displacement. Besides the expected discrepancies related to the different methodologies employed in the development of the capacity curves, it is also worth mentioning that the lower displacement capacity estimated herein could be also due to the fact that a lower inter-story height was considered in this study, as well as P-delta effects, which tend to cause an earlier collapse in the frame.

The introduction of the infill panels induced an increase in the initial stiffness and overall strength, and consequently, a substantial decrease in the period of vibration by approximately 50% (see Figure 5.14). The influence of this feature in the structural capacity is demonstrated on Figure 5.16, where the mean capacity curves for one hundred pre-code frames with four storeys (with and without the masonry infills) are depicted. For a randomly selected frame, a nonlinear dynamic analysis was also performed using the ground motion record from the 2007 Portuguese earthquake (magnitude of 5.8Mw and PGA of 0.04 g).

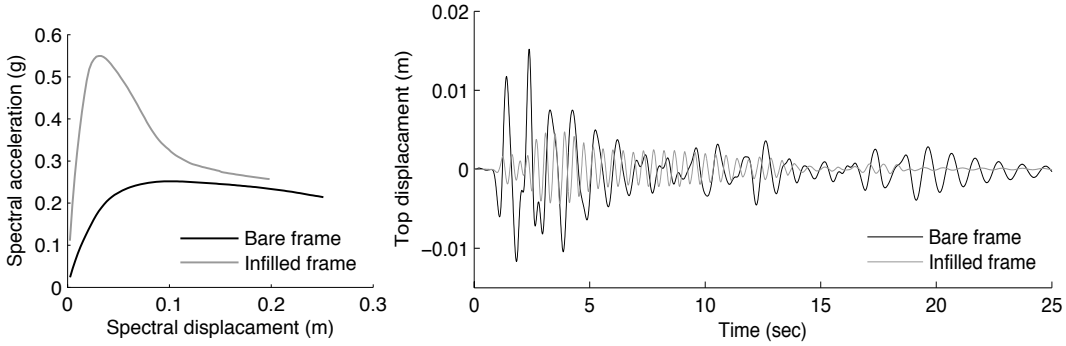

Figure 5.16 – Mean capacity curve for a sample of a hundred of pre-code frames with 4 storeys (left) and top displacement time history of a single frame of the same building typology (right).

The variation between the structural and dynamic characteristics of the bare and infill frames seemed to be in agreement with recent studies (e.g. Dolsek and Fajfar, 2008; Ozcebe, 2011; Uva et al., 2012).

5.4.3. Fragility functions

The selection of the ground motion parameter to represent each ground motion record is of fundamental importance, as each intensity measure type has a specific correlation with damage. Macroseismic intensities (e.g. MMI, EMS) could be a natural choice since there is a direct relationship between the intensity levels and the severity of damage in different building typologies. However, keeping track of the intensity at the location where the record was captured is not common and furthermore, macroseismic intensity does not take into account the influence of the frequency content on the structural response. Peak ground motion (e.g. PGA, PGV) also shares this last shortcoming. The influence of the frequency content on the ground motion can be considered by choosing spectral acceleration or displacement to represent each record (Bommer *et al.*, 2002). The period for which these spectral

ordinates are computed also influences considerably the uncertainty in each limit state curve. In the European project SYNER-G, more than four hundred fragility functions were collected (SYNER-G, 2011), and in those that adopted spectral ordinates, the elastic period (T_{el}) was the most common choice. In few cases, the employment of the yielding period (T_y) or the period at each limit state (T_{LSi}) was also observed. Using T_{el} might seem advantageous as it can be easily estimated (instrumentally or analytically) however, the damage introduced in the structures even for weak motion (cracking of the concrete), causes an elongation of the period of vibration, thus changing their dynamic properties. The coefficient of correlation (R^2) between the intensity measure levels and the cumulative percentage of frames for each limit state was estimated within a range of periods for each limit state for the six building typologies, and is illustrated in Figure 5.17 for pre-code low-rise and post-code high-rise RC frames. The mean coefficient of correlation is also presented and the period for which the maximum correlation was observed for each limit state curve is marked with a vertical dashed line. The spectral acceleration for T_{el} seems to perform poorly, with a mean coefficient of correlation value of 0.65.

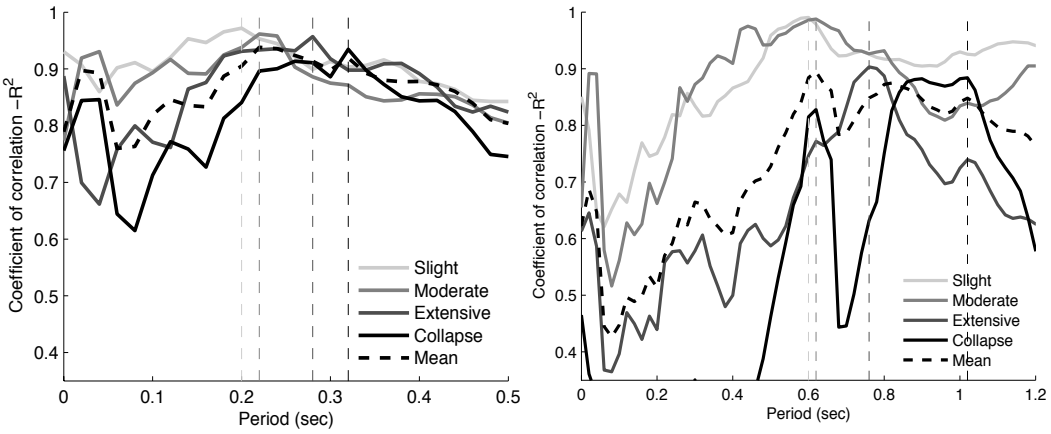

Figure 5.17 - Variation of the coefficient of correlation between the intensity measure levels and the cumulative percentage of frames in each damage state for pre-code low-rise (left) and post-code high-rise (right) RC structures, as a function of the period.

It is fair to state that the variation of the coefficient of correlation as a function of the period changes differently depending on the limit state. For slight or moderate damage, a smaller elongation of the period is observed due to a lower structural degradation of the frames and thus, a better correlation is observed for shorter periods. On the other hand, for extensive damage or collapse, a better performance is observed with longer periods, as frames sustaining such damage are likely to have

their dynamic properties more altered. For the case of pre-code low rise RC frames, the mean coefficient of correlation is considerably lower (0.74) for T_{el} (0.11 sec) and reaches its maximum (0.92) for a value very close to the optimal period for the moderate damage limit state, which defines the threshold after which the frames begin to sustain plastic deformations (yielding point). This behaviour was also verified for the limit state curves of the remaining building typologies. For this reason, it was decided to employ the spectral acceleration for the yielding period as the representative measure of each ground motion record. Moreover, (T_y) can be easily extracted from the capacity curves ($T_y = 2\pi\sqrt{Sd_y/Sa_y}$) or through the employment of simplified formulae (e.g. Crowley and Pinho, 2004; Crowley and Pinho, 2006).

The cumulative percentage of frames exceeding each limit state at each ground motion record is presented in Figure 5.18, along with the associated limit state curves derived from the scatter of points using the least squares method. As previously mentioned, a set of fragility curves has been developed according to each damage criterion: global drift or inter-story drift.

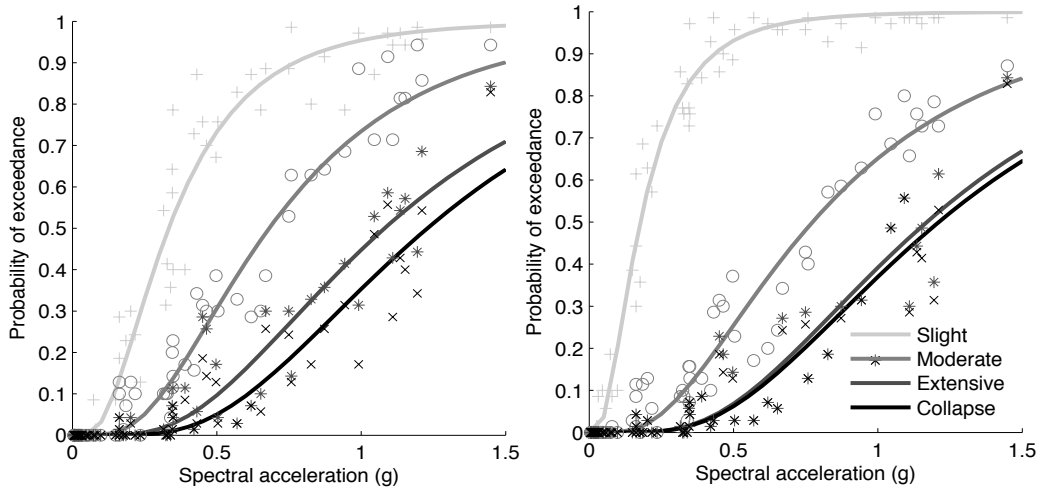

Figure 5.18 - Fragility model for pre-code low-rise RC buildings, considering the global drift (left) and inter-story drift (right) damage criteria.

Each fragility function was assumed to follow a cumulative lognormal distribution, with logarithmic mean (λ) and logarithmic standard deviation (ζ). The results for all the building typologies according to the assumed damage criterion are described in Table 5.6.

Table 5.6 – Logarithmic mean (λ), logarithmic standard deviation (ζ) and coefficient of correlation (R^2) for each limit state fragility function, according to the adopted damage criterion.

Damage criterion		Global drift				Inter-story drift			
Limit State		Slight	Moderate	Extensive	Collapse	Slight	Moderate	Extensive	Collapse
RC LR PC T_y=0.23 sec	λ	-1.098	-0.384	0.078	-1.098	-1.734	-0.257	0.157	0.191
	ζ	0.652	0.612	0.593	0.652	0.701	0.661	0.570	0.576
	R^2	0.812	0.931	0.866	0.812	0.668	0.922	0.823	0.815
RC MR PC T_y=0.39 sec	λ	-1.435	-0.828	-0.292	-0.113	-2.246	-1.025	-0.269	-0.130
	ζ	0.493	0.483	0.388	0.429	0.110	0.527	0.394	0.445
	R^2	0.698	0.862	0.878	0.857	0.392	0.822	0.845	0.853
RC HR PC T_y=0.74 sec	λ	-1.756	-1.210	-0.635	-0.299	-2.845	-1.398	-0.245	-0.032
	ζ	0.434	0.381	0.386	0.358	0.397	0.236	0.539	0.584
	R^2	0.760	0.864	0.848	0.637	0.423	0.815	0.645	0.591
RC LR C T_y=0.21 sec	λ	-0.464	0.043	0.329	0.744	-1.286	-0.145	0.354	0.722
	ζ	0.623	0.603	0.639	0.637	0.631	0.678	0.621	0.619
	R^2	0.823	0.835	0.784	0.753	0.576	0.853	0.772	0.763
RC MR C T_y=0.30 sec	λ	-0.951	-0.491	-0.064	0.525	-2.172	-0.883	-0.056	0.513
	ζ	0.326	0.257	0.386	0.607	0.398	0.374	0.396	0.617
	R^2	0.738	0.783	0.790	0.503	0.394	0.769	0.797	0.552
RC HR C T_y=0.61 sec	λ	-2.855	-1.143	-0.218	0.547	-1.873	-0.992	-0.473	-0.116
	ζ	0.577	0.298	0.362	0.676	0.368	0.269	0.280	0.321
	R^2	0.429	0.819	0.553	0.453	0.802	0.841	0.724	0.418

The appraisal of the coefficient of correlation throughout the various fragility functions indicates a lower dispersion of the data when adopting a global drift damage criterion, mainly for the first two limit state curves. This reduced scatter does not necessarily signify a lower variability in the vulnerability functions, as each limit state fragility function contributes differently to the resulting loss ratio. As demonstrated in section 5.3.4, extensive damage and collapse limit state curves have a greater damage ratio, and will thus have a greater influence in the variability of the vulnerability curves.

5.4.4. Vulnerability functions

As mentioned in section 5.3.2.3, after each nonlinear dynamic analysis, the residual inter-story drift was extracted and a statistical procedure employed to assess whether the frame should be demolished or repaired. This aspect is very important from a loss assessment point of view, as buildings with excessive residual drift are likely to be demolished, thus increasing the total loss. For this reason, another set of fragility functions was derived, considering this additional amount of frames that should be defined as collapsed, rather than sustaining moderate or extensive damage. In Figure 5.19, the percentage of nonlinear dynamic analysis in which a frame was classified as collapsed due to excessive residual inter-story drift is presented.

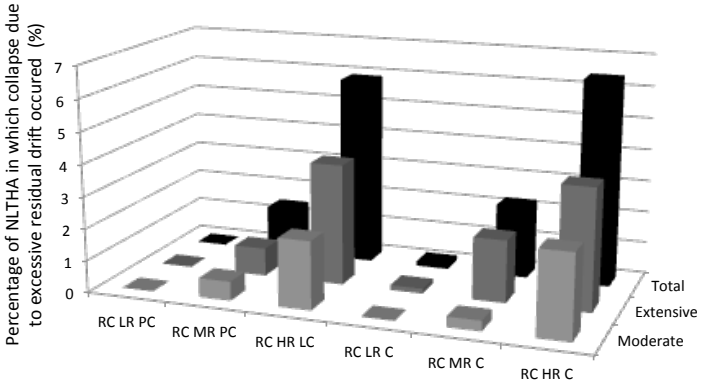

Figure 5.19 - Percentage of nonlinear dynamic analysis (per damage state and in total), in which collapse occurred due to excessive residual inter-story drift.

The cases of collapse due to residual drift were observed more often in frames with a higher number of storeys, and only when moderate or extensive damage was observed. This aspect does not influence the slight or moderate limit state curves, as the cumulative number of frames under each limit state remains the same. It does, however, have a direct impact in the extensive damage or collapse curves, as the number of frames with at least such a level of damage will increase. Higher levels of residual deformations in post-code frames, rather than in pre-code ones, were also observed. This greater likelihood of occurrence of permanent drifts in systems capable of withstanding large displacements is also indicated by Miranda and Ramirez (2012). In Figure 5.20, a set of fragility functions for pre-code high-rise RC frames is presented with and without the consideration of the impact of excessive residual inter-story drift.

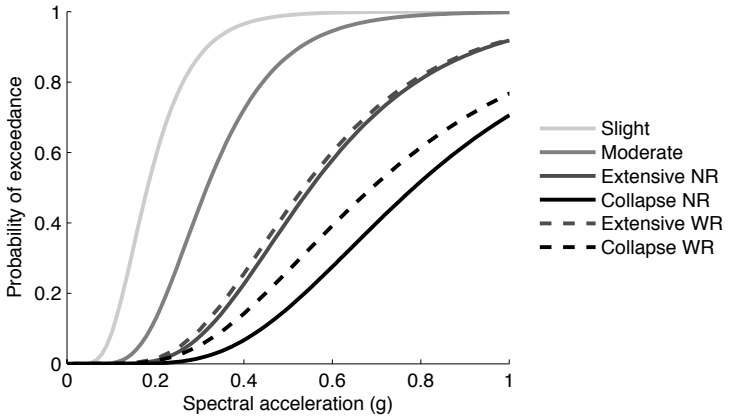

Figure 5.20 - Fragility model for pre-code high-rise RC frames with (WR) and without (NR) considering collapse due to excessive residual inter-story drift.

After the computation of the fragility model considering this feature, the consequence model described in section 5.3.4 was used to derive vulnerability

functions. In this process, for a set of intensity measure levels, the percentage of buildings in each damage state are computed and multiplied by the respective damage ratio, thus obtaining a loss ratio for each intensity measure level. The consideration of the large spectrum of uncertainties considered in this study, impose a significant variability of loss ratio at each intensity measure level. In order to evaluate this uncertainty, a statistical method was implemented that allowed the estimation of the 10% and 90% percentiles. This method consists of a continuous bootstrap sampling with replacement from the original dataset (Wasserman, 2004). The resulting mean vulnerability functions and associated percentiles are depicted in Figure 5.21, for the global drift (black) and inter-story drift (grey) damage criteria.

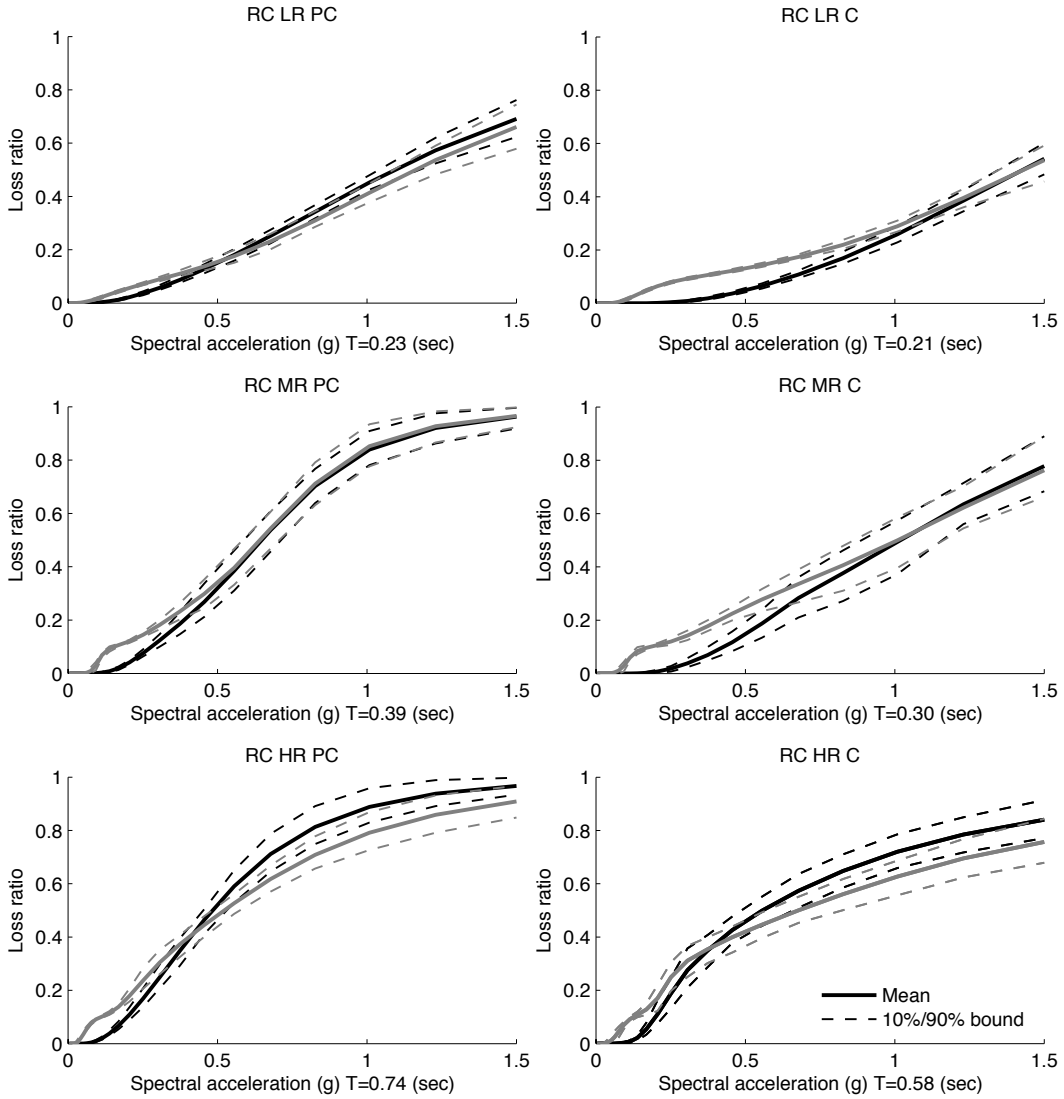

Figure 5.21 - Vulnerability model for RC building in Portugal assuming a global drift (black) and an inter-storey drift (grey) damage criteria.

5.5. Final remarks

The structural characteristics of typical Portuguese reinforced concrete buildings were thoroughly examined in this study. Hundreds of building drawings from different regions in Portugal were collected and analysed with the purpose of deriving the statistical distribution of a set of geometrical properties. These results can be used to carry out investigations regarding the seismic vulnerability of the RC building stock in Portugal, or employed directly in seismic risk methodologies such as the Displacement-Based Earthquake Loss Assessment (DBELA) (Crowley *et al.*, 2004; Bal *et al.*, 2010). Despite the useful contribution that this statistical study might provide to future endeavours in the area of the vulnerability assessment of the Portuguese building stock, it is clear by the number of failed Chi-square tests, that the size of the analysed sample of RC buildings needs to be further increased. Furthermore, it is also important to recognize that the results presented herein are based on the observations of the drawings and technical specifications, which might vary from what has been built in reality.

The geometric and material probabilistic distributions were employed to generate hundreds of RC frames through Monte Carlo simulation, representative of six building typologies, organized according to their number of storeys and design code level. The dynamic and structural characteristics of these frames were compared, and it was concluded that a fair agreement existed between previous analytical and empirical studies. A sample of one hundred frames was tested against one hundred ground motion records, leading to ten thousand nonlinear dynamic analyses for each building typology. For each analysis, the global drift and the inter-story drift were employed to allocate each frame in a damage state, according to a five level damage scale (none, slight, moderate, extensive and collapse). For each damage criterion, a fragility model was derived for the six building typologies, using spectral acceleration for the yield period as the representative measurement of the ground motion. Taking into consideration the eventual demolition due to excessive residual inter-story drift, a second set of fragility functions were also created. The consideration of the residual inter-story drifts caused a considerable increase in the extensive and collapse limit state curves for mid-rise and high-rise building typologies, but no significant changes in the low-rise fragility functions. This second set of fragility functions was combined with a consequence model to derive a vulnerability model.

The distribution of the loss ratios at each intensity measure level was evaluated through the employment of a bootstrap method, allowing the estimating of 10% and 90% percentile curves. The evaluation of the vulnerability functions revealed an increase in the seismic vulnerability with the height of the building. Furthermore, the vulnerability functions produced using the maximum inter-story drift seemed to lead to higher loss ratios at low intensity measure levels. This aspect could be due to the fact that in the adaptation of the original scale proposed by Rossetto and Elnashai (2003) to the one considered herein, "slight" and "light" damage states were merged into one, and combined with a damage ratio of 10%. Such ratio might be excessively high for the first damage state of this scale. Nevertheless, a fair agreement is observed between the vulnerability functions from each damage criterion for low- and mid-rise building typologies. With regards to the uncertainty in the loss ratio, a similar variability was obtained regardless of the chosen damage criterion.

The results obtained herein were employed in a probabilistic seismic risk assessment for mainland Portugal, as presented in the following Chapter. The two sets of vulnerability functions were included within a logic tree framework, thus allowing a better characterization of the epistemic uncertainty in the vulnerability.

Chapter 6

Seismic Risk Assessment for mainland Portugal

Silva, V., Crowley, H., Pinho, R., Varum, H. (2013) "Seismic Risk Assessment for mainland Portugal". *Bulletin of Earthquake Engineering*, in review.

6.1. Summary

The assessment of the seismic risk at a national scale represents an important resource in order to introduce measures that may reduce potential losses due to future earthquakes. This evaluation results from the convolution of three components: seismic hazard, structural vulnerability and exposure data. In this study, a review of existing studies focusing on each one of these areas is carried out, and used together with data from the 2011 Building Census in Portugal to compile the required input models for the evaluation of seismic hazard and risk. In order to better characterize the epistemic uncertainty in the calculations, several approaches are considered within a logic tree structure, such as the consideration of different seismic source zonations, the employment of vulnerability functions derived based on various damage criteria and the employment of distinct spatial resolutions in the exposure model. The aim of this Chapter is thus to provide an overview of the recent developments regarding the different aspects that influence the seismic hazard and risk in Portugal, as well as an up-to-date identification of the regions that are more vulnerable to earthquakes, together with the expected losses for a probability of exceedance of 10% in 50 years. The results from the present study were obtained

through the OpenQuake-engine, the open-source software for seismic risk and hazard assessment presented in Chapter 2.

6.2. Introduction

Portugal is located in the southwest part of the Eurasian plate, near the meeting of the African and North-American plates, thus subjected to offshore seismic events with large to very large magnitude (such as the well-known 1755 Lisbon earthquake) and moderate to large onshore earthquakes (Moreira, 1989). This tectonic environment induces low to moderate seismic hazard, which in countries similar to Portugal, has caused considerable economic and human losses (Barata, 2005). Moreover, more than half of the Portuguese building stock is comprised of masonry structures, which is a construction typology that is typically more vulnerable to earthquakes, and is therefore at significant risk even when only subjected to moderate events (Vicente *et al.*, 2010). This panorama strengthens the need for a reliable and comprehensive evaluation of the seismic risk in Portugal, and strategic development of risk mitigation actions. Such measures can include the prioritization of regions within a country where retrofitting/strengthening campaigns of the building stock should take place, creation of insurance and reinsurance schemes to transfer the financial burden due to reconstruction from the governments to the private sector, planning of urban/regional-scale emergency response and definition of regulations to endorse seismic-proof construction practices. As discussed by Spence (2004), the intervention of the governments in the enforcement of rigorous seismic design codes and in the creation of regulations that facilitate the retrofitting/strengthening of existing buildings, can also contribute effectively to the reduction of seismic risk.

The evaluation of seismic risk involves the combination of three main components: a probabilistic seismic hazard model, a set of vulnerability functions capable of describing the distribution of percentage of loss for a set of intensity measure levels and an exposure model defining the spatial distribution of elements exposed to the seismic hazard. In this Chapter, a review of the most relevant studies that somehow contributed to the understanding of seismic hazard and risk in Portugal was carried out.

For what concerns the seismic hazard, an existing seismic source model (Vilanova and Fonseca, 2007) was combined with a set of ground motion prediction equations recently proposed for the tectonic environment in the vicinity of Portugal (Delavaud *et al*., 2012; Vilanova *et al*., 2012; Stewart *et al*., 2012). An additional model describing the spatial distribution of V_{s30} values was developed, for the purposes of considering ground motion amplification due to soil conditions. Regarding the structural vulnerability of the building stock, a new set of vulnerability functions for the RC buildings was developed in Chapter 5, whilst for the remaining typologies, existing capacity curves (Carvalho *et al.,* 2002) were combined with the Capacity Spectrum Method (ATC-40, 1996) to derive a vulnerability function for each typology. For what concerns the development of the exposure model, information from the Building Census of 2011 was employed, together with building statistics from the Portuguese Statistical Office [33], to create a dataset capable of providing the geographic position, vulnerability class and replacement cost of residential buildings in mainland Portugal. These three components were provided as input to the open-source software for seismic hazard and risk assessment presented in Chapter 2, and hazard and loss exceedance curves were calculated, as well as hazard and risk maps for a probability of exceedance of 10% in 50 years. The results from this study identify the zones in the country where the seismic risk is higher and where, therefore, risk mitigation actions should be introduced with higher priority. The disaggregation of losses based on building typology also indicated which type of building construction is more vulnerable to earthquakes, allowing the development of retrofitting interventions more suitable for this type of structure.

6.3. Review of existing studies

The great number of human losses observed in the earthquakes in Romania (1977) and former-Yugoslavia (1979), triggered several studies in the area of seismic risk mitigation in 1980's (Vicente, 2008). Later, the period 1990 to 1999 was decreed by the United Nations as the International Decade for Natural Disaster Reduction, also propelling many efforts within the assessment of seismic risk. A number of hazard and risk studies that covered partially or completely the territory of mainland Portugal are presented herein, beginning with international efforts and finishing with those with a regional or local scale.

One of the first initiatives for the understanding of the seismic hazard at a global level was the Global Seismic Hazard Assessment Program (GSHAP) (Giardini, 1999). This project begun in 1992 and its main objective was the creation of seismic hazard models for the different regions in the world. The GSHAP was concluded in 1999 with the publication of the first global hazard map of peak ground acceleration for a return period of 475 years. The activities carried out within GSHAP, with special focus in the Ibero-Maghreb region (Algeria, Portugal, Spain and Tunisia) are described in detail in Jimenez *et al.* (1999, 2001). More recently, another initiative with the same global extent that will cover not only seismic hazard, but also seismic risk, was founded. This initiative, denominated Global Earthquake Model (GEM) [2], has the objective of developing best practice, datasets, models and tools for seismic hazard and risk assessment through collaboration with local experts around the world.

Regarding endeavours at a European scale, three undergoing initiatives can be mentioned, each one focusing in unique components of seismic risk. The SHARE project (2009-2013) [34] has the main objective of creating a homogeneous seismic hazard model for Europe, selecting a set of ground motion prediction equations compatible with the European tectonic environment and producing a European seismic hazard map. In parallel, another project denominated SYNER-G (2009-2013) [35] is evaluating the structural fragility of buildings, infrastructures and networks, and a unified methodology for the evaluation of the physical and socio-economic systemic vulnerability is being defined. The third initiative (NERA, 2010-2014) [36], facilitates the sharing of information and collaboration of many institutions from the different areas of seismic risk; one of the outputs of this project will be a building exposure model covering all European countries. It is also worth mentioning another two projects, RISK-EU (2001-2004) (Mouroux and Brun, 2006) and LESSLOSS (2004-2007) (Calvi and Pinho, 2004), both of which are already completed. In these initiatives, the seismic hazard and structural vulnerability of several European cities (including Lisbon) were evaluated, and the results were employed to calculate the associated seismic risk.

At a smaller scale, Pelaez and Casado (2002) conducted a probabilistic seismic hazard assessment covering the Iberian Peninsula, through an approach that combined both zonified (area sources) and non-zonified (smoothed seismicity)

probabilistic methodologies. Thus, hazard maps for peak ground acceleration were produced for 100, 475 and 975 year return periods.

Concerning the territory of mainland Portugal, two main studies can be mentioned: Vilanova and Fonseca (2007) and Sousa (2006). In the first study, a seismic hazard model for Portugal is proposed using a logic tree approach to characterize the various epistemic uncertainties such as seismic sources characterization, selection of ground motion prediction equations, earthquake catalogues and methodologies to derive the magnitude-frequency relationship parameters. This effort resulted in the creation of a national hazard map for peak ground acceleration for a probability of exceedance of 10% in 50 years. In the second study by Sousa (2006), a seismic risk assessment was carried out, using the seismic hazard model from Sousa (1996), and several simplified methodologies for the building vulnerability assessment and a detailed exposure model compiled based on data from the Building Census of 2001. Sousa (2006) calculated human and economic loss maps (see Figure 6.1) for several return periods, as well as loss maps for two deterministic events equivalent to the historical earthquakes of Lisbon in 1755 and Benavente in 1909.

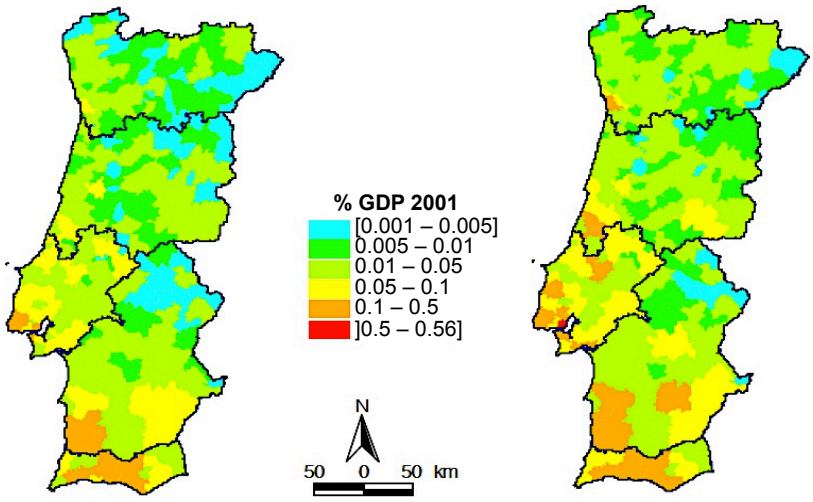

Figure 6.1 – Economic loss map for a return period of 475 (left) and 975 (right) years, (adapted from Sousa, 2006).

With regards to studies at a regional or local scale, it is worth mentioning the studies of Campos-Costa *et al.* (2009) for the Metropolitan Area of Lisbon, Sousa *et al*. (2010) for the province of Algarve, Vicente *et al.* (2010) for the downtown of the city of Coimbra, and the vulnerability assessment of the old city of Seixal by Ferreira *et al*. (2012).

6.4. Description of the input models

6.4.1. Probabilistic seismic hazard model

Despite the occurrence of strong earthquakes in the last century, instrumental strong-motion data for Portugal is very scarce and therefore most of the seismic hazard studies have been built upon historical data and macroseismic information, which usually has a much larger uncertainty. From the review of the previous studies presented in Section 6.3, it was decided to follow the probabilistic seismic hazard model proposed by Vilanova and Fonseca (2007), with a re-evaluation of the ground motion prediction equations. This model is a recent proposal that addressed in detail the national tectonic characteristics, considered a large spectrum of epistemic and aleatory uncertainties and took into consideration several previous studies in its formulation. Area sources were employed to define the seismicity according to two zonations: one comprising eleven area sources drawn based on the isoseismal configurations from historical events, and a second one adapted from the work of Pelaez and Casado (2002), comprising of eight area sources. Mainland Portugal was assumed as a stable continental region, whilst the areas offshore of south and southern Spain were defined as active shallow crustal regions. The earthquake catalogue was strongly based on the data from the IGN [37] (instrumental) and the work of Oliveira (1986) (historical). From this working catalogue (CA), a secondary one was extracted (CB), in which only events with a low error in magnitude were included. The source zone characterization, tectonic regionalization and working earthquake catalogue are illustrated in Figure 6.2.

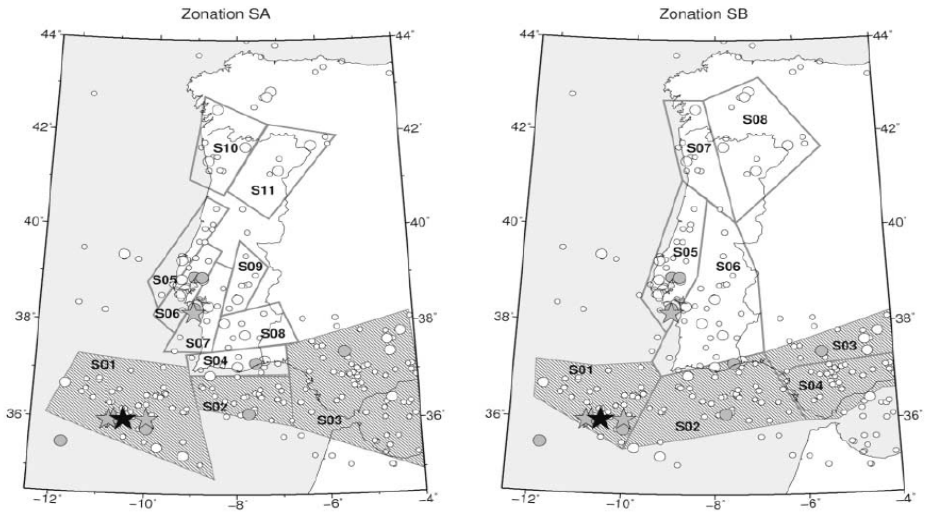

Figure 6.2 – Source zonation and earthquake catalogue (adapted from Vilanova and Fonseca, 2007).

For the computation of the recurrence rates, Vilanova and Fonseca (2007) used two methodologies, proposed by Stepp (1972) (RA) and Albarello *et al.* (2001) (RB), and two minimum moment magnitudes, 4.0 and 4.6, comprising four branches of the logic tree. For the definition of the maximum magnitude for each area source, the historical records were used in one branch, and the historical maximum magnitude increased by 0.5 magnitude units in another branch. The weights defined by Vilanova and Fonseca (2007) for each branch of the logic tree were maintained and its structure is illustrated in Figure 6.3.

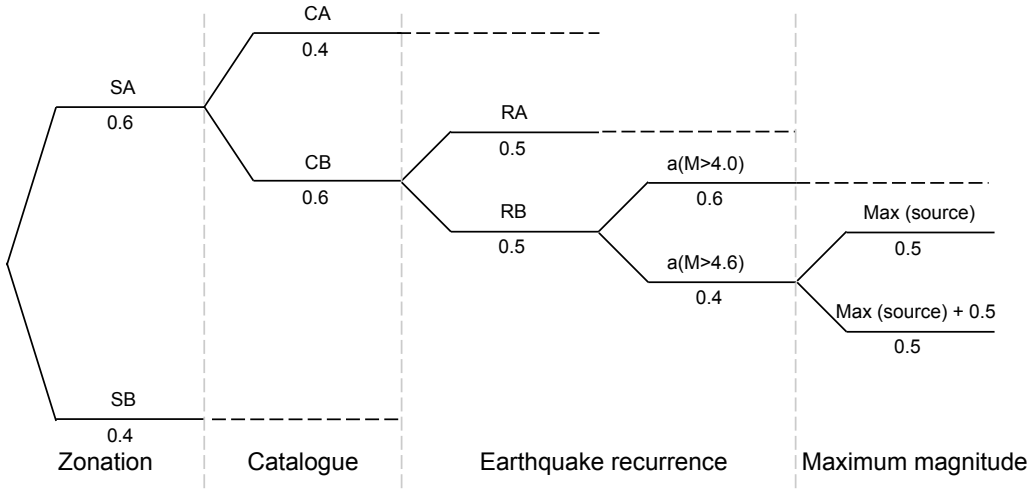

Figure 6.3 – Logic tree used for the hazard calculations defining the epistemic uncertainties in the seismic source model (adapted from Vilanova and Fonseca, 2007).

6.4.2. Selection of ground motion prediction equations

Ground motion attenuation models are probably the factor that influences most the seismic hazard (Pelaez and Casado, 2002), as well as the seismic risk (Crowley *et al*., 2005). The selection of these models needs to be done considering several aspects, such as the tectonic regionalization, distance and magnitude applicability, period range (for spectral ordinates), ability to model site effects, region wave propagation characteristics, amongst others. Regarding the seismic hazard model that was adopted herein, Vilanova and Fonseca (2007) proposed the employment of three ground motion prediction equations, Ambraseys *et al*. (1996), Toro *et al*. (1997) and Atkinson and Boore (1997), applied on both tectonic regions with the weights of 0.2, 0.4 and 0.4, respectively. A more recent scheme has been proposed as part of the European project SHARE, as described in Delavaud *et al*. (2012), for SCR (Stable Continental Region) and ASCR (Active Shallow Crustal Region). In this effort,

the applicability and performance of some existing ground motion prediction equations was evaluated through comparison with empirical data and expert judgement. Table 6.1 presents the resulting selected ground motion prediction equations and respective weight for each region.

Table 6.1 - Ground motion prediction scheme for SCR and ASCR proposed by Delavaud *et al.* (2012).

Stable continental region (SCR)		Active shallow crustal region (ASCR)	
GMPE	Weight	GMPE	Weight
Campbell (2003) [1*]	0.20	Akkar and Bommer (2010) [2*]	0.35
Toro (2002) [1]	0.20	Cauzzi and Faccioli (2008) [2]	0.35
Akkar and Bommer (2010) [2*]	0.20	Zhao *et al.* (2006) [3]	0.10
Cauzzi and Faccioli (2008) [2]	0.20	Chiou and Youngs (2008) [2*]	0.20
Chiou and Youngs (2008) [2*]	0.20		

[1] Attenuation model developed for stable continental regions.
[2] Attenuation model developed for active shallow crustal regions.
[3] Attenuation model developed for subduction areas.
[*] Attenuation models that were tested against data for Western Iberia by Vilanova *et al*. (2012).

In In addition to the models in Table 6.1, the models by Atkinson and Boore (2006), Douglas *et al.* (2006) and Atkinson (2008) were also considered as applicable to SCR, and the model by Boore and Atkinson (2008) was considered for ASCR, by the majority of the experts. Notwithstanding the value and pioneering character of this study, it is important to understand that such recommendations were compiled with the intention of providing the best arrangement for the European territory in general and thus, they may not fulfil the requirements for some specific regions. In fact, no empirical verification was carried out for SCR (the predominant regime in the region of interest in this study) due to the lack of a homogenous dataset.

The ASCR near Portugal proved to be considerably different from other active shallow crustal regions in Europe, due to a very low attenuation which is typically observed in SCR, rather than a high to very high attenuation, frequently reported in other regions of the same regime (e.g. Pyrenees) (Casado *et al*., 2000; Vilanova *et al*., 2007). Moreover, in a recent study conducted by Vilanova *et al*. (2012) in which the performance of a set of ground motion prediction equations were evaluated against instrumental and historical data from Western Iberia, it was concluded that attenuation models developed for SCR (namely Atkinson and Boore (2006), Campbell (2003) and Atkinson (2008)) tended to provide better results for both onshore and offshore events, whilst attenuation models developed for ASCR (namely Chiou and Youngs (2008) and Boore and Atkinson (2008)) performed

poorly, consistently underestimating the ground shaking. The model proposed by Akkar and Bommer (2010) was also evaluated in this effort and proved to deliver reasonable results, mainly for long period spectral ordinates.

In a recent study performed by Stewart *et al.* (2012) on the selection of a global set of ground motion prediction equations for the Global Earthquake Model initiative [2], in which the results from the SHARE project and Vilanova *et al.* (2012) were already taken into consideration, Atkinson and Boore (2006) and Pezeshk *et al.* (2011) attenuation models are suggested as the most appropriate for SCR. The studies above were developed with the final purpose of providing guidance to improve the accuracy and reliability of probabilistic seismic hazard assessment. For this reason, the ability of modelling the influence of local soil conditions, which is a fundamental feature in seismic risk, was not given particular attention. The consideration of site effects is specially important in Portugal, since a considerable portion of the population resides in areas susceptible to ground motion amplification, as described in the following section.

At the light of all of these findings, as well as the need to model ground motion amplification, it was decided not to employ the attenuation models from Toro (2002), Campbell (2003) and Pezeshk *et al.* (2011), since all of them provide ground motion only for rock (V_{s30}=2800 m/s). The attenuation models from Chiou and Youngs (2008) and Boore and Atkinson (2008) were also excluded due to a consistent underestimation of the ground motion reported by Vilanova *et al*. (2012). Overall, the models from Boore and Atkinson (2006) and Akkar and Bommer (2010) seemed to fulfil the requirements of the region of interest and to be in agreement with the suggestions from recent state-of-the-art reports, hence, both models were applied to the whole region with a weight of 0.7 and 0.3, respectively.

It is also recognized herein that the use of ground motion prediction equations capable of considering local soil conditions is not the only option to model site effects. Alternatively, the ground motion can be computed for rock, and modified afterwards through the employment of amplification factors based on the type of soils (e.g. Choi and Stewart, 2005), as recommended by many building design codes (e.g. CEN, 2004; BSSC, 2004). However, such approach brings in the additional uncertainty from the estimation of those amplification factors and they are not yet implemented in the OpenQuake-engine, which has been used for the calculations presented herein.

It is also important to acknowledge the GMPEs developed specifically for Portugal by Carrilho and Oliveira (1997) and Carvalho (2008). However, the former model was developed based on seismic events with magnitudes (m_b) between 2.8 and 4.9, which hampers its employment in studies with seismic sources with a maximum magnitude considerably above this range. The latter model instead employed artificial ruptures produced through a stochastic finite-fault method, however it has not yet been published in an international peer-reviewed journal, which is a fundamental criterion for the selection of GMPEs (Cotton *et al.*, 2006; Stewart *et al.*, 2012).

6.4.3. Consideration of site effects

The influence of local soil conditions in earthquake ground motion has been recognised for many decades and its impact is evident through the observation of damage in several past events. In the 1985 Michoacán (M_s = 8.1) earthquake, only moderate damage was reported in the vicinity of the epicentre, whilst in Mexico City located 350 km away, extensive damage was observed (Kramer, 1996). Similar effects were registered in the 1755 Lisbon (M_w=8.5-9.0) earthquake, in which the southern town of Faro was partially destroyed and the town of Tavira, built in hard limestone and located only 30 km away, experienced much lower ground shaking and barely any building damage (Chester, 2001).

Despite the recognition of the effects of local site conditions on the intensity of ground motion, in general, its consideration in building design codes was not properly introduced until the 1970s (Kramer, 1996). Portugal, however, was one of the first countries in the world to adopt a design code (RSCCS in 1958), with guidelines of how to consider in a very simplified manner the lateral loads due to a seismic event. Later, in 1961, this code was replaced by RSEP, which already included some provisions regarding site effects. This code, as well as the more recent ones (RSA, 1983; CEN, 2004), recommend the use of coefficients that modify the ground motion at a given location based on the type of soil, which needs to be classified by the practitioner or other experts, since there is no national map of soil conditions.

The use of the average velocity of seismic shear waves in the top 30 meters layer (V_{s30}) has become a very common standard to characterize seismic site conditions. The United States design code (BSSC, 2004) requires specifically this measurement

to represent the local site conditions, and in the European EC8 design code (CEN, 2004), guidelines are also provided to classify the soil based on this parameter. In addition, many ground motion prediction equations (e.g. Atkinson and Boore (2006); Chiou and Youngs, 2008), which are fundamental for seismic hazard and risk assessment, have been calibrated against seismic station site conditions described with V_{s30} values (Wald and Allen, 2007).

The acquisition of V_{s30} values at a large scale requires a significant investment of economic and human resources, and has only been done nationally or locally in few regions in the World (e.g. California (USA), Italy, Taiwan, Thessaloniki (Greece), Australia). The recognition of the challenges in carrying out the effort to collect V_{s30} in large areas or in less developed countries, propelled the development of simplified methodologies to derive first-order V_{s30} values, mainly for the purposes of estimating post-earthquake human and economic losses and assessing seismic hazard and risk. Wills and Claham (2006) established a correlation between a set of geology units and V_{s30} values for California, whilst Wald and Allen (2007) proposed a methodology that uses medium to high resolution slope topography to obtain proxy V_{s30} values, based on the assumption that stiffer materials (high-velocity) are more likely to maintain a steep slope while deep basin sediments are deposited mainly in environments characterized by a lower velocity. This approach has been subsequently revised in Allen and Wald (2009).

In this study, a V_{s30} map was developed according to each of the aforementioned approaches and incorporated in the logic tree as an additional branching level, as described in the following section.

6.4.3.1. V_{s30} mapping for Portugal

If poorly estimated, site effects can introduce a significant error in seismic risk results, due to the under- or over-estimation of the ground motion. It is thus important to understand how the V_{s30} values are going to be handled by the seismic hazard and risk software. In the case presented herein, the OpenQuake-engine uses ground motion prediction equations that require the definition of a V_{s30} value for each location where the seismic hazard/risk are going to be computed. If such parameter is not available at a given location, the OpenQuake-engine uses the closest V_{s30} value. For the purposes of creating a V_{s30} map for Portugal, an evenly spaced grid of 5x5 km^2 was used to estimate V_{s30} values, through the employment of

the simplified methodologies proposed by Wills and Claham (2006) and Wald and Allen (2007). For the former methodology, which relies on the geological units, a dataset from the Portuguese Environmental Agency [38] has been used, which provides the type of rock and associated period of genesis. Then, each geological unit was related to one of the categories described by Wills and Claham (2006) (California) to define the respective V_{s30} value. For the geological units not covered by Wills and Claham (2006), the work of Stewart *et al.* (2008) (Italy) was used. Table 6.2 contains the correspondence between the most common Portuguese geological units (at least representing 1% of the national surface) and the ones from the aforementioned studies.

Table 6.2 - Correspondence between the geological units in Portugal and the equivalent categories in Wills and Clahan (2006) and Stewart *et al*. (2008).

Area %	Geological units in Portugal	Equivalent geological category	V_{s30} m/sec
25.8	Granites and similar rocks (Cambrian)	Crystalline rocks, Cretaceous granitic rocks, Jurassic metamorphic rocks, schist, and Precambrian gneiss(1)	748 ± 430
13.0	Schists, grayswackes (Precambrian and Cambrian)	Crystalline rocks, Cretaceous granitic rocks, Jurassic metamorphic rocks, schist, and Precambrian gneiss(1)	748 ± 430
11.9	Schists and graywackes (Silurian)	Crystalline rocks, Cretaceous granitic rocks, Jurassic metamorphic rocks, schist, and Precambrian gneiss(1)	748 ± 430
10.6	Shales, graywackes, sandstones (Carboniferous and Devonian)	Franciscan complex rock, including melange, sandstone, shale, chert, and greenstone(1)	782 ± 359
7.7	Sandstones, more or less argillaceous limestone, sands, gravels, clays (Miocene and Pliocene)	Quaternary (Pleistocene) sand deposits(1)	302 ± 46
6.2	Sands, rounded pebbles, sandstones poorly consolidated, clays (Pliocene and Pleistocene)	Quaternary (Pleistocene) sand deposits(1)	302 ± 46
3.7	Planaltic gravel, Beira Baixa arcosic deposits, coarse to conglomeratic sandstones and of thin grain, limestone (Miocene)	Tertiary (mostly Miocene, Oligocene, and Eocene) sandstone units(1)	515 ± 215
3.1	Conglomerates, sandstones, limestone,dolomitic limestone, argillaceous limestone, marls (Jurassic)	Dolomitic limestone and limestone (Jurassic)(2)	1000
2.1	Dunes and eolic sands (Holocene)	Quaternary (Holocene) alluvium in major channels where the alluvium is expected to be coarse(1)	354 ± 82
2.1	Schists, amphibolic schists, amphibolites, micaschists, grayswackes, quartzite, carbonated rocks, gneiss (Precambrian)	Crystalline rocks, Cretaceous granitic rocks, Jurassic metamorphic rocks, schist, and Precambrian gneiss(1)	748 ± 430
1.9	Limestone, dolomitic limestone, argillaceous limestone, marls (Jurassic)	Dolomitic limestone and limestone (Jurassic) (2)	1000
1.8	Alluvium (Holocene)	Quaternary (Holocene) alluvium(1)	280 ± 74

1.7	Sandstones, conglomerates, limestone, dolomitic limestone (Cretaceous)	Cretaceous sandstone(1)	566 ± 199
1.3	Quartzite (Devonian, Silurian and Ordovician)	Crystalline rocks, Cretaceous granitic rocks, Jurassic metamorphic rocks, schist, and Precambrian gneiss(1)	748 ± 430
1.2	Shales, quartzites, amphibolites (Precambrian)	Crystalline rocks, Cretaceous granitic rocks, Jurassic metamorphic rocks, schist, and Precambrian gneiss(1)	748 ± 430
1.1	Sands and gravels (Pleistocene)	Quaternary (Pleistocene) alluvium(1)	387 ± 142

(1) Equivalent geological category taken from Wills and Clahan (2006).
(2) Equivalent geological category taken from Stewart *et al.* (2008).

For what concerns the approach proposed by Wald and Allen (2007) to estimate V_{s30} values based on the topography, the global STRM30 dataset (Farr and Kobrick, 2000) with a 30 arcsec spatial resolution was employed. The territory of Portugal was assumed as stable continental and the correspondence between V_{s30} and slope range is described in Table 6.3.

Table 6.3 - Relation between V_{s30} values and topographic slope (Allen and Wald, 2009).

Vs30 range (m/sec)	Value used (m/sec)	Slope range (m/m)
<180	180	< 2.0 x e-5
180-240	210	2.0 x e-5 – 2.0 x e-3
240-300	270	2.0 x e-3 – 4.0 x e-3
300-360	330	4.0 x e-3 – 7.2 x e-3
360-490	425	7.2 x e-3 – 0.013
490-620	555	0.013 – 0.018
620-760	690	0.018 – 0.025
>760	760	>0.025

Figure 6.4 presents the V_{s30} spatial distribution for Portugal obtained with each of the two simplified methodologies followed. A good agreement between these two approaches is observed, mainly in the north, centre and western part of the territory. For the inner-southern region of Portugal instead, significantly lower V_{s30} values are provided by the topographic-based methodology. The discrepancies between these maps highlight the zones where further investigation should be carried out, preferably through field measurements.

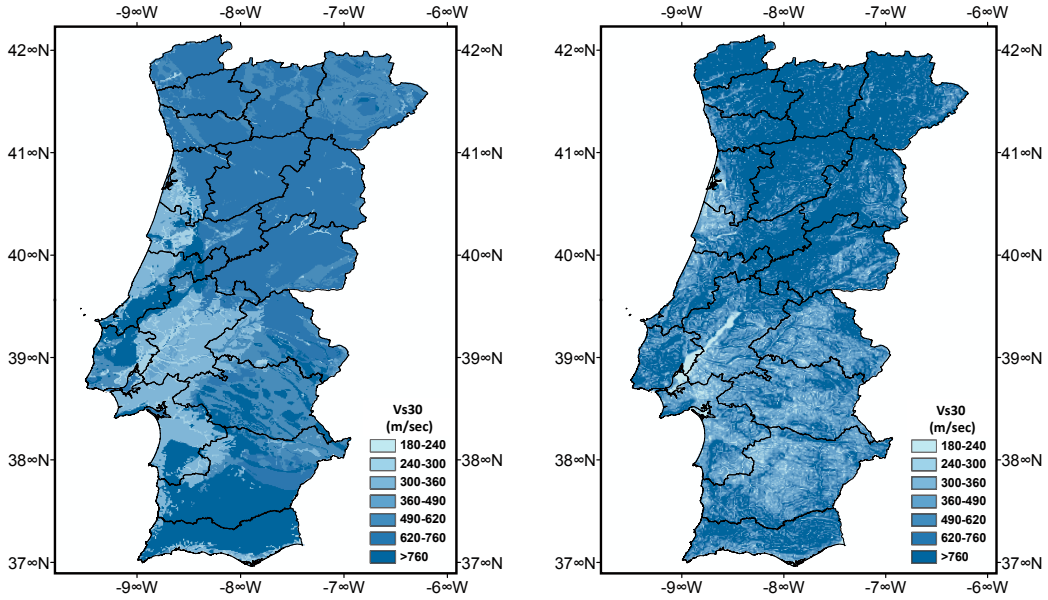

Figure 6.4 - V_{s30} map based on the methodology proposed by Wills and Clahan (2006) (left) and Wald and Allen (2009) (right).

An additional dataset with the average V_{s30} values (based on the two aforementioned approaches) was computed and from this map it was estimated that approximately 93% of the Portuguese mainland territory is comprised of rock/very stiff soils (V_{s30} > 360 m/s according to the Eurocode 8 (CEN, 2004) soil classification). However, regions where softer soils exist are greatly populated. By crossing the population distribution dataset LandScan™ 2009 developed by the Oak Ridge national Laboratory (Dobson *et al.*, 2000) with the average V_{s30} map, it was possible to estimate the distribution of population per soil type, leading to the results presented in Figure 6.5.

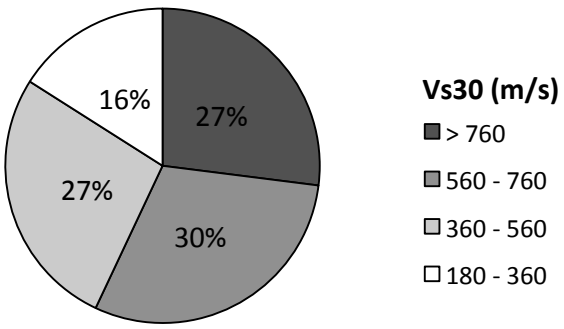

Figure 6.5 – Distribution of population per each soil type category for Portugal mainland.

Regarding V_{s30} field measurements in Portugal, it is worth mentioning the on-going project SCENE (Site Conditions Evaluation for National seismic hazard

Estimation) (Narciso *et al*., 2012), which aims to create a database of shear wave velocity for mainland Portugal, including also the results from other related projects at a regional scale, such as ERSTA (Carvalho *et al*., 2008), CAPSA (Carvalho *et al*., 2009) for the province of Algarve, NEFITAG [39] (still in progress) for the Lower Tagus Valley. The simplified methodologies employed in this study have been validated (Narciso *et al*., 2012) against a set of instrumental measurements, concluding that both approaches performed roughly equally. For this reason, both V_{s30} maps were given equal weight in the logic tree, for the seismic risk calculations.

6.4.4. Exposure model

The development of an exposure model capable of providing information about the location, value and vulnerability classification of the exposed elements at a national scale might be a very challenging task, often only achievable through the use of Census data (e.g. Erdik *et al*., 2003 (Turkey); Sousa, 2006 (Portugal); Crowley *et al*., 2008 (Italy)) or using other datasets to approximate building distribution, such as population datasets (Jaiswal *et al*., 2010). In this work, the 2011 Building Census data at the parish level was used as the main component for the development of a first exposure model. Then, this model was used to derive a second one, with a spatial re-distribution of the assets within each parish according to the population dataset LandScan™ 2009.

6.4.4.1. Portuguese building stock

Census surveys have been undertaken in Portugal since 1864 with a 10 years periodicity, but information about the building portfolio was only included after 1970. In the present work, the Building Census data from 2011 for residential buildings is considered, thus disregarding public infrastructures and exclusively commercial or industrial buildings. In 2011, 3,544,389 residential buildings were reported, housing 5,878,756 dwellings. Amongst the various attributes considered in the Building Census survey, the type of construction, year of construction and number of floors have been used herein to define a set of building classes. The first attribute is organized in five categories: reinforced concrete (RC); masonry with concrete floors (M1); masonry with timber floors (M2); weak masonry (M3), comprised by adobe, rubble stone or rammed earthen units; and others (OT), comprised of wooden and steel structures.

The year of construction plays an important role in classifying the building portfolio according to the level of seismic design. In Portugal, the first design codes that contained provisions regarding the consideration of seismic action date from 1958 (RSCCS) and 1961 (RSEP). However, such recommendations were overly simplified and could not impose effectively an adequate seismic performance. Later, in 1983, a new and much more demanding design code (RSA) was introduced, which is still in use nowadays, along with the Eurocodes [40]. Thus, buildings constructed before 1983 are categorized as pre-code (PC), whilst the ones built after are termed post-code (C). Nevertheless, it is important to understand that for the case of masonry buildings (even those built recently), there were no guidelines to ensure seismically resistant construction practices and the verification of seismic action could even be neglected for masonry buildings of reduced size.

Regarding the number of floors, three categories are considered herein: up to three storeys as low-rise (LR), between four and six storeys as mid-rise (MR) and more than six storeys as high-rise (HR). The percentage of buildings from each construction typology according to the number of stories and date of construction is illustrated in Figure 6.6.

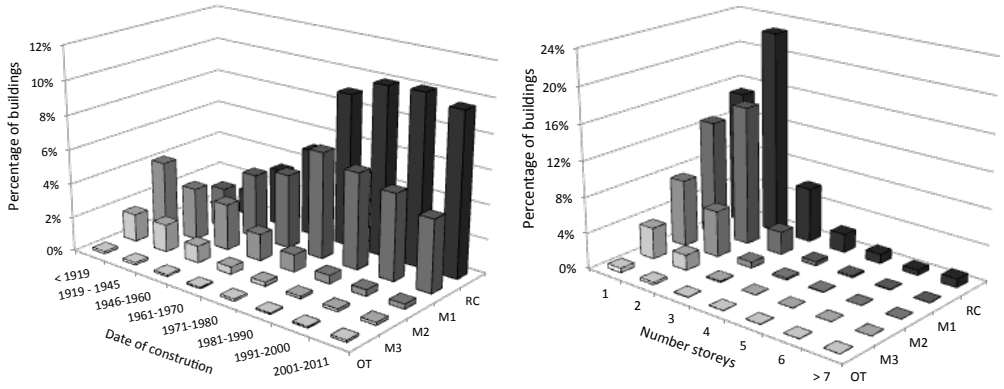

Figure 6.6 - Distribution of buildings according to type of construction, year of construction and number of storeys.

The building stock is comprised of 50.6% masonry buildings (M1, M2 and M3), 48.6% of reinforced concrete (RC) buildings, and 0.8% of other typologies (OT). Despite this distribution, RC buildings tend to have more storeys (thus containing more dwellings) and therefore it has been estimated that this building typology hosts about 60% of the Portuguese population. For what concerns the date of construction, almost 62% of the building stock has been built before the

introduction of the 1983 design code (RSA) and, more specifically regarding the RC buildings, it has been estimated that only 51% were designed while the RSA design code was already in force. This implies that more than 6 million people live in structures that might not adequately withstand the effects of an eventual seismic event.

6.4.4.2. Development of the exposure model

Using the previously described categories, a set of classes has been defined to distinguish each construction typology according to its seismic vulnerability, as described in Table 6.4. For the sake of simplicity, high-rise masonry has been merged with the mid-rise masonry, and the buildings classified as "Other" were added to the M3 category, as they only represent 0.05% and 0.83% of the building stock, respectively.

Table 6.4 - Vulnerability classes for Portuguese building stock.

Construction type	Number of floors	Design level	Vulnerability Class	Percentage (%)
RC	Low-rise	Pre-code	RC LR PC	21
		Post-code	RC LR C	23
	Mid-rise	Pre-code	RC MR PC	2
		Post-code	RC MR C	2
	High-rise	Pre-code	RC HR PC	< 1
		Post-code	RC HR C	1
M1	Low-rise	Pre-code	M1 LR PC	18
		Post-code	M1 LR C	12
	Mid-rise	Pre-code	M1 MR PC	< 1
		Post-code	M1 MR C	< 1
M2	Low-rise	Pre-code	M2 LR PC	12
		Post-code	M2 LR C	1
	Mid-rise	Pre-code	M2 MR PC	< 1
		Post-code	M2 MR C	< 1
M3	Low-rise	-	M3 LR PC	6

Combining the classification from Table 6.4 with the data from the Building Census survey of 2011, a parish-based exposure model containing the number of buildings from each vulnerability class was created. For the purposes of computing the seismic hazard for each asset, it was assumed that all of the building locations could be represented by the centroid of the associated parish area, which is a common assumption when performing seismic risk assessment at a large scale (e.g.

Bommer *et al.*, 2002; Sousa, 2006; Crowley *et al.*, 2008; Campos-Costa *et al.*, 2009). However, this aggregation of the elements at a single location per parish can introduce a significant error for the larger regions with a very unbalanced spatial distribution of the building stock and seismic hazard, as the ground motion at the area centroid might be significantly different from that at the actual location of the assets. In order to investigate this issue, a second exposure model was created, in which a redistribution of the building stock per parish was performed based on the population distribution dataset LandScan™ 2009. This dataset uses an algorithm to allocate population count in an evenly spaced grid with a 30 arc sec spatial resolution (which in Portugal represents approximately 0.75 km^2), based on parameters such as proximity to roads and train lanes, terrain slope, land cover and night-time lights (Dobson *et al.*, 2000). The buildings were then distributed across this grid proportionally to the amount of population estimated at each grid cell. In this way, the assets within each parish are shifted to the regions where human activity is more evident. In Figure 6.7, the resulting exposure models in terms of total number of buildings per unit of area are illustrated.

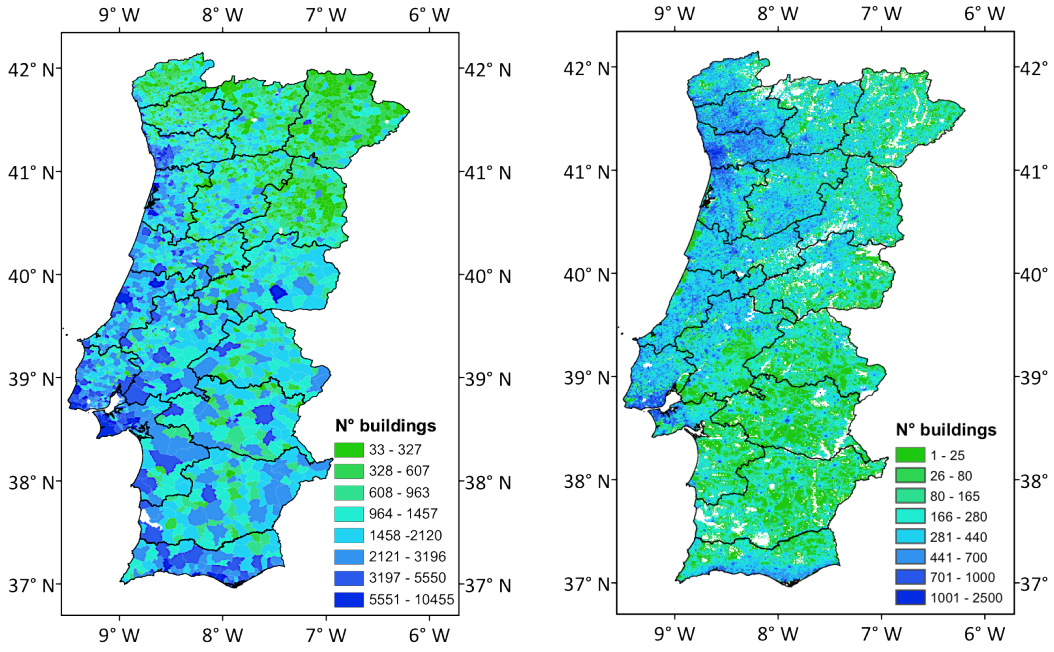

Figure 6.7 - Exposure model for Portugal following a parish-based (left) and 30 arc sec grid (right) resolutions.

Estimation of building economic value

The spatial distribution of building count is a fundamental component for earthquake scenario damage assessment, which can then be used to create post-

disaster emergency plans or to design risk mitigation strategies. However, in order to estimate the associated economic losses, it is necessary to attribute a building cost to each typology. In this study, this building cost is established as the required monetary value to construct a building with the same characteristics according to nowadays costs, herein termed as the replacement cost. This value naturally depends on the location and total area of the building. Regarding the first parameter, the Portuguese government establishes reference construction costs (Directive nº 291, 2011), based on three zones: Type 1, capital of districts and other major cities; Type 2, counties located in urban areas; Type 3, counties located in rural areas. Table 6.5 presents these costs per area.

Table 6.5 – Construction costs for each zone according to Directive nº 291 (2011).

Zone	Type 1	Type 2	Type 3
Cost (€/m²)	743.7	650.1	589.0

The total area per building has been computed by multiplying the average number of dwellings per building by the average area per dwelling. The estimation of the dwellings per building has been carried out as a function of the number of floors, as taller buildings tend to comprise more dwellings than shorter ones. In order to take into consideration the variation in these two parameters across the country, it was decided to use the data from the Building Census 2011 at the level of the five regions delimited by the Coordinating Committee for Regional Development (CCRD). The average number of dwellings as a function of the number of floors is depicted in Figure 6.8 and the average area per dwelling is presented in Table 6.6.

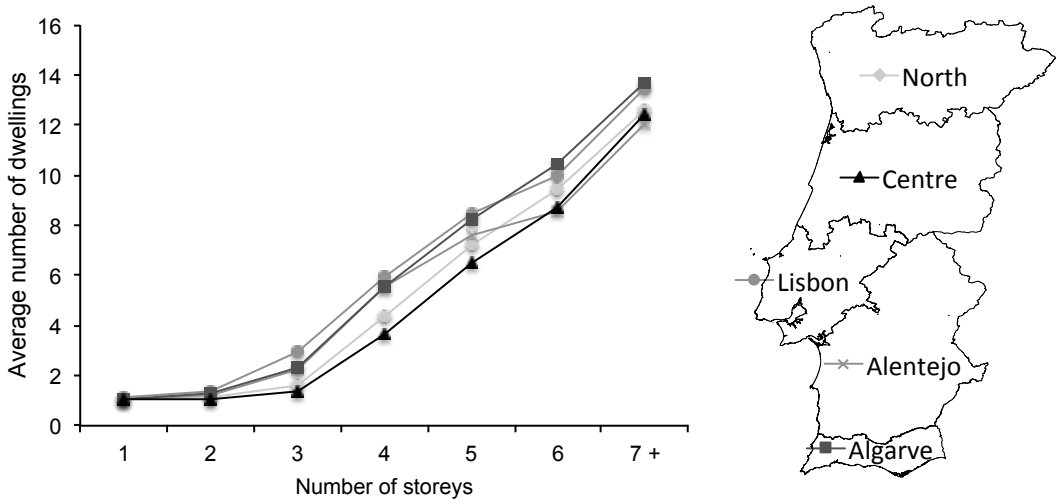

Figure 6.8 – Average number of dwelling in function of the number of floors for each CCRD region.

Table 6.6 - Area per dwelling for each CCRD region.

CCRD region	Alentejo	Algarve	Centre	Lisbon	North
Area (m²)	97.1	87.3	111.1	102.5	107.5

Finally, the replacement cost for each vulnerability class will be calculated through the following formula:

$$R_{cost} = \sum_{j=1}^{n} \sum_{i=1}^{m} b_{i,j} \times d_j \times A_{location} \times C_{location} \quad (6.1)$$

in which R_{cost} stands for the replacement cost for a given vulnerability class; $b_{i,j}$ stands for the buildings with j number of floors; d_j stands for the number of dwellings given the j number of floors and $A_{location}$ and $C_{location}$ represent the area per dwelling and cost per area given the location of the building, respectively.

6.4.5. Vulnerability model

In this study, the seismic loss calculations were performed through the employment of a vulnerability model, which describes the probability distribution of loss ratios for a set of intensity measure levels. The seismic vulnerability of the reinforced concrete building typologies was the target of a comprehensive study, presented in Chapter 5, which resulted in the development of a new set of vulnerability functions. Masonry building typologies were not considered in the aforementioned study and therefore, a simplified approach is employed herein to derive a set of masonry vulnerability functions by combining the Capacity Spectrum Method (ATC40, 1996) with the capacity curves proposed by Carvalho *et al*. (2002).

Not withstanding the recent studies regarding the structural behavior of masonry buildings in Portugal (e.g. Coelho *et al*. 2011; Costa, 2011), a robust vulnerability model covering the most common masonry building typologies does not seem to be currently available in the literature. In the European project LESSLOSS (2004-2007) (Calvi and Pinho, 2004), various fragility functions previously derived by Carvalho *et al.* (2002) using the simplified methodology from HAZUS (FEMA, 1999) were used. This approach relies on a capacity curve constructed based on a group of parameters (related to the design of the structure), which is used to extract a set of spectral displacements (one per limit state) according to pre-defined global drift thresholds. Each spectral displacement is used as the median of a cumulative lognormal distribution, with a given pre-established logarithmic standard deviation,

to represent the respective limit state fragility function. These fragility functions can be used together with capacity spectrum-based methodologies (e.g. N2 - Fajfar, 1999; Capacity Spectrum Method - ATC40, 1996) in seismic loss assessment. However, it is important to understand that these curves are defined in terms of spectral ordinates for a period of vibration and viscous damping that varies for each intensity measure level. This impedes their employment in common seismic risk methodologies in which the losses are calculated directly from the seismic action, which is derived through the employment of ground motion prediction equations, as these methodologies require the seismic excitation to be defined at a fixed period of vibration and viscous damping. For this reason, a simplified methodology is employed herein to compute a set of fragility functions for the masonry typologies M1, M2 and M3 (as defined in Table 6.4), using spectral acceleration at the yield period to represent the seismic action. The seismic performance of masonry typologies M1 and M2 was assumed to be identical and hence, just a set of vulnerability functions is derived for them.

Carvalho *et al*. (2002) computed a set of capacity curves (*Sa* versus *Sd*) for each masonry building typology, categorized according to the number of storeys and seismic design approach. In the present study, a large number of demand spectra defined according to the spectral shape of Eurocode 8 (CEN, 2004) was combined with the aforementioned capacity curves using the Capacity Spectrum Method (ATC-40, 1996) to assess which demand spectrum intersects the global drift threshold of each limit state. Then, using the peak ground acceleration of the matching demand spectrum at each limit state, the spectral acceleration for the yielding period and 5% viscous damping was computed based on the aforementioned spectral shape, and used as the median of the cumulative lognormal function representative of the associated limit state fragility curve, as defined by the following formula:

$$P_D(D \geq d|Sa) = \Phi\left[\frac{1}{\beta}\ln\left(\frac{Sa}{\overline{Sa}}\right)\right] \tag{6.2}$$

where Φ stands for the standard normal cumulative distribution function, $\overline{Sa}$ represents the median spectral acceleration for each limit state and β is the logarithmic standard deviation. Regarding the latter parameter, FEMA and NIBS (1999) describe a procedure to estimate the β parameter that takes into

consideration several sources of variability such as the uncertainty in the damage state threshold, the uncertainty in the capacity of the building and the variability in the ground motion. In addition, standard values of β calculated based on pre-established building typologies, heights, damage states and seismic design levels are also provided. In the present study, due to lack of information regarding some of the aforementioned sources of variability, a decision was made to adopt these standard values of β in the derivation of the fragility model. In order to clarify this procedure, in Figure 6.9, the resulting demand spectra for the four limit states and respective fragility functions for a three storeys masonry building are illustrated.

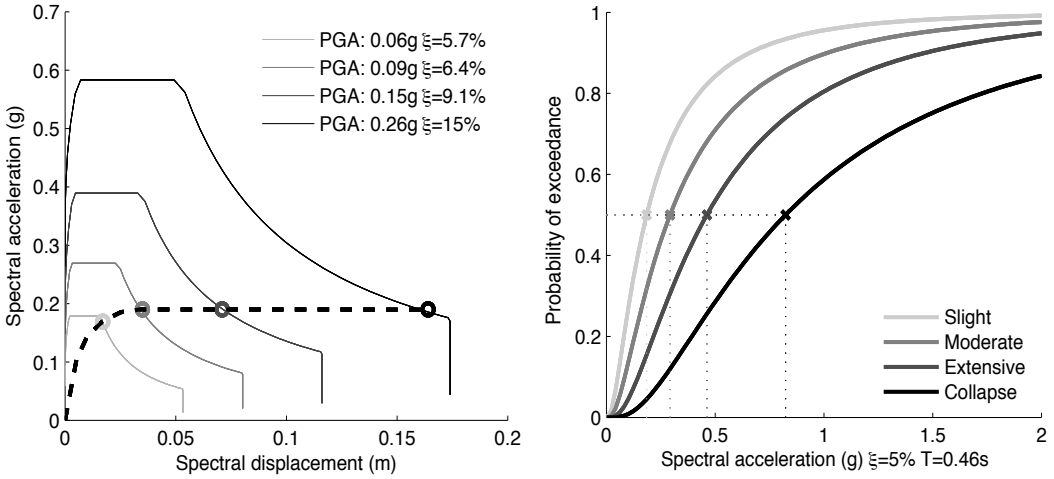

Figure 6.9 - Performance points for each limit state and associated acceleration spectrum (left), and resulting fragility model for a masonry building with 3 storeys (right).

This procedure was carried out for all the capacity curves of masonry buildings with 1, 2, 3, 4, and 5-6 storeys. Then, for each of the building typologies considered herein (which consider a range of number of storeys), a weighted average of the logarithmic mean and standard deviation for each limit state curve was calculated, based on the percentage of buildings of each height within the building class. For example, for the building typology M2 LR C, the fragility curves for 1 storey had a weight of 58%, 2 storeys were used with a weight of 37% and 3 storeys had a 5% weight. The logarithmic mean and logarithmic standard deviation of each limit state fragility function for the five masonry typologies are presented in Table 6.7.

Table 6.7 - Logarithmic mean (λ) and logarithmic standard deviation (ζ) for each limit state fragility function.

Damage state		Slight		Moderate		Extensive		Collapse	
Building typology	T_y (sec)	λ (g)	ζ (g)	λ (g)	ζ (g)	λ (g)	ζ (g)	λ (g)	ζ (g)
M1,2 LR PC	0.25	-1.42	1.15	-1.24	1.19	-0.96	1.20	-0.38	1.18
M1,2 LR C	0.25	-1.35	0.99	-1.16	1.05	-0.85	1.10	-0.22	1.08
M1,2 MR PC	0.61	-1.73	0.99	-1.27	0.97	-0.81	0.90	-0.08	0.88
M1,2 MR C	0.61	-1.72	0.91	-1.16	0.92	-0.67	0.87	0.13	0.91
M3 LR	0.23	-1.76	1.15	-1.61	1.19	-1.45	1.20	-1.04	1.18

Each set of fragility functions was converted into a vulnerability function, through the employment of a consequence model. In this process, the percentage of buildings in each damage state is computed at each intensity measure level, and multiplied by the respective damage ratio (ratio of cost of repair to cost of replacement), obtaining in this manner, a loss ratio for each level of spectral acceleration. The consequence model applied herein was described in 5.3.4, and it is the product of an evaluation of four models for different regions (Italy, Greece, Turkey and California), assuming the following damage ratios: slight damage – 0.1; moderate damage – 0.3; extensive damage – 0.6 and collapse – 1.0. In Figure 6.10, the final set of vulnerability functions for the masonry building typologies is depicted.

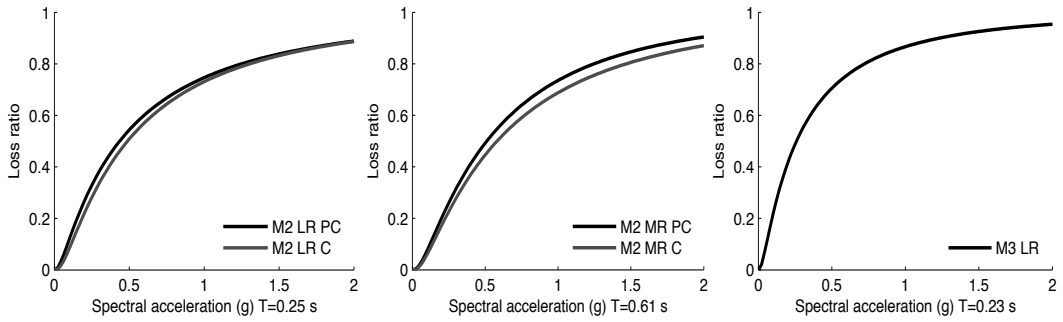

Figure 6.10 - Vulnerability functions for M2 low-rise (a), mid-rise (b) and M3 low-rise (c) typologies.

6.5. Results

6.5.1. Seismic hazard

The OpenQuake-engine, the open source platform for seismic hazard and risk assessment presented in Chapter 2, was used for the calculation of seismic hazard curves and maps. The Classical PSHA-based hazard calculator was employed. This calculator uses the classical PSHA approach (Cornell, 1968; McGuire, 2004)

following the methodology presented by Field *et al.* (2003) to compute a hazard curve for a 50 years time span (probability of exceeding a set of intensity measure levels within a given interval of time) at each site, for each of the possible 128 paths of the previously described logic tree. The employment of a spatial resolution of 0.01x0.01 decimal degrees for the hazard calculations, led to approximately 10 million hazard curves for each intensity measure type. From this set of hazard curves, the mean, 16th and 84th percentiles were calculated, and used to derive seismic hazard maps (see Figure 6.11) for a probability of exceedance of 10% in 50 years (equivalent to a return period of 475 years, commonly used as the reference for seismic design purposes).

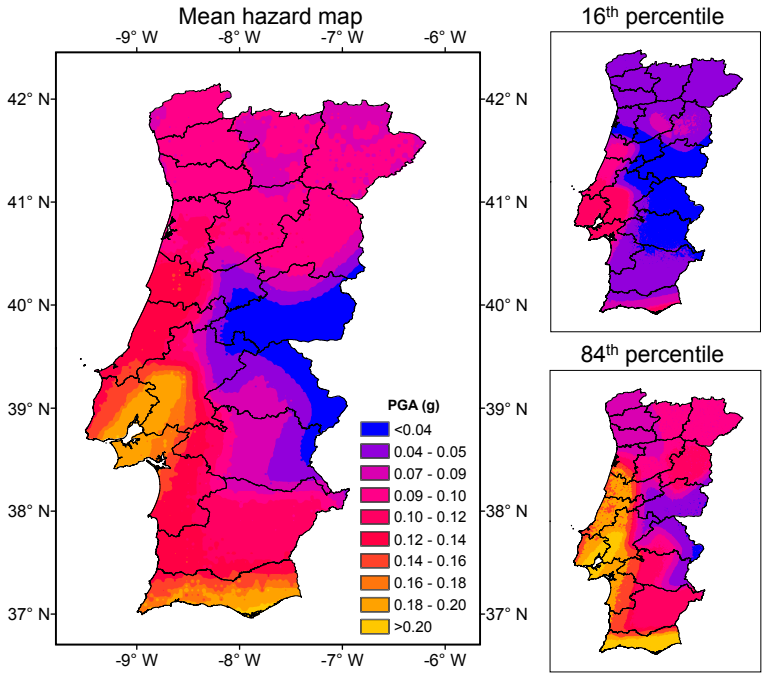

Figure 6.11- Mean seismic hazard map and 16th and 86th percentile maps in peak ground acceleration (g) for rock, for a probability of exceedance of 10% in 50 years (return period of 475 years).

The spatial distribution of the hazard and range of peak ground acceleration obtained in this study is in agreement with the results proposed by Vilanova and Fonseca (2007) (who originally developed the seismic source model adopted herein), despite the different GMPE scheme considered between these two studies. Vilanova and Fonseca (2007) carried out a comprehensive comparison between hazard assessments for this region, concluding that for the 475 years return period, studies that relied on peak ground acceleration (Oliveira *et al.*, 1999; Jiminez *et al.*, 1999) present a pattern with higher hazard in the Lower Tagus Valley and Algarve,

whilst for studies based on intensity data (Sousa, 1996; Pelaez and Casado, 2002), a higher hazard is obtained in the southwest of mainland Portugal. The former trend (higher hazard in the Lower Tagus Valley and Algarve) was also observed in the present study.

6.5.2. Seismic risk

The seismic risk assessment of mainland Portugal was also carried out using the OpenQuake-engine. In order to take into consideration the influence of soil conditions, a new set of hazard curves was derived, considering the two V_{s30} models presented in section 6.4.3.1 as an additional branching level in the logic tree. This set of curves was provided to the Classical PSHA-based Risk calculator, together with the vulnerability model (see section 6.4.5) and the two exposure models (parish- and grid-based, as described in section 6.4.4.2), in order to calculate a loss exceedance curve (probability of exceeding a set of losses within a given interval of time, taken as 50 years herein) for each asset, considering each possible path of the logic tree. Using the set of loss exceedance curves for each asset, a mean loss map for a 10% probability of exceedance in 50 years was computed for the two exposure models, as presented in Figure 6.12 and Figure 6.13, along with the 16th and 84th percentile results.

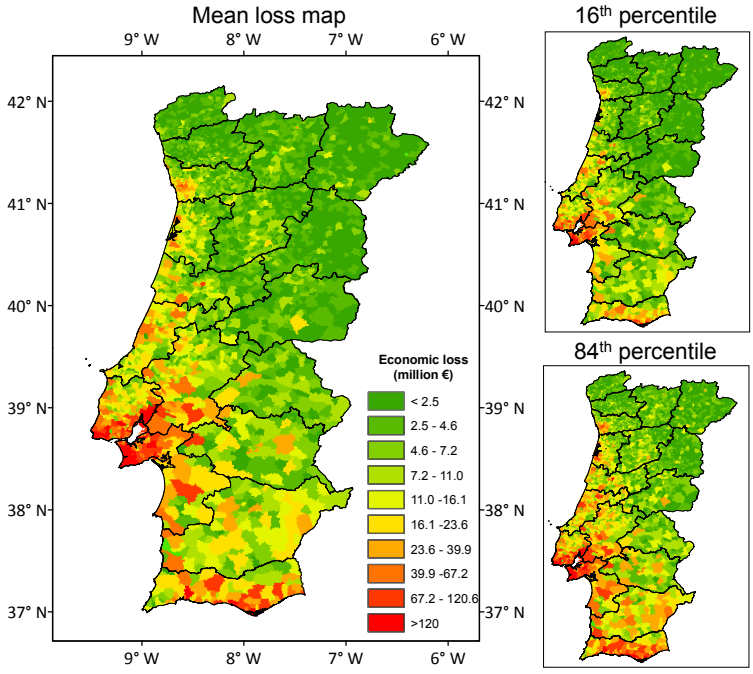

Figure 6.12 – Economic loss map for a probability of excedance of 10% in 50 years (475 years return period), considering the parish-based exposure model.

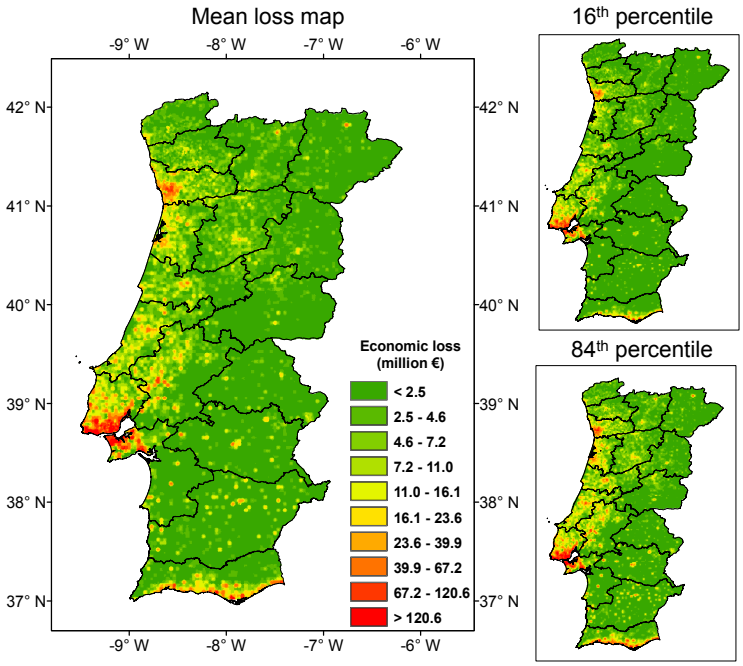

Figure 6.13 - Economic loss map for a probability of excedance of 10% in 50 years (475 years return period), considering the grid-based exposure model.

The estimated economic losses in mainland Portugal are mostly concentrated in the western region and the south (Algarve). In the region above the Lower Tagus Valley, despite the decrease in the seismic hazard, significant economic losses are still expected, due to the presence of a large amount of adobe masonry buildings (vulnerability class M3) in soft soils, which can amplify the spectral acceleration by a factor of 1.5 for short periods and 2.0 for longer periods (Stewart *et al.*, 2012). The mean aggregated economic loss for the 475 year return was has been estimated as 56.4 ± 7.9 billion and 56.1 ± 7.8 billion euro for the parish-based and grid-based exposure model, respectively. Both approaches seem to provide similar results, probably due to the fact that the spatial resolution of the parish-based exposure was already fine enough, thus not changing significantly the position of the assets.

It is important to understand that the process of aggregating the losses throughout the region of interest may underestimate the total loss value, particularly at high return periods, because the approach chosen for the calculations (classical PSHA) does not take into consideration the spatial correlation of the intra-event residuals (Jayaram and Baker, 2010), nor the correlation of loss ratio between buildings of the same vulnerability class. In order to take these two aspects properly into account, a probabilistic event-based approach would have to be followed where the losses are calculated event-by-event, which would lead to an aggregated loss

exceedance curve (representative of the whole exposure model) with higher probabilities of exceeding large losses (e.g. Park *et al.*, 2007; Crowley *et al.*, 2008). However, the employment at a national scale of the probabilistic event-based methodology, as it is currently implemented in the OpenQuake-engine, would require sampling of millions of earthquake ruptures, making this approach very computational demanding. Nevertheless, for a study of this magnitude, with such a wide spectrum of uncertainties, this aggregation of the losses can still be a reasonable indicator of the trend of total economic losses for this return period. In addition, the impact of spatial correlation of the ground motion residuals is more pronounced when considering longer return periods (Park *et al.*, 2007), as opposed to the 475 years adopted herein.

In order to understand which building typologies are contributing more to the overall economic loss, the losses per building typology have been aggregated, as presented in Figure 6.14, for the two exposure models. The error bars indicate the 16th and 84th percentile of the building typology-based aggregated loss.

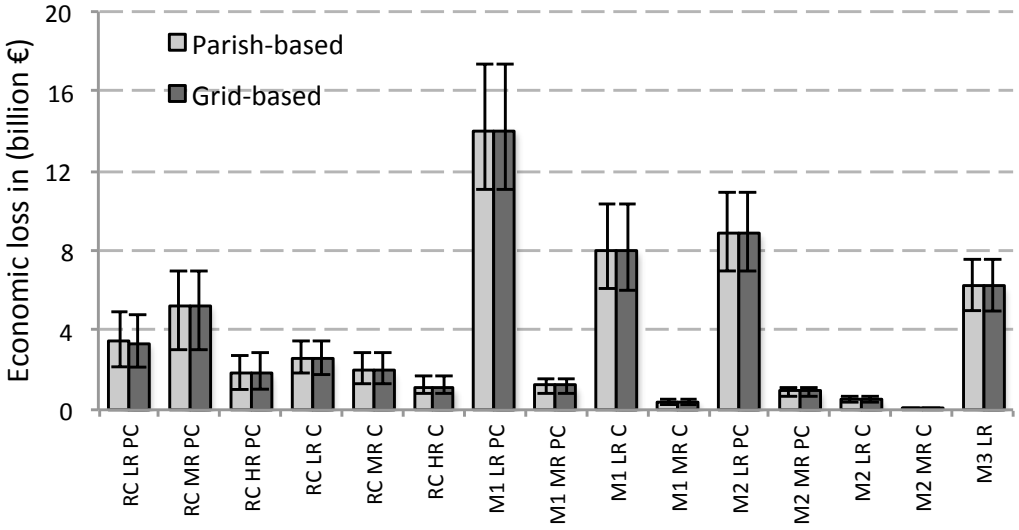

Figure 6.14 - Economic loss per building typology, for a probability of exceedance of 10% in 50 years (return period of 475 years). The error bars indicate the 16th and the 84th percentiles.

The disaggregation of the economic losses according to the building typology indicates that the masonry typologies (M1, M2 and M3) are responsible for more than 70% of the losses, which is a predictable scenario considering the large proportion of this type of construction in Portugal (51%), associated with its high seismic vulnerability (see section 5.3). Although some masonry typologies present reduced losses, which could indicate a low likelihood of damage due to ground

shaking, these low values are actually due to the fact that they represent only a small fraction of the building stock. To evaluate the respective vulnerability (independently of the exposure) the aggregated losses for each building typology have been normalized by the respective total economic value, as illustrated in Figure 6.15.

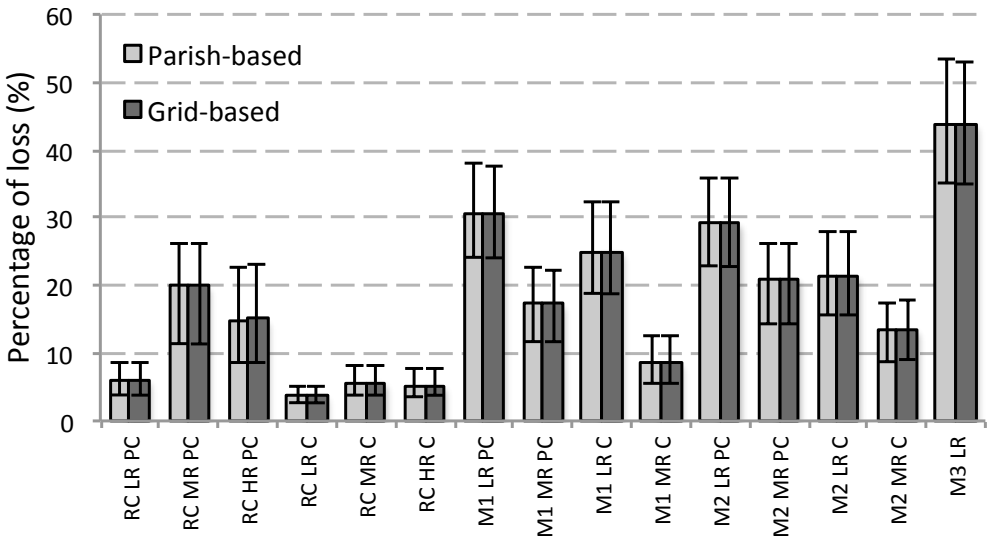

Figure 6.15 – Percentage of economic loss per building typology, for a probability of exceedance of 10% in 50 years (return period of 475 years). The error bars indicate the 16th and the 84th percentiles.

The normalization of the aggregated losses indicates a high percentage of loss for the low-rise masonry typologies and pre-code reinforced concrete buildings. The overall percentage of loss has been estimated as 15.7 % of the whole building stock, which represents about 31.8% of the Portuguese gross domestic product (GDP) of 2011.

In the work of Campos-Costa *et al.* (2009), in which a probabilistic seismic risk assessment was carried out for the Metropolitan Area of Lisbon, an economic loss of approximately 12 billion Euro was estimated for a return period of 475 years. Considering the same region of interest, an economic loss of 22 billion Euro has been calculated in the present study. In order to compare these two values that represent losses from epochs 10 years apart, both aggregated losses were normalized using the GDP [41] of the respective year. A slightly decrease in the aggregated losses is observed, from 12.7% of the 2001 GDP, to 12.3% of the 2011 GDP. Furthermore, in the probabilistic seismic risk assessment carried out by Sousa (2006) for mainland Portugal, an aggregated average annual loss (AAL) of 257 million Euro was computed, whilst in this study, an average AAL of 265 million Euro,

with a standard deviation of 65 million Euro was obtained. When normalized, these parameters become 0.29% and 0.15% of the GDP of the respective years.

6.6. Final remarks

The seismic hazard and risk for mainland Portugal has been thoroughly investigated using up-to-date models, methods and data. The evaluation of the seismic hazard in mainland Portugal revealed some significant differences regarding the hazard map of the design code (RSA) currently in force. Such differences are more pronounced around the Lower Tagus Valley and in the south (Algarve), which are regions responsible for a great portion of the gross domestic product.

In the evaluation of the distribution of V_{s30} values in mainland Portugal, a fair agreement was observed between the two simplified methodologies (geology- and topography-based) in the centre and north, but considerable differences in the southeast part were observed. In order to decrease the uncertainty in this area, field measurements should be performed. It was concluded that most of the territory is comprised of rock or hard soil, but regions with soft soils that are greatly populated also exist. This site effects model is expected to be improved once the results from the projects that are currently experimentally measuring V_{s30} values throughout Portugal will be released.

Data from the 2011 Building Census survey was employed to derive an exposure model capable of providing the spatial distribution of building replacement cost for a set of building typologies, categorized based on type of construction, number of storeys and date of construction. The aggregated replacement cost for the Portuguese building stock has been estimated to be approximately 358 billion euro. It is important to mention that a number of simplifications and assumptions had to be followed in order to estimate the replacement cost for each building typology, such as the number of dwellings per building or the average living area per dwelling. Such parameters probably depend on the date and type of construction, however, until such statistics are available, it was decided that the adoption of a generic set of parameters can still provide an indicative replacement cost. A simple comparison between the exposure models illustrated in Figure 6.7 and the seismic hazard map depicted in Figure 6.11 reveals that an important fraction of the building stock is located in zones with high levels of seismic hazard.

A detailed physical fragility/vulnerability model to characterize all of the Portuguese building stock was not previously available in the literature. A new set of vulnerability functions for the RC building stock based on an analytical methodology was derived in Chapter 4, whilst for the masonry typologies, a simplified approach was adopted based on existing capacity curves (Carvalho *et al*. 2002). A study to investigate the seismic vulnerability of the masonry typologies (which are simultaneously the most common and vulnerable construction in Portugal) considering the Portuguese geometric and material properties and characteristic failure mechanisms should be developed in the future.

The seismic risk map for the probability of exceedance of 10% in 50 years identified the Lower Tagus Valley and the southwest of Portugal as the highest risk-prone regions. The economic losses per building typology indicated that the masonry typologies are the most seismically vulnerable, and therefore the ones for which strengthening/retrofitting should be focused. In the work of Campos-Costa *et al.* (2009), it has been shown that applying selective retrofitting interventions in the Metropolitan Area of Lisbon building stock could reduce the economic risk by an amount of 36% for all return periods. A comparison of the results estimated herein with previous studies considering the 2001 building stock indicates similar levels of seismic risk for the Metropolitan Area of Lisbon, and lower levels of risk at a national level, though such differences are within the estimated bounds of epistemic uncertainty.

Chapter 7

Conclusions and future developments

7.1. Conclusions

The activities developed within this thesis addressed three main areas: 1) development of an open-source tool for seismic hazard and risk assessment; 2) evaluation of existing analytical methods to derive vulnerability functions and development of a novel methodology with this purpose; 3) study of the physical vulnerability of Portuguese RC buildings and evaluation of probabilistic seismic risk in mainland Portugal.

The input models, calculation workflows and main results of the risk calculators that currently compose OpenQuake-engine have been described and through the exemplificative case study applications presented for Turkey, it has been demonstrated that OpenQuake-engine already offers several functionalities and a wide spectrum of output for seismic risk assessment, even recognizing that it is still in a developing phase.

The evaluation of the various methodologies to derive vulnerability functions showed that unlike what is obtained when analysing individual structures, no notable differences were observed in the fragility/vulnerability functions or risk parameters when employing different methodologies. Such findings are of substantial importance for large-scale initiatives that aim to develop

fragility/vulnerability models for a large number of building typologies (e.g. Global Earthquake Model), since post-earthquake damage data may not be available for every region or building type, and consequently, an analytical approach might have to be adopted. Performing dynamic analysis to produce vulnerability functions for all the building types within a given region could soon become computationally unfeasible, but the conclusions of this study suggest that NSPs can be used as a valid alternative for the assessment of the seismic vulnerability.

Recognizing that even the alternative methodologies (NSPs) can demand a significant computational effort and require a considerable calculation time, a simplified approach to assess the seismic vulnerability of building has been developed. This methodology is build upon the displacement-based earthquake loss assessment (DBELA) (Crowley *et al.*, 2004; Bal *et al.*, 2010) and allows the derivation of fragility functions considering a large spectrum of uncertainties. It is recognised that such simplified methodology should only be employed to assess regular buildings, with a low- to high-rise height (less than 10 storeys), since it does not capture some phenomena such as torsion effects or the influence of higher modes of vibration. Nevertheless, regular buildings within such height represent the large majority of typical building portfolios.

Due to its modular and flexible architecture, this method can be applied using a wide variety of intensity measure types and its damage scale can be easily modified. This framework has been developed as an open source effort and can be found in a public code repository at GitHub [3]; the fragility and vulnerability models produced with this tool can be directly used in the open source software, OpenQuake-engine, for seismic hazard and risk assessment.

Regarding the investigation of the seismic vulnerability of the Portuguese reinforced concrete building stock, various geometric and material properties were analysed through the evaluation of hundreds of drawings and technical specifications of real building distributed across the country. These results can be are valuable for the seismic performance of the RC buildings in Portugal, or to employ directly in seismic risk methodologies such as the Displacement-Based Earthquake Loss Assessment. It is important, however, to recognize that such results are based on what was observed in the drawings and technical specifications, which might vary from what was executed in reality.

The RC building stock was organized into six typologies based on the height and design code level. For each typology, a set of fragility functions was derived, using nonlinear time history analysis and two damage state criteria: maximum global drift and maximum inter-storey drift. These fragility models were converted into vulnerability functions, using a consequence model. The latter model was estimated based on various proposals for other countries. This study resulted in a set of vulnerability functions that can be used directly in loss estimation or seismic risk assessment.

An assessment of the seismic hazard and risk in Portugal was carried out, resulting in a hazard and risk map corresponding to a return period of 475 years. The estimated levels of ground motion throughout mainland Portugal were slightly higher than the values for which buildings are currently being designed, mainly in the Lower Tagus Valley region and in the province of Algarve. For what concerns the economic losses in residential buildings, it has been estimated that for the considered return period, a loss of 15.7% of the total building stock value (about 56 billion euro) is expected. These losses are mainly concentrate in the Metropolitan Area of Lisbon and south of Portugal. The disaggregation of the overall loss according to each building typology showed that masonry buildings are responsible for a great portion of the losses (70%).

Summarizing, the research carried out in this thesis contributed to the dissemination of open-source tools, which might support individuals or institutions assessing seismic hazard and risk in a transparent and uniform manner. The results regarding the evaluation of the methodologies to derive vulnerability models demonstrated that satisfactory results can still be achieved when simplified approaches are adopted, such as the methodology developed in this work. Finally, the seismic risk situation for mainland Portugal has been reviewed, highlighting the regions and type of construction where risk mitigation actions should be explored.

7.2. Future developments

Several improvements that could enhance the accuracy and reliability of the methodologies and results produced within this thesis have been identified. These

improvements are described herein, in addition to some initial insight on activities already initiated.

For what concerns the development of the open-source software for seismic hazard and risk assessment (OpenQuake-engine), several functionalities are planned to be implemented, such as the disaggregation of losses, the employment of nonlinear analytical methodologies for the estimation of damage (e.g. Capacity Spectrum Method (Freeman, 2004)) or the consideration of other elements such as networks or infrastructures.

Currently, the probabilistic framework presented in the third chapter can only support 2D analysis, which hampers the appraisal of plan irregularities or torsional effects. Thus, extending this framework to 3D analysis is part of the future activities. Once such platform is available, the seismic vulnerability of the Portuguese building stock will be re-evaluated, considering not only a moment-resisting frame structural system, but also the possible presence of shear walls, elevator shafts and stair wells.

In the investigation of the material and geometric properties of the reinforced concrete buildings in Portugal, it was not possible to obtain drawings from all the districts. Moreover, the probabilistic distribution derived for some of the geometric parameters (e.g. beam depth and width for buildings constructed after the 1983 design code) did not satisfied the Chi-square test. For these reasons, the sample of real RC buildings will be substantially increased, focusing on the regions where few or none buildings have been collected.

With regards to the seismic vulnerability of masonry buildings, a decision was made to employ a simplified methodology to derive a set of vulnerability functions, as the focus of this research work was on reinforced concrete buildings. The collection of drawings and technical specifications for this building typology represents a more challenging exercise, as often such documents are not stored by governmental institutions. The lack of information regarding the geometry and materials complicates the application of analytical methodologies to assess the

physical vulnerability, as was done herein for the reinforced concrete typologies. In order to overcome this issue, a campaign to collect information from drawings and field measurements will be executed, in cooperation with the project "Earthquake loss assessment of the Portuguese building stock", funded by the Foundation for the Technology and Science (FCT). When the necessary information for the structural modelling of this type of buildings will be compiled, analytical methodologies to derive vulnerability functions will be explored.

A novel consequence model capable of relating physical damage with percentage of loss, considering the structural characteristics of the Portuguese building stock and reconstruction practices is also part of the future activities. In this study, a controlled Monte Carlo sampling procedure will be employed to generate hundreds of structures, which will be tested using nonlinear time history analysis. The evolution of the damage in each structural element (e.g. beams, columns, shear walls) will be investigated for a set of increasing intensity measure levels. Thus, a set of percentages of loss will be estimated, using the number of elements that needs to be replaced/repaired at each intensity measure level.

For what concerns the probabilistic seismic risk of mainland Portugal, improvements in the input models are already being done in order to reduce or remove some of their limitations. Some of these improvements include the application of the area and fault source model from the European project SHARE and the employment of the site model (V_{s30} mapping) that will be produced by the SCENE project.

The probabilistic seismic risk estimated in this work is currently being used to calculate integrated risk, considering a set of social vulnerability and resilience indicators. These indicators may include wealth per capita, insurance availability, number of hospital beds per inhabitant, levels of education, amongst others. Such assessment will allow understanding what are the social indicators leading the risk in Portugal and what are the districts where such direct losses could be aggravated or reduced.

Finally, a number of earthquake scenarios are being investigated, considering three events: the historical 1755 Lisbon earthquake, the 1909 Benavente

earthquake and the offshore event of 1969. The exposure and vulnerability models already developed in this work are being employed, and economic and human losses throughout mainland Portugal are being calculated for these events. Such results are fundamental to develop post-disaster emergency plans, raise awareness of risk, or to identify the regions where risk mitigation actions should be concentrated.

REFERENCES

A

Abo El Ezz, A. (2008). "Deformation and strength based assessment of seismic failure mechanisms for existing RC frame buildings". MSc Thesis, ROSE School, Pavia, Italy.

Abrahamson, N. A. (2006). "Seismic hazard: Problems with current practice and future developments". *Proceedings of the 1st European Conference on Earthquake Engineering and Seismology*, Geneva, Switzerland.

Ahmad, N., Crowley, H., Pinho, R. (2010). Analytical fragility functions for reinforced concrete and masonry buildings and building aggregates. UPAV-Internal Report, Pavia, Italy.

Akkar, S., Sucuoglu, H., Yakut, A. (2005). "Displacement-based fragility functions for low- and mid-rise ordinary concrete buildings". *Earthquake Spectra*, 21(4):901-927.

Akkar, S., Bommer, J. (2010). "Empirical equations for the prediction of PGA, PGV and spectral accelerations in Europe, the Mediterranean region and the Middle East". *Seismological Research Letters*, 81(2):195-206.

Akyuz, S., Uyan, M. (1992). "A study on the concrete steel bars used in Turkey". *Technical Journal Turkish Assembly Civil Engineering*, 35:497-508 (in turkish).

Albarello, D., Camassi, R., Rebez, A. (2001). "Detection of space and time heterogeneity in the completeness of a seismic catalogue by a statistical approach: an application to the Italian area". *Bulletin of the Seismological Society of America*, 91:1694-1703.

Allen, T. I., Wald, D. J., Hotovec, A. J., Lin, K., Earle, P. S., Marano, K. D. (2008). An Atlas of ShakeMaps for selected global earthquakes. U.S. Geological Survey Open-File Report 2008-1236.

Allen, T., Wald, D. (2009). "On the Use of High-Resolution Topographic Data as a Proxy for Seismic Site Conditions (Vs30)". *Bulletin of the Seismological Society of America*, 99:935-943.

Almunia, J. A. S. (1993). Evaluación del comportamiento funcional y de la seguridad estructural de puentes existentes de hormigón armado y pretensado. PhD Thesis, Universitat Politècnica de Catalunya, Barcelona, Spain (in Spanish).

Ambraseys, N., Simpson, K., Bommer, J. (1996). "Prediction of horizontal response spectra in Europe", *Earthquake Engineering and Structural Dynamics*, 25:371-400.

Antoniou, S., Pinho, R. (2004a). "Development and verification of a displacement-based adaptive pushover procedure". *Journal of Earthquake Engineering*, 8(5):643-661.

Antoniou, S., Pinho, R. (2004b). "Development and verification of a displacement-based adaptive pushover procedure". *Journal of Earthquake Engineering*, 8(5):643-661.

ATC-40 (1996). Seismic Evaluation and Retrofit of Concrete Buildings, Volumes 1 and 2, Report No. ATC-40, Applied Technology Council, Redwood City,

California, USA.

Atkinson, G., (2008). "Ground-motion prediction equations for eastern North America from a referenced empirical approach: Implications for epistemic uncertainty". *Bulletin of the Seismological Society of America*, 98(3):1304-1318.

Atkinson, G., Boore, D. (1997). "Some comparisons between recent ground motion relations". *Seismological Research Letters,* 68:24-40.

Atkinson, G., Boore, D. (2006). "Earthquake ground-motion prediction equations for eastern North America". *Bulletin of the Seismological Society of America*, 96(6):2181-2205.

Azevedo, J., Guerreiro, L., Bento, R., Lopes, M. e Proença, J. (2009). "Seismic vulnerability of lifelines in the greater Lisbon area". *Bulletin Earthquake Engineering*, 8, 157-180

B

Bakıra, P. G., Boduroglu, H. M. (2002) "Earthquake Risk and Hazard Mitigation in Turkey". *Earthquake Spectra* 28(3):427-447.

Baez, J. I., Miranda, E., (2000). "Amplification factors to estimate inelastic displacement de- mands for the design of structures in the near field". *Proceedings of the 12th World Conference on Earthquake Engineering,* Auckland, New Zealand.

Bal, I., Yildiz, M., (2005). "Evaluation of concrete quality of existing buildings in the regional municipalities of Istanbul". *Journal of the Turkish Chamber Civil Engineering*, 80:10-7.

Bal, I., Crowley, H., Pinho, R. (2005). Displacement-based earthquake loss assessment: Method development and application to Turkish building stock. IUSS Press: Pavia, Italy.

Bal, I., Crowley, H., Pinho, R. (2008a) "Displacement-based earthquake loss assessment for an earthquake scenario in Istanbul", Journal of Earthquake Engineering, 12: S2, 12-22.

Bal, I., Crowley, H., Pinho, R., Gulay, F. (2008b). "Detailed assessment of structural characteristics of Turkish RC building stock for loss assessment models", *Soil Dynamics and Earthquake Engineering*, 28:914-932.

Bal, I., Crowley, H., Pinho, R. (2010). Displacement-based earthquake loss assessment: Method development and application to Turkish building stock, ROSE Research Report 2010/02, IUSS Press, Pavia, Italy.

Barata, M. (2005). "The Lisbon earthquake of 1st November 1755 - a historical perspectives approach". *Proceedings of the international conference 250th anniversary of the 1755 Lisbon earthquake*, Lisbon, Portugal.

Bogaziçi (2002). Earthquake Risk Assessment for Istanbul Metropolitan Area. Final Report, Kandilli Observatory and Earthquake Research Center, Istanbul, Turkey.

Bommer, J. J. (2002). Basics of Seismology and Seismic Hazard Assessment. Course Notes at European School for Advanced Studies in Reduction of Seismic Risk (ROSE School), Pavia, Italy.

Bommer, J. J., Martínez-Pereira, A. (1999) "The effective duration of earthquake strong motion". *Journal of Earthquake Engineering*, 3(2):127-172.

Bommer, J. J., Spence, R., Erdik, M., Tabuchi, S., Aydinoglu, N., Booth, E., Re, D. D., Pterken, D. (2002). "Development of an Earthquake Loss Model for Turkish Catastrophe Insurance". *Journal of Seismology*, 6:431-446.

Bommer, J. J., Abrahamson, N. A. (2006). "Why do Modern Probabilistic Seismic Hazard Analyses Often Lead to Increased Hazard Estimates?". *Bulletin of the Seismological Society of America*, 96:1967-1977.

Bommer, J. J., Scherbaum, F. (2008). "The use and misuse of logic-trees in Probabilistic Seismic Hazard Analysis", *Earthquake Spectra*, 24(4), 997-1009.

Boore, D., Atkinson, G. (2008). "Ground-motion prediction equations for the average horizontal component of PGA, PGV, and 5%-damped PSA at spectral periods between 0.01s and 10.0s". *Earthquake Spectra*, 24(1):99-138.

Borzi, B., Pinho, R., Crowley, H. (2008). "Simplified pushover-based vulnerability analysis for large-scale assessment of RC buildings". *Engineering Structures*, 30:804-820.

Bracci, J. M, Kunnath, S. K, Reinhorn, A. M. (1997). "Seismic Performance and Retrofit Evaluation of Reinforced Concrete Structures". *Journal of Structural Engineering*; 123(1):3–10.

Bradley, B. A. (2010). "Epistemic uncertainties in component fragility functions". *Earthquake Spectra*, 26(1):41-62.

BU-ARC (2002). Earthquake Risk Assessment for Istanbul Metropolitan Area. Project Report, Boğaziçi University and American Red Cross, Boğaziçi University Publications, Istanbul, Turkey.

BSSC (2004). NEHRP Recommended provisions for seismic regulations for new buildings and other structures, 2003 edition (FEMA 450), Building Seismic Safety Council, National Institute of Building Sciences, Washington, D.C., USA.

C

Calvi, G. M. (1999). "A displacement-based approach for the vulnerability evaluation of classes of buildings". *Journal of Earthquake Engineering*, 26:1091-1112.

Calvi, G.M., Pinho, R. (2004). LESSLOSS - A European integrated project on risk mitigation for earthquakes and landslides. IUSS Press, Pavia, Italy.

Calvi, M., Pinho, R., Magenes, G., Bommer, J., Restrepo-Vélez, L., Crowley, H. (2006). "Development of Seismic Vulnerability Assessment Methodologies over the past 30 years", *ISET Journal of Earthquake Technology*, 43(3):75-104.

Campbell, K. (2003). "Prediction of strong ground motion using the hybrid empirical method and its use in the development of ground-motion (attenuation) relations in eastern North America", *Bulletin of the Seismological Society of America*, 93:1012-1033.

Campbell, K., Bozorgnia, Y. (2008). "NGA ground motion model for the geometric mean horizontal component of PGA, PGV, PGD and 5% damped linear elastic response spectra for periods ranging from 0.01 to 10s". *Earthquake Spectra,* 24(1):139-171.

Campos-Costa, A., Sousa, M. L., Carvalho, A., Coelho, E. (2009). "Evaluation of seismic risk and mitigation strategies for the existing building stock: application of LNECloss to the metropolitan area of Lisbon". *Bulletin of Earthquake*

Engineering, 8:119-134.

Carrilho, F., Oliveira, C. (1997). "Preliminary analysis of the first digital recordings obtained in the Portuguese seismographic network - Attenuation studies". *Natural Hazards*, 14:241-261.

Carvalho, A. (2008). Modelação estocástica da acção sísmica em Portugal continental. PhD thesis, Instituto Superior Técnico, Lisbon, Portugal (in Portuguese).

Carvalho, E.C., Coelho, E., (2001). Seismic assessment, strengthening and repair of structures, ECOEST2-ICONS report no. 2, European Commission - Training and Mobility of Researchers Programme.

Carvalho, E. C., Coelho, E., Campos-Costa, A., Sousa, M. L., Candeias, P. (2002). "Vulnerability evaluation of residential buildings in Portugal". *Proceedings of the 12th European Conference on Earthquake Engineering,* London, United Kingdom.

Carvalho, J., Dias, R., Pinto, C., Leote, J., Mendes-Victor, L. (2008). "A Soil Classification for Seismic Hazard Assessment and Mitigation of the Algarve". *Proceedings of the 14th World Conference on Earthquake Engineering*, Beijing, China.

Carvalho, J., Torres, L., Castro, R., Dias, R., Mendes-Victor, L. (2009). "Seismic Velocities and Geotechnical data Applied to the Soil Microzoning of Western Algarve, Portugal". *Journal of Applied Geophysics*, 68, 249-258.

Casado, C., Palacios, S., Delgado, J., Peláez, J. (2000). "Attenuation of intensity with epicentral distance in the Iberian Peninsula". *Bulletin of the Seismological Society of America*, 90:34-47.

Casarotti, C., Pinho, R. (2007). "An adaptive capacity spectrum method for assessment of bridges subjected to earthquake action". *Bulletin of Earthquake Engineering*; **5**(3):377–390.

Casarotti, C., Monteiro, R., Pinho, R. (2009). "Verification of spectral reduction factors for seismic assessment of bridges". *Bulletin of the New Zealand Society for Earthquake Engineering*, 42(2):111-121.

Cauzzi, C., Faccioli, E. (2008). "Broadband (0.05 to 20 s) prediction of displacement response spectra based on worldwide digital records". *Journal of Seismology*, 12(4):453-475.

CEN (2004). Eurocode 2: Design of concrete structures. European Committee for Standardization, Brussels, Belgium.

CEN (2005). Eurocode 8: Design of Structures for Earthquake Resistance - Part 1: General rules, seismic actions and rules for buildings. European Committee for Standardization, Brussels, Belgium.

Chester, K. (2001). "The 1755 Lisbon earthquake". *Progress in Physical Geography*, 25(3):363-383.

Chiou, B., Youngs, R. (2008). "An NGA model for the average horizontal component of peak ground motion and response spectra". *Earthquake Spectra*, 24(1):173-215.

Choffat, P., (1912). "Le tremblement de terre du 23 Avril 1909 dans le Ribatejo". *Revista de Obras Públicas e Minas*, Tomo XLIII, Imprensa Nacional, Lisboa, Portugal (in French).

Choi, Y., Stewart, J., (2005). "Nonlinear site amplification as function of 30 m shear wave velocity". *Earthquake Spectra*, 21(1):1-30.

Chopra, A. K., Goel, R. K., (2000). "Evaluation of NSP to estimate seismic deformation: SDF systems". Journal of Structural Engineering, 126(4):482-490.

Chopra, A. K., Goel, R. K. (2002). "A modal pushover analysis procedure for estimating seismic demands for buildings". *Earthquake Engineering & Structural Dynamics*; 31(3):561–582.

Colombi, M., Borzi, B., Crowley, H., Onida, M., Meroni, F., Pinho, R. (2008). "Deriving vulnerability curves using Italian earthquake damage data". *Bulletin of Earthquake Engineering,* 6(3):485-504.

Cornell, C. A. (1968). "Engineering seismic risk analysis". *Bulletin of the Seismological Society of America*, 58:1583-1606.

Costa, A., Arêde, A., Costa, A., Oliveira, C. (2011). "Out-of-plane behaviour of existing stone masonry buildings: experimental evaluation". *Bulletin of Earthquake Engineering,* 10(1):93-111.

Cotton, F., Scherbaum, F., Bommer, J., Bungum, H. (2006). "Criteria for selecting and adjusting ground-motion models for specific target regions: Application to central Europe and rock sites". *Journal of Seismology*, 10(2):137-156.

Crowley, H., Pinho, R. (2004). "Period-height relationship for existing European reinforced concrete buildings". *Journal of Earthquake Engineering*, 8(1):893-119.

Crowley, H., Pinho, R., Bommer, J. J. (2004). "A probabilistic displacement-based vulnerability assessment procedure for earthquake loss estimation". *Bulletin of Earthquake Engineering*, 2:173-219.

Crowley, H., Bommer, J. J. (2006). "Modelling Seismic Hazard in Earthquake Loss Assessment with Spatially Distributed Exposure". *Bulletin of Earthquake Engineering*, 4(3):249-273.

Crowley, H., Bommer J. J., Pinho, R., Bird, J. (2005). "The impact of epistemic uncertainty on an earthquake loss model". *Earthquake Engineering and Structural Dynamics*, 34:1653-1685.

Crowley, H., Pinho, R., Bommer, J.J., Bird, J.F. (2006). Development of a Displacement-Based Method for Earthquake Loss Assessment. IUSS Press, Pavia, Italy.

Crowley, H., Colombi, M., Crempien, J., Erduran, E., Lopez, M., Liu, H., Mayfield, M., Milanesi, M. (2010). GEM1 Seismic Risk Report: Part 1, GEM Technical Report 2010-5. GEM Foundation, Pavia, Italy.

Crowley, H., Bommer J.J., Stafford, P.J. (2008) "Recent developments in the treatment of ground-motion variability in earthquake loss models". *Journal of Earthquake Engineering*, 12 (1), 71-80.

Crowley, H., Borzi, B., Pinho, R., Colombi, M., Onida, M. (2008). "Comparison of two mechanics-based methods for simplified structural analysis in vulnerability assessment". *Advances in Civil Engineering*, 2008:19.

Crowley, H., Miriam, C., Borzi, B., Faravelli, M., Onida, M., Lopez, M., Polli, D., Meroni, F. (2009). "A comparison of seismic risk maps for Italy". *Bulletin of Earthquake Engineering,* 7(1):149-180.

Crowley, H., Pinho, R. (2006). "Simplified equations for estimating the period of

vibration of existing buildings". *Proceedings of the 1st European Conference on Earthquake Engineering and Seismology*, Geneva, Switzerland.

Cummins, J. D., Mahul, O. (2009). Catastrophe Risk Financing in Developing Countries: Principles for Public Intervention. The World Bank, Washington D.C., USA.

D

Danciu, L., Monelli, D., Pagani, M., Wiemer, S. (2010). GEM1 Hazard: Review of PSHA software, GEM Technical Report 2010-2, GEM Foundation, Pavia, Italy.

Daniell, J. E., Wenzel, F., Khazai, B. (2010). "The Cost of Historic Earthquakes Today – Economic Analysis since 1900 through the use of CATDAT". *Proceedings of the Australian Earthquake Engineering Society Conference*, Perth, Australia.

Dawe, J. L, Seah, C. K. (1988). "Lateral load resistance of masonry panels in flexible steel frames". *Proceedings of the 8th International brick and block masonry conference*, Dublin, Ireland.

Delavaud, E., Cotton, F., Akkar, S., Scherbaum, F., Danciu, L., Beauval, C., Drouet, S., Douglas, J., Basili, R., Sandikkaya, M. A., Segou, M., Faccioli, E., Theodoulidis, N. (2012). "Toward a ground-motion logic tree for probabilistic seismic hazard assessment in Europe". *Journal of Seismology*, 16(3):451-473.

Demircioglu, M. B., Sesetyan, K., Durukal, E., Erdik, M. (2007). "Assessment of Earthquake Hazard in Turkey". *Proceedings of the 4th International Conference on Earthquake Geotechnical Engineering*, Thessaloniki, Greece.

Di Pasquale, G., Goretti, A. (2001). "Vulnerabilità funzionale ed economica degli edifici residenziali colpiti dai recenti eventi sismici italiani". *Proceedings of the 10th national conference "L'ingegneria Sismica in Italia"*, Potenza-Matera, Italy.

Directive n°291 (2011). Preços da habitação por metro quadrado de área útil. Decreto-Lei n° 329-A/2000. Lisbon, Portugal (in Portuguese).

Dobson, J., Bright, E., Coleman, P., Durfee, R., Worley, B. (2000). "LandScan: a global population database for estimating populations at risk". *Photogrammetric Engineering and Remote Sensing*, 66:849-857.

Dolšek, M., Fajfar, P. (2005). "Simplified non-linear seismic analysis of infilled reinforced concrete frames". *Earthquake Engineering & Structural Dynamics*; 34(1):49–66.

Dolšek, M., Fajfar, P. (2008). "The effect of masonry infills on the seismic response of a four storey reinforced concrete frame - a deterministic assessment". *Engineering Structures*, 30(7):1991-2001.

Douglas, J., Bungum, H., Scherbaum, F. (2006). "Ground-motion prediction equations for southern Spain and southern Norway obtained using the composite model perspective". *Journal of Earthquake Engineering*, 10(1):33-72.

Dumova-Jovanoska, E. (2004). "Fragility Curves for RC Structures in Skopje Region". *Proceedings of the 13th World Conference on Earthquake Engineering*, Vancouver, Canada.

E

Elnashai, A. S. (2001). "Advanced inelastic static (pushover) analysis for earthquake

applications". *Structural Engineering & Mechanics*, 12(1): 51–69.

Enomoto, T., Schmitz, M., Abeki, N., Masaki, K., Navarro, M., Rocavado, V., Sanchez, A. (2000). "Seismic risk assessment using soil dynamics in Caracas, Venezuela". *Proceedings of the 12th World Conference in Earthquake Engineering*, Auckland, New Zealand.

Erberik, M. A. (2008) "Fragility-based assessment of typical mid-rise and low-rise RC buildings in Turkey" *Engineering Structures* 30(5), 1360-1374.

Erdik, M. (2007). Discussion of: ''Istanbul at the threshold: an evaluation of the seismic risk in Istanbul,'' by Pyper Griffiths, J.H., Irfanoglu, A, Pujol, S., *Earthquake Spectra*, 23(1):63–75.

Erdik, M., Aydinoglu, N., Fahjan, Y., Sesetyan, K., Demircioglu, M., Siyahi, B., Durukal, E., Ozbey, C., Biro, Y., Akman, H., Yuzugullu O. (2003). "Earthquake Risk Assessment for Istanbul Metropolitan Area", *Earthquake Engineering and Engineering Vibration*, 2(1).

Espinoza, F. (1999). Determinación de las características dinámicas de estructuras. PhD Thesis, Universidad Politécnica de Catalunya, Barcelona, Spain (in spanish).

F

Fajfar, P. (1999). "Capacity spectrum method based on inelastic demand spectra". *Earthquake Engineering and Structural Dynamics*, 28(9):979-993.

Farinha, J. S. B. (1955). "Acção dos sismos sobre as construções. Simpósio sobre a acção dos sismos e a sua consideração no cálculo das construções". *Boletim da Ordem dos Engenheiros*, no 22. Lisbon, Portugal (in Portuguese).

Farr, G., Kobrick, M. (2000). "Shuttle Radar Topography Mission produces a wealth of data". *EOS* 81, 583–585.

FEMA-273 (1997). NEHRP Guidelines for the Seismic Rehabilitation of Buildings. Report No. FEMA 273. Federal Emergency Management Agency, Washington D.C., USA.

FEMA-440 (2005). Impovement of Nonlinear Static Seismic Analysis Procedures. Federal Emergency Management Agency, Washington D.C., USA.

FEMA-443 (2003). HAZUS-MH Technical Manual. Federal Emergency Management Agency, Washington D.C., USA.

FEMA and NIBS, (1999). Earthquake loss estimation methodology – HAZUS 99. Federal Emergency Management Agency and National Institute of Buildings Sciences, Washington D. C., USA.

Fernandes, C., Melo, J., Varum, H., Costa, A. (2011) "Comparative analysis of the cyclic behavior of beam-column joints with plain and deformed reinforcing bars", *IBRACON Structures and Materials Journal*, 4(1):147-172.

Ferreira, T., Vicente, R., Varum, H., Costa, A., Mendes da Silva, J.A.R. (2012) "Seismic vulnerability assessment of the old city centre of Seixal, Portugal". *Proceedings of the 15th WCEE, World Conference on Earthquake Engineering*, Lisbon, Portugal.

Field, E, Jordan, T., Cornell, C. (2003). "OpenSHA: A Developing Community-Modelling Environment for Seismic Hazard Analysis". *Seismological Research Letters*, 74:406-419.

França, J. A., (1989). Lisboa: urbanismo e arquitectura. Instituto de Cultura e Língua

Portuguesa, Lisbon, Portugal (in Portuguese).

Freeman, S., Nicoletti, J., Tyrell, J. (1975). "Evaluation of Existing Buildings for seismic risk - A case study of Puget Sound Naval Shipyard, Bremerton, Washington". *Proceedings of the 1st U.S. National Conference on Earthquake Engineering*, Berkley, USA.

Freeman, S., (2004). "Review of the development of the capacity spectrum method". *ISET Journal of Earthquake Technology*, 41:1-13.

G

Gamba, P., Cavalca, D. Jaiswal, K., Huyck, C., Crowley, H. (2014). "The GED4GEM Project: Development of a Global Exposure Database for the Global Earthquake Model Initiative". *Proceedings of the 15th WCEE, World Conference on Earthquake Engineering*, Lisbon, Portugal.

GEM (2011a). OpenQuake Manual. Available from URL: http::://openquake.org.

GEM (2011b). OpenQuake Book. Available from URL: http::://openquake.org.

Giardini, D. (1999) "The Global Seismic Hazard Assessment Program (GSHAP) 1992-1999". Summary Volume. *Annali di Geofisica*, 42(6):957-1230.

Giuffrè, A., Pinto, P.E. (1970). "Il comportamento del cemento armato per sollecitazioni cicliché di forte intensità", Giornale del Génio Civile (in Italian).

Glaister, S., Pinho, R. (2003). "Development of a simplified deformation based method for seismic vulnerability assessment". *Journal of Earthquake Engineering*, 7:107-140.

GNDT-SSN (1994). "Scheda di esposizione e vulnerabilità e di rilevamento danni di primo livello e secondo livello (muratura e cemento armato)". Gruppo Nazionale per la Difesa dai Terremoti, Roma, Italy (in Italian).

Griffiths, J. P., Irfanoglu, A., Pujol, S. (2007). "Istanbul at the Threshold: An Evaluation of the Seismic Risk in Istanbul". *Earthquake Spectra,* 23(1):63-75.

Grunthal, G. (1998). European Macroseismic Scale. Chaiers du Centre Européen de Géodynamique et de Séismologie, vol. 15 Luxembourg.

Gulkan, P., Sozen, M. A. (1974) "Inelastic Responses of Reinforced Concrete Structure to Earthquake Motions". *ACI Journal Proceedings*, 71(12):604-610.

H

Hancilar, U., Durukal, E., Franco, G., Deodatis, G., Erdik, M., Smyth., A. (2006). "Probabilistic Vulnerability Analysis: An Application to A Typical School Building in Istanbul". *Proceedings of the 1st European Conference on Earthquake Engineering and Seismology*, Geneva, Switzerland.

Hashemi, A., Mosalam, K. (2007). Seismic Evaluation of Reinforced Concrete Buildings Including Effects of Masonry Infill Walls. PEER Report 2007/100, Pacific Earthquake Engineering Research Center, University of California, Berkeley, USA.

J

Jaiswal, K., Wald, D., Porter, K. (2010). "A global building inventory for earthquake

loss estimation and risk management". *Earthquake Spectra*, 26:731-748.

Jayaram, N. (2010). Probabilistic Seismic Lifeline Risk Assessment using Efficient Sampling and Data Reduction Techniques. PhD Thesis, Stanford University, California, USA.

Jayaram, N., Baker, J. W. (2009). "Correlation model for spatially distributed ground motion intensities". *Earthquake Engineering and Structural Dynamics,* 38(15):1687-1708.

Jayaram, N., Baker, J. W. (2010). "Efficient sampling and data reduction techniques for probabilistic seismic lifeline risk assessment". *Earthquake Engineering & Structural Dynamics*, 39(10):1109-1131.

Jayaram, N., Lin, T., Baker, J. (2011). "A Computationally Efficient Ground-Motion Selection Algorithm for Matching a Target Response Spectrum Mean and Variance". *Earthquake Spectra*; 27(3):797-815.

JICA (2002). The Study on a Disaster Prevention/Mitigation Basic Plan in Istanbul Including Seismic Microzonation in the Republic of Turkey. Final Report, Japanese International Cooperation Agency, Japan.

Jimenez, M., Garcia, M., GSHAP Ibero-Maghreb Working Group (1999). "Seismic hazard assessment in the Ibero-Maghreb region", *Annals of Geophysics*, 42:1057-1066.

Jimenez, M., Giardini, D., Grunthal, G., SESAME Working Group (2001). "Unified seismic hazard modelling throughout the Mediterranean region", *Bolletino di Geofisica*, 42:3-18.

JCSS (2001). Probabilistic Model Code - Working document. Joint Committee for Structural Safety. Available from URL: www.jcss.ethz.ch/.

K

Kalkan, E., Kunnath, S. K. (2006). "Adaptive Modal Combination Procedure for Nonlinear Static Analysis of Building Structures". *Journal of Structural Engineering*, 132(11):1721-1731.

Kalkan, E., Gülkan, P., Yilmaz, N., Celebi, M. (2008). Probabilistic Seismic Hazard Mapping of the Marmara Region. Report No. 08-01, Earthquake Engineering Research Center.

Kappos, A. J., Chryssanthopoulos, M. K., Dymiotis, C. (1999). "Uncertainty analysis of strength and ductility of confined reinforced concrete members". *Engineering Structures*, 21:195-208.

Kappos, A., Panagopoulos, G., Panagiotopoulos, C., Penelis, G. (2006). "A hybrid method for the vulnerability assessment of R/C and URM buildings". *Bulletin of Earthquake Engineering*, 4(4):391-413.

Katsanos, E. I, Sextos, A. G., Manolis, G. D. (2010). "Selection of earthquake ground motion records: A state-of-the-art review from a structural engineering perspective". *Soil Dynamics and Earthquake Engineering*, 26:157-169.

Kirçil, M., Polat, Z. (2006). "Fragility analysis of mid-rise R/C frame buildings". *Engineering Structures*, 28(9):1335-1345.

Kobayashi, H., Vidal, F., Feriche, D., Samano, T., Alguacil, G. (1996) "Evaluation of dynamic behaviour of building structures with microtremors for seismic

microzonation mapping". *Proceedings of the 11th World Conference in Earthquake Engineering*, Acapulco, México.

Kramer, S. (1996). Geotechnical Earthquake Engineering. New Jersey, Prentice Hall.

Krawinkler, H., Seneviratna, G. (1998). "Pros and cons of a pushover analysis of seismic performance evaluation". *Engineering Structures*, 20(4-6):452–464.

L

Lagomarsino S., Giovinazzi, S. (2006). "Macroseismic and Mechanical Models for the Vulnerability Assessment of Current Buildings". *Bulletin of Earthquake Engineering, Special Issue "Risk-Ue Project",* 4(4).

Lang, K. (2002). Seismic Vulnerability of Existing Buildings. PhD Thesis, Swiss Federal Institute for Technology, Zurich, Switzerland.

LESSLOSS (2005). Report on Building Stock Data and Vulnerability Data for each Case Study. Deliverable Report D84 available from URL http://www.lessloss.org/.

Lin, Y. Y., Chang, K. C., Wang, Y. L. (2004). "Comparison of displacement coefficient method and capacity spectrum method with experimental results of RC columns". *Earthquake Engineering & Structural Dynamics*, 33:35-48.

Lopes, L. (2012). "Dificuldades práticas na avaliação da segurança sísmica de estruturas existentes". MSc Thesis, University of Aveiro, Aveiro, Portugal (in Portuguese).

M

Martinez, W. L., Martinez, A. R. (2002). Computational statistics handbook with Matlab. Chapman & Hall/CRC, New York, USA.

McGuire, R. R. (2004). Seismic hazard and risk analysis. Earthquake Engineering Research Institute Publication No. MNO-10, Second monograph series.

Melo, J., Varum, H., Rossetto, T., Costa, A. (2012). "Experimental response of RC columns built with plain bars under unidirectional cyclic loading". *Proceedings of the 15th World Conference on Earthquake Engineering*, Lisbon, Portugal.

Mirza, S. A., MacGregor, J. G. (1979). "Variability of mechanical properties of reinforcing bars". *Journal of the Structural Division ASCE*, 105, Vol ST5:921-937.

Monteiro, R. (2011). Probabilistic Seismic Assessment of Bridges. PhD Thesis, University of Porto, Porto, Portugal.

Moreira, V. (1989). Seismicity of the Portuguese continental margin, in Earthquakes at North-Atlantic Passive Margins: Neotectonics and Postglacial Rebound. Kluwer Academic Publishers, 533-545.

Mouroux, P., Brun, B. T. L. (2006). "Presentation of RISK-UE Project". *Bulletin of Earthquake Engineering*, 4:323-339.

MunichRe (2012). Topics Geo: Natural catastrophes 2011 Analyses, assessments, positions. 2012 Issue, Munich, Germany.

N

Narciso, J., Vilanova, S., Lopes, I., Oliveira, C., Carvalho, J., Pinto, C., Borges, J., Nemser, E. (2012). "Developing a Site-Conditions Map for Seismic Hazard Assessment in

Portugal". *Proceedings of the 15th World Conference on Earthquake Engineering*, Lisbon, Portugal.

Navarro, M., Oliveira, C. S. (2004). "Evaluation of dynamic characteristics of reinforced concrete buildings in the City of Lisbon". *Proceedings of the 4th Assembly of the Portuguese-Spanish of Geodesy and Geophysics*, Figueira da Foz, Portugal.

Neves, F., Costa, A., Vicente, R., Oliveira, C., Varum, H. (2011). "Seismic vulnerability assessment and characterisation of the buildings on Faial Island, Azores". *Bulletin of Earthquake Engineering,* 10(1):27-44.

Newmark, N. M. (1959). "A method of computation for structural dynamics". *Journal of the Engineering Mechanics Division*, ASCE, 85(3):67-94.

NZSEE (2005). Assessment and improvement of the structural performance of buildings in earthquakes, Study Group Draft. New Zealand Society for Earthquake Engineering.

O

Oliveira, C. S. (1986). A simicidade histórica e a revisão do catálogo sísmico. Laboratório Nacional de Engenharia Civil, Proc. 36/11/7368, Lisbon, Portugal (in Portuguese).

Oliveira, C. S. (1988). Distribuição dos danos ocorridos em Lisboa aquando dos principais sismos históricos. Protecção Civil, Vol. 1, no 4, Serviço Nacional de Protecção Civil, Lisbon, Portugal (in Portuguese).

Oliveira, C. S., Sousa, M. L., Campos Costa, A. (1999). "Contribuição para a revisão da acção sísmica em Portugal continental no contexto do eurocódigo 8". *Proceedings of the 4th National Conference on Earthquake Engineering*, Faro, Portugal (in Portuguese).

Oliveira, C. S., Navarro, M. L. (2010). "Fundamental periods of vibration of RC buildings in Portugal from in-situ experimental and numerical techniques". *Bulletin of Earthquake Engineering*, 8:609-642.

Özcebe, S. (2011). Identification of Initial Damage States in Displacement-Based Assessment of Existing RC Buildings. MSc Thesis, ROSE School, Pavia, Italy.

Ozmen, H., B., Inel, M., Meral, E., Bucakli, M. (2010). "Vulnerability of Low and Mid-Rise Reinforced Concrete Buildings in Turkey". *Proceedings of the 14th European Conference of Earthquake Engineering*, Ohrid, Macedonia.

P

Pagani M., Danciu, L., Monelli, D., Wössner, J., Wiemer, S., Field, E. H. (2010a). "Toward a unified PSHA input data model and code: a proposal based on the GEM1 experience". *Proceedings of the 14th European Conference of Earthquake Engineering*, Ohrid, Macedonia.

Pagani, M., Monelli, D., Crowley, H., Danciu, L., Field, E. H., Wiemer, S., Giardini, D. (2010b). GEM1 Hazard: Description of input models, calculation engine and main results. GEM Technical Report 2010-3. GEM Foundation, Pavia, Italy.

Papaila, A. (2011). Seismic fragility curves for reinforced concrete buildings. MSc

Thesis, University of Patras, Patras, Greece.

Papanikolaou, V., Elnashai, A. (2005). Evaluation of Conventional and Adaptive Pushover Analysis I: Methodology. *Journal of Earthquake Engineering*, 9(6):923-941.

Park, J., Bazzurro, P., Baker, J. (2007). "Modelling spatial correlation of ground motion intensity measures for regional seismic hazard and portfolio loss estimation". *Proceedings of the 10th International Conference on Application of Statistic and Probability in Civil Engineering* (ICASP10), Tokyo, Japan.

Paulay, T., Priestley, M. J. N. (1992). Seismic Design of Reinforced Concrete and Masonry Buildings. John Wiley and Sons, Inc., New York, USA.

Pelaez, M. J. A., Casado, C., Romero, J. H. (2002). "Deaggregation in magnitude, distance, and azimuth in the south and west of the Iberian Peninsula", *Bulletin of Seismological Society of America*, 92:2177-2185.

Pelaez, M. J. A., Casado, C. (2002). "Seismic hazard estimate at the Iberian Peninsula". *Pure Applied Geophysics*, 159:2699-2713.

Petersen, Mark D., Frankel, Arthur D., Harmsen, Stephen C., Mueller, Charles S., Haller, Kathleen M.,Wheeler, Russell L., Wesson, Robert L., Zeng, Yuehua, Boyd, Oliver S., Perkins, David M., Luco, Nicolas, Field, Edward H., Wills, Chris J., and Rukstales, Kenneth S., 2008, Documentation for the 2008 Update of the United States National Seismic Hazard Maps: U.S. Geological Survey Open-File Report 2008–1128.

Pezeshk, S., Zandieh, A., Tavakoli, B. (2011). "Hybrid Empirical Ground-Motion Prediction Equations for Eastern North America Using NGA Models and Updated Seismological Parameters". *Bulletin of the Seismological Society of America*, 101(4):1859-1870.

Pinho, R. (2012) "GEM: a participatory framework for open, state-of-the-art models and tools for earthquake risk assessment worldwide". *Proceedings of the 15th World Conference on Earthquake Engineering*, Lisbon, Portugal.

Pinho, R., Bommer, J. J., Glaister, S. (2002). "A simplified approach to displacement-based earthquake loss estimation analysis". *Proceedings of the 12th European Conference on Earthquake Engineering*, London, England.

Pipa, M., (1993). Ductilidade de Elementos de Betão Armado Sujeitos a Acções Cíclicas - Influência das Características Mecânicas das Armaduras. PhD Thesis, IST/LNEC, Lisbon, Portugal (in Portuguese).

PRB (2010). World population data sheet. Population Reference Bureau, Washington D.C., USA.

Priestley M. J. N. (1998). "Displacement-based approaches to rational limit states design of new structures". *Proceedings of the 11th European Conference on Earthquake Engineering*, Rotterdam, The Netherlands.

Priestley, M. J. N., Calvi, G. M., Kowalsky, M. J. (2007). Displacement-based Seismic Design of Structures. IUSS Press, Pavia, Italy

R

Ramirez, C., M., Miranda, E. (2012). "Significance of residual drifts in building earthquake loss estimation". *Earthquake Engineering & Structural Dynamics*,

41:1477-1493.
RBA (1935). Regulamento para o Emprego de Betão Armado, Decreto-Lei nº 4036, Lisbon, Portugal (in Portuguese).
REBA (1967). Regulamento de Estruturas de Betão Armado, Decreto-Lei nº 47723, Lisbon, Portugal (in Portuguese).
Rezaeian, S., Bozorgnia, Y., Idriss, I. M., Campbell, K., Abrahamson, N., Silva, W. (2012). Spectral Damping Scaling Factors for Shallow Crustal Earthquakes in Active Tectonic Regions. PEER Report no 2012/01, Pacific Earthquake Engineering Research Center, California, USA.
RGEU (1951). Regulamento Geral das Edificações Urbanas, Decreto-Lei nº 38382, Lisbon, Portugal (in Portuguese).
Rodrigues, H., Varum, H., Costa, A. (2010). "Simplified macro-model for infill masonry panels". *Journal of Earthquake Engineering*, 14:390-416.
Rodrigues, H., Arêde, A., Varum, H., Costa, A. G. (2012). "Experimental evaluation of rectangular reinforced concrete column behaviour under biaxial cyclic loading". *Earthquake Engineering and Structural Dynamics*, 10.1002/eqe.2205.
Rossetto, T., Elnashai, A. (2003). "Derivation of vulnerability functions for European-type RC structures based on observational data". *Engineering Structures.* 25(10), 1241-1263.
Rossetto, T., Elnashai, A. (2005) "A new analytical procedure for the derivation of displacement-based vulnerability curves for populations of RC structures". *Engineering Structures* 27(3):397-409.
Rota, M., Penna, A., Strobbia, C. (2008). "Processing Italian damage data to derive typological fragility curves". *Soil Dynamics & Earthquake Engineering*, 28(10-11):933–947.
RSA (1983). Regulamento de Segurança e Acções para Estruturas de Edifícios e Pontes, Decreto-Lei n.º235/83, Lisbon, Portugal (in Portuguese).
RSCCS (1958). Regulamento de Segurança das Construções Contra os Sismos, Decreto-Lei nº41658, Lisbon, Portugal (in Portuguese).
RSEP (1961). Regulamento de Solicitações em Edifício e Pontes, Decreto-Lei n.º44041, Lisbon, Portugal (in Portuguese).

S

Sabetta, F., Goretti, A., Lucantoni, A. (1998). Empirical fragility curves from damage surveys and estimated strong ground motion. *Proceedings of the 11th European Conference on Earthquake Engineering*, Paris, France.
Sattar, S., Liel, A. (2010). "Seismic Performance of the Reinforced Concrete Frame Structures with and without Masonry Infill Walls". *Proceedings of the 9th US national and 10th Canadian conference on Earthquake Engineering,* Toronto, Canada.
Scott, B. D., Park, R., Priestley, M. J. N. (1982). "Stress-Strain Behavior of Concrete Confined by Overlapping Hoops at Low and High Strain Rates". *ACI Journal Proceedings*, 79(1):13-27.
Shome, N., Cornell, C. A., Bazzurro, P., Carballo, J. E., (1998). "Earthquakes, records and nonlinear responses", *Earthquake Spectra*, 14:469-500.

Singhal, A., Kiremidjian, S. (1997). A method for earthquake motion–damage relationships with application to reinforced concrete frames. NCEER report, NCEER-97-0008, SUNY at Buffalo, USA.

Sorensen, M. B., Stromeyer, D., Grünthal, G. (2008). "Estimation of macroseismic intensity – new attenuation and intensity vs. ground motion relations for different parts of Europe". *Proceedings of the 14th World Conference on Earthquake Engineering,* Beijing, China.

Sousa, M. L. (1996). Modelos probabilistas para avaliaçao da casualidade sísmica em Portugal continental. MSc thesis, Instituto Superior Técnico, Lisbon, Portugal (in Portuguese).

Sousa, M. L. (2006). Risco sísmico em Portugal continenal. PhD thesis, Instituto Superior Técnico, Lisbon, Portugal (in Portuguese).

Sousa, M. L., Campos Costa, A. C. (2009). "Ground motion scenarios consistent with probabilistic seismic hazard disaggregation analysis. Application to Mainland Portugal". *Bulletin of Earthquake Engineering*, 7:127-147.

Sousa, M. L., Coelho, E., Martins, A. (2010). "Vulnerabilidade sísmica e danos no parque hoteleiro da região do Algarve". *Proceedings of the 10th National Conference on Earthquake Engineering*, Aveiro, Portugal (in Portuguese).

Sozen, M. (2006). From Düzce to the city. Advances in Earthquake Engineering for Urban Risk Reduction, NATO Science Series, Springer.

Spence, R. (2004). "Risk and regulation: can improved government action reduce the impacts of natural disasters?". *Building Research & Information*, 32(5).

Spence, R. (2007). Earthquake disaster scenario prediction and loss modelling for urban areas. LESSLOSS Report - 2007/07, IUSS press, Pavia, Italy.

Stafford-Smith, B., Carter, C., (1969). "A method for the analysis of infilled frames". *Proceedings of the ICE*, 44:31-48.

Stepp, J. (1972). "Analysis of completeness in the earthquake sample in the Puget Sound area and its effect on statistical estimates of seismic hazard". *Proceedings of the International Conference on Microzonation for Safer Construction Research and Applications*, Seattle, USA.

Stewart, J., Javanbarg, M., Di Alessandro, C., Bozorgnia, Y., Abrahamson, N., Boore, D., Campbell, K., Delavaud, E., Erdik, M., Stafford, P. (2012). Selection of a Global Set of Ground Motion Prediction Equations. Technical Report, GEM Foundation, Pavia, Italy.

Stewart, J., Scasserra, G., Lanzo, G., Mollaioli, F., Bazzurro, P. (2008). Critical evaluation of Italon strong motion data and comparison to NGA ground motion prediction equations, Technical Report UCLA SGEL 2008/03, Structural and Geotechnical Engineering Laboratory, University of California, Los Angeles, USA.

Strasser, F. O., Bommer, J. J., Sesetyan, K., Erdik, M., Cagnan, Z., Irizarry, J., Goula, X., Lucantoni, A., Sabetta, F., Bal, I. E., Crowley, H., Lindholm, C. (2008). "A comparative study of European earthquake loss estimation tools for an earthquake scenario in Istanbul". *Journal of Earthquake Engineering*, 12(S2):246–256.

SYNER-G (2011). Fragility functions for common RC building types in Europe. Deliverable 3.1. Available from URL: http://www.vce.at/SYNER-G/.

T

Thomas, P., Wong, I., Abrahamson, N. (2010). Verification of Probabilistic Seismic Hazard Analysis Computer Programs. PEER Report 2010/106, Pacific Earthquake Engineering Research Center, University of California, Berkeley, USA.

Toro, G., Abrahamson, N. A., Schneider, J. (1997). "Model of strong ground motions from earthquakes in central and eastern North America: best estimates and uncertainties". *Seismological Research Letters*, 68:41-57.

Toro, G. (2002). Modification of the Toro et al. (1997) attenuation equations for large magnitudes and short distances. Technical Report, Risk Engineering, Inc.

Turkish Design Code (2007). Specifications for the building to be constructed in earthquake hazardous areas. Ministry of public works and Settlement, Ankara, Turkey.

U

UNISDR (2009). "Global Assessment Report on Disaster Risk Reduction 2009". Report, United Nations International Strategy for Disaster Reduction Secretariat, Geneva, Switzerland.

Uva, G., Porco, F., Fiore, A. (2012). "Appraisal of masonry infill walls effect in the seismic response of RC framed buildings: A case study", *Engineering Structures*, 34:514-526.

V

Vacareanu, R., Radoi, R., Negulescu, C. Aldea, A. (2004). "Seismic vulnerability of RC buildings in Bucharest, Romania". *Proceedings of the 13th World Conference on Earthquake Engineering,* Vancouver, Canada.

Vamvatsikos, D., Cornell, A. C. (2002). "Incremental dynamic analysis". *Earthquake Engineering & Structural Dynamics*, 31(3):491-514.

Vamvatsikos, D., Cornell, C. (2005). "Developing efficient scalar and vector intensity measures for IDA capacity estimation by incorporating elastic spectral shape information". *Earthquake Engineering and Structural Dynamics*, 34:1573-1600.

Vargas, Y. F., Pujades, L. B., Barbat, A. H. (2010). "Probabilistic assessment of the global damage in reinforced concrete structures". *Proceedings of the 14th European conference on Earthquake Engineering,* Ohrid, Macedonia.

Vicente, R. (2008). Strategies and methodologies for urban rehabilitation interventions. The vulnerability assessment and risk evaluation of the old city centre of Coimbra. PhD Thesis, University of Aveiro, Aveiro, Portugal (in Portuguese).

Vicente, R., Parodi, S., Lagomarsino, S., Varum, H., Mendes Silva, J. (2010). "Seismic vulnerability and risk assessment: case study of the historic city centre of Coimbra, Portugal". *Bulletin of Earthquake Engineering*, 9(4):1067-1096.

Vilanova, S., Fonseca, J. (2007). "Probabilistic seismic-hazard assessment for Portugal". *Bulletin of the Seismological Society of America*, 97:1702-1717.

Vilanova, S., Fonseca, J., Oliveira, C. S. (2012). "Ground-Motion for Seismic Hazard

Assessment in Western Iberia". *Bulletin of the Seismological Society of America*, 102:169-184.

W

Wald, D., Allen, T. (2007). "Topographic Slope as a Proxy for Seismic Site Conditions and Amplification". *Bulletin of the Seismological Society of America*, 97:1379-1395.

Wasserman, L. (2004) All of Statistics: A Concise Course on Statistical Inference. Springer, New York, USA.

Watson-Lamprey, J., Abrahamson, N. A. (2006). "Selection of ground motion time series and limits on scaling". *Soil Dynamics & Earthquake Engineering*, 26:477-482.

Wells, D. L., Coppersmith, K. J. (1994). "New empirical relationships among magnitude, rupture length, rupture width, rupture area, and surface displacement". *Bulletin of Seismological Society of America,* 84:974-1002.

Wills, C. J., Clahan, K. B. (2006). "Developing a map of geologically defined site-condition categories for California". *Bulletin of the Seismological Society of America*, 96:1483-1501.

Z

Zhao, J., Zhang, J., Asano, A., Ohno, Y., Oouchi, T., Takahashi, T., Ogawa, H., Irikura, K., Thio, H.K., Somerville, P., Fukushima, Y., Fukushima, Y. (2006). "Attenuation relations of strong ground motion in Japan using site classification based on predominant period". *Bulletin of the Seismological Society of America*, 96(3):898-913.

Web References

1. OpenQuake repository: https://github.com/gem/openquake/tree/master/docs/schema
2. Global Earthquake Model: http://www.globalquakemodel.org/
3. DBELA Github repository: https://github.com/VSilva/DBELA/
4. OpenQuake: http://www.openquake.org/
5. SELENA: http://www.norsar.no/pc-35-68-SELENA.aspx - developed by the Norwegian Seismic Array (NORSAR) in Kjeller, Norway.
6. EQRM: http://www.ga.gov.au/hazards/earthquakes.html - developed by the Geoscience Australia (GA) in Canberra, Australia.
7. ELER: http://www.koeri.boun.edu.tr/depremmuh/eski - developed by the Kandilli Observatory and Earthquake Research Institute (KOERI) in Istanbul, Turkey.
8. QLARM: http://www.wapmerr.org/qlarm.asp - developed by the World Agency of Planetary Monitoring and Earthquake Risk Reduction (WAPMERR) in Geneva, Switzerland.
9. CEDIM: http://www.cedim.de - developed by the Center for Disaster Management and Risk Reduction Technology (CEDIM) in Potsdam, Germany.
10. CAPRA: http://www.ecapra.org/software - Central America Probabilistic Risk Analysis, an initiative from the World Bank.
11. RiskScape: http://www.riskscape.org.nz - developed by the Geological and Nuclear

Sciences (GNS) in Lower Hutt, New Zealand.

12. LNECLoss: http://www-ext.lnec.pt/LNEC/DE/NESDE - developed by the Laboratório Nacional de Engenharia Civil (LNEC) in Lisbon, Portugal.
13. MAEviz: http://rcp.ncsa.uiuc.edu/maeviz/about.html - developed by the Mid-America Earthquake Center (MAE Center) in Illinois, USA.
14. OpenRisk: http://www.risk-agora.org - developed by the Scawthorn, Porter and Associates (SPA Risk).
15. Celery project: http://celeryproject.org/
16. RabbitMQ project: http://www.rabbitmq.com/
17. QuakeML markup language – http://www.quakeml.org
18. NRML, Natural Risk Markup Language: https://github.com/gem/nrml/
19. GEM Building Taxonomy: http://www.nexus.globalquakemodel.org/gem-building-taxonomy/
20. Matlab: http://www.mathworks.com/
21. OpenSEES: http://opensees.berkeley.edu/
22. Italian strong motion database ITACA: http://itaca.mi.ingv.it/ItacaNet/
23. Japan strong motion database: http://www.k-net.bosai.go.jp/
24. Iran strong Motion Network (ISMN): http://www.bhrc.ac.ir/ismn/Index.htm/
25. New Zealand strong motion database (GENET): http://www.geonet.org.nz/resources/basic-data/strong-motion-data/
26. Turkish strong motion database (Daphne): http://daphne.deprem.gov.tr:89/2K/daphne_v4.php/
27. European strong motion database: http://www.isesd.hi.is/
28. PEER strong motion database: http://peer.berkeley.edu/smcat/
29. Global strong motion database (COSMOS): http://www.cosmos-eq.org/
30. Portuguese Census Survey 2011: http://censos.ine.pt/
31. French Accelerometric Network (RAP): http://www-rap.obs.ujf-grenoble.fr/
32. Swiss Earthquake Database (SED): http://seispc2.ethz.ch/strong_motion/home.jsp
33. Portuguese Statistical Office: http://www.ine.pt/
34. SHARE project: http://www.share-eu.org/
35. SYNER-G project: http:// www.vce.at/SYNER-G/
36. NERA project: http://www.nera-eu.org/
37. Instituto Geofráfico Nacional: http://www.ign.es/
38. Portuguese Environmental Agency: http://www.apambiente.pt/
39. NEFITAG: http://www.lneg.pt/iedt/projectos/336/
40. Eurocodes repository: http://eurocodes.jrc.ec.europa.eu/
41. World Bank data: http://data.worldbank.org/country/portugal/